Advances in Materials Science and Engineering

Advances and New Challenges for Recycled Aggregate Concrete

Lead Guest Editor: Ana S. Guimarães
Guest Editors: J. M. P. Q. Delgado, Robert Černý, and Antonio G. De Lima

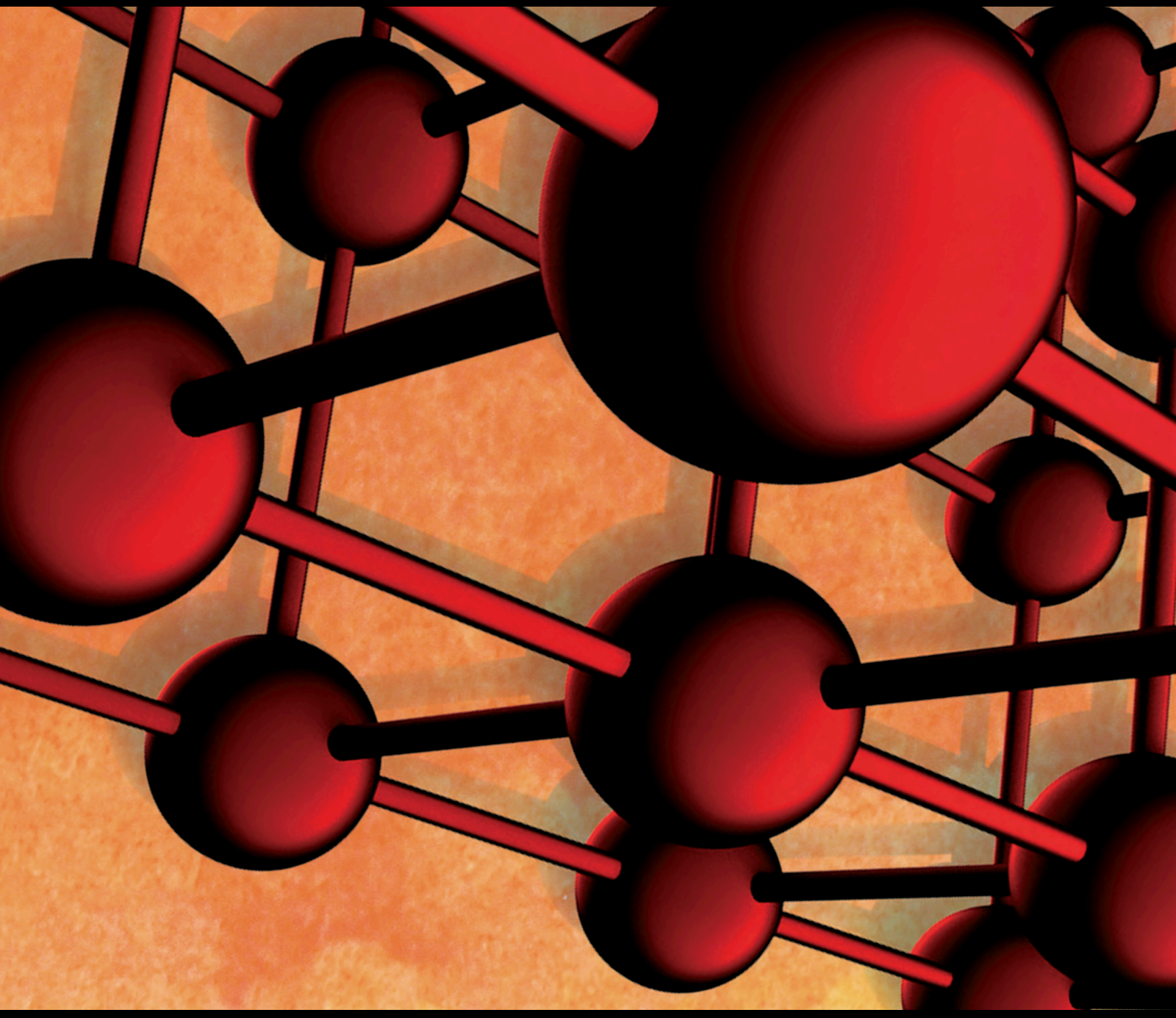

Advances and New Challenges for Recycled Aggregate Concrete

Advances in Materials Science and Engineering

Advances and New Challenges for Recycled Aggregate Concrete

Lead Guest Editor: Ana S. Guimarães
Guest Editors: J. M. P. Q. Delgado, Robert Černý, and Antonio G. De Lima

Contents

Hindawi
Advances in Materials Science and Engineering
Volume 2021, Article ID 9891634, 2 pages
https://doi.org/10.1155/2021/9891634

Editorial

Advances and New Challenges for Recycled Aggregate Concrete

A. S. Guimarães,[1] **J. M. P. Q. Delgado**,[1] **Robert Černý**,[2] **and A. G. Barbosa de Lima**[3]

[1]*CONSTRUCT-LFC, Faculty of Engineering, University of Porto, Rua Dr. Roberto Frias s/n, Porto 4200-465, Portugal*
[2]*Department of Materials Engineering and Chemistry, Faculty of Civil Engineering, Czech Technical University in Prague, Thákurova 7/2077, 166 29 Prague 6, Czech Republic*
[3]*Department of Mechanical Engineering, Federal University of Campina Grande, Av: Aprígio Veloso, 882, Campina Grande 58429-900, Brazil*

Correspondence should be addressed to A. S. Guimarães; anasofia@fe.up.pt

Received 27 November 2021; Accepted 27 November 2021; Published 3 December 2021

The world's waste production is at its highest level ever following the development of new world powers. This is particularly evident in construction/demolition activities, which have one of the largest contributions to the economic growth and waste generation, therefore requiring stricter policies to encourage sustainability.

Concrete is the favourite choice as a construction material among civil engineers around the globe for decades, due its better performance, longer life, and low maintenance cost. However, the continuous necessity and increase for raw materials of concrete, especially coarse aggregate, due to a rapid building construction, tends to increase the danger of early exhaustion of the natural resources. The recycled coarse aggregate plays a great role as an alternative raw material that can replace the natural coarse aggregate for concrete. With the wave of sustainability on construction, new sustainable and reusable construction materials are needed. One such material is recycled aggregate concrete.

This special issue had a good acceptation by the scientific community with several papers submitted and 7 papers accepted for publication. A considerable number of experimental papers address new research advances and applications in recycled aggregate concrete. K. H. Younis et al. present an experimental research study that investigates the effect of utilizing metakaolin on the behaviour of recycled aggregate concrete. Based on the experimental results, the authors showed that metakaolin reduces the workability of the recycled aggregate concrete mixes; however, the use of metakaolin improves the compressive, splitting tensile, and flexural strengths and the elastic modulus of recycled aggregate concrete.

Z. Yao et al. analyse the static and dynamic mechanical characteristics of the coal gangue concrete used to replace coarse and fine aggregates in concrete, in mine support structures. Their results showed, between others, that the addition of coal gangue fine aggregate has a positive effect and the addition of coal gangue coarse aggregate has a negative effect, on the impact energy of the initial and final cracks of concrete. Moreover, the dynamic strength of concrete was improved with the addition of coal gangue fine or coarse aggregate; the incorporation of coal gangue coarse aggregate made the concrete shear surface smooth; and the given impacting pressure of the concrete with coal gangue coarse aggregate has greater particle breakage.

R. Berenguer et al. present an experimental work related to the partial substitution of Portland cement by sugar cane bagasse in order to reduce clinker in concrete volume, responsible for high emission of CO_2 to the atmosphere. An experimental campaign with cementitious pastes was carried out to evaluate the durability properties' changes due to sugar cane bagasse ash use. The results showed that samples containing 15% of sugar cane bagasse ash unveiled good results in terms of durability, indicating that concrete structure with sugar cane ash research is a new and important scientific topic to be highlighted.

Y. Zhang et al. analyse the mechanical performance of concrete with recycled aggregates from concrete pavements. The experimental results showed that the strength of recycled concrete decreases with increasing water-cement ratio and as the replacement rate of recycled aggregates increases, the optimal sand ratio decreases.

I. H. Yang et al. experimentally analyse the structural behavior of concrete beams containing recycled coarse aggregates. The results showed that the crack pattern of the recycled coarse aggregate beams was similar to that of the natural coarse aggregate beams; however, the recycled coarse aggregate beams exhibited smaller crack spacing than the natural coarse aggregate beams. The flexural strength was marginally affected by the recycled coarse aggregate content; however, the ductility of the beam was not significantly influenced by the recycled coarse aggregate content.

L. Zhu and Z. Zhu present a review of the potential use of waste clay brick as a binder and aggregate substitute in mortar and concrete. The literature review showed that the complete replacement of natural aggregates with recycled clay brick aggregate is feasible and it could reduce the consumption of natural resources and encourage the reuse of construction waste.

Finally, Y. Wang et al. present an experimental study related to the effect of prewetting time and shrinkage reducing agents on shrinkage volume and concrete strength through a series of concrete shrinkage and strength tests. The experimental campaign showed that an appropriate amount of shrinkage reducing agent and adjustment of prewetting time of coal gangue ceramsite are necessary to reduce the shrinkage rate and improve the stability of the specimen. As demonstrated by the authors, this is of great significance to wide application of lightweight aggregate concrete with coal gangue ceramsite.

We hope that readers of this special issue will find not only accurate experimental data and updated reviews on the application of recycled aggregates on concrete structures and elements but also important questions to be resolved. This special issue includes essentially experimental developments, providing a self-contained major reference that is appealing to both the scientists and the engineers. At the same time, these topics will be going to encounter a variety of scientific and engineering disciplines, such as chemical, civil, and agricultural engineering.

Conflicts of Interest

The Editors declare that they have no conflicts of interest.

A. S. Guimarães
J. M. P. Q. Delgado
Robert Cerný
A. G. Barbosa de Lima

Hindawi
Advances in Materials Science and Engineering
Volume 2020, Article ID 8829713, 17 pages
https://doi.org/10.1155/2020/8829713

Research Article

Recycled Aggregate Concrete including Various Contents of Metakaolin: Mechanical Behavior

Khaleel H. Younis,[1,2] **Abdulfattah A. Amin**,[1] **Hemin G. Ahmed**,[3] **and Shelan M. Maruf**[1]

[1]*Department of Road Construction, Erbil Technology Institute, Erbil Polytechnic University, Erbil, Iraq*
[2]*Civil Engineering Dept., Tishk International University, Erbil, Iraq*
[3]*Surveying Dept., Erbil Technology Institute, Erbil Polytechnic University, Erbil, Iraq*

Correspondence should be addressed to Khaleel H. Younis; khaleel.younis@epu.edu.iq and Shelan M. Maruf; shelan.maruf@epu.edu.iq

Received 2 September 2020; Revised 26 November 2020; Accepted 1 December 2020; Published 17 December 2020

Academic Editor: Antonio G. De Lima

This experimental research investigates the effect of utilizing metakaolin (MK) on the behavior of recycled aggregate concrete (RAC). The RAC incorporates recycled coarse aggregate (RCA) originated from crushing construction and demolition waste. The investigated parameters were RCA and MK contents. Tests of workability and mechanical properties such as compressive strength, splitting tensile strength, flexural strength, and modulus of elasticity were conducted to evaluate the influence of MK on workability and mechanical behavior of RAC. In total, 19 mixes were prepared. These mixes are divided into four groups. Group zero (G0) includes a reference mix containing normal coarse aggregate (NCA) and 3 mixes made with 35%, 70%, and 100% of RCA. Each one of the other three groups (G1, G2, and G3) was made with one content of the three contents of RCA, and each group includes five mixes made with the contents of 4%, 8%, 12%, 16%, and 20% of MK. Empirical models among the mechanical properties of the RAC mixes were developed and compared with models of standard codes of practice such as ACI 318, BS 8110, and Eurocode 2. It was found that MK reduces the workability of the RAC mixes. Nonetheless, the outcomes reveal that MK can improve the compressive, splitting tensile, and flexural strengths and the elastic modulus of RAC. This strength improvement enhances as the content of MK increases. The proposed models for the mechanical properties of RAC made with MK showed good correlations. The developed model for modulus of elasticity is quite close to the Eurocode 2 model, whereas the models of ACI 318 and BS 8110 underestimate the values of the modulus of elasticity.

1. Introduction

As a result of the population growth, economic development, and urbanization, construction activities and demolishing works are increasing rapidly worldwide [1]. Constructing new buildings and demolishing the old ones are among these construction and demolishing activities. Although such works and activities are vital in most of the communities in the world, they cause several environmental concerns and sustainability issues that are globally recognized [2] such as the depletion of the natural resources and changes in ecosystems. Construction and demolishing activities result in massive quantities of waste which is known as construction and demolition waste (CDW). Worldwide, the annual generation of CDW is estimated at 0.5 billion tons [3, 4]. The environmental concerns that are associated with such substantial quantitate of CDW include the use of significant parts of land to dump these wastes and the contamination of soils. To alleviate the effects of these concerns, the construction industry and researchers have examined various ways as solutions to these concerns. One solution is the utilization of CDW in concrete. It can be recycled and reused as coarse and fine aggregates. The usage of CDW as recycled coarse aggregate (RCA) in concrete can

conserve our environment, save vast areas of land, and mitigate natural resource depletion [5].

For decades, the feasibility of the utilization of recycled aggregate in concrete production has been considered by many scholars [6]. Despite the fact that the utilization of CDW in concrete is beneficial in terms of the aforementioned environmental aspects, its use is limited [7, 8]. The main obstacle against the use of RCA is the inferior characteristics of such aggregate in comparison with the normal aggregates. The performance of the concrete that contains such aggregate is also lower than that of the concrete made with normal aggregate [4, 9]. This has been confirmed by previous studies [3–5, 10, 11]. The concrete made with RCA possesses low strength, high water absorption, high porosity, high shrinkage, and creep [4, 5, 11]. The content of the RCA determines the level of the decrease in the strength of the concrete. The recycled aggregate concrete (RAC) shows lower compressive strength than natural aggregate concrete (NAC) by up to 40% [12]. Additionally, the RAC exhibits lower splitting tensile strength by up to 25% [4]. Furthermore, the use of RCA in concrete results in lower flexural strength by up to 30% [5]. This behavior of RAC is the main reason behind the limitations (only 20–30) imposed by most of the international codes of practice on the RCA content that should be used to replace the NAC, in particular for structural applications [2]. The fact that the RCA particles have a heterogeneous nature in terms of its composition is the main reason causing such behavior of RAC. The RCA particles are characterized with the residual mortar attached to its surface [8]. This attached mortar possesses high porosity, low density, and microcracks which all together lead to RCA with weak and loose microstructure which in turn adversely affect the performance of RAC. The imperfections in the microstructure of the RCA particles also result in weak and uncompact interfacial transition zone (ITZ) between the recycled coarse aggregate particles and cement paste [8]. This has been recognized by several studies [7, 9, 13–15] and identified as a factor leading to low strength of RAC.

The low quality of RAC has pushed scholars to examine different methods to improve its properties and enhance the characteristics of RCA. One example is removing the residual mortar on the surface of RCA which was applied employing various approaches [2, 9]. Although these approaches resulted in enhanced properties of RCA, they were accompanied with shortcomings like low durability, high consumption of energy, and cost issues [4, 8]. Therefore, other studies have attempted other approaches such as the use of reactive powders that are very fine in size and possess cementitious characteristics. Reactive powders such as fly ash (FA), ground blast furnace slag (GBFS), silica fume (SF), and metakaolin (MK) have been used to improve the properties RAC [4, 16–18]. Studies have reported that such materials can enhance the mechanical properties, improve the durability, and modify the microstructure of RAC [18]. Most of these studies have attributed the improvement in the performance of RAC due to the use of these reactive powders (minerals admixtures) to the filling ability, the pozzolanic reaction, the alteration in the concrete pore structure, and compact ITZ [4, 8, 19]. Although there are many studies that dealt with improving RAC using SF, FA, and GBFS, limited work can be found when it comes to the inclusion of MK in such concrete.

Metakaolin (MK) is an alumina-silicate material that is derived from clay or soils that contain high levels of kaolinite. MK is obtained after the clay soils are exposed to high temperatures (650–900°C) for thermal activation. MK differs from other mineral admixtures (SF, FA, and GBFS) in that its production can be well controlled to minimize composition's variation and achieve high purity as well as obtain high pozzolanic reactivity [20, 21]. MK can significantly improve the strength performance as well as the durability behavior of NAC [20, 22]. These benefits of MK are ascribed to the pozzolanic reaction of MK and its high surface area (small size of its particles). The pozzolanic reaction usually develops when the SiO_2 in the MK reacts with calcium hydrates (CH) (a product of the cement-hydration process) with the presence of water. Such chemical reaction leads to the development of more C–S–H gel which is responsible for the strength of the cement paste. The pozzolanic reaction alters the pore structure of the cement paste as well as refines the microstructure of the concrete which can improve the performance of concrete [20, 21, 23]. There are many research studies that examined the influence of the MK on the performance of NAC in both conditions, fresh and hardened [20]. A reduction in the workability and increase in the setting time of the NCA were reported due to the usage of MK [20, 23]. This was linked to the high surface area of the MK [20]. Furthermore, MK can improve the compressive strength of NAC at both early and late ages with more effectiveness at early ages. It was also found that the extent of the strength improvement increases with the increase of the MK content [20, 22, 23]. It was observed that the typical contents that can enhance the performance of NAC were in the range of 5–20% by cement mass [20].

Few experimental studies can be found on the effect of the use of MK on the performance of RAC [18, 24–26]. The influence of the addition of 15% of MK on the performance of RAC made with 50% and 100% RCA was reported in [18]. The authors found that 15% of MK improved the strength in compression, splitting tensile, and resistance to penetration of chloride by 10%, 18%, and 32%, respectively, for RAC made with 100% RCA. Another study which was conducted in [26] reported that the inclusion of 10% of MK enhanced the compressive strength of RAC. Replacing 10% of cement with MK resulted in significant improvement in compressive strength, splitting tensile, and elastic modulus [24, 25]. Others reported strength and durability enhancement with the use of 20% of MK in RAC incorporating 100% RCA [25].

As there are limited numbers of studies that have dealt with enhancing the behavior of RAC using MK, the current study aims at examining the outcomes of utilizing MK to help upgrading the mechanical properties of RAC. The study examines the influences of replacing the OPC with MK at various dosages on the behavior of RAC. To assess the influence of MK on the mechanical behavior of RAC mixtures, mechanical properties such as compressive strength, splitting tensile strength, and flexural strength of RAC were evaluated. The modulus of elasticity was also assessed for all mixtures. Utilizing the experimental results with the

employment of the regression analysis method, empirical relationships between the mechanical properties of the RAC mixes made with MK were developed. These developed relationships were compared with models proposed by the standard codes of practice such as ACI 318, BS 8110, and Eurocode 2. The outcomes of the current study may contribute in the promotion of the feasibility of using RAC in many applications of civil engineering.

2. Materials and Methodology

2.1. Materials. Ordinary Portland cement (OPC) type CEMI 42.5R was utilized in the current research. It fulfills the specifications of Iraqi standards. It is produced by Mas Company which is based in north of Iraq (Sulaymaniyah). The chemical composition of the OPC is presented in Table 1, while the physical characteristics of the OPC are shown in Table 2.

Natural coarse aggregate and recycled coarse aggregate were used in this study. The former was river aggregate (gravel). The maximum aggregate size is 20 mm. It had absorption capacity of 1.1% and specific density of 2.64. The coarse recycled aggregate was recycled concrete-based aggregate derived from crushing old concrete structural elements. The RA had specific gravity and water absorption of 2.45 and 3.3%, respectively. Normal sand was used as fine aggregate in the current work, and it had a maximum size of 4.75 mm.

The metakaolin utilized in the current work was a commercial type produced by the BASF Company of chemicals. It is a reactive mineral admixture in the form of very fine white powder as can be seen in Figure 1(a). The average particle size of the metakaolin is around 1 μm. The chemical composition of the metakaolin is presented in Table 1, while the physical properties are presented in Table 2. Figure 1 shows a scanning electron microscopy image of the MK used in the current study.

2.2. Mixes, Variables, and Mix Proportioning. The total number of prepared and investigated mixes in this study is nineteen concrete mixtures. Table 3 shows the designation of all mixes, study's variables, and mix proportions. The variables of the mixes are the content of RCA (three contents) and the content of MK (five contents). The NCA was replaced with RCA in three contents (35%, 70%, and 100%). The contents of the MK were 4%, 8%, 12%, 16%, and 20%. The investigated mixes were divided into four groups. Group zero (reference group) includes four mixes: one made with NCA and three mixes made with the three contents of RCA (35%, 70%, and 100%). Each one of the other three groups was made with one content of the three contents of RCA, and each group includes five mixes made with the five contents of the MK (4%, 8%, 12%, 16%, and 20%) (see Table 3). The mixtures were prepared using the same water/binder ratio (0.46) with cement quantity of (375 kg/m^3) and water quantity of (172.5 kg/m^3). The rest of the mix proportions are shown in Table 3. An adjustment to the amount of the mix water was made in the mixes containing RCA, to take into consideration the water absorption of the RCA.

2.3. Mixing, Casting, and Curing. All experimental procedures were made in a concrete laboratory under ambient conditions. To mix the components of the concrete mixtures, a concrete tilting drum mixer that has a capacity of 0.12 m^3 was employed. The mixing steps of the concrete were as follows. In the first step, the dry coarse aggregate was added to the mixer and mixed with part of the mixing water for 2 minutes. In the case of mixes with RCA, after the first step, the coarse aggregate was left in the mixer for a period of ten minutes to let the RCA absorb water to attain the saturated surface dry condition (SSD). In the second step, the sand, binders (OPC and/or MK), and the remaining part of the mixing water were put in the mixes and all ingredients were mixed for 3 more minutes. When the mixing is completed, concrete was cast in different types of molds. Thereafter, proper compaction using vibrating table was conducted and all molds were covered and kept to cure in the lab conditions for 24 h. Then, the specimens were extracted from the molds and moved to tanks containing water for further curing till the specified age for testing.

2.4. Specimens and Tests

2.4.1. Workability (Slump) Test. The evaluation of the workability of the fresh concrete in all mixtures was conducted through the slump test. The test was done as per BS EN 12350-2:2009 [27].

2.4.2. Compressive Strength Test. To evaluate the compressive strength of the hardened concrete, a universal hydraulic machine with 2000 kN capacity was utilized. The test was done following the BS EN 12390-3 [28]. The test was performed on cubic specimens of 100 mm (see Figure 2). It was obtained at ages of 7, 28, and 90 days.

2.4.3. Splitting Tensile Strength Test. The test of splitting tensile strength was performed following the standard test of BS EN 12390-6 [29]. The same machine used for the compressive strength was also used for this test. The specimens were cylinders of 100 × 200 mm as can be seen in Figure 3. For each mix, three cylinders were tested at the age of 28 days.

2.4.4. Flexural Strength Test. The test of flexural strength was performed as per the guidelines of BS EN 12390-5 [30]. Prisms of 100*100*500 mm were used to determine the flexural strength of all mixes (see Figure 4), and for each mix, after 28 days of curing, three specimens were tested.

2.4.5. Modulus of Elasticity Test. The test of modulus of elasticity was undertaken as per ASTM C469-02 [31]. Concrete cylindrical samples of 150*300 mm were made to conduct this test (see Figure 5). For all mixes, the test was conducted at the age of 28 days.

Table 1: Chemical analysis of OPC and MK.

Material	SiO_2	Al_2O_3	Fe2O3	CaO	MgO	SO_3	Na_2O	K2O	Na_2Oeq
CEM I	20.88	4.98	2.96	65.7	0.76	2.82	0.28	0.44	0.50
MK	57.6	30.1	6.6	1.0	0.98	—	—	0.58	—

Table 2: Physical characteristics of OPC and MK.

Material	CEM I	MK
Color	Gray	White
Specific gravity	3.15	2.5
Fineness (cm2/g)	2400	12800

3. Results

3.1. Workability (Slump) Test. Workability of all concrete mixtures was assessed by the slump test. Table 4 illustrates the slump values of all mixes. It was observed that the workability of mixes encompassing RCA in G0 is lower than that of the reference mix (N00). The slump values decreased from 125 mm for the mix with NCA to 100, 85, and 80 mm when the NCA was replaced with 30%, 70%, and 100% of RCA. This decrease in slump value depends on the RCA content (when the RCA content increases, the slump value reduces). The adverse effect of the use of RCA in concrete is also reported by others [4, 8, 32]. This slump value decrease can be partly related to the rough surface of the RCA and mainly to the high absorption capacity of the RCA compared with that of the NCA [4, 32] (see Table 4).

The effect of the use of MK on the workability of the mixes made with RCA (mixes of G1, G2, and G3) is shown in Figure 6. It can be seen that the content of the MK adversely affects the slump values of these regardless of the percentage of the RCA. There is a general decrease trend in the workability of the mixes made with 30%, 70%, and 100% RCA as the content of the MK increases as can be seen in Figure 7. For example, for mixes in G1 (RCA = 35%), these mixes lost about 10%, 15%, 20%, 20%, and 30% of their workability (compared to the reference group) when 4%, 8%, 12%, 16%, and 20% of the OPC were replaced with MK. Higher ratios of workability loss were recorded with mixes with higher contents of RCA (70% and 100% in G2 and G3) (see Figure 7). The drop in the workability of concrete due to adding MK was also reported in [20, 22, 24]. This workability loss is attributed to the very small size of the particles of MK compared to the particles of the OPC, which can be clearly identified in Table 2 when we compare the surface area of the two powders. Higher surface area requires more water to achieve suitable workability [20]. One more reason could be the forces of van der Waals, which can be considered as the source to the development of agglomeration and electrostatic attraction between the particles of any powder, and these are more dominant with powders having high surface area [33]. These agglomeration and electrostatic attraction hinder the movement of the matrix, hence reducing the workability of concrete.

3.2. Compressive Strength. Table 4 shows the outcomes of the compressive strength test at the ages of 7, 28, and 90 days of all mixes. The results at 28 days, which are the average of three specimens for each mix, are also presented in Figure 8. As far as the results of the reference group (G0) are concerned, generally mixes with RCA exhibited lower compressive strength than mix N00 regardless of the age of the concrete at testing time. The degree of strength reduction depends on the content of RCA. For example, at the age of 28 days, the strength of the reference mix which includes NCA decreased by 12%, 20%, and 30% when the NCA was replaced by 35%, 70%, and 100% of RCA as it is clear in Figure 8. A decrease in strength due to replacing NCA by RCA was reported by others [4, 10, 14]. This decrease in strength can be related to the lower quality of the RCA particles compared to NCA. The lower quality is due to the adhered mortar existing on the surface of the RCA which is characterized with microcracks and voids, hence resulting in low strength and stiffness and high water absorption and porosity concrete [14]. This nondense adhered mortar also deteriorates the cement paste and the RCA bond, leading to the development of weak interfacial transition zone (ITZ) [8, 34, 35]. Indeed, weak ITZ increases the propagation of the cracking process under loading, causing early failure and lower strength.

The influence of the use of MK on the compressive strength of concrete mixtures made with RCA (in groups G1, G2, and G3) can be seen in Table 4 and Figure 8. The general trend that can be identified is a positive strength enhancement regardless of the content of both RCA and MK. The influence of the percentage of MK on the compressive strength and the recycled aggregate concretes is presented and discussed based on the normalized strength. The strength of the mixes is normalized with the reference mixes (G0): N00, R350, R700, and R1000. Normalized strength means that the average compressive strength of the mix is divided on the average compressive strength of the reference mix. The normalized strengths to that of the N00 mix are illustrated in Figure 9, while the normalized strength of the mixes with RCA that contain MK to that of RCA mixes without MK are presented in Figure 10.

The normalized strength of the mixes made with 35%, 70%, and 100% RCA to that of the mix N00 are shown in Figures 9(a), 9(b) and 9(c). Regardless of the content of RCA, the general strength enhancement in the compressive strength of the RCA mixtures due to the use of MK can be observed. The strength enhancement increases with the increase in the content of MK, in particular at RCA content of 35%, as can be seen in Figures 9(a), 9(b), and 9(c). However, the optimum content of MK that leads to a compressive strength equal/or comparable strength to that of the mix N00 (made with NCA) varies according to the

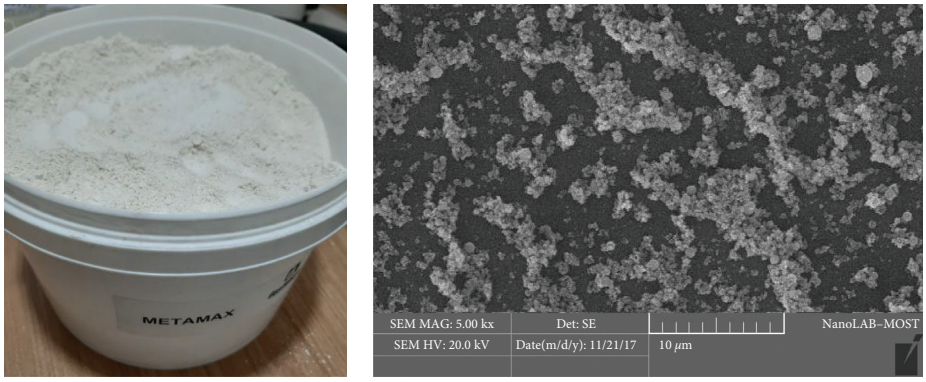

(a) (b)

Figure 1: Metakaolin used in current study. (a) Metakaolin powder. (b) Scanning electron microscopy image.

Table 3: Mix designation and proportioning.

Group	Mix designation	% of metakaolin[a]	Cement	Metakaolin	Water	Coarse Agg. (natural)	Coarse Agg.(recycled)	Fine Agg.
Reference group or G0	N00	0	375	0	172.5	1092	0	711
	R350	0	375	0	172.5	710	359	711
	R700	0	375	0	172.5	328	718	711
	R1000	0	375	0	172.5	0	1026	711
G1	R354	4	360	15	172.5	710	359	711
	R358	8	345	30	172.5	710	359	711
	R3512	12	330	45	172.5	710	359	711
	R3516	16	315	60	172.5	710	359	711
	R3520	20	300	75	172.5	710	359	711
G2	R704	4	360	15	172.5	328	718	711
	R708	8	345	30	172.5	328	718	711
	R7012	12	330	45	172.5	328	718	711
	R7016	16	315	60	172.5	328	718	711
	R7020	20	300	75	172.5	328	718	711
G3	R1004	4	360	15	172.5	0	1026	711
	R1008	8	345	30	172.5	0	1026	711
	R10012	12	330	45	172.5	0	1026	711
	R10016	16	315	60	172.5	0	1026	711
	R10020	20	300	75	172.5	0	1026	711

[a]By cement mass.

content of RCA (see Figure 9). For example, for the mixes made with 35% RCA, a content of MK which is equal to 12% is enough to get normalized strength of 1.0 which means similar strength to that of mix N00 (see Figure 9(a))). This also means that the use of 12% of MK instead of OPC can compensate the 12% compressive strength loss of mix N00 when 35% of NCA was replaced with RCA. Figure 9(b)) shows that for the mix containing 70% of RCA, to reach a comparable strength to that of mix N00, 20% of the OPC should be replaced with MK. For the mix made with 100% RCA, even 20% of MK did not result in comparable strength to the reference mix as 20% of MK led to a normalized strength of 0.9 as can be seen in Figure 9(c). This means that when the NCA is fully replaced with RCA, 90% of the compressive strength of the mix N00 can be obtained by replacing 20% of the OPC with MK.

The beneficial influence of utilizing MK on the compressive strength of the mixes containing RCA can be justified by three mechanisms. The first mechanism is physical while the second and the third mechanisms are chemical [8]. The physical one can be elucidated by the filling capability of MK particles. The very fine particles of the MK as mineral admixture can play a key role in filling microvoids and pores on the surface of the RCA and in modifying the microstructure of the concrete and making it denser [22]. Indeed, this mechanism helps in enhancing the density of the concrete and hence improving the compressive strength of the concrete. The chemical mechanism can be described by the pozzolanic reaction of the MK [20]. This reaction usually develops due to the high content of silicon dioxide in the MK. The silicon dioxide reacts with the calcium hydroxide (CH) which is a part of production of the cement hydration; this reaction leads to the production of more calcium-silicate-hydrates (C–S–H), the main production that enhances the strength of concrete [9]. Therefore, this chemical mechanism also results in improving the

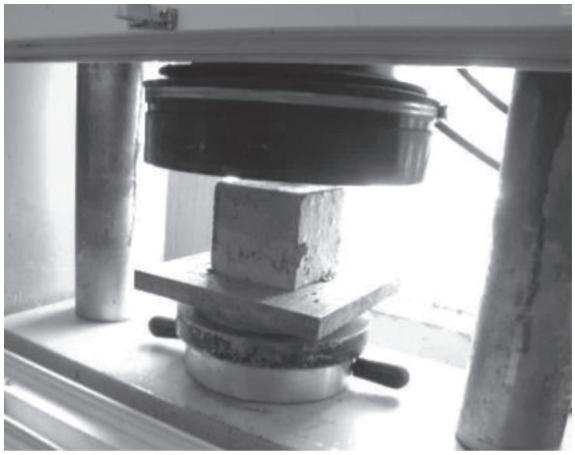

Figure 2: Specimen under compression machine.

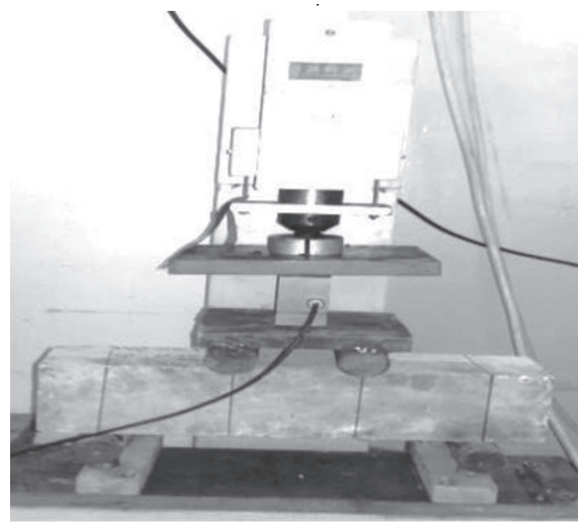

Figure 4: Specimen under bending machine.

Figure 3: Specimen prepared for splitting tensile test.

Figure 5: Specimen prepared for the modulus of elasticity test.

compressive strength of the RCA mixes. Thus, this is why the level of the strength improvement rises as the content of the MK increases, as can be seen in Figure 9. The third mechanism is by speeding up the reaction between the water and the cement particles which is well known as hydration process. This increase in the rate of the hydration process is due to the high surface area of the small particles of the MK. The acceleration of the hydration process acts as a booster for the pozzolanic reaction, hence improving the compressive strength of concrete [20].

The normalized strength of the mixes made with MK and 35%, 70%, and 100% RCA to that of the mixes without MK is shown in Figures 10(a), 10(b), and 10(c). Regardless of the content of RCA, a clear rise in the compressive strength of the RCA mixtures due to the addition of MK can be observed. This strength increase is directly connected to the increase in the content of the MK (see Figures 10(a), 10(b), and 10(c)). Nonetheless, the extent of strength increase also depends on the RCA content. For instance, at 35% of RCA content, the strength increase can reach up to 19% when the OPC was replaced with 20% of MK, whereas at the same content of the MK, the strength increase rises to 23% and 29% for the RCA of 70% and 100%, respectively (see Figure 10).

This compressive strength enhancement could be due to the strengthening of the RCA by the MK. This strengthening can be achieved by (1) filling up the microcracks and voids on the surface of the RCA and (2) eliminating the porosity of the adhered mortar on the RCA surface. Moreover, the improvement of the quality of RCA surface not only increases the strength of the RCA itself but also enhances the ITZ between the RCA and the cement paste. Another reason for the strength enhancement of the RAC mixes could be the nucleation effect since the existence of several zones of nucleation could help in providing a more uniform and homogenized distribution of the strength-responsible gel C–S–H in the concrete [36]. This, in turn, leads to a denser pore structure of the concrete resulting in higher strength of concrete. These reasons with the pozzolanic reaction effect can together justify the strength enhancement of the RCA mixes incorporating MK compared to those without MK.

Table 4: Results of workability and compressive strength of all mixes.

Group	Mix designation	Slump (mm)	Compressive strength (MPa)		
			7 days	28 days	90 days
Reference group or G0	N00	125	33.2	44.8	49.7
	R350	100	27.6	39.4	42.6
	R700	85	24.6	35.7	39.3
	R1000	80	21.4	31.4	34.2
G1	R354	90	27.5	41.0	45.5
	R358	85	29.1	42.2	47.6
	R3512	80	31.0	44.9	50.3
	R3516	80	30.4	45.3	52.6
	R3520	70	33.3	46.9	55.3
G2	R704	80	26.7	38.2	42.0
	R708	75	26.9	39.6	44.8
	R7012	70	28.6	42.1	48.4
	R7016	60	29.8	43.2	50.1
	R7020	60	30.3	43.9	50.9
G3	R1004	80	22.3	33.3	37.9
	R1008	75	23.9	35.2	40.4
	R10012	75	25.8	37.4	43.7
	R10016	65	26.5	38.9	45.9
	R10020	60	29.6	40.5	48.5

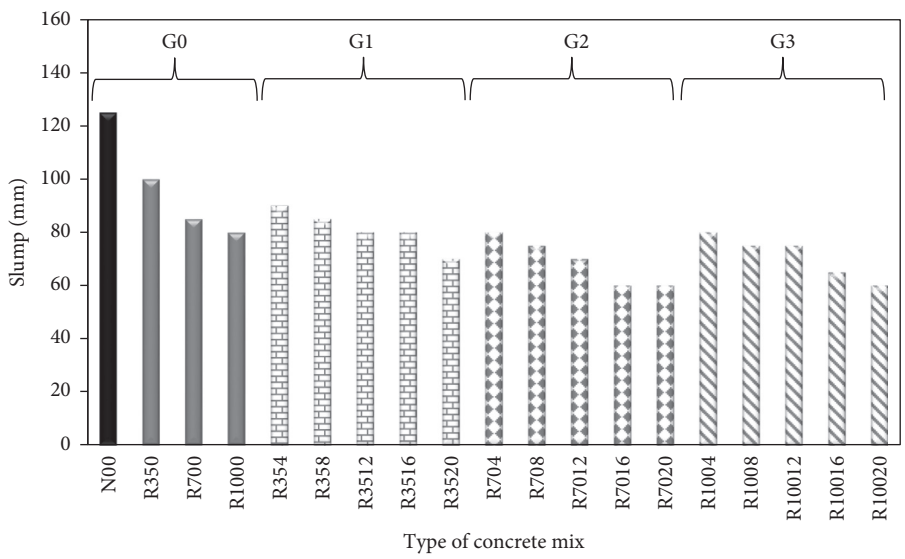

Figure 6: Slump values of all mixes.

The rate of the strength increase is also related to the content of MK. This rate is high up to 12% of MK content, but after that, this rate slows down as can be seen in Figure 11. This behavior is similar for all RCA contents (35%, 70%, and 100%).

The influence of curing time or the age of concrete at testing on the development of the compressive strength of the mixtures is presented in Figure 12. This figure shows the rate of strength development over time for the mixes with and without MK. Figure 12(a)) shows the strength development of the reference mixes (group G0) made without MK, while Figure 12(b)) depicts the strength development for the mixes made with 20% MK. From Figures 12(a) and 12(b), it can be observed that rate of strength development for the mixes including MK is higher than those without MK particularly after the age of 28 days and up to 90 days. Thus, the effect of MK on the strength of the RCA mixes is more influential at early ages than later ages. This is very clear in Figure 12(c)) which compares the rate of development of strength of the mixes with and without MK.

3.3. Splitting Tensile Strength. The splitting tensile strength results of the cylindrical samples after curing for 28 days of mixes made with and without MK are presented in Table 5. The normalized strength (to the mix N00 and to the mixes of RCA without MK) is also presented in Table 5. The splitting

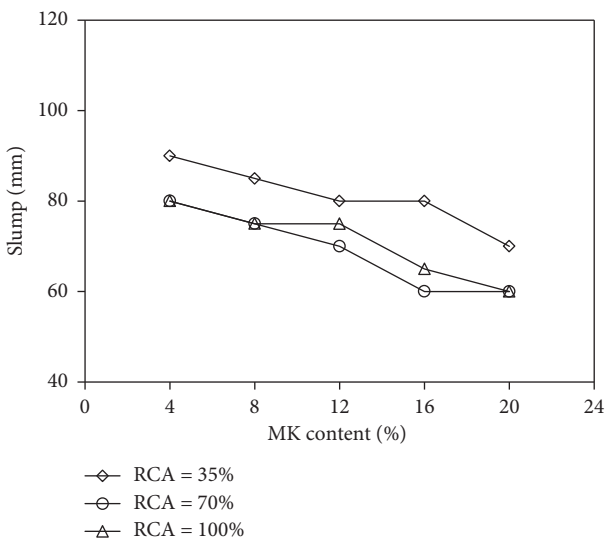

Figure 7: Effect of MK content on the slump values at various contents of RCA.

tensile values (MPa) are also shown in Figure 13. These results represent the average of three cylindrical samples.

In the reference group (G0), the trend of the results of the splitting tensile strength is similar to the trend of the results of the compressive strength. The splitting tensile strength of mixes made with RCA exhibited lower strength than that of the reference mix N00. The splitting tensile strength of mixes R350, R700, and R1000 dropped to 3.94, 3.57, and 3.45 MPa compared to 4.03 MPa of mix N00. This means that the concrete lost about 2%, 11%, and 14% of its strength when the NCA was replaced with RCA at contents of 35%, 70%, and 100%, respectively, as shown in Table 5. Similar behavior was also observed by other studies [5, 14] for recycled coarse aggregate concrete. The loss of splitting tensile strength of the mixes made with RCA is because of the weaknesses in the RCA particles related to the adhered mortar which is considered as weak and cracked surface. The weak bond between the cement paste and the RCA particles caused by the loosely attached mortar also results in a weak ITZ, thus extending the possibility of the existence of flaws and weak points that promote cracking in these zones and decreasing the splitting tensile strength of the concrete [4, 8, 34].

The results of the mixes in groups G1, G2, and G3 reveal the positive effect of using various contents of MK on the splitting tensile strength of these mixes (see Table 5). Regardless of the content of RCA, low contents of MK (4% and 8%) show no or very slight strength enhancement, whereas high contents (12%, 16%, and 20%) resulted in strength enhancement that reached comparable values to that of the reference mix. For example, the tensile strength of mix made with 35% of RCA increased to reach a comparable value to that of mix N00 only at 20% of MK, while for the mixes made with 70% and 100% RCA, MK contents of 16% and 20% led to the same strength of mix N00. On the other hand, at the MK content of 20%, the normalized tensile strength of the mixes with 35%, 70%, and 100% RCA was about 1.06, 1.11, and 1.15, respectively, compared to the strength of the same mixes without MK.

The better splitting tensile strength due to the inclusion of MK is because of the strengthening of the top surface of the RCA by the filling ability of the very fine particles of the MK. Furthermore, the contribution of the MK in enhancing the ITZ is also a factor that can enhance the splitting tensile strength of concrete. Moreover, the pozzolanic reaction of the MK can also positively affect the splitting tensile strength of the RCA [8, 20].

3.4. Flexural Strength. The results of the flexural strength measured on prisms with dimensions of 500*100*100 mm and loaded using four-point bending test are presented in Table 6. These results are the average of three samples tested after 28 days of curing. The normalized strength (to the mix N00 and to the mixes of RCA without MK) is also illustrated in Table 6. Figure 14 shows the flexural strength values in MPa.

The mixes made with recycled coarse aggregates in the reference group showed lower flexural strength than that of mix N00. The higher the content of the RCA, the higher the loss of the flexural strength compared to mix N00. For example, the flexural strength decreased from 5.02 MPa to 4.65, 4.25, and 4.08 MPa when the NCA was replaced by 35%, 70%, and 100% of RCA, respectively, as can be seen in Table 6 and Figure 14. Hence, the concrete loses about 7%, 15%, and 19% of its flexural strength when 35%, 70%, and 100% of the NCA were replaced by RCA, respectively. As explained in Sections 3.3 and 3.4, the drop in the flexural strength due to the inclusion of the RCA can be attributed to loose and cracked surface of the RCA, the weak bond between the RCA and the cement paste, and the porous ITZ [13, 14]. All these reasons can act as early failure initiatives leading to lower flexural strength.

Nonetheless, these reductions in flexural strength of the mixes made with RCA can be compensated by replacing the OPC with MK as can be seen in Table 6. The use of MK improves the flexural strength of these mixes almost at all contents of the MK but the level of improvement depends on the content of RCA. For instance, at 35% of RCA, even at low contents of MK (4%, 8%, and 12%), comparable (to that of the reference mix N00) flexural strength can be achieved, whereas high contents of MK (16% and 20%) are needed to get the same comparable flexural strength (see the normalized strength in Table 6) for the mixes made with 70% and 100% RCA. Comparison of the results of the RCA mixes made with and without MK reveals that all contents of MK increase the flexural strength of these mixes, and the higher the content of MK, the higher the flexural strength of the mix. At 20% of the MK, the flexural strength of the mixes made with 35%, 70%, and 100% of RCA increased by 16%, 15%, and 22%, respectively, compared to the same mixes but without MK. This beneficial effect of the MK on the RCA concrete is also reported in [20, 24]. The flexural strength improvement can be elucidated by the same explanations previously mentioned in Sections 3.2 and 3.3 which are the strengthening of the RCA particles, the refinement in the

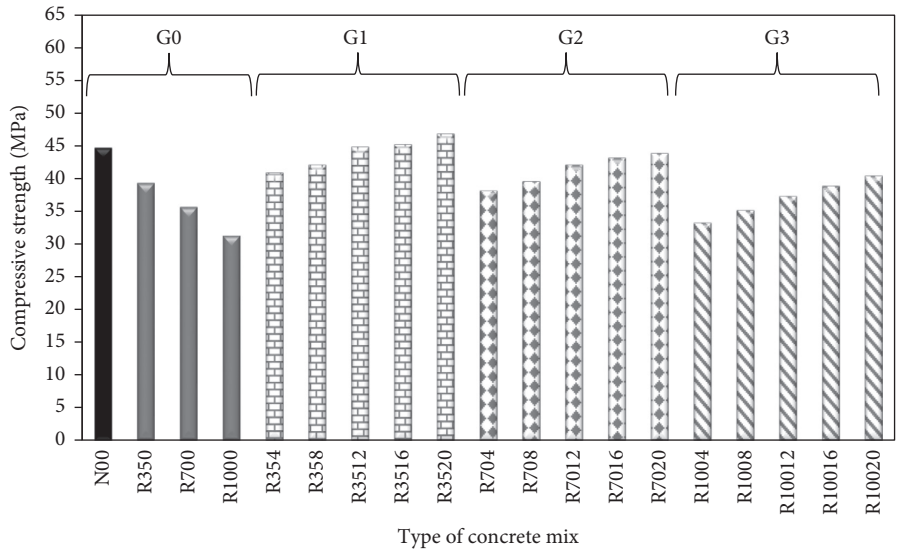

Figure 8: Compressive strength of all mixes at age of 28 days.

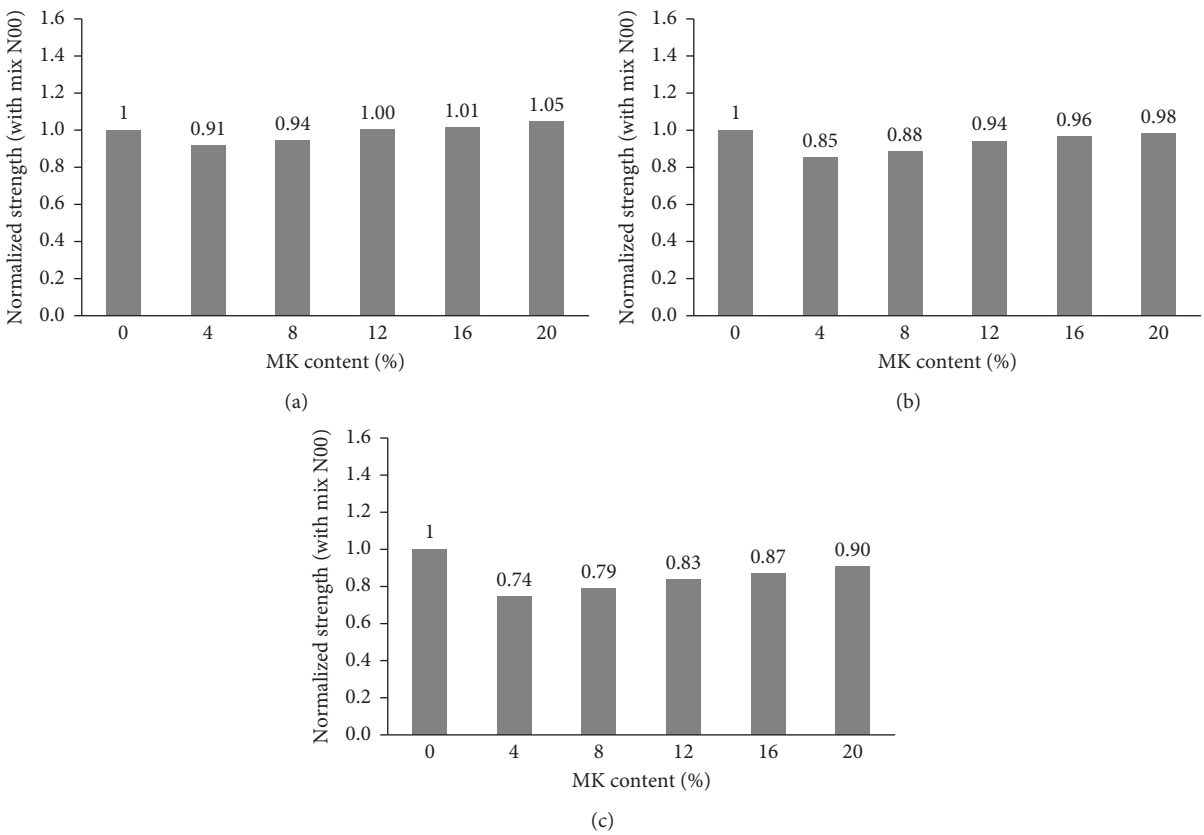

Figure 9: Normalized strength (with mix N00) for mixes. (a) RCA = 35%. (b) RCA = 70%. (c) RCA = 100%.

microstructure of the paste, and the densification in the interfacial transition zone.

3.5. Modulus of Elasticity (Ec). The results of the elastic modulus determined using cylindrical concrete samples are illustrated in Table 7. These results are the average of three samples tested at the age of 28 days. The normalized strength (to the mix N00 and to the mixes of RCA without MK) is also shown in Table 7. Figure 15 shows the values of the elastic modulus in GPa.

Figure 15 shows that the modulus of elasticity of the RCA mixes in the reference group (G0) is lower than the value of the mix N00. The elastic modulus of the mix N00 reduced

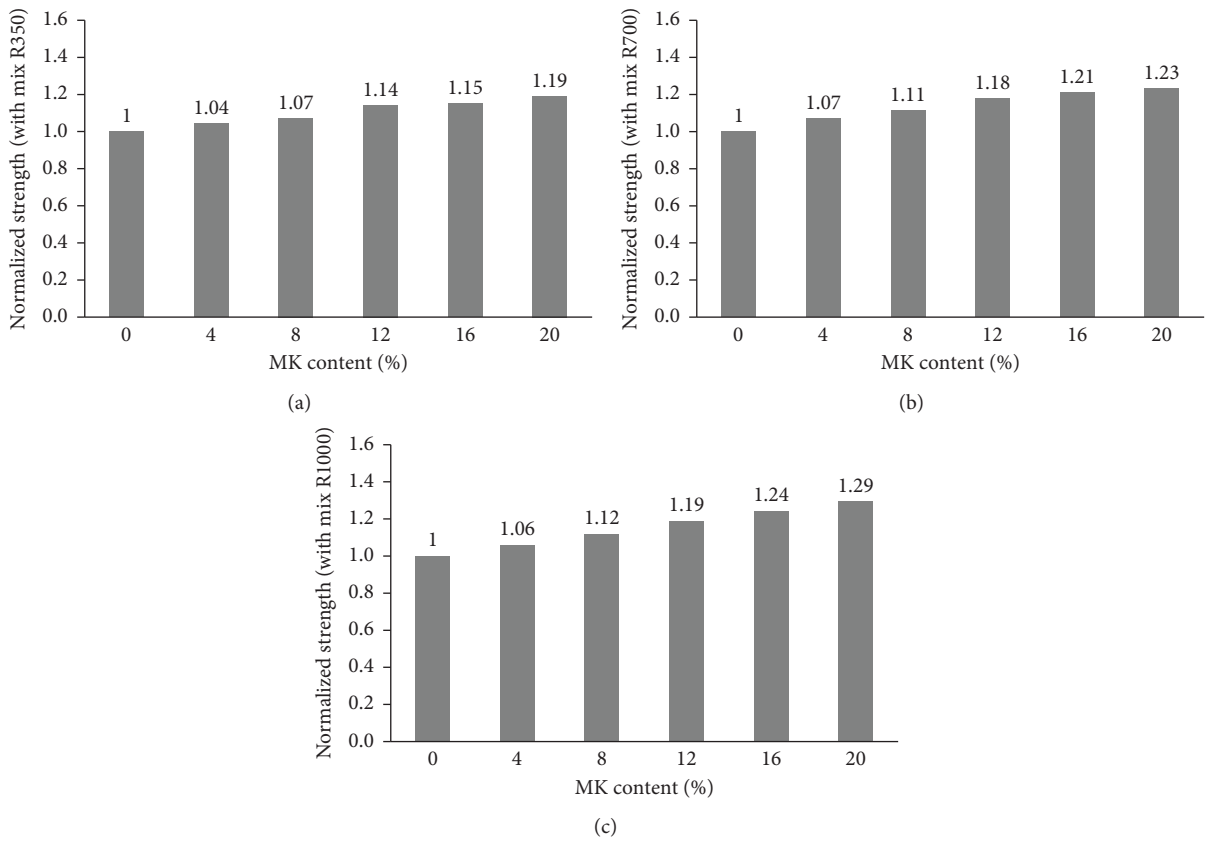

Figure 10: Normalized strength (with the mix of RCA without MK) for mixes. (a) RCA = 35%. (b) RCA = 70%. (c) RCA = 100%.

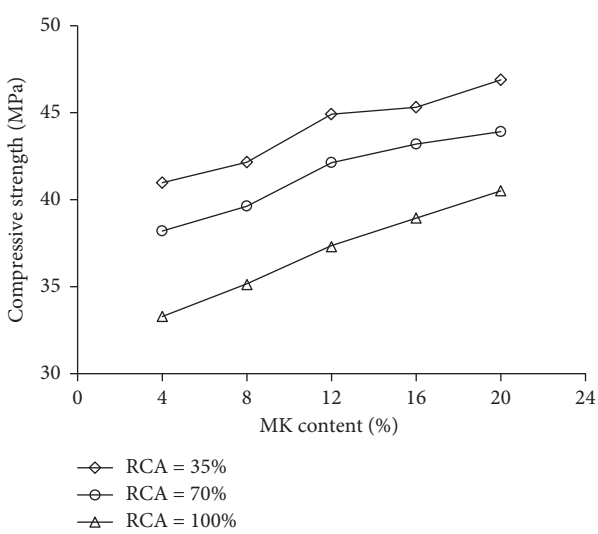

Figure 11: Influence of the MK on the compressive strength of the RCA mixes.

from 37.4 GPa to 32.1, 31.0, and 30.1 GPa when the NCA was replaced with 35%, 70%, and 100% of RCA, respectively. As can be seen, the reduction in elastic modulus depends on the RCA content; the higher the RCA content, the higher the drop in modulus of elasticity. This reduction due to the use of RCA represents 14%, 17%, and 20% for the R350, R700, and R1000 compared to the elastic modulus of mix N00. The reduction in the modulus of elasticity due to the use of RCA is lower than the reduction in the compressive strength. At 100% of RCA, the compressive strength reduced by 30%, whereas the modulus of elasticity decreased by 20%.

The loss of stiffness (elastic modulus) as a result of using RCA could be due to the characteristics of the RCA particles. As mentioned previously, these particles are inherently weak because of the porous nature of its surface which results from microcracks and voids in attached mortar existing on the top surface of these particles. The porous ITZ caused by the weak bond between the RCA and the cement paste also contributes to the loss of the elastic modulus of RCA mixes. Indeed, these flaws (cracks and voids) decrease the ability to withstand loads and weaken the stiffness of the concrete leading to lower elastic modulus [4, 8, 13].

The advantageous effect of the partial substitution of OPC with MK on the elastic modulus is clear in Table 7. The improvement of the modulus of elasticity increases as the MK content increases. The higher values were obtained at 20% of MK content. For example, at 20% of MK, the elastic modulus of the mixtures with 35%, 70%, and 100% RCA achieved 98%, 96%, and 89% of the that of the reference mix N00; this means that the loss of elastic modulus of these mixes of RCA was reduced from 14%, 17%, and 20% to 2%, 4%, and 11% when 20% of MK was used (see normalized strength in Table 7). The improvement in the modulus of elasticity of the RCA mixes due to the inclusion of MK could be due to the modification on the

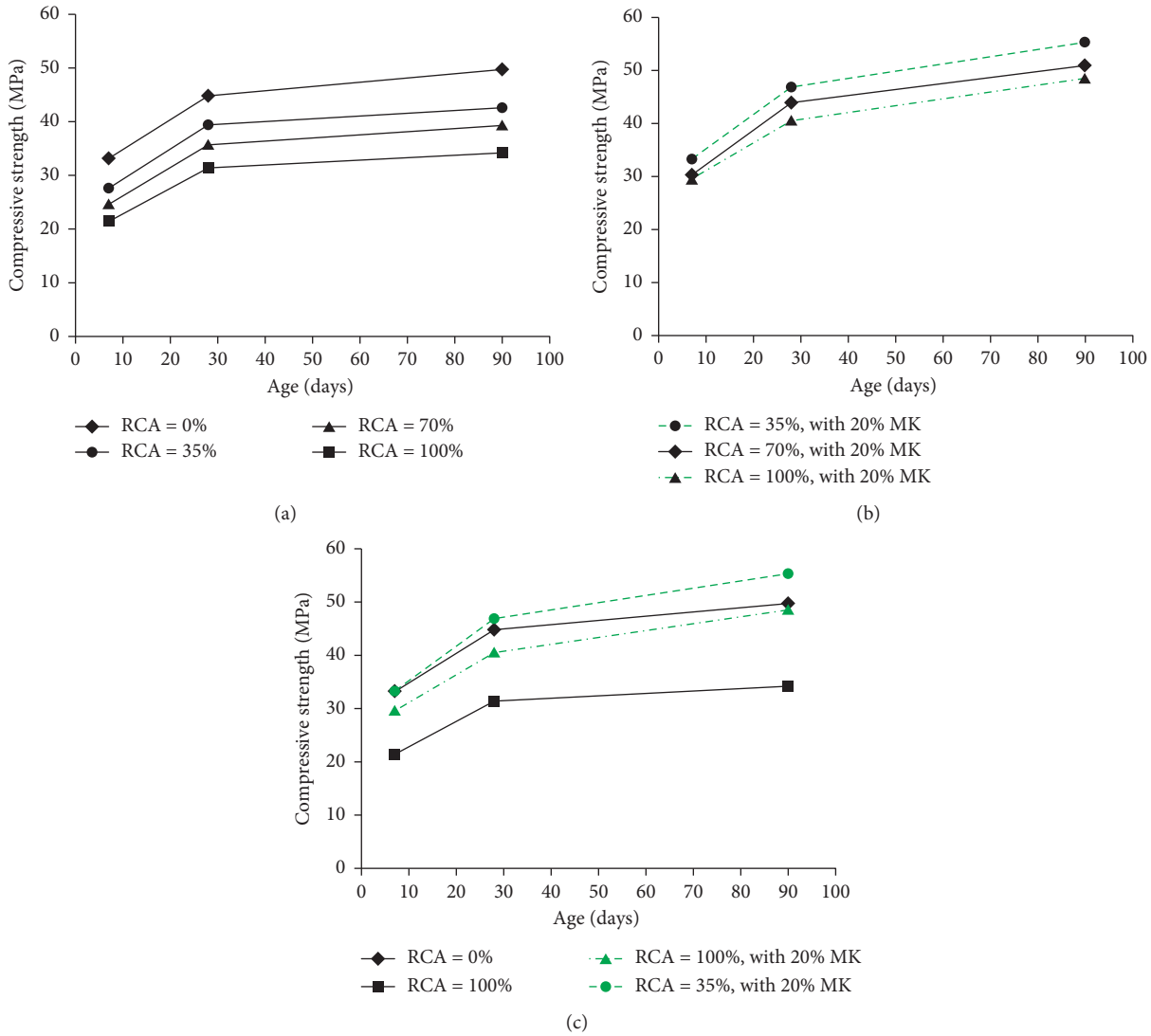

Figure 12: Strength development over time. (a) Mixes without MK. (b) Mixes with 20% of MK. (c) Comparing several mixes in (a) and (b).

Table 5: Results of splitting tensile strength (strength values and normalized strength).

Group	Mix designation	Splitting tensile		
		Strength (MPa)	Normalized (to mix N00)	Normalized (to mixes: R350/R700/R1000)
Reference group or G0	N00	4.03	1	—
	R350	3.94	0.98	1
	R700	3.57	0.89	1
	R1000	3.45	0.86	1
G1	R354	3.69	0.91	0.94
	R358	3.71	0.92	0.94
	R3512	3.91	0.97	0.99
	R3516	3.85	0.96	0.98
	R3520	4.17	1.03	1.06
G2	R704	3.51	0.87	0.98
	R708	3.57	0.88	1.00
	R7012	3.79	0.94	1.06
	R7016	3.93	0.97	1.10
	R7020	3.97	0.99	1.11
G3	R1004	3.26	0.81	0.94
	R1008	3.80	0.94	1.10
	R10012	3.74	0.93	1.08
	R10016	3.97	0.98	1.15
	R10020	4.05	1.00	1.17

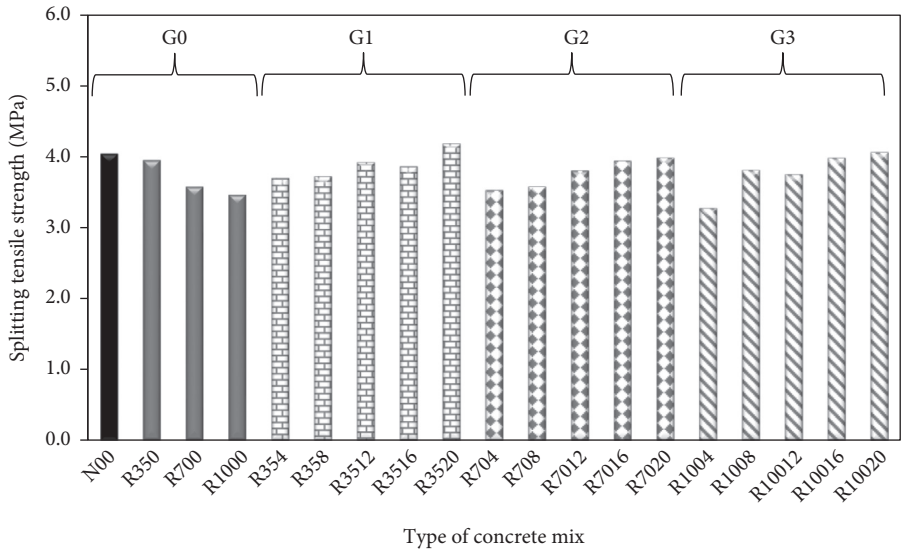

Figure 13: Splitting tensile strength at the age of 28 days.

Table 6: Results of flexural strength of all mixes (strength values and normalized strength).

Group	Mix designation	Flexural		
		Strength (MPa)	Normalized (to mix N00)	Normalized (to mixes: R350/R700/R1000)
Reference group or G0	N00	5.02	1	—
	R350	4.65	0.93	1
	R700	4.25	0.85	1
	R1000	4.08	0.81	1
G1	R354	4.84	0.96	1.04
	R358	4.89	0.97	1.05
	R3512	4.94	0.98	1.06
	R3516	5.07	1.01	1.09
	R3520	5.39	1.07	1.16
G2	R704	4.28	0.85	1.01
	R708	4.36	0.87	1.03
	R7012	4.63	0.92	1.09
	R7016	4.77	0.95	1.12
	R7020	4.87	0.97	1.15
G3	R1004	4.03	0.80	0.99
	R1008	4.54	0.90	1.11
	R10012	4.86	0.97	1.19
	R10016	4.87	0.97	1.19
	R10020	4.98	0.99	1.22

surface of the RCA particles and pore structure of the cement paste. The high surface area of the MK particles contributes to fill up the microcracks on the RCA leading to a strong RCA. The pozzolanic reaction helps in refining the pore structure of the paste and the ITZ by consuming the Ca (OH) existing on the surface of the concrete and forming more C–S–H gel which improves the modulus of elasticity (stiffness) of the concrete [20, 24].

3.6. Empirical Formulas among Mechanical Properties. In this part, the obtained results of the mechanical properties including compressive strength, splitting tensile strength, flexural strength, and modulus of elasticity were used to develop empirical equations among these properties. Moreover, the developed empirical equations were compared with the standard equation available in the codes of practice such as ACI 318-02 (American Concrete Institute) [37], BS 8500 [38] (British standards), and EU-code EN-2004 (Euro code) [39]. The aim is to assess the suitability of using the current equations introduced by available codes of practice to estimate the mechanical properties of recycled aggregate concrete containing MK.

3.6.1. Splitting Tensile Strength vs. Compressive Strength. Figure 16 shows the relations between the compressive strength and splitting tensile strength of all mixes made with RCA. The experimental data from the compression and tensile tests were used to develop the relation between these two mechanical properties. Using linear regression analysis,

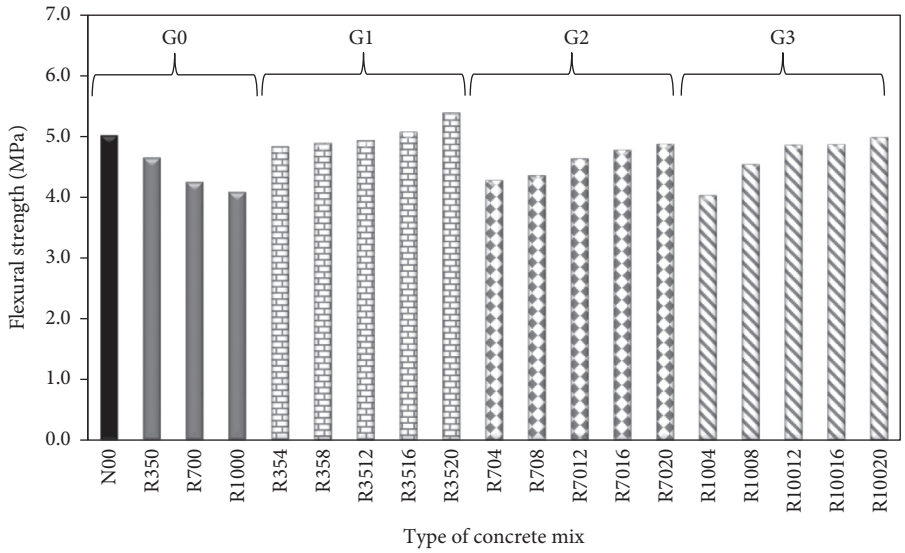

Figure 14: Flexural strength after 28 days of curing.

Table 7: Modulus of elasticity (results and normalized values).

Group	Mix designation	Modulus of elasticity		
		Value (GPa)	Normalized (to mix N00)	Normalized (to mixes: R350/R700/R1000)
Reference group or G0	N00	37.4	1	—
	R350	32.1	0.86	1.0
	R700	31.0	0.83	1.0
	R1000	30.1	0.80	1.0
G1	R354	33.9	0.91	1.06
	R358	34.1	0.91	1.06
	R3512	35.0	0.94	1.09
	R3516	35.7	0.95	1.11
	R3520	36.8	0.98	1.15
G2	R704	33.6	0.90	1.08
	R708	33.7	0.90	1.09
	R7012	34.4	0.92	1.11
	R7016	35.3	0.94	1.14
	R7020	36.0	0.96	1.16
G3	R1004	31.1	0.83	1.03
	R1008	31.6	0.84	1.05
	R10012	32.7	0.87	1.09
	R10016	33.2	0.89	1.10
	R10020	33.3	0.89	1.11

a regression equation can be developed from this figure. It can be seen that there is a correlation coefficient (R^2) of 0.55 between the compressive strength and the splitting tensile strength of the mixes made with RCA. The equation can be expressed as follows (from Figure 16):

$$f_{sp} = 0.8\left(f_c\right)^{0.4}, \tag{1}$$

where f_{sp} is the splitting tensile strength and fc is the compressive strength of the concrete.

3.6.2. Flexural Strength vs. Compressive Strength. The experimental results of the flexural and compression tests of all mixtures containing RCA are plotted and shown in Figure 17. It can be seen that there is a correlation between the two properties, and the correlation coefficient (R^2) is equal to 0.71. It was found that the best equation that best fits all the results is a power equation as can be seen in Figure 17. The equation that represents this relation can be expressed as follows:

$$f_r = 0.49\left(f_c\right)^{0.61}, \tag{2}$$

where f_r is the splitting tensile strength and fc is the compressive strength of the concrete.

3.6.3. Elastic Modulus vs. Compressive Strength. Figure 18 depicts the experimental data from the compression and modulus of elasticity (Ec) tests of all mixes made with RCA.

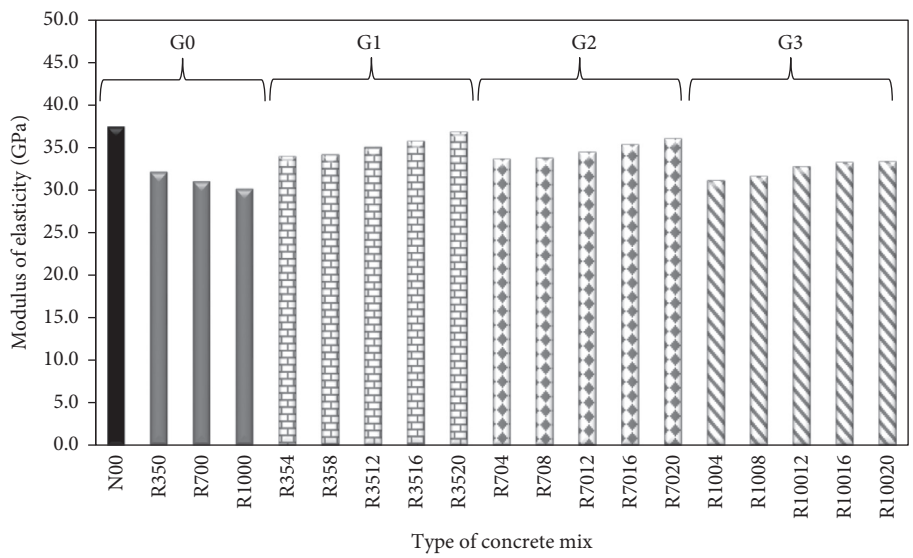

Figure 15: Modulus of elasticity after 28 days of curing.

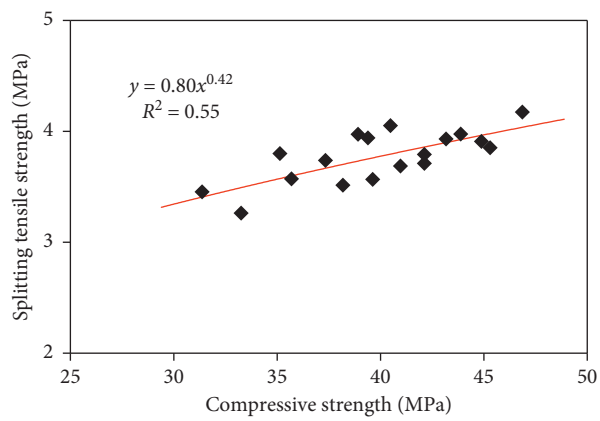

Figure 16: Correlation between splitting tensile strength and compressive strength of the mixes with RCA.

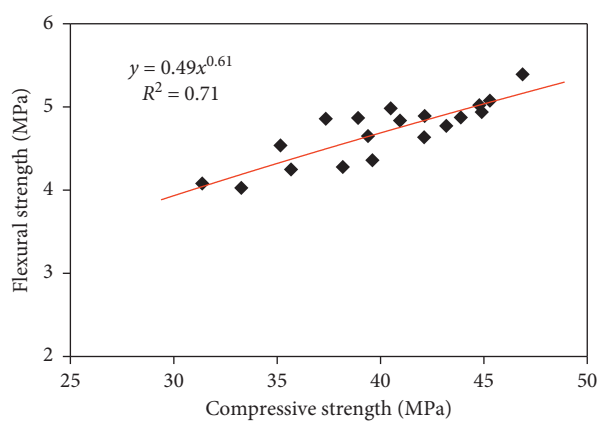

Figure 17: Correlation between flexural strength and compressive strength of the mixes with RCA.

These results were used to develop the relation between these two mechanical properties. From this figure and by using linear regression analysis, a regression equation can be developed. The figure shows that there is a strong correlation between the compressive strength (fc in MPa) and the elastic modulus (Ec in GPa) of all concretes made with RCA. The strong relationship is supported by the very high correlation coefficient R^2 which is equal to 0.92 as can be seen in

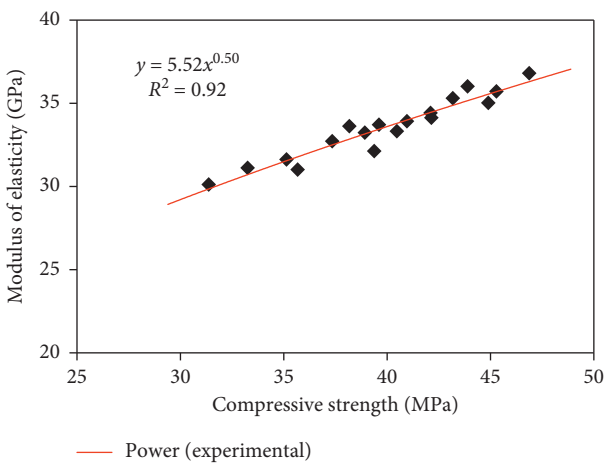

Figure 18: Correlation between modulus of elasticity and compressive strength of the mixes with RCA.

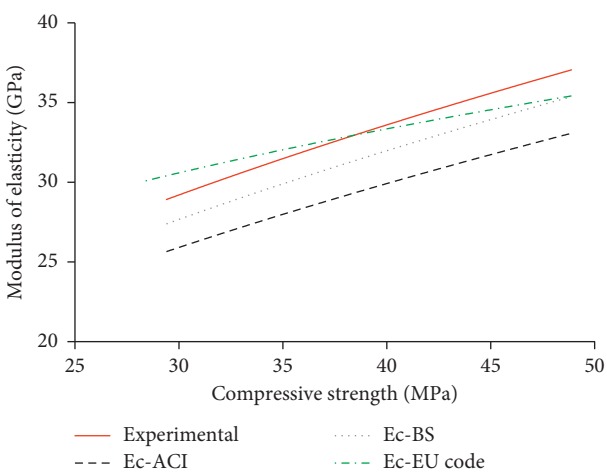

Figure 19: Comparing the developed empirical equation of E_c with the standard codes of practice.

Figure 18. The developed equation is a power equation and can be expressed as follows:

$$E_c = 5.52\sqrt{f_c}. \quad (3)$$

From equation (3) ($Ec = 5.52\sqrt{fc}$), the elastic modulus of the RCA concrete mixes with or without MK can be predicted using its compressive strength. To assess the validity of this model, we should compare it with other models from international codes of practice. The ACI 318-02 model for predicting E_c for natural aggregate concrete is $E_c = 4.7\sqrt{f_c}$. The BS 8110 proposes the model $E_c = 5\sqrt{fc}$ to estimate E_c for normal concrete. The Euro code EN-2004 uses the model $E_c = 22\,(f_{ck}/10)^{0.3}$. The results of the experiments of this study were used to predict the Ec value of each mix using the models proposed by these codes of practice. The results of predicted Ec are depicted in Figure 19. For comparison reasons, the results of the empirical model to estimate Ec developed in this study are also plotted in Figure 19. It can be seen that the estimated Ec using the developed model is higher than that of the BS and the ACI models. This means that these models underestimate Ec of the mixes with RCA (with and without MK). This could be due to the fact that this model includes both mixes of RCA, modified with MK and those have no MK . The mechanical properties of the mixes with RCA were improved using MK meaning higher strength than mixes without MK and even higher than the reference mix N00 in some cases which could be the reason that led the developed model to appear above the models of these codes. However, the developed model is more comparable to the model of Eurocode 2 as can be seen in Figure 19. This model slightly overestimates Ec of the current study up to fc in the range of 38–42 MPa and slightly underestimates the Ec value after this range of strength. Hence, the Eurocode can better estimate Ec of the RAC mixes made with or without MK.

4. Conclusions

In the current research, mechanical performance of RAC including various contents of RCA and incorporating different dosages of MK, as cement replacement, is examined. The following conclusions are highlighted based on the outcomes of current work.

(i) Replacing NCA with RCA reduces the workability of concrete. This reduction increases with the increase of RCA content. When 100% of the NCA was replaced with RCA, the concrete loses about 36% of its slump value. This can be due to the rough surface of the RCA and the high absorption capacity of the RCA particles.

(ii) The use of MK as partial replacement of the OPC decreases the workability of RAC. The decrease in workability is attributed to the percentage of MK. A decrease of up to 52% was observed for the mix made with 100% RAC and 20% MK. This is due to the high surface area of the MK particles and because of the agglomeration and electrostatic attraction that hinder the movement of the matrix, hence decreasing workability.

(iii) The utilization of RCA at contents of 35%, 70%, and 100% decreases the compressive strength of the NAC by 12%, 20%, and 30%, reduces the splitting tensile strength by 2%, 11%, and 14%, reduces the flexural strength by 7%, 155, and 19%, and reduces the modulus of elasticity by 14%, 17%, and 19%, respectively. This is because of the low quality of the RCA resulting from the attached mortar and the weak and porous ITZ.

(iv) The partial replacement of OPC with MK at contents 4%, 8%, 12%, 16%, and 20% can improve the compressive strength of RAC. At 20% of MK, the compressive strength increases to reach a value that is comparable to that of the NAC mix and higher than that of RAC without MK by 19%, 23%, and 29%. This strength enhancement is due to

physical/chemical mechanisms. The former is achieved by the filling ability of the very fine particles of the MK, whereas the latter is developed by the pozzolanic reaction of the MK which contributes to densifying the ITZ of the RAC.

(v) The influence of MK on the strength of the RCA mixes is more influential at early ages than later ages. Mixes including MK exhibit higher rate of strength development than those without MK particularly after the age of 28 days and up to 90 days.

(vi) Just as the trend of the compressive strength, the splitting tensile strength, flexural strength, and modulus of elasticity (at all contents of RCA) increase as the content of MK increases. For the RAC mix made with 100% RCA and 20% of MK, splitting tensile strength, flexural strength, and modulus of elasticity increased by 17%, 22%, and 11% compared to the RAC mix without MK.

(vii) Empirical equations (models) among the mechanical properties of the RAC mixes made with MK were developed. These equations show correlations between compressive strength and other mechanical properties as R^2 was 0.55 (for the splitting tensile strength), 0.71 (for the flexural strength), and 0.92 (for the elastic modulus).

(viii) The developed empirical model of the elastic modulus is more comparable to the model developed by Eurocode 2 (EN-2004) standard, whereas the models of the ACI 318-02 and BS 8110-1 underestimate the results of the elastic modulus in comparison with the developed model in this study.

Data Availability

The data used to support the findings of this study are included within the article.

Conflicts of Interest

The authors declare that they have no conflicts of interest.

Acknowledgments

The authors acknowledge the support and help provided by Erbil Polytechnic University and Tishk International University.

References

[1] P. K. Mehta and P. J. M. Monteiro, *Concrete: Microstructure, Properties, and Materials*, McGraw-Hill, New York, USA, 2006.

[2] K. H. Younis, "Restrained shrinkage behaviour of concrete with recycled materials," Ph. D Thesis in Civil and Structural Engineering, University of Sheffield, Sheffield, UK, 2014, http://etheses.whiterose.ac.uk/id/eprint/5966.

[3] V. W. Y. Tam and C. M. Tam, *Re-use of Construction and Demolition Waste in Housing Developments*, Nova Science Publishers, New York, USA, 2008.

[4] K. H. Younis and K. Pilakoutas, "Strength prediction model and methods for improving recycled aggregate concrete," *Construction and Building Materials*, vol. 49, pp. 688–701, 2013.

[5] W. Chen, R. Jin, Y. Xu et al., "Adopting recycled aggregates as sustainable construction materials: a review of the scientific literature," *Construction and Building Materials*, vol. 218, pp. 483–496, 2019.

[6] N. Kisku, H. Joshi, M. Ansari, S. K. Panda, S. Nayak, and S. C. Dutta, "A critical review and assessment for usage of recycled aggregate as sustainable construction material," *Construction and Building Materials*, vol. 131, pp. 721–740, 2017.

[7] T. Xie, A. Gholampour, and T. Ozbakkaloglu, "Toward the development of sustainable concretes with recycled concrete aggregates: comprehensive review of studies on mechanical properties," *Journal of Materials in Civil Engineering*, vol. 30, no. 9.

[8] K. H. Younis and S. M. Mustafa, "Feasibility of using nanoparticles of SiO2 to improve the performance of recycled aggregate concrete," *Advances in Materials Science and Engineering*, vol. 2018, Article ID 1512830, 11 pages, 2018.

[9] V. W. Y. Tam, C. M. Tam, and K. N. Le, "Removal of cement mortar remains from recycled aggregate using pre-soaking approaches," *Resources, Conservation and Recycling*, vol. 50, no. 1, pp. 82–101, 2007.

[10] V. W. Y. Tam, K. Wang, and C. M. Tam, "Assessing relationships among properties of demolished concrete, recycled aggregate and recycled aggregate concrete using regression analysis," *Journal of Hazardous Materials*, vol. 152, no. 2, pp. 703–714, 2008.

[11] M. Gomes and J. de Brito, "Structural concrete with incorporation of coarse recycled concrete and ceramic aggregates: durability performance," *Materials and Structures*, vol. 42, no. 5, pp. 663–675, 2009.

[12] V. W. Y. Tam and C. M. Tam, "Parameters for assessing recycled aggregate and their correlation," *Waste Management and Research*, vol. 27, no. 1, pp. 52–58, 2009.

[13] A. Katz, "Treatments for the improvement of recycled aggregate," *Journal of Materials in Civil Engineering*, vol. 16, no. 6, pp. 597–603, 2004.

[14] V. W. Y. Tam and C. M. Tam, "Diversifying two-stage mixing approach (TSMA) for recycled aggregate concrete: TSMAs and TSMAsc," *Construction and Building Materials*, vol. 22, no. 10, pp. 2068–2077, 2008.

[15] H. Y. Khaleel and M. M. Shelan, "Application of nano materials to enhance mechanical performance and microstructure of recycled aggregate concrete," in *Proceedings of the 4th International Engineering Conference on Developments in Civil and Computer Applications IEC2018*, Erbil Ploytechnic University and Ishik University: Erbil-Iraq, February 2018.

[16] K. H. Younis, F. F. Jirjis, G. J. Khoshnaw, and H. Brham, "Experimental study on performance of recycled Aggregate Concrete: effect of reactive microfillers," *International Journal of Civil Engineering and Technology*, vol. 10, no. 1, pp. 2566–2576, 2019.

[17] S. C. Kou, C. S. Poon, and D. Chan, "Influence of fly ash as a cement addition on the hardened properties of recycled aggregate concrete," *Materials and Structures*, vol. 41, no. 7, pp. 1191–1201, 2008.

[18] S.-C. Kou, C.-S. Poon, and F. Agrela, "Comparisons of natural and recycled aggregate concretes prepared with the addition of different mineral admixtures," *Cement and Concrete Composites*, vol. 33, no. 8, pp. 788–795, 2011.

[19] M. L. Berndt, "Properties of sustainable concrete containing fly ash, slag and recycled concrete aggregate," *Construction and Building Materials*, vol. 23, no. 7, pp. 2606–2613, 2009.

[20] R. Siddique and J. Klaus, "Influence of metakaolin on the properties of mortar and concrete: a review," *Applied Clay Science*, vol. 43, no. 3-4, pp. 392–400, 2009.

[21] P. Duan, Z. Shui, W. Chen, and C. Shen, "Effects of metakaolin, silica fume and slag on pore structure, interfacial transition zone and compressive strength of concrete," *Construction and Building Materials*, vol. 44, pp. 1–6, 2013.

[22] M. Antoni, J. Rossen, F. Martirena, and K. Scrivener, "Cement substitution by a combination of metakaolin and limestone," *Cement and Concrete Research*, vol. 42, no. 12, pp. 1579–1589, 2012.

[23] E. Guneyisi, M. Gesoglu, S. Karaoğlu, and K. Mermerdaş, "Strength, permeability and shrinkage cracking of silica fume and metakaolin concretes," *Construction and Building Materials*, vol. 34, no. 0, pp. 120–130, 2012.

[24] R. Muduli and B. B. Mukharjee, "Effect of incorporation of metakaolin and recycled coarse aggregate on properties of concrete," *Journal of Cleaner Production*, vol. 209, pp. 398–414, 2019.

[25] K. Kapoor, S. P. Singh, and B. Singh, "Permeability of self-compacting concrete made with recycled concrete aggregates and metakaolin," *Journal of Sustainable Cement-Based Materials*, vol. 6, no. 5, pp. 293–313, 2018.

[26] N. Singh and S. P. Singh, "Carbonation and electrical resistance of self compacting concrete made with recycled concrete aggregates and metakaolin," *Construction and Building Materials*, vol. 121, pp. 400–409, 2016.

[27] BS EN 12350-2, *Testing Fresh Concrete – Part 2: Slump Test*, British Standards Institution, London, UK, 2009.

[28] BS EN 12390-3:2009, *Testing Hardened Concrete Part 3: Compressive Strength of Test Specimens*, British Standards Institution, London, UK, 2009.

[29] BS. EN. 12390:6-2009, *Testing Hardened Concrete Part 6: Splitting Tensile Strength of Test Specimens*, British Standard Institution, London, UK, 2009.

[30] BS EN 12390-5:2009, *Testing Hardened Concrete Part 5: Flexural Strength of Test Specimens*, British Standards Institution, London, UK, 2009.

[31] ASTM C642-13, *Standard Test Method for Density, Absorption, and Voids in Hardened Concrete. 2103*, American Standards for Testing and Materials, ASTM ASTM International, West Conshohocken, PA, USA, 2013.

[32] J. Li, H. Xiao, and Y. Zhou, "Influence of coating recycled aggregate surface with pozzolanic powder on properties of recycled aggregate concrete," *Construction and Building Materials*, vol. 23, no. 3, pp. 1287–1291, 2009.

[33] M. Nehdi, S. Mindess, and P.-C. Aıitcin, "Rheology of high-performance concrete: effect of ultrafine particles," *Cement and Concrete Research*, vol. 28, no. 5, pp. 687–697, 1998.

[34] W. Li, C. Long, V. W. Y. Tam, C.-S. Poon, and W. Hui Duan, "Effects of nano-particles on failure process and microstructural properties of recycled aggregate concrete," *Construction and Building Materials*, vol. 142, no. Supplement C, pp. 42–50, 2017.

[35] V. W. Y. Tam, X. F. Gao, and C. M. Tam, "Microstructural analysis of recycled aggregate concrete produced from two-stage mixing approach," *Cement and Concrete Research*, vol. 35, no. 6, pp. 1195–1203, 2005.

[36] H. Moosberg-Bustnes, B. Lagerblad, and E. Forssberg, "The function of fillers in concrete," *Materials and Structures*, vol. 37, no. 2, pp. 74–81, 2004.

[37] ACI 231r-10, *Report On Early-Age Cracking: Causes, Measurement, And Mitigation, In ACI Committee 231*, American Concrete Institute, Farmington Hills, U.S.A, 2010.

[38] BS 8500-2, *Concrete Complementary British Standard to BS EN 206 Part 1 -Part 2: Specification for Constituent Materials and Concrete,* British Standard Institiution, London, UK, 2006.

[39] BS EN 1992-1-1:2004, *Eurocode 2: Design of Concrete Structures — Part 1-1: General Rules and Rules for Buildings*, British Standard Institution, London, UK, 2004.

Hindawi
Advances in Materials Science and Engineering
Volume 2020, Article ID 8874191, 16 pages
https://doi.org/10.1155/2020/8874191

Research Article

Experimental Study on Dynamic Mechanical Properties of Coal Gangue Concrete

Zhishu Yao, Yu Fang, Weihao Kong, Xianwen Huang, and Xuesong Wang

School of Civil Engineering and Architecture, Anhui University of Science and Technology, Huainan, Anhui, China

Correspondence should be addressed to Zhishu Yao; zsyao@aust.edu.cn

Received 3 September 2020; Revised 7 November 2020; Accepted 11 November 2020; Published 23 November 2020

Academic Editor: J. M. P. Q. Delgado

In order to study the static and dynamic mechanical characteristics of the coal gangue concrete used in the mine support structure, the compressive strength test, the drop weight impact test, and the Split Hopkinson Pressure Bar (SHPB) test were conducted. The compressive strength, initial and final impacting energy, dynamic strength, and failure characteristic of concrete were obtained of the concrete single-doped with coal gangue coarse aggregate, single-doped with coal gangue fine aggregate, and codoped with coal gangue coarse and fine aggregates. The results show that (1) it is feasible that employing coal gangue to replace natural coarse and fine aggregates in concrete can prepare C30 and C40 concrete; (2) the addition of coal gangue fine aggregate has a positive effect on the impact energy of the initial and final cracks of concrete, while the addition of coal gangue coarse aggregate has a negative effect on it; (3) compared with the static strength, the dynamic strength of concrete is improved no matter whether coal gangue is added to concrete; (4) the incorporation of coal gangue coarse aggregate will make the concrete shear surface smooth; (5) at the given impacting pressure, the concrete with coal gangue coarse aggregate has greater particle breakage and those with coal gangue fine aggregate has less. The research of this study can be a reference for the application of gangue concrete in mine support structures.

1. Introduction

In recent years, the concept of sustainable development and ecological environmental protection has become deeply rooted in the hearts of people, and various countries have begun to attach importance to the protection of the natural environment and ecological balance [1–3]. In China, in order to protect the natural environment, many areas have implemented prohibit hillside mining prohibitions, which can result in problems for the supply of concrete aggregate for mine support near mountainous areas. In order to solve the concrete aggregate supply problem for mine support structures, scholars have tried to use coal gangue produced in the process of coal mining as concrete aggregate [4–7]. Coal gangue is the solid waste with the largest amount of emission in the process of coal mining. It is generally treated by way of placement in a storage yard, which takes up space in the storage yard, pollutes the environment, and affects the green development of the coal industry [8–10]. Using wasted coal gangue as concrete aggregate can reduce the environmental pollution caused by coal gangue stacking and protect the environment; further, it can reduce the demand for natural sand and rocks, as well as saving resources, which is an effective way to turn waste into high-value materials. Therefore, this research proposes having coal gangue directly crushed and screened under a mine as the construction technology to be used for coal gangue concrete preparation. This method not only solves the environmental problems caused by coal gangue but also addresses the concrete aggregate supply problem, giving it a good application prospect [9, 11, 12].

Compressive strength is part of the basic mechanical indexes of concrete, and it is also the judgment standard for concrete whether available for engineering application [13, 14]. Zhang et al. [5] studied the compressive strength of concrete with coal gangue and concluded that the compressive strength and splitting tensile strength might reduce when the coal gangue was mixed in the concrete and the reducing amplitude increased with the increase of mixing ratio. After that, for considering the working situation of concrete bearing cyclic loading, Li et al. [15] studied the compressive strength of concrete mixed with coal gangue

under cyclic loading and obtained, that, at the given cyclic loading, the concrete with coal gangue has worse compressive strength than those without coal gangue. This result was explained by the accumulation of damage characteristics and the low strength of coal gangue. For supporting engineering of concrete with coal gangue corroded by acid solution, a series of concrete tests were conducted by Li et al. [3] and concluded that, in premise of low concrete strength requirements (less than 10 MPa), it is completely feasible to use coal gangue to replace the concrete coarse aggregate in acid solution. Then, for improving the compressive strength of concrete with coal gangue with high strength requirements, Ma et al. [11, 16] try to incorporate the appropriate alkali activator in coal gangue concrete. The experimental results demonstrate that the addition of an appropriate alkali activator can improve the compressive strength of coal gangue concrete. A large number of studies show that the direct addition of coal gangue in concrete is tended to reduce the compressive strength. Hence, it is essential to measure the compressive strength of coal gangue concrete and check the strength requirements before engineering application.

In coal mine support structures, except for the static pressure generated by the rock [17–19], the concrete is often subjected to dynamic load caused by construction and stope. However, fewer studies were conducted on the dynamic characteristic of concrete, especially in the concrete of coal gangue. Hence, for supporting coal mine supporting engineering, it is necessary to study the dynamic properties of concrete with coal gangue [20–22]. For measuring the dynamic properties of concrete, the drop weight impact test [23] and the SHPB (Split Hopkinson Pressure Bar) impact test [24] are proposed in recent years. The results of the drop weight impact test can better present the impact damage energy of the specimen [25]. Abid et al. [26, 27] studied the impact failure characteristics of fiber-reinforced concrete by this method and analyzed the failure characteristic of concrete under impact loading. Through SHPB tests, the dynamic stress-strain relationship of concrete can be obtained [28]. By this method, Lee et al. [24] studied the dynamic stress-strain relationship of concrete and put forward a prediction model of concrete dynamic strength. At present, there is no relevant studies on the dynamic properties of concrete with coal gangue, which limits the promotion and application of coal gangue concrete.

Based on the above analysis, for supporting a coal mine supporting engineering in Huainan, China, the static and dynamic mechanical properties of coal gangue concrete were studied. In this paper, the compressive strength, initial and final impacting energy, dynamic strength, and failure characteristic of concrete were obtained of single-doping coal gangue coarse aggregate, single-doping coal gangue fine aggregate, and codoping coal gangue coarse and fine aggregates. The obtained results may be used for supporting the coal mine engineering.

2. Materials and Solutions

2.1. Test Materials. The cementitious materials used in the test were P.C32.5 and P.O42.5 Portland cement. The natural coarse aggregate was limestone macadam with continuous gradation, and the particle size range was 4.75–20 mm. Natural fine aggregate was Huaihe River sand with a fineness modulus of 2.628. The water-reducing agent was PCA-1 polycarboxylic high-performance water-reducing agent, which is transparent and colorless, and the water-reducing rate was 25–35%. The coal gangue used in this experiment was taken from the undisturbed coal gangue of the Dingji Coal Mine in Huainan. After being crushed by a crusher and sieved by a square-hole screen, fine aggregate with a particle size of 0.15–4.75 mm and coarse aggregate of continuous grading test of 4.75–20 mm were obtained. The fineness modulus of the coal gangue fine aggregate was 2.830. The rock strength test results and the chemical composition of the coal gangue samples are shown in Tables 1 and 2, respectively.

It can be seen from Table 2 that, in the chemical composition of coal gangue, the mass fractions of SiO_2 and Al_2O_3 accounted for a large proportion: 50.86% and 12.37%, respectively. According to the classification relationship between the chemical composition of coal gangue and rock type, it was preliminarily determined that the coal gangue belonged to sandstone gangue. Compared with the seven indicators of coal gangue resource utilization (coal gangue type, rock type, fixed carbon content (FC_{ad}), total sulfur content ($S_{,d}$), Al_2O_3/SiO_2 ratio, Fe_2O_3 content, and $CaO + MgO$ content), the chemical composition of the coal gangue met the requirements for coarse and fine aggregates of cement concrete [3, 4, 6] (Figures 1 and 2).

2.2. Mixture Proportion and Specimen Preparation. According to the Specification for Mix Proportion Design of Ordinary Concrete (JGJ55-2019) [29], the benchmark mix design of concrete is shown in Table 3.

On the basis of C30 and C40 benchmark concrete mix proportions, coal gangue concrete was prepared by single-doped and codoped gangue coarse and fine coal gangue aggregate. Based on the pretest results and existing relevant research [7, 30], the replacement rates of coarse and fine aggregates of coal gangue were set at 100% and 30%, respectively. The test scheme is shown in Table 4.

For each ratio, 18 pieces of $100 \times 100 \times 100$ mm cube specimens and 20 pieces of $\Phi 70 \times 35$ mm cylindrical specimens were made to measure the compressive strength, falling weight impact performance, and SHPB impact performance of concrete. After pouring the test block, it was allowed to stand at room temperature for 24 h and then was removed from the mold. After numbering, it was placed into a curing box at a temperature of $20 \pm 2^{\circ}C$ and humidity of 97% for standard curing.

2.3. Test Methods

2.3.1. Experimental Study on Compressive Strength of Coal Gangue Concrete. The compressive strength of concrete was tested according to "The Standard for Test Methods of Mechanical Properties of Ordinary Concrete" (GB/T50081-2019) [31]. In this test, cube specimens with a size of

Table 1: Uniaxial compressive strength of noncombustible coal gangue.

Coal gangue sample	#1	#2	#3
Average rock strength (MPa)	57.64	60.31	65.26

Table 2: Main chemical constituents of coal gangue.

Chemical composition	Loss	SiO_2	Fe_2O_3	Al_2O_3	CaO	f-CaO	MgO	SO_3	$\sum$
Gangue (%)	17.31	50.86	6.3	12.37	7.43	0	3.81	0.13	98.21

Figure 1: Undisturbed coal gangue.

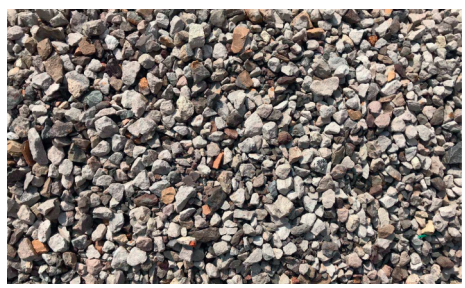

Figure 2: Coal gangue coarse aggregate.

Table 3: Test reference mix ratio.

Group	Natural coarse aggregate (kg/m^3)	Natural fine aggregate (kg/m^3)	Cement (kg/m^3)	Water (kg/m^3)	W/C
C30	1117.9	685.1	350	147	0.42
C40	1118.2	656.8	380	144	0.38

Table 4: Test scheme.

Group	Number	Coarse gangue coarse aggregate	Coal gangue fine aggregate	Natural coarse aggregate	Natural fine aggregate (%)
C30	NAC	0	0	100%	100
	N-SFC	0	30%	100%	70
	N-SAC	100%	0	0	100
	N-SC	100%	30%	0	70
C40	NAC	0	0	100%	100
	N-SFC	0	30%	100%	70
	N-SAC	100%	0	0	100
	N-SC	100%	30%	0	70

$100 \times 100 \times 100$ mm were used, and each group was poured with 3 pieces. The test results were averaged and multiplied by a conversion factor of 0.95. A WAW-1000C microcomputer-controlled electrohydraulic servo universal testing machine was used for the test. The loading speed was set at 0.5 MPa/s. The test device is shown in Figure 3.

2.3.2. Drop Weight Impact Test of Coal Gangue Concrete. As shown in Figure 4, according to the concrete drop impact test method recommended by the American Concrete Association [26], the impact resistance of the specimens was measured by using a self-made drop weight impact test device. The support of the drop weight impact

Figure 3: Compressive strength test equipment.

Figure 4: Drop weight impact test instrument.

test device was a horizontal rigid plate. A steel vertical cylinder was set in the test. The drop weight was lifted to the groove position set at the top of the vertical cylinder. Because the diameter of the cylinder was slightly larger than the diameter of the falling hammer, the lifting height of the falling weight could be accurately controlled. In addition, the center of the groove, the steel strand on the pulley, and the center of the test piece were connected to the three lines and were perpendicular to the upper surface of the test piece, thus ensuring that the drop point of the hammer did not deviate from the center of the test piece during the test. The drop weight smashed a force-transmitting steel ball (diameter: 63.5 mm) from a certain height freely to the center of the test piece and then transmitted the impact energy to the test piece. This cycle was repeated, and the number of initial cracking impacts ($N1$) and complete damage impacts ($N2$) of the 8 test pieces was recorded. By comparing the impact times of different specimens at the same height and calculating the impact energy consumption of each group of concrete according to the relevant formula, the impact resistance of the concrete was evaluated. The drop weight impact test device included a drop weight, a force-transmitting steel ball, a vertical pipe, a fixed baffle, a pair of pulleys, a steel vertical cylinder, and a rigid support; further, a nonelastic and smooth steel strand was used as the traction line of the pulley.

After the experiment, the initial crack energy and failure energy of each group of concrete were calculated according to the following formula:

$$W = N \cdot mgh, \tag{1}$$

where W stands for the impact energy, N stands for the impact times corresponding to initial cracking or complete failure, m stands for the weight of the drop weight (4.5 kg), g stands for the acceleration of gravity (9.8 N/kg), and h stands for the impact height of the drop hammer (457 mm).

2.3.3. SHPB Impact Test of Coal Gangue Concrete. The dynamic impact test of SHPB was carried out with a Φ75 mm Split Hopkinson Pressure Bar at the Impact Dynamics Laboratory of Anhui University of Science and Technology. The SHPB test device was mainly composed of an impact rod, an incident rod, a transmission rod, and an absorption rod. The data acquisition system was mainly composed of a strain gauge, a velocity measuring device, a dynamic strain gauge, waveform storage, and a software processing system [28, 32, 33]. The impact bar, incident rod, transmission rod, and absorption rod were all steel compression rods with a density of 7850 kg/m^3, an elastic modulus of 210 GPa, and a longitudinal wave impedance of 5190 m/s. Figures 5(a) and 5(b) show the SHPB test device and the gas pressure control and data acquisition system, respectively.

In order to satisfy the assumption of one-dimensional stress wave and stress-strain uniformity, the following measures were taken during the SHPB test:

(1) A cylinder specimen with a diameter of 35 mm and a length diameter ratio of 0.5 was used (as shown in Figure 6(a)).

(2) The sample was ground to ensure that the surface unevenness of the sample was controlled within 0.05 mm, and the unevenness of both ends was controlled within 0.03 mm (as shown in Figure 6(b)).

(3) A certain thickness of ultralight clay was adsorbed at the front end of the incident rod (as shown in Figure 6(c)).

(4) Before the experiment, it was ensured that the specimen and the compression bar were coaxial, and in order to reduce the friction between the specimen and the pressure bar, vaseline was applied on both ends of the sample.

The specific test process mainly included the following steps:

(a) (b)

Figure 5: The SHPB experimental equipment. (a) SHPB test device. (b) Gas pressure control and data acquisition system.

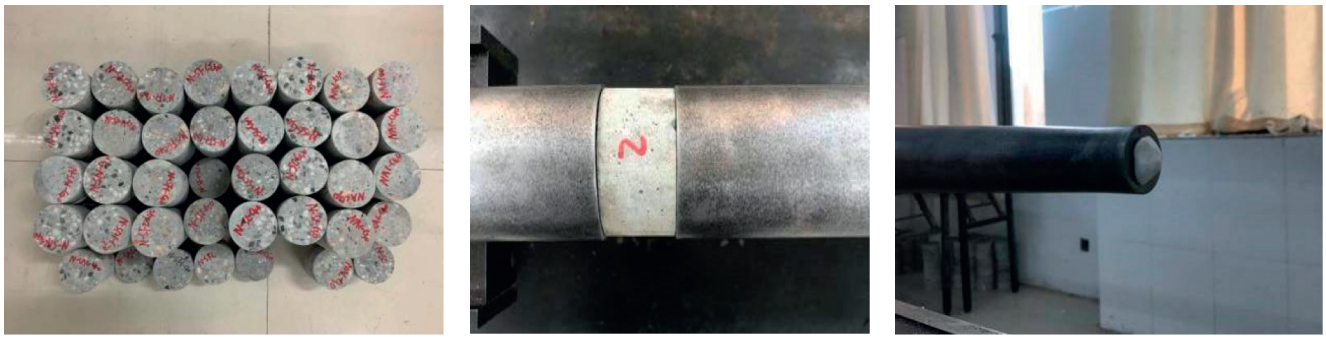

(a) (b) (c)

Figure 6: SHPB test specimen. (a) Specimen. (b) Specimen installation. (c) Superlight clay as shaper.

(1) Experiment preparation: before the experiment, we checked whether the SHPB experiment device and all equipment of the whole system were in normal operation. The positions of the impact bar, incident bar, and transmission rod were adjusted to ensure that the central axis of the three rods coincided. The instrument was tested to adjust the parameter values, and then the trigger voltage, bridge voltage, gain, and other parameters were set.

(2) Specimen installation: in order to reduce the friction between the specimen and the pressure bar, vaseline was applied on the end faces of the test piece and the pressure bar, and then the specimen was pressed so that it was firmly clamped between the incident rod and the transmission rod. Next, the specimen was wrapped with a towel to prevent fragments from flying away. Finally, the ultralight clay was bonded to the front end of the incident rod.

(3) Formal experiment: the inflation switch was started, the acquisition switch was turned on, and when it rose to the set gas pressure, the impact rod was activated and the impact test was carried out.

(4) The data were saved and the specimen damage was recorded.

3. Experimental Results and Discussion

3.1. Compressive Strength of Coal Gangue Concrete. The failure cross section and compressive strength test results of coal gangue concrete are shown in Figure 7.

As shown in Figure 7, comparing the failure modes of each group of concrete test blocks, it was found that the failure modes of coal gangue concrete and ordinary concrete were similar. After the failure of each group of specimens, they all appeared as "reversely connected quadrangular pyramids," but each exhibited different failure characteristics. For the N-SFC group, it was the destruction of the cement mortar and the interface between some natural coarse aggregates and cement mortar. The natural aggregate in the concrete was relatively complete, and the fractured section was uneven. The combination of coarse aggregate and cement mortar was one of a "weak" mortar wrapped around a "strong" aggregate. For the N-SAC and N-SC groups, not only were there cement mortar damage and separation failure between the coal gangue coarse aggregate and the mortar, but also the coal gangue coarse aggregate itself was broken, so the damaged section was relatively flat. The combination of gangue coarse aggregate and cement mortar was a "strong" mortar wrapped around a "weak" aggregate.

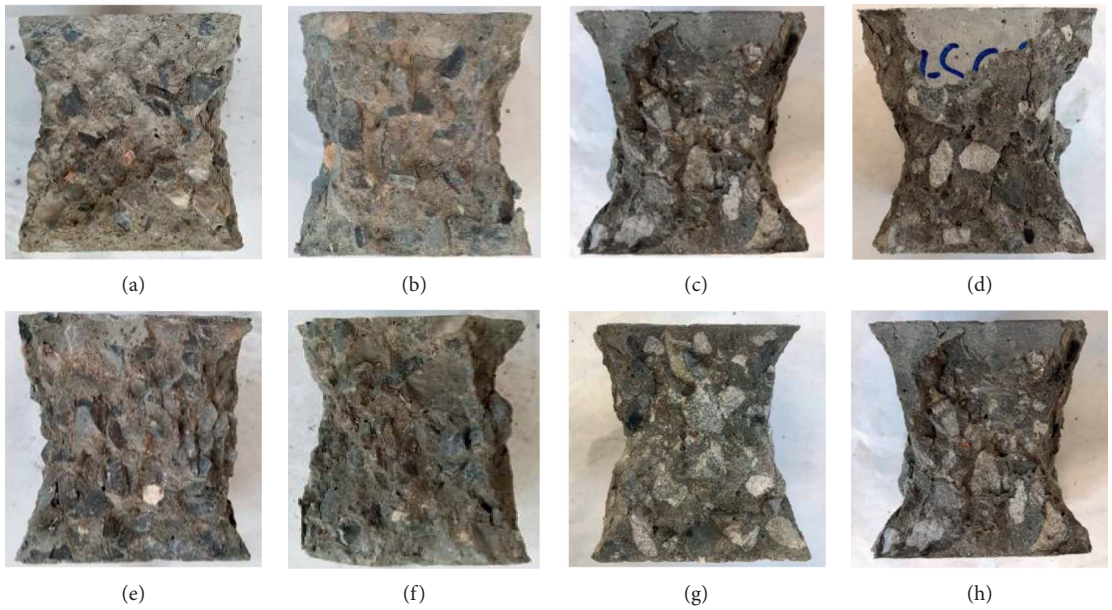

Figure 7: Concrete failure section. (a) NAC-C30. (b) N-SFC-C30. (c) N-SAC-C30. (d) N-SC-C30. (e) NAC-C40. (f) N-SFC-C40. (g) N-SAC-C40. (h) N-SC-C40.

Comparing the compressive strengths of N-SFC, N-SAC, N-SC, and NAC under the two preparation strengths in Table 5, it was found that the 3-day strengths all reached more than 50% of the 28-day strength, the 7-day strengths all reached more than 70% of the 28-day strength, the 28-day strengths all reached the design strength requirements, the 60-day strength increased by 5–10% compared with the 28-day strength, and the 90-day intensity was 10–18% higher than the 28-day intensity. This shows that the compressive strength of coal gangue concrete with age is basically the same as that of ordinary concrete under the same design strength. The ultimate compressive strength of coal gangue concrete increases with age, but the growth rate becomes increasingly slower.

Comparing the measured strength and preparation strength of the doped coal gangue concrete in Table 5, under the C30 preparation strength, it was found that the 28-day strength of the concrete doped with coal gangue was greater than 38.23 MPa [29], which meets the requirements of the concrete preparation strength. Under the C40 preparation strength, the 28-day strength of the concrete single-doped with coal gangue was greater than 48.23 MPa [29], which meets the requirements of concrete preparation strength. Therefore, it can be concluded that the use of coal gangue to replace natural coarse and fine aggregates in concrete can work to completely prepare C30 and C40 concrete that meets the requirements and realizes the resource utilization of coal gangue.

Figure 8 shows the destruction surface of different groups at C30 preparation strength, and greater difference appeared at the destruction surface. For the NAC and N-SFC, it was observed that the destruction surface is rough. And for the N-SAC and N-SC, the destruction surface is smooth, especially for the N-SAC. The difference in the destruction surface can be explained by the lower strength of coal gangue and the better "gangue-cement" contacting surface. In the traditional concrete analysis, the strength characteristic of the internal structure of concrete in descending order is coarse aggregate, mortar, and contacting surface between coarse aggregate and mortar. When the coal gangue was used to replace the fine aggregate, the lower strength of the coal gangue will not change the strength characteristic of the internal structure of concrete. While the strength characteristics of each component in concrete may change when the concrete is single-doped with coarse aggregate or codoped with coal gangue coarse and fine aggregate, which shows that the strength of the bearing skeleton (coarse aggregate) decreases and the contact surface (contact surface between coarse aggregate and mortar) increases, which will lead to the shear surface of concrete not develop along the interface between aggregate and mortar, but along the interior of coal gangue. Therefore, the shear plane of concrete is relatively flat, especially when the coarse aggregate of concrete is coal gangue.

3.2. Impact Resistance of Coal Gangue Concrete. The drop weight impact test results of coal gangue concrete are shown in Figures 8–10.

It can be seen from Figures 9 and 10 that the failure morphology of the N-SFC, N-SAC, and N-SC specimens under the impact load under the two preparation strengths is similar to that of ordinary concrete NAC. The phenomenon of "destruction once cracked" occurred, showing obvious brittle cracking.

It can be seen from Figure 11 that the influence of single-doped and codoped coal gangue coarse and fine aggregates on the amount of concrete initial cracking and final cracking was roughly the same under different preparation strengths, and the regularity was relatively strong. With single-doped

Table 5: Compressive strength of concrete after conversion.

Group	Numbering	Compressive strength (MPa)					Compressive strength growth rate			
		3 days	7 days	28 days	60 days	90 days	3–7 days	7–28 days	28–60 days	60–90 days
C30	NAC	26.45	31.50	39.94	43.42	46.42	0.191	0.268	0.087	0.069
	N-SFC	24.34	31.08	44.67	49.10	52.94	0.277	0.437	0.099	0.078
	N-SAC	23.30	31.12	39.07	42.47	43.91	0.336	0.255	0.087	0.034
	N-SC	22.39	31.35	41.83	45.67	47.43	0.400	0.334	0.092	0.039
C40	NAC	36.14	41.87	48.62	53.04	55.92	0.159	0.161	0.091	0.053
	N-SFC	31.29	40.32	54.42	59.42	60.96	0.289	0.35	0.092	0.053
	N-SAC	29.46	41.74	47.34	50.11	52.50	0.417	0.134	0.059	0.034
	N-SC	27.89	42.00	49.79	53.65	55.69	0.506	0.185	0.078	0.038

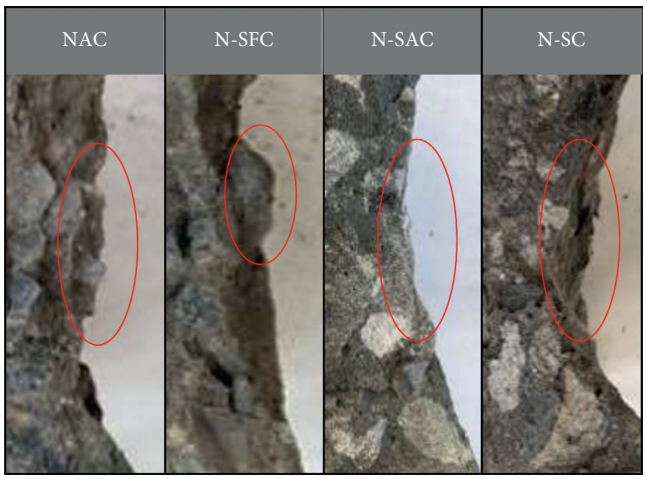

Figure 8: Destruction surface.

Figure 9: Initial cracking state of concrete. (a) NAC-C30. (b) N-SFC-C30. (c) N-SAC-C30. (d) N-SC-C30. (e) NAC-C40. (f) N-SFC-C40. (g) N-SAC-C40. (h) N-SC-C40.

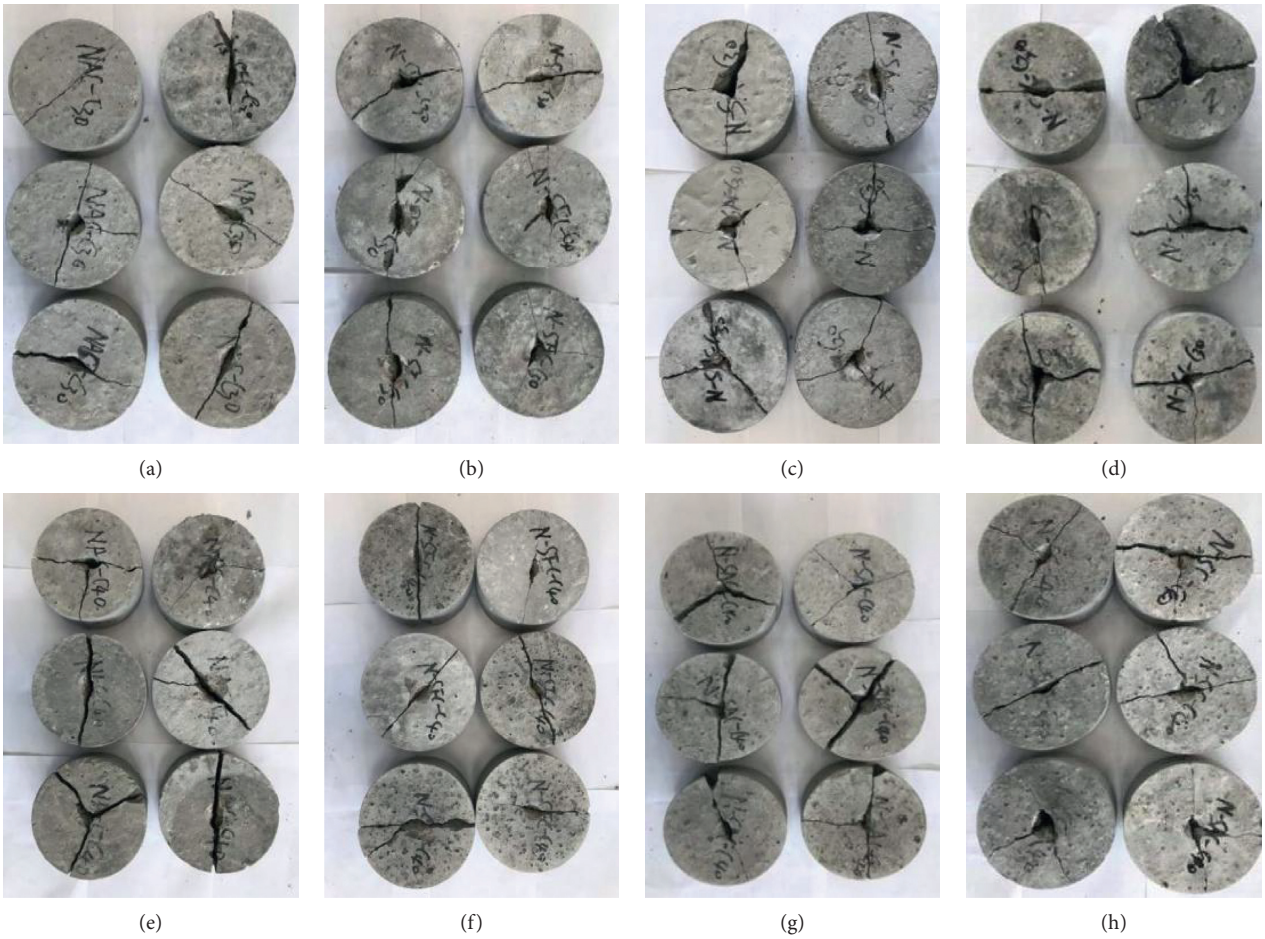

Figure 10: Final cracking state of concrete. (a) NAC-C30. (b) N-SFC-C30. (c) N-SAC-C30. (d) N-SC-C30. (e) NAC-C40. (f) N-SFC-C40. (g) N-SAC-C40. (h) N-SC-C40.

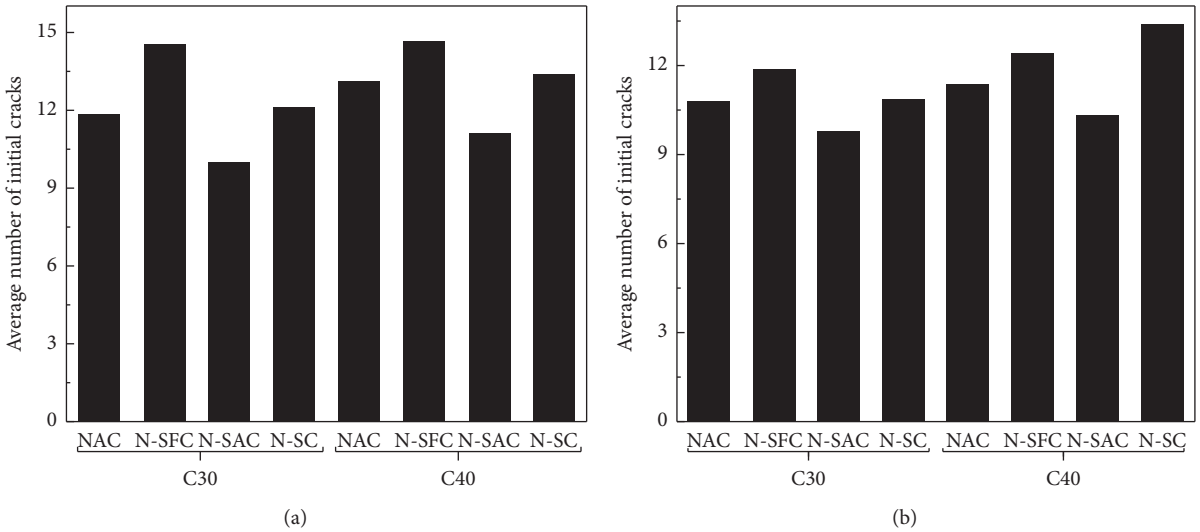

Figure 11: Comparison of impact resistance times of coal gangue concrete. (a) Initial cracking. (b) Final cracking.

coal gangue fine aggregate, the average impact resistance of the initial and final cracking of the two kinds of preparation strengths for coal gangue fine aggregate concrete was greater than that of ordinary concrete. With single-doped coal gangue coarse aggregate, the average impact resistance of the initial and final cracking of the two kinds of preparation

strengths for coal gangue coarse aggregate concrete was less than that of ordinary concrete. With codoped coal gangue coarse and fine aggregates, the average impact resistance of the initial cracking of the two kinds of preparation strengths for coal gangue concrete was greater than that of ordinary concrete, while the final cracking was equal to that of ordinary concrete. The results show that the single-doped coal gangue fine aggregate can increase the average impact resistance of the initial and final cracking of the concrete, and the single-doped coal gangue coarse aggregate can reduce the average impact resistance of the initial and final cracking of concrete. On the basis of doping coal gangue coarse aggregate, adding the appropriate amount of coal gangue fine aggregate can increase the impact resistance of the initial and final cracking of coal gangue concrete.

When the preparation strength was C30 and C40, the initial cracking impact energy of the concrete single-doped with coal gangue fine aggregate was 292.2 and 294.2 J, the final cracking impact energy was 239.8 and 249.9 J (the definition of final cracking impact energy is the energy from the initial cracking impact to the final crack impact), and the average failure energy was 266 and 272.1 J, respectively. Compared with ordinary concrete (the initial, final, and average cracking impact energy of C30 and C40 were 237.8, 217.7, 227.8, 264.0, 229.8, and 246.9 J, resp.), the impact energy of the initial and final cracking of N-SAC-C30 and N-SAC-C40 increased by 22.9%, 10.2%, 11.4%, and 8.7%, and the average failure energy of N-SAC-C30 and N-SAC-C40 increased by 16.8% and 10.2%, respectively.

The initial cracking impact energy of the concrete single-doped with coal gangue coarse aggregate of the C30 and C40 concrete was 201.5 and 223.7 J, the final cracking impact energy was 197.5 and 207.6 J, and the average failure energy was 199.5 and 215.7 J, respectively. Compared with ordinary concrete, the impact energy of initial and final cracking of N-SFC-C30 and N-SFC-C40 decreased by 15.2%, 9.3%, 15.4%, and 9.7%, and the average failure energy of N-SFC-C30 and N-SFC-C40 decreased by 12.4% and 12.6%, respectively.

The initial cracking impact energy of the concrete codoped with coal gangue coarse and fine aggregates was 243.9 and 270.1 J, the final cracking impact energy was 219.7 and 229.8 J, and the average failure energy was 231.8 and 250 J, respectively. Compared with ordinary concrete, the impact energy of initial cracking of C30 and C40 concrete increased by 2.6% and 2.3%, the impact energy of final cracking of C30 and C40 concrete increased by 0.9% and 0.1%, and the average failure energy of N-SC-C30 and N-SC-C40 increased by 1.7% and 1.3%, respectively. Compared with the concrete single-doped with coal gangue aggregate, the impact energy of initial and final cracking of N-SC-C30 and N-SC-C40 increased by 21%,11.1%, 20.7%, and 10.7%, and the average failure energy of N-SC-C30 and N-SC-C40 concrete increased by 16.2% and 15.9%, respectively.

Based on the above analysis, it can be found that the impact resistance of concrete single-doped with coal gangue fine aggregate is higher than the concrete single-doped with coal gangue coarse aggregate. This is related to the porous structure and low strength of coal gangue. As shown in Figure 12, by observing the SEM pictures of coal gangue and limestone flat section, it can be found that the microstructure of coal gangue is porous, while the microstructure of limestone is dense; there is a significant difference between the two. It should be noted that, in the concrete structure system, the coarse aggregate is generally used as the main bearing structure, while the fine aggregate and cementitious material are generally used as the force transmission structure. In the concrete single-doped with coal gangue fine aggregate, the coarse interface of coal gangue fine aggregate makes the cementitious material and concrete fine aggregate form a good force transmission structure. At this time, the lower strength of coal gangue has little influence on the mechanical structure of concrete, so the impact strength of concrete single-doped with coal gangue fine aggregate increases. In the concrete single-doped with coal gangue coarse aggregate, as the main bearing structure, the low strength of coal gangue weakens the mechanical structure of concrete. At this time, the good contact characteristics of coal gangue and cementitious materials have little influence on the mechanical structure of concrete, so the impact strength of concrete single-doped with coal gangue coarse aggregate decreases.

3.3. Dynamic Compressive Strength of Coal Gangue Concrete. The average dynamic compressive strengths of coal gangue concrete under different gas pressures are shown in Figure 13.

As shown in Figure 13, the dynamic compressive strength growth law of coal gangue concrete and ordinary concrete is basically the same. Compared with the static compressive strength, the dynamic compressive strength of each group of concrete specimens under the two kinds of preparation strengths has different degrees of improvement, and the dynamic compressive strength also increases with the increase of impact gas pressure. Comparing the dynamic compressive strength under 0.4, 0.5, 0.6, and 0.7 MPa gas pressure with the static compressive strength, under the design strength of C30, the ordinary concrete increased by 11.2%, 16.5%, 25.1%, and 31.3%, respectively; the concrete single-doped with coal gangue fine aggregate increased by 9.8%, 17.0%, 23.0%, and 30.4%, respectively; the concrete single-doped with coal gangue coarse aggregate increased by 10.6%, 13.5%, 22.2%, and 28.1%, respectively; and the concrete codoped with coal gangue coarse and fine aggregates increased by 9.1%, 14.7%, 21.4%, and 30.4%, respectively. Under the design strength of C40, the ordinary concrete increased by 13.5%, 21.3%, 25.5%, and 32.2%, respectively; the concrete single-doped with coal gangue fine aggregate increased by 8.3%, 13.7%, 20.5%, and 30.1%, respectively; the concrete single-doped with coal gangue coarse aggregate increased by 13.2%, 17.2%, 20.8%, and 25.8%, respectively; and the concrete codoped with coal gangue coarse and fine aggregates increased by 11.0%, 18.0%, 22.3%, and 26.1%, respectively.

Figure 14 shows the failure morphology of different types of concrete specimens under different impact pressures. Under 0.4 MPa impact gas pressure, different numbers

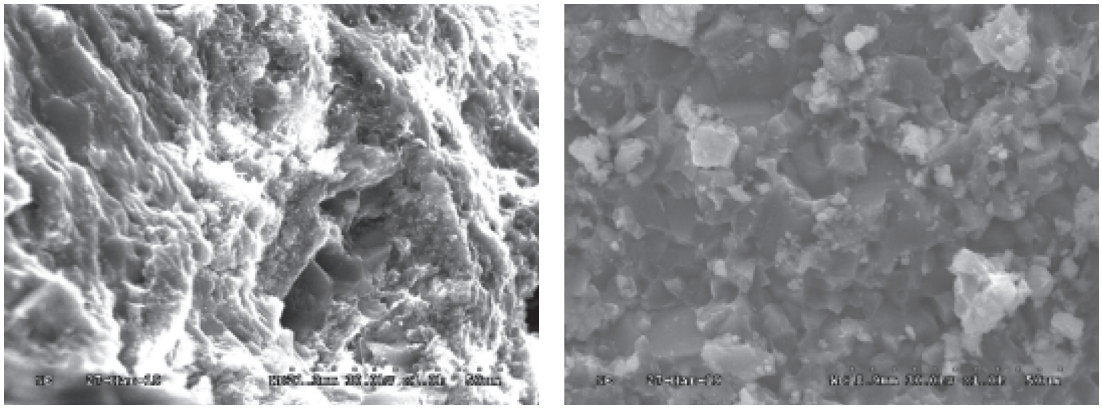

(a) (b)

Figure 12: SEM image of coal gangue and limestone. (a) Microstructure of coal gangue. (b) Microstructure of gravels.

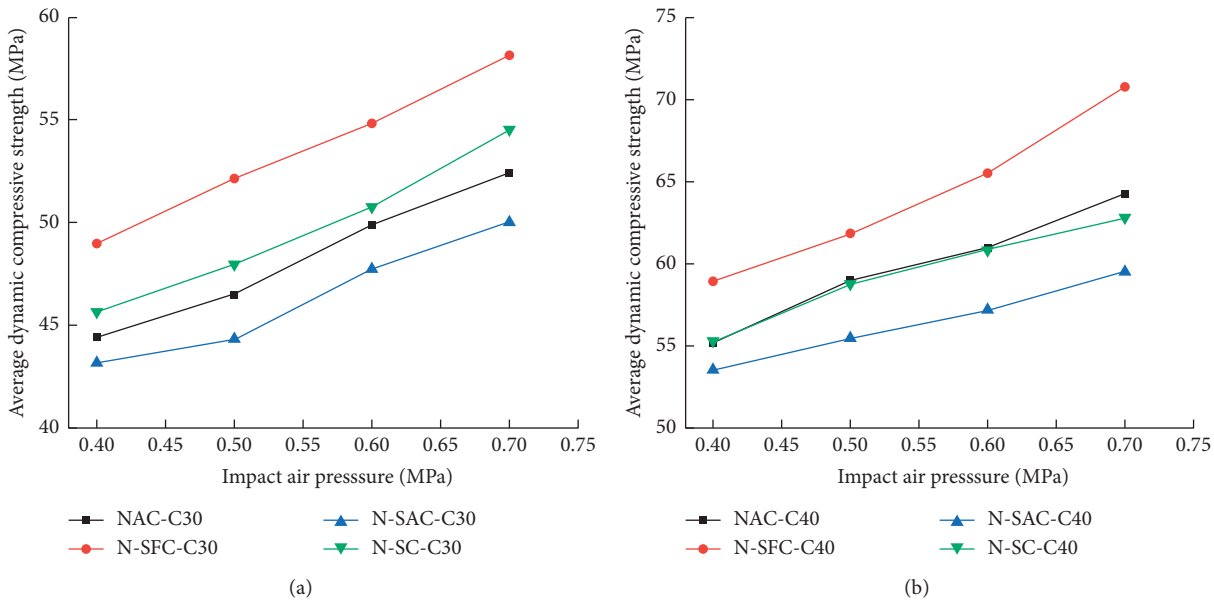

Figure 13: Coal gangue concrete destruction characteristics under different gas pressures. (a) C30 groups. (b) C40 groups.

and widths of cracks appeared on the surface of each group of specimens with two kinds of preparation strengths, and the specimens were relatively complete when they were destroyed. With the increase of impact gas pressure, the specimens became more and more broken. When the impact gas pressure was further increased to 0.7 MPa, the concrete specimens of each group were almost completely broken.

It can be seen from Figure 15 that the average particle size of the fragmentation of each group of specimens decreased with the increase of impact gas pressure. When the impact gas pressure was 0.4 MPa, each group of specimens of the two kinds of preparation strengths was relatively complete. When the impact gas pressure was 0.5 MPa, the order of the average particle size of the crushing block was N-SFC > N-SC > N-SAC > NAC when the preparation strength was C30, and the order of the average particle size of the crushing block was N-SFC > N-SC > NAC > N-SAC when the preparation strength was C40. When the impact gas pressure was 0.6 MPa, the order of the average particle size of the crushing block was N-SFC > N-SC > N-SAC > NAC when the preparation strength was C30, and the order of the average particle size of the crushing block was N-SFC > NAC > N-SC > N-SAC when the preparation strength was C40. When the impact gas pressure was 0.7 MPa, the order of the average particle size of the crushing block was N-SFC > NAC > N-SC > N-SAC when the preparation strength was C30, and the order of the average particle size of the crushing block was N-SFC > NAC > N-SC > N-SAC when the preparation strength was C40. In summary, under the impact load, the average particle size of the single-doped coal gangue fine aggregate concrete specimen was generally higher than that of ordinary concrete, and the average particle size of the single-doped coal gangue coarse aggregate concrete specimen was generally lower than that of ordinary concrete, while the average particle size of the codoped coal gangue coarse and fine

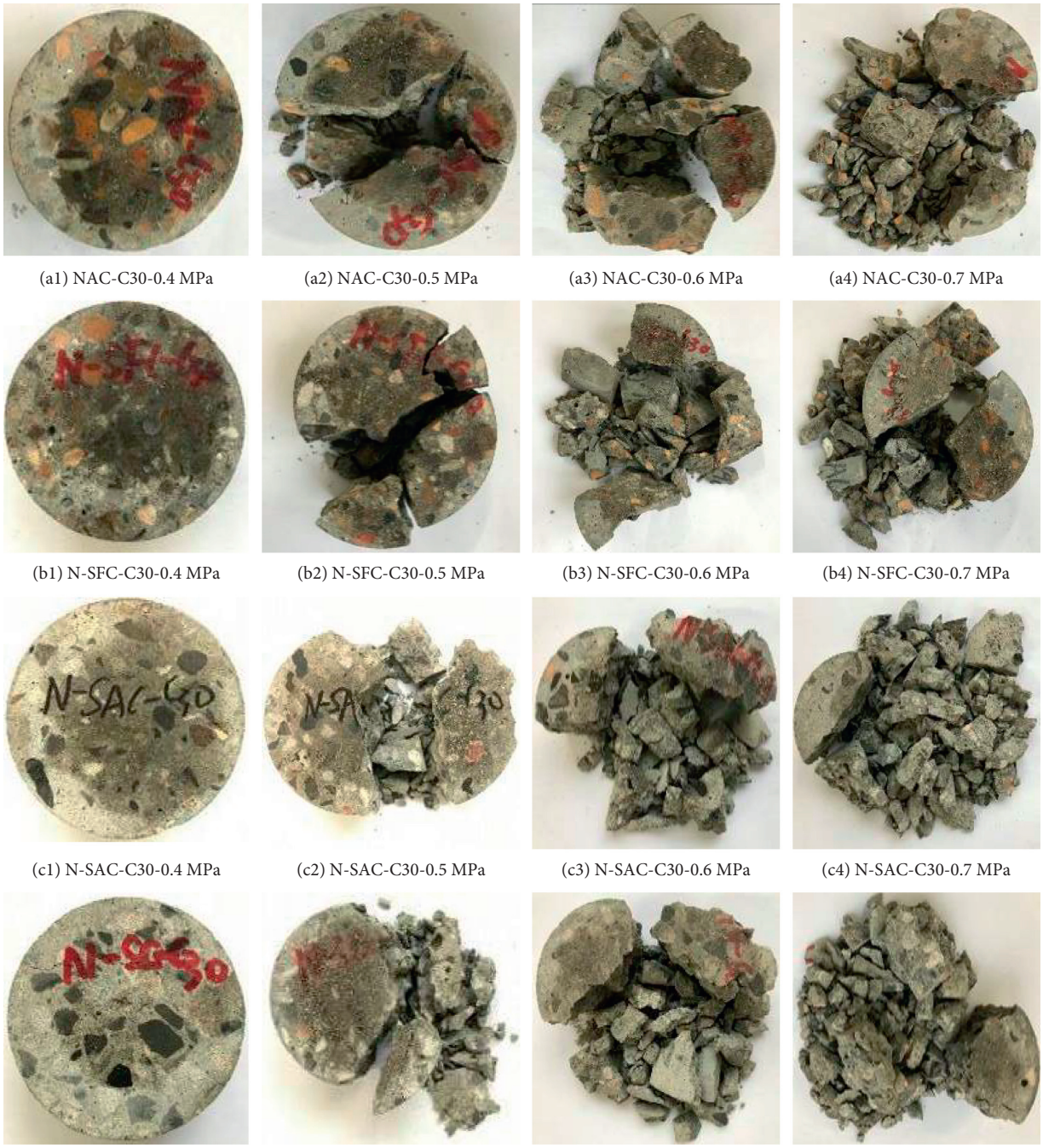

(a1) NAC-C30-0.4 MPa (a2) NAC-C30-0.5 MPa (a3) NAC-C30-0.6 MPa (a4) NAC-C30-0.7 MPa

(b1) N-SFC-C30-0.4 MPa (b2) N-SFC-C30-0.5 MPa (b3) N-SFC-C30-0.6 MPa (b4) N-SFC-C30-0.7 MPa

(c1) N-SAC-C30-0.4 MPa (c2) N-SAC-C30-0.5 MPa (c3) N-SAC-C30-0.6 MPa (c4) N-SAC-C30-0.7 MPa

(d1) N-SC-C30-0.4 MPa (d2) N-SC-C30-0.5 MPa (d3) N-SC-C30-0.6 MPa (d4) N-SC-C30-0.7 MPa

Figure 14: Continued.

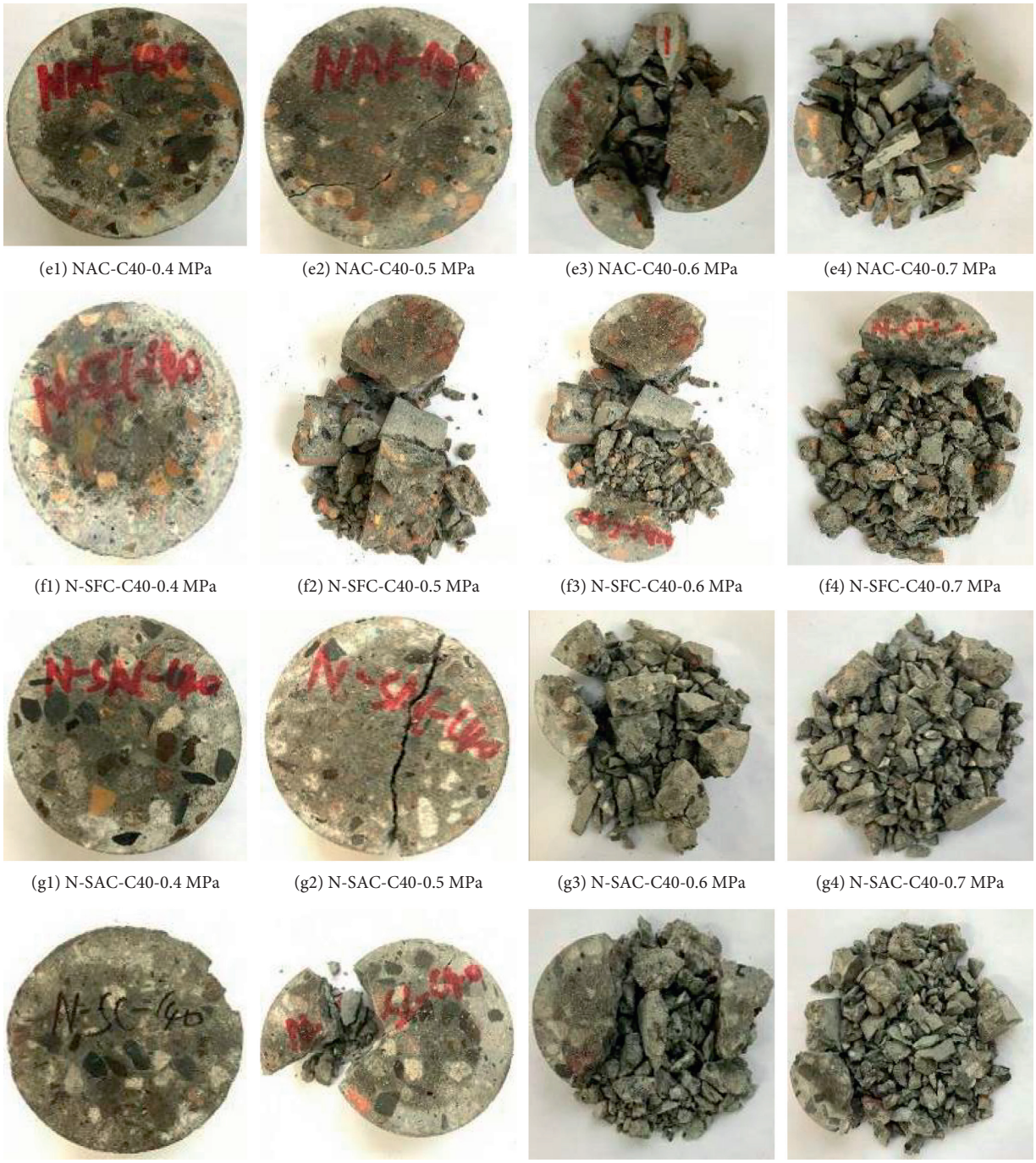

(e1) NAC-C40-0.4 MPa (e2) NAC-C40-0.5 MPa (e3) NAC-C40-0.6 MPa (e4) NAC-C40-0.7 MPa

(f1) N-SFC-C40-0.4 MPa (f2) N-SFC-C40-0.5 MPa (f3) N-SFC-C40-0.6 MPa (f4) N-SFC-C40-0.7 MPa

(g1) N-SAC-C40-0.4 MPa (g2) N-SAC-C40-0.5 MPa (g3) N-SAC-C40-0.6 MPa (g4) N-SAC-C40-0.7 MPa

(h1) N-SC-C40-0.4 MPa (h2) N-SC-C40-0.5 MPa (h3) N-SC-C40-0.6 MPa (h4) N-SC-C40-0.7 MPa

Figure 14: Impact specimen after crushing.

aggregate concrete specimen was larger than that of the single-doped coal gangue coarse aggregate concrete. The coal gangue fine aggregate can inhibit the expansion of cracks in concrete to a certain extent so that the concrete has good integrity when damaged.

Existing studies have shown that the distribution and evolution of many irregular pores, cracks, and other mesodefects in concrete materials satisfy statistically self-similar characteristics. The impact damage of concrete is a phenomenon in which these damage defects in the material are continuously generated and expanded under the action of dynamic impact load, eventually leading to the nonlinear damage of the concrete material. Therefore, the fractal theory was used to analyze the fragment size distribution of concrete after impact failure.

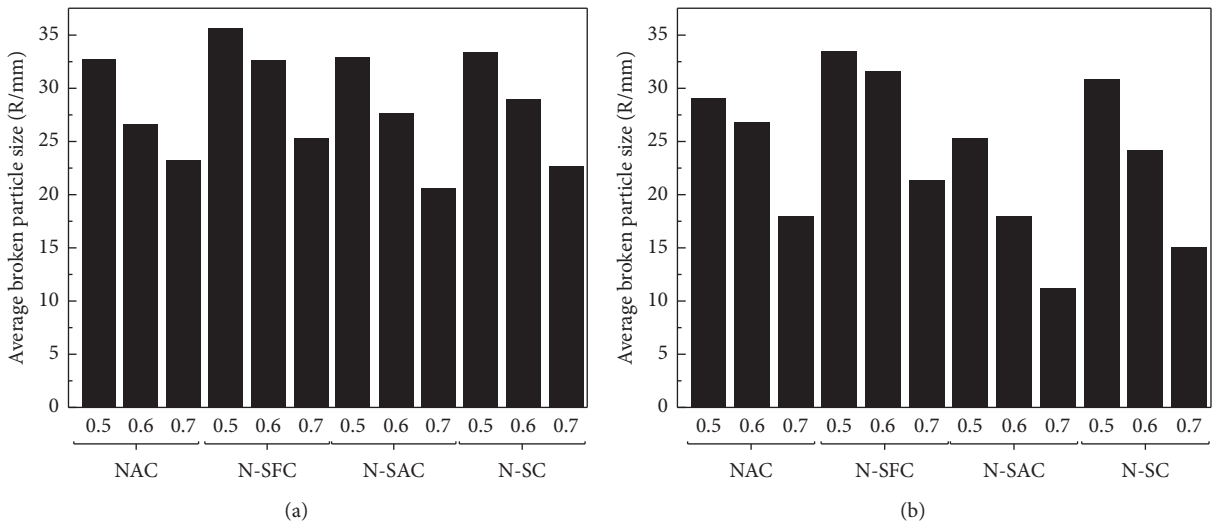

Figure 15: Average particle size after SHPB impact. (a) C30 groups. (b) C40 groups.

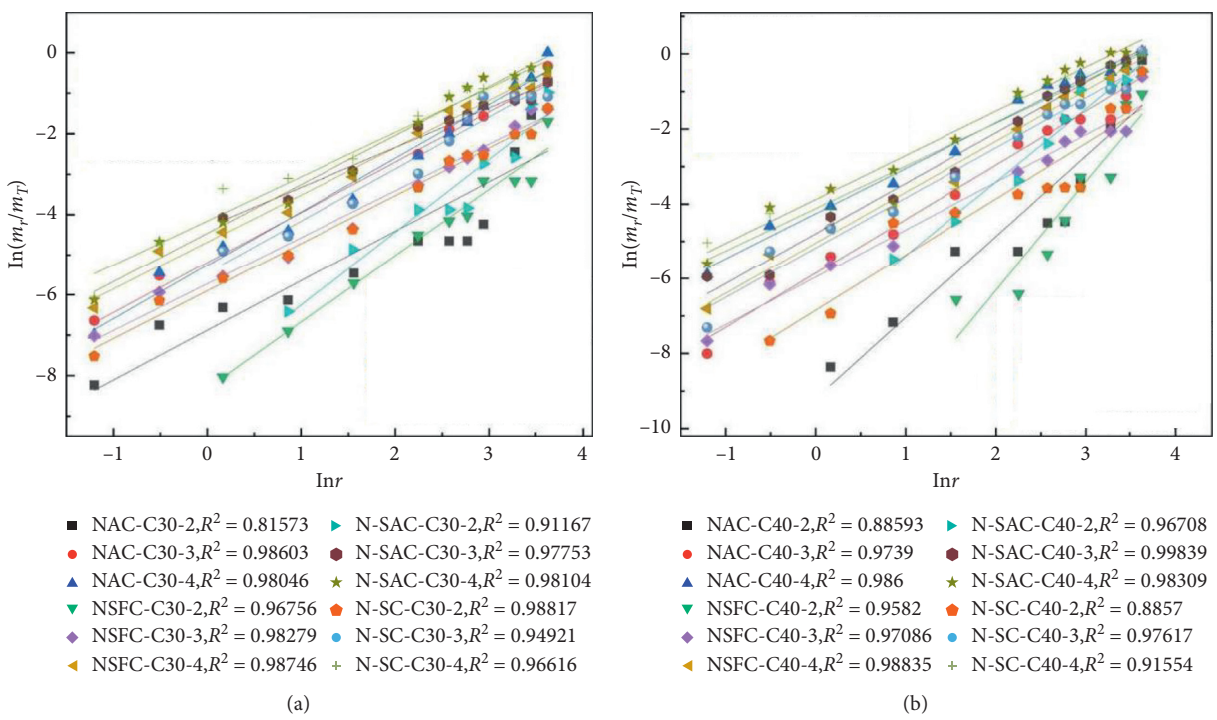

Figure 16: $\ln(m_r/m_T) - \ln r$ curves. (a) C30 configuration strength. (b) C40 configuration strength.

The calculation formula of concrete fragmentation is as follows:

$$\ln y = \ln\left(\frac{m_r}{m_T}\right) = b\ln\left(\frac{r}{r_m}\right), \tag{2}$$

where m_r stands for the cumulative mass of fragments with particle size less than r, g; m_T stands for the total amount of fragments, g; r_m stands for the maximum size of fragments, mm; r stands for the fragment size, mm; and b stands for the distribution parameter, that is, the slope of the typical $\ln(m_r/m_T) - \ln r$ relationship curve.

Figure 16 is the typical $\ln(m_r/m_T) - \ln r$ relationship curve of each group of concrete under C30 and C40 configuration strengths. It can be seen from Figure 16 that the slope of the fitting curve between coal gangue concrete and ordinary concrete gradually decreases with the increase of impact pressure when the strength is C30 and C40. According to Figure 14, it can be found that the degree of fragmentation of the test piece is gradually increasing, and the proportion of small particle size fragments continues to increase, indicating that the mass distribution of the test piece continues to move to the small particle size end with the increase of impact pressure.

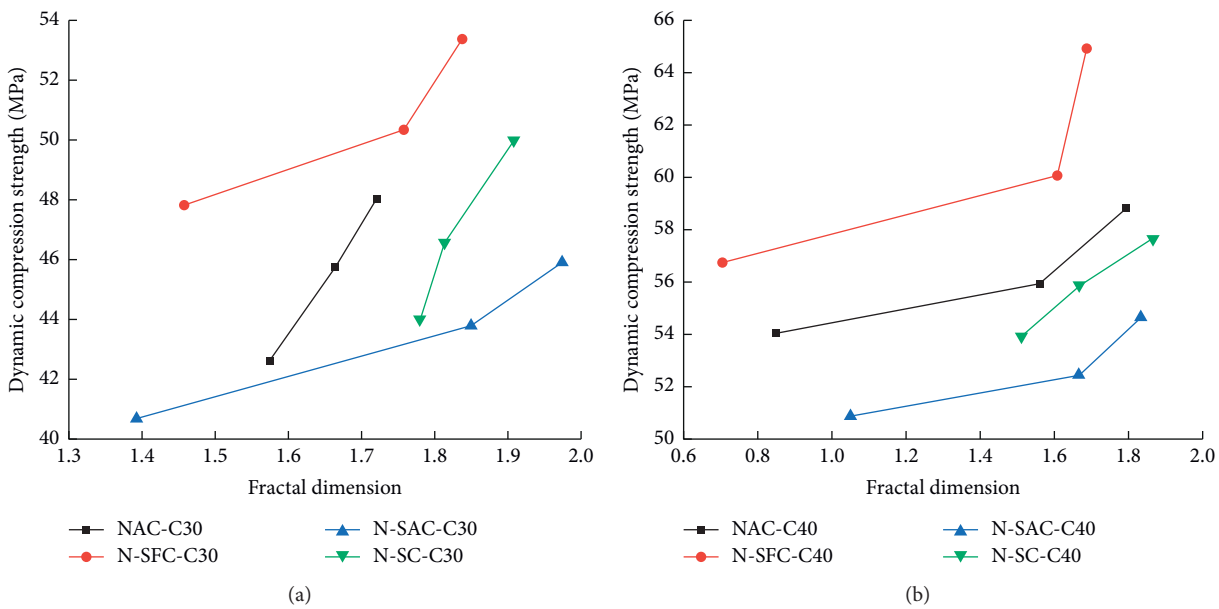

Figure 17: Relationship between fractal dimension and dynamic compressive strength index of concrete. (a) C30 groups. (b) C40 groups.

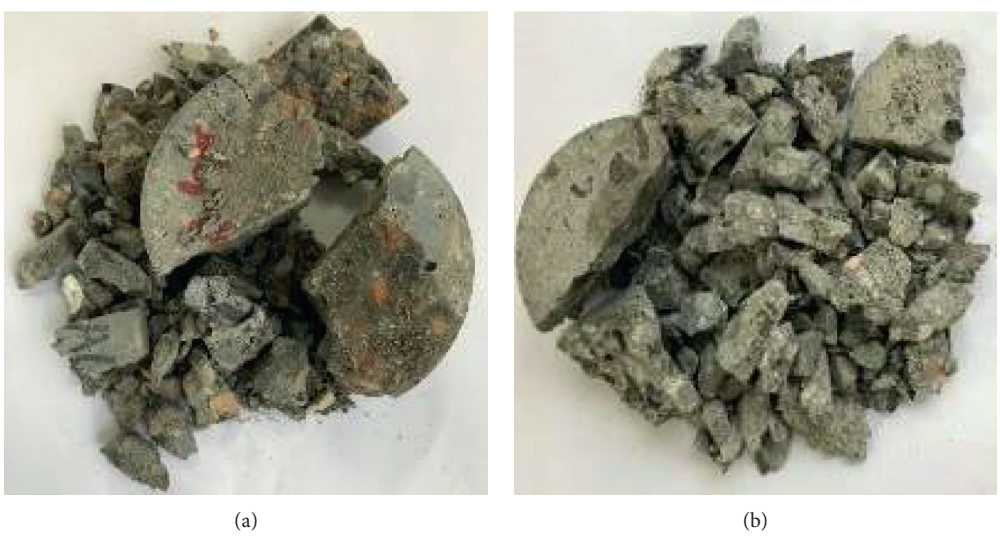

Figure 18: N-SFC and N-SAC after crushing. (a) N-SFC. (b) N-SAC.

According to the literature [34], the relationship between the fractal dimension D of the concrete specimen damaged by impact and the slope k of the typical $\ln(m_r/m_T) - \ln r$ curve corresponding to Figure 16 is $D = 3 - b$. Therefore, the representative data were selected to draw the relationship between the fractal dimension D and its dynamic compressive strength index after the specimen was damaged under different impact pressures, as shown in Figure 17.

It can be seen from Figure 17 that, with the increase of the impact gas pressure, the fractal dimension of each group of concrete gradually increases, which is similar to the change trend of the dynamic compressive strength of concrete with the impact gas pressure. This shows that the higher the dynamic compressive strength of concrete, the larger the fractal dimension, and there is a good positive correlation between the fractal dimension of concrete and the dynamic compressive strength. This is due to the impact load being greater and the generation and evolution of internal defects and damage in the concrete being stronger, thus resulting in more complete damage, which increases the number of fragments, decreases the size of the specimen after impact damage, and then leads to the fractal dimension of the specimen increase.

Based on the above analysis, it can be found that, as shown in Figure 18(a), the fractal dimension of concrete single-doped with coal gangue fine aggregate is smaller; that is, the average size of broken particles is larger. As shown in Figure 18(b), the fractal dimension of concrete single-doped with coal gangue coarse aggregate is larger; that is, the average size of the broken particles is smaller. The reason is

mainly related to the lower strength characteristics of coal gangue. For the concrete single-doped with coal gangue fine aggregate, under the impact load, due to the high strength of the coarse aggregate, the concrete cracks develop along the interface between the coarse aggregate and the mortar, so the broken concrete will form block distribution with block stone as the main body. For the concrete single-doped with coal gangue coarse aggregate because of the low strength of coal gangue coarse aggregate, the concrete cracks will develop along the interior of the block stone, so the concrete has a higher degree of fragmentation under dynamic load. Therefore, it can be concluded that, in the coal gangue concrete, when the coal gangue replaces the concrete fine aggregate, the concrete crushing degree is low; when the coal gangue replaces the concrete coarse aggregate, the concrete crushing degree is higher.

4. Conclusions

In order to study the feasibility of concrete doped with coal gangue in the application of mine supporting structure, in this research, coal gangue is used to replace coarse and fine aggregate in concrete, and its static (compressive strength) and dynamic (impact characteristics and dynamic compressive strength) characteristics are studied. The conclusions are as follows:

(1) According to the strength requirements of mine supporting concrete, the design strength of coal gangue concrete is C30 and C40, respectively. The results of the compressive strength test show that the uniaxial compressive strength of concrete single-doped with coal gangue coarse aggregate, single-doped with coal gangue fine aggregate, and codoped with coal gangue coarse and fine aggregates can meet the design strength requirements of C30 and C40 concrete, which indicates that it is feasible to use coal gangue to replace concrete fine aggregate and coarse aggregate or both to prepare C30 and C40 concrete.

(2) The initial and final crack impact energy of coal gangue concrete obtained by drop weight impact test are compared with that of ordinary concrete. Under the C30 design strength, the concrete single-doped with coal gangue fine aggregate increases by 22.9% and 11.4%; the concrete single-doped with coal gangue coarse aggregate decreases by 15.2% and 15.4%; the concrete codoped with coal gangue coarse and fine aggregates increases by 2.6% and 0.9%, respectively. Under the C40 design strength, the concrete single-doped with coal gangue fine aggregate increased by 10.2% and 8.7%, the concrete single-doped with coal gangue coarse aggregate decreased by 9.3% and 9.7%, and the concrete codoped with coal gangue coarse and fine aggregates increased by 2.3% and 0.1%, respectively. The main reason for this difference is that the coal gangue fine aggregate can optimize the force transfer structure of mortar and the coal gangue coarse aggregate can weaken the bearing structure of concrete.

(3) Comparing the dynamic compressive strength obtained by the SHPB impact test under 0.4–0.7 MPa gas pressure with the static compressive strength, under the design strength of C30, the concrete single-doped with coal gangue fine aggregate increased by 9.8–30.4%, the concrete single-doped with coal gangue coarse aggregate increased by 10.6–28.1%, and the concrete codoped with coal gangue coarse and fine aggregates increased by 9.1–30.4%. Under the design strength of C40, the concrete single-doped with coal gangue fine aggregate increased by 8.3–30.1%, the concrete single-doped with coal gangue coarse aggregate increased by 13.2–25.8%, and the concrete codoped with coal gangue coarse and fine aggregates increased by 11.0–26.1%.

(4) According to the crushing characteristics of coal gangue concrete under different gas pressures, it can be found that, with the increase of gas pressure, the fractal dimension of coal gangue concrete increases and the degree of fragmentation increases. In addition, it can be found that the crushing degree of concrete with coal gangue coarse aggregate is greater than that with coal gangue fine aggregate, which can be explained by the fact that the lower strength of coal gangue may not limit the development of cracks.

Data Availability

The data used to support the findings of this study are included within the article.

Conflicts of Interest

The authors declare no conflicts of interest.

Acknowledgments

This research was supported by the National Natural Science Foundation of China (nos. 51674006 and 51778004), the Anhui University Discipline Professional Talented Person (no. gxbjZD09), Anhui Provincial Natural Science Foundation Youth Project (1908085QE185), Anhui Provincial College of Natural Science Research Key Project (KJ2018A0098), Project Funded by China Postdoctoral Science Foundation (2018M642502), and the Science Research Foundation for Young Teachers in Anhui University of Science and Technology (QN2017211).

References

[1] X. Huang, A. Zhou, W. Wang, and P. Jiang, "Characterization of the dynamic properties of clay-gravel mixtures at low strain level," *Sustainability*, vol. 12, no. 4, p. 1616, 2020.

[2] J. M. P. Q. Delgado, F. A. N. Silva, A. C. Azevedo, D. F. Silva, R. L. B. Campello, and R. L. Santos, "Artificial neural networks to assess the useful life of reinforced concrete elements deteriorated by accelerated chloride tests," *Journal of Building Engineering*, vol. 31, Article ID 101445, 2020.

[3] L. Li, G. Long, K. Ma et al., "Preparation of green low strength mixture for foundation reinforcement treatment by using fly ash and waste coal gangue," *Materials*, vol. 13, no. 3, p. 664, 2020.

[4] M. Zhou, Y. Dou, Y. Zhang, Y. Zhang, and B. Zhang, "Effects of the variety and content of coal gangue coarse aggregate on the mechanical properties of concrete," *Construction and Building Materials*, vol. 220, pp. 386–395, 2019.

[5] Y. Zhang, Q. Wang, M. Zhou, Y. Fang, and Z. Zhang, "Mechanical properties of concrete with coarse spontaneous combustion gangue aggregate (SCGA): experimental investigation and prediction methodology," *Construction and Building Materials*, vol. 255, Article ID 119337, 2020.

[6] L. Qin and X. Gao, "Properties of coal gangue-Portland cement mixture with carbonation," *Fuel*, vol. 245, pp. 1–12, 2019.

[7] M. Xiao, F. Ju, and Z.-q. He, "Research on shotcrete in mine using non-activated waste coal gangue aggregate," *Journal of Cleaner Production*, vol. 259, Article ID 120810, 2020.

[8] Y. Zhang and T.-C. Ling, "Reactivity activation of waste coal gangue and its impact on the properties of cement-based materials - a review," *Construction and Building Materials*, vol. 234, Article ID 117424, 2020.

[9] H. Ma, H. Zhu, C. Wu, H. Chen, J. Sun, and J. Liu, "Study on compressive strength and durability of alkali-activated coal gangue-slag concrete and its mechanism," *Powder Technology*, vol. 368, pp. 112–124, 2020.

[10] R. Wu, S. Dai, S. Jian, H. Jun, H. Tan, and B. Li, "Utilization of solid waste high-volume calcium coal gangue in autoclaved aerated concrete: physico-mechanical properties, hydration products and economic costs," *Journal of Cleaner Production*, vol. 278, Article ID 123416, 2020.

[11] M. Hongqiang, C. Hongyu, Z. Hongguang et al., "Study on the drying shrinkage of alkali-activated coal gangue-slag mortar and its mechanisms," *Construction and Building Materials*, vol. 225, pp. 204–213, 2019.

[12] L. Li, G. Long, C. Bai, K. Ma, M. Wang, and S. Zhang, "Utilization of coal gangue aggregate for railway roadbed construction in practice," *Sustainability*, vol. 12, no. 11, p. 4583, 2020.

[13] Chinese Standard GB/T 50107-2010, "China ministry of housing and urban-rural development," *Standard for Evaluation of Concrete Compressive Strength*, China Construction Industry Press, Beijing, China, 2010, in Chinese.

[14] W. L. Li, "Experimental study on strength and crack resistance of coal gangue aggregate concrete mixed with glass fiber and fly ash," *Building Structure*, vol. 50, no. 13, pp. 49–53, 2020.

[15] Y. J. Li, C. Pan, S. K. Zhang, D. H. Li, H. T. Guan, and Z. S. Zhang, "Experimental study on damage of coal gangue concrete under cyclic load," *Bulletin of the Chinese Ceramic Society*, vol. 38, no. 08, pp. 2531–2535, 2019.

[16] H. Ma, H. Zhu, H. Chen, Y. Ni, X. Xu, and Q. Huo, "Shrinkage-reducing measures and mechanisms analysis for alkali-activated coal gangue-slag mortar at room temperature," *Construction and Building Materials*, vol. 252, Article ID 119001, 2020.

[17] J. X. Zhang, W. L. Chen, and R. J. Yang, "Experimental study on basic properties of coal gangue aggregate," *Journal of Building Materials*, vol. 6, no. 13, pp. 739–743, 2010.

[18] C.-l. Wang, W. Ni, S.-q. Zhang, S. Wang, G.-s. Gai, and W.-k. Wang, "Preparation and properties of autoclaved aerated concrete using coal gangue and iron ore tailings," *Construction and Building Materials*, vol. 104, no. 104, pp. 109–115, 2016.

[19] M. Zhou, G. N. Li, Q. Zhang, and H. B. Cui, "Study on application of spontaneous combustion coal gangue aggregate in ready-mixed concrete," *Journal of Building Materials*, vol. 5, no. 18, pp. 830–835, 2015.

[20] J.-X. Lin, Y. Song, Z.-H. Xie et al., "Static and dynamic mechanical behavior of engineered cementitious composites with PP and PVA fibers," *Journal of Building Engineering*, vol. 29, Article ID 101097, 2020.

[21] G. Murali, R. Gayathri, V. R. Ramkumar, and K. Karthikeyan, "Two statistical scrutinize of impact strength and strength reliability of steel fibre-reinforced concrete," *KSCE Journal of Civil Engineering*, vol. 22, no. 1, pp. 257–269, 2018.

[22] Y. Hao, H. Hao, G. P. Jiang, and Y. Zhou, "Experimental confirmation of some factors influencing dynamic concrete compressive strengths in high-speed impact tests," *Cement and Concrete Research*, vol. 52, pp. 63–70, 2013.

[23] A. Badr, A. F. Ashour, and A. K. Platten, "Statistical variations in impact resistance of polypropylene fibre-reinforced concrete," *International Journal of Impact Engineering*, vol. 32, no. 11, pp. 1907–1920, 2006.

[24] S. Lee, K.-M. Kim, J. Park, and J.-Y. Cho, "Pure rate effect on the concrete compressive strength in the split Hopkinson pressure bar test," *International Journal of Impact Engineering*, vol. 113, pp. 191–202, 2018.

[25] T. Abirami, M. Loganaganandan, G. Murali et al., "Experimental research on impact response of novel steel fibrous concretes under falling mass impact," *Construction and Building Materials*, vol. 222, pp. 447–457, 2019.

[26] S. R. Abid, M. L. Abdul-Hussein, N. S. Ayoob, S. H. Ali, and A. L. Kadhum, "Repeated drop-weight impact tests on self-compacting concrete reinforced with micro-steel fiber," *Heliyon*, vol. 6, no. 1, Article ID e3198, 2020.

[27] M. Nili and V. Afroughsabet, "Combined effect of silica fume and steel fibers on the impact resistance and mechanical properties of concrete," *International Journal of Impact Engineering*, vol. 37, pp. 879–886, 2010.

[28] Y. B. Lu and Q. M. Li, "A correction methodology to determine the strain-rate effect on the compressive strength of brittle materials based on SHPB testing," *International Journal of Protective Structures*, vol. 2, no. 1, pp. 127–138, 2011.

[29] Chinese Standard JGJ 55-2019, "China ministry of housing and urban-rural development," *Specification for Mix Proportion Design of Ordinary Concrete*, China Construction Industry Press, Beijing, China, 2019, in Chinese.

[30] C. Liu, X. Deng, J. Liu, and D. Hui, "Mechanical properties and microstructures of hypergolic and calcined coal gangue based geopolymer recycled concrete," *Construction and Building Materials*, vol. 221, no. 221, pp. 691–708, 2019.

[31] Chinese Standard GB/T 50081-2019, "China ministry of housing and urban-rural development," *Standard for Test Methods of Concrete Physical and Mechanical Properties*, China Construction Industry Press, Beijing, China, 2019, in Chinese.

[32] S. Feng, Y. Zhou, Y. Wang, and M. Lei, "Experimental research on the dynamic mechanical properties and damage characteristics of lightweight foamed concrete under impact loading," *International Journal of Impact Engineering*, vol. 140, Article ID 103558, 2020.

[33] M. Z. N. Khan, Y. Hao, H. Hao, and F. u. A. Shaikh, "Mechanical properties and behaviour of high-strength plain and hybrid-fiber reinforced geopolymer composites under dynamic splitting tension," *Cement and Concrete Composites*, vol. 104, Article ID 103343, 2019.

[34] P. Liu, D. Hu, Q. Wu, and X. Liu, "Sensitivity and uncertainty analysis of interfacial effect in SHPB tests for concrete-like materials," *Construction and Building Materials*, vol. 163, pp. 414–427, 2018.

Hindawi
Advances in Materials Science and Engineering
Volume 2020, Article ID 6907834, 16 pages
https://doi.org/10.1155/2020/6907834

Research Article

Durability of Concrete Structures with Sugar Cane Bagasse Ash

R. Berenguer,[1,2] N. Lima,[3] A. C. Valdés,[4] M. H. F. Medeiros,[4] N. B. D. Lima,[1] J. M. P. Q. Delgado,[5] F. A. N. Silva,[6] A. C. Azevedo,[5] A. S. Guimarães,[5] and B. Rangel[7]

[1]*Department of Fundamental Chemistry, Federal University of Pernambuco, Recife 50740-540, PE, Brazil*
[2]*Department of Civil Engineering, Federal University of Pernambuco, Recife 50740-540, PE, Brazil*
[3]*Polytechnic School, University of Pernambuco, Recife 50720-001, PE, Brazil*
[4]*Department of Civil Construction, Federal University of Paraná, Curitiba 81531-980, PR, Brazil*
[5]*CONSTRUCT-LFC, Civil Engineering Department, Faculty of Engineering, University of Porto, Porto 4200-465, Portugal*
[6]*Civil Engineering Department, Pernambuco Catholic University, Pernambuco, Recife 50050-900, Brazil*
[7]*CONSTRUCT-GEQUALTEC, Civil Engineering Department, Faculty of Engineering, University of Porto, Porto 4200-465, Portugal*

Correspondence should be addressed to J. M. P. Q. Delgado; jdelgado@fe.up.pt

Received 10 July 2020; Revised 2 September 2020; Accepted 19 September 2020; Published 5 October 2020

Academic Editor: Francesco Ruffino

The environmental impact of cement production increased significantly in the previous years. For each ton of cement produced, approximately a ton of carbon dioxide is emitted in decarbonation (50%), clinker furnace combustion (40%), raw materials transport (5%), and electricity (5%). Green strategies have been advanced to reduce it, adding natural or waste materials to substitute components or reinforce the mortar, like fibers or ashes. Sugar cane bagasse ash is a by-product generated from sugar boilers and alcohol factories with capacity to be used in concrete production. Composed mainly of silica, it can be used as mortar and concrete mineral admixture, providing great economic and environmental advantages, particularly in regions with sugar culture and industrial transformation like Brazil. In this research, a study of partial substitution of Portland cement by sugar cane bagasse (SCB) is analyzed, in order to reduce clinker in concrete volume, responsible for high emission of CO_2 to the atmosphere. An experimental campaign with cementitious pastes was carried out to evaluate the durability properties' changes due to SCB ash use. Samples containing 15% of sugarcane bagasse ash unveiled good results in terms of durability, indicating that concrete structure with sugar cane ash research is a new and important scientific topic to be highlighted.

1. Introduction

In some research centers, concrete's environmental impact is being studied. An environmental impact assessment was investigated by Saffari et al. [1] for Shahrood (Iran) cement, revealing that plant contaminations were identified in air, soil, landscape, and ecology environment. In China, for instance, studies concluded that, in the last decades, the Chinese cement industry has implemented several sustainable strategies in solid wastes and recycling materials have been used in its production [2]. As a result, Hossain et al. evaluated two green strategies to reduce Hong Kong industries' emission of CO_2 in cement production: one using glass powder obtained locally from glass bottle waste and the other adding biofuel obtained from local wood waste [3]. Both strategies reduced 12% of total gases emission and 15% of energy consumption in cement production [3]. Wilk et al. [4] reported a solution for cement industry to estimate asbestos-cement products' quantity used at polish industry, which is the use of Random Forest algorithm [4]. Aspects of environmental and economic potential of the use of limestone calcined clay cement were investigated in Cuba, comparing it with commercial zeolite cement [5]. The authors concluded that a low amount of CO_2 was produced and that it has the potential to be commercialized also in countries where trucks can make 100 km distance transport from clay deposit to cement plant.

Recently, advances to improve sustainable cement production were reported [6–14]. Chen et al. [7] employed cements' life cycle impact assessment to ascertain different processes and cement plant variabilities aspects. The results revealed differences between cement production processes in the studied plants set. It was concluded that variations are greater than 40%, mainly due to lack of pollutant content in accurate measurements [7]. This result indicates that studies of green strategies, which are capable of reducing cement production environmental impact, must be pursued. In this sense, Gursel and Ostertag [15] investigated strategies for embodied energy and environmental impacts on reduction of cement usage and aggregate consumption in concrete employed in Singapore. Two cases were considered: (i) the use of materials (cement and aggregate) prepared in Singapore and (ii) the use of materials imported from Malaysia. It was concluded that, using Malaysian cement and aggregates instead of the corresponding Singapore materials, the high-strength concrete potential and embodied energy reduced to 11% and 31%, respectively.

The effects of by-products' usage and waste materials as supplementary cementitious systems have been also extensively investigated [16–29]. As a result, fly ashes [21, 27], metakaolin [30], geopolymers [31, 32], slags (such as steel slags) [24, 25], and sugar cane bagasse ash [33–36] were added to green concrete. The sugar cane bagasse ash is a by-product resulting from factories' sugar and alcohol boilers [33–36]. Composed mainly of silica (SiO_2), it can be used as mineral admixture in concrete mortar with great economic and environmental advantages. In this sense, new applications can be destined and provided when waste ashes are incorporated in cement matrices. In particular, the sugar cane bagasse ashes are, in general, discarded, when they could be employed, for example, in the cement-based materials such as concrete and mortars that emit lower levels of CO_2 in the atmosphere [37].

This work intends to contribute to the research of partial substitution of Portland cement by sugar cane bagasse (SCB) to reduce the consumption of clinker in concrete volume responsible for high emission of CO_2. A new use can be provided when incorporated into cement matrices: the leftovers of bagasse can be used to generate energy and the tailings in concrete and mortars production.

2. Materials and Methods

2.1. Materials. This work presents characterization and analyses of sugar cane bagasse ash potential through chemical, physical, and mineralogical methods in order to evaluate its pozzolanicity by direct and indirect techniques. Through accelerated techniques of environmental aggressiveness, the durability of concrete structures with this material is analyzed. Two samples of sugar cane bagasse ash were used:

(i) SCBA-A: collected from a wood oven in a pizzeria in the Metropolitan Region of Recife, Brazil, and used as an energy source and to burn to heat during the pizza cooking

(ii) SCBA-B: collected from sugar cane mill located in the city of Palmares, Pernambuco, Brazil, and resulting from sugar derivatives production burning process in heating the boilers

2.2. Materials Characterization. The following techniques were employed in order to characterize physical, chemical, and mineral properties of the SCBA-A and SCBA-B systems to support their rational use and viability to be added in mortar and concrete manufactures: (1) scanning electron microscopy (SEM) analysis, (2) particle size distribution, (3) specific mass, (4) specific area, (5) unit mass, (6) fire loss (FL), and (7) thermogravimetric analysis (TG-DTG). The samples used in characterization and subsequent specimen molding analysis were obtained from the SCBA-A and SCBA-B, dried at 105°C, and passed through 20 min sieving process at 70 rpm speed to obtain the passing fraction by opening sieve of 0.075 mm.

The morphology of SCBA-A and SCBA-B was evaluated by scanning electron microscopy (SEM) technique. For morphology analysis, a TESCAN scanning electron microscope (SEM), MIRA3 model, 10 kV voltage, and SE detector (EDS) were used.

2.2.1. Physical Properties. For particle size distribution, a CILAS 1090 laser granulometer was used through dry and wet route. According to the analysis method used, the particle size is given by the respective circumscribe circumference diameter. Thus, rods and particles with long lamellar shape or particle agglomeration are visualized in scanning electron microscopy (SEM) analysis through secondary electron detectors (SE), and the equipment (CILAS 1090 laser granulometer) considers particle length as the diameter, impairing the results analysis.

Portland cement (PC-V), metakaolin (MET), active silica (SIL), fly ash (FA), and sugarcane bagasse ash (SCBA-A and SCBA-B) specific mass were determined by the helium gas pycnometer method (recommended by ABNT NBR 16605 [38]), using AccuPyc 1330 V2.01-Micromeritics device. The material specific surfaces were determined using the Blaine Semi-Automatic ACMEL BSA 1 permeability equipment, according to standard NBR 16372 [39].

2.2.2. Chemical Properties. In order to validate the results of muffle fire loss obtained, thermogravimetric tests were employed. The analyses were conducted on STA 449 F3 JUPITER NETZSCH simultaneous analysis equipment. The experimental conditions used were as follows: inert atmosphere (N_2), maximum flow of 100 ml/min and heating range of 30°C to 1000°C, with a heating rate of 10°C/min, with sample port (alumina crucible), and mass approximately around 20 mg ± 0.5 and purge of 50°C/min.

For the chemical analysis of precursor materials, the technique and semiquantitative analysis by X-ray fluorescence (XRF) spectrometry were employed. In this sense, the chemical characterization of the precursor materials was obtained using Shimadzu equipment, model XRF 1800.

2.3. Pozzolanicity Experiments

2.3.1. Direct Method. The water/binders ratio of 0.48 and a mixture of 20 g of cement with 9.60 g of water, for the reference material (REF), and 20 g of cement with 11.04 g of water and 3 g of added material, for SCBA-A, SCBA-B, FA, MET, and SIL, were considered. The samples were moulded and after 24 h were demoulded and added to properly identified submerged cure. Further, the samples were submitted to thermogravimetric analysis with 28, 63, and 91 days of age.

On the other hand, the thermogravimetric analyses were performed by using an STA 449 F3 JUPITER NETZSCH analysis equipment. The experimental conditions were as follows: inert atmosphere (N_2), maximum flow of 100 ml/min, initial heating range of 30°C to 1000°C, with a heating rate of 10°C/min, and mass approximately around 20 mg ± 0.5 and purge of 50 C/min. From equations (1) to (6), the chemically combined water content (AQC) related to C-S-H and hydrated aluminate phases formation, calcium hydroxide $Ca(OH)_2$, and calcium carbonate content ($CaCO_3$) were calculated:

$$CH_1 = \frac{(H_2O \times 100)}{A}, \quad (1)$$

$$CO_2 = \frac{(PCO_2 \times 100)}{B}, \quad (2)$$

$$C_aCO_{3real} = CO_2 - \text{Approx}, \quad (3)$$

$$CH_2 = \frac{(C_aCO_{3real} \times C)}{100}, \quad (4)$$

$$AQC = AQC_{total} - CH, \quad (5)$$

$$Ca(OH)_2 = CH_1 + CH_2, \quad (6)$$

where H_2O is the water loss that happens in the thermal event of portlandite decomposition, "A" is the molar water mass of H_2O, PCO_2 is the water loss that happens in the thermal decarbonation event, "B" is the molar mass of the CO_2, "Approx." is the approximate 5% of the carbonate content present in the CP-V ARI, "C" is the molar mass of $Ca(OH)_2$, "AQC_{total}" is the mass loss occurring in the thermal event ranging from 100 to 600°C, $CH_1 = CH_2$ is the mass loss that occurs in the thermal event ranging from 350 to 450°C, "AQC" is the chemically combined water, $Ca(OH)_2$ is the total portlandite content, and $CaCO_3$ is the calcium carbonate content.

In addition, the modified Chapelle's method was employed by considering 1 g of material to evaluate "pozzolanic material" (m_2) and 2 g of calcium oxide (m_3) should be weighed. Immediately thereafter, 250 ml of CO_2-free distilled water should be added and measured in an Erlenmeyer flask heated to 90 ± 5°C, with stirring in a container simultaneously for 16 h. Subsequently, to test with the pozzolanic material, the same procedures are performed for blank assay containing only calcium oxide determination under the same conditions. Further, 250 ml of sucrose solution was added to Erlenmeyer with material evaluated, "pozzolanic material" and calcium oxide, which was shaken for 15 min. 50 ml of this solution was pipetted out and titrated with 0. 1 M chlorine hydroxide solution using 1 g/l of phenolphthalein solution as an indicator. The volume consumed in titration was noted (V_2). The same procedure was performed with blank assay, noting the volume spent (V_3). The pozzolanic activity index by modifying Chapelle's method can be calculated according to equation (7), corresponding to the amount of calcium hydroxide used (in mg) per gram of pozzolanic material:

$$I_{Ca(OH)_2} = \frac{28 \times (V_3 - V_2) \times Fc}{m_2}, \quad (7)$$

where $I_{Ca(OH)2}$ is the pozzolanic activity index corresponding to the fixed calcium hydroxide content (m_l), m_2 is the pozzolanic material mass (g), V_2 is HCl 0.1 M consumed assay with pozzolan solution volume (ml), V_3 is the HCl 0.1 M consumed in the assay with reference solution volume (mL), and "Fc" is the HCl for a concentration of 0.1 M correction factor (Fc = 1.32).

2.3.2. Indirect Method. For the electrical conductivity analysis, the loss of a solution of calcium electrical conductivity hydroxide P.A. was measured, based on the research of Raverdy et al. [40] and Lúxan et al. [41]. In this sense, a 1000-second analysis period was considered to verify sewage sludge ash pozzolanic activity among other supplementary materials. This time interval was fixed as being sufficient to analyze the sugarcane bagasse ashes. In this sense, 1050 ml of distilled water was heated to 60 ± 2°C, and this temperature was determined due to similarity with Portland cement hydration initial temperature. After the water reached the ideal temperature and stabilized, 840 mg of $Ca(OH)_2$ P.A. (minimum of 95% purity) was added. The container was then sealed, and the solution was kept under constant agitation at 700 rpm for a period of 1 hour.

Subsequently, 200 ml of this solution was used and it was transferred to the 250 ml beaker under the same conditions; and rubber stopper was inserted firmly, together with conductivity cell and thermometer. Finally, 4 g of the studied materials (SCBA-A, SCBA-B, FA, MET, and SIL) was added to the $Ca(OH)_2$ solution, through the appropriate tube fixed to the stopper. Portland cement's performance index in the material pozzolanic activity was determined following part of the physical and chemical requirements proposed by NBR 12653 [42]. According to this standard, minimum physical requirements for a material are considered pozzolanic: a minimum of 90% performance index with Portland when compared with control.

The material pozzolanic reaction used was evaluated by determining performance index with Portland cement according to NBR 5752 [43]. Two different mortar compositions suggested by the standard were used: (i) mortar A, containing only Portland CP II F-32 cement as binder, and (ii) mortar B, containing 25% of material analyzed as pozzolanic (SCBA-A and SCBA-B), replacing cement. The materials used in this assay are described in Table 1. In this

Table 1: Determination of pozzolanic activity index with cement.

Materials	Mass (g)			
	Mortar A	Mortar B (SCBA-A)	Mortar B (SCBA-B)	Water/binder
CP II F-32	624 ± 0.4	468 ± 0.4	468 ± 0.4	0.48
Pozzolanic material	—	156 ± 0.2	156 ± 0.2	0.48
Sand normalized by IPT NBR 7214 (2015)	1872.0	1872.0	1872.0	—
Water	300 ± 0.2	300 ± 0.2	300 ± 0.2	—

sense, six cylindrical specimens with a diameter of 5 cm × height of 10 cm (5 cm × 10 cm) of mortar moulded for each trace were made and, after 28 days, were ruptured by axial compression according to NBR 5739 [44].

2.4. Durability. The durability tests were performed by considering the following strategies: accelerated carbonation, total absorption, capillarity, and immersion with the objective of efficiency analyses of mineral materials addition. The cylindrical specimens with a diameter of 5 cm × height of 10 cm (5 cm × 10 cm) were moulded according to NBR 7215 [45]. Using a normal sand described in NBR 7214 [46], the sugarcane bagasse ash from the pizzeria (SCBA-A), the sugarcane bagasse ash from the plant (SCBA-B), the fly ash (FA), the metakaolin (MET), the active silica (SIL), and the Portland CPV-ARI cement (REF) were tested.

The mixture employed in the cylindrical specimen processing was 5 cm × 10 cm (1 : 3 : 0.48), that is, 624 g of cement and 1872 g of sand with 300 ml of water. Regarding the addition levels, 15% addition (93.6 g of mineral) to cement was used for materials used in this research (SCBA-A, SCBA-B, FA, MET, and SIL). The choice of 15% addition is according to Berenguer et al. [37]. Further, 24 specimens were made with 15% (SCBA-B, FA, MET, and SIL) addition and 6 specimens without mineral addition (references), in which all 30 samples were employed in the accelerated carbonation tests. In addition, 20 specimens were made with 15% and 5 reference specimens were used in the absorption capillary and immersion assays. Finally, for the analysis of the accelerated migration of chloride ions, 10 specimens with a diameter of 10 cm × height of 20 cm were prepared by considering a ratio of 1 : 1.51 : 2.06 : 0.48 between cement, sand, and gravel. In addition, the water/cement ratio with 45% gravel, A% = 10.50, $\alpha = 0.55$, and cement consumption (kg/m^3) = 465.61 was considered. Among these 10 samples, 8 were samples with mineral additions (SCBA-B, FA, MET, and SIL), and 2 were corresponding to reference systems with absence of mineral additions.

2.4.1. Water Absorption by Capillarity and Immersion. The water absorption tests by capillarity followed the procedures and recommendations of NBR 9779 [47]. It provides mass measurements and water absorption height in mortars. After 28 days of submerged curing, the specimens were packed in an oven in a 45 ± 2°C temperature with internal ventilation until mass constancy for the remaining 23 days to perform the test. A 45 ± 2°C constant temperature was maintained to preserve the integrity of Portland cement hydration products.

In a container installed in an environment with a constant temperature of 23 ± 2°C, the specimens were positioned on a metal support, filling the container with water at a constant level of 5 mm ± 1 mm above the lower face. The saturated mass was determined after 3 h, 6 h, 24 h, 48 h, and 72 h. Previously, the excess water was removed with damp cloth and after each step, it was returned to the container with constant water slide. Then, the experiments were performed on three cylindrical mortar specimens, 5 cm × 10 cm, for each trait described, and the absorption of water by capillarity is calculated according to

$$A_w = \frac{M_{sat} - M_s}{S}, \tag{8}$$

where A_w is the water absorption by capillarity (g/cm^2); M_{sat} is the saturated mass of the specimen which remains with one of the faces in contact with water for the specified period (g); M_s is the mass of the dry specimen, as soon as it reaches 23 ± 2°C temperature (g), and S is the cross-sectional area (cm^2).

According to NBR 9778 [48], samples were taken to an oven for 72 h at a 45 ± 2°C temperature. According to Berenguer et al. [37], to maintain the Portland cement hydration products' integrity, samples were kept in an oven with internal ventilation until mass constancy for 23 days, with a 45 ± 2°C temperature for later tests. Soon after, dry samples masses were determined and recorded; at the second moment samples were immersed in water at a (23 ± 2)°C temperature for 72 h, with the aid of hydrostatic scale, and the mass of immersed samples was determined. The assay was performed for each mixture on three cylindrical mortar specimens with 5 cm × 10 cm and the immersion water absorption was calculated by

$$A_{\%} = \frac{M_{sat} - M_s}{M_s} \times 100, \tag{9}$$

where M_{sat} is the saturated sample mass after immersion and M_s is the sample dried mass.

2.4.2. Determination of Void Indexes. According to NBR 9778 [48], the total water absorption test enables the calculation of cylindrical specimens void index, I_v (%). This index is associated with pores total volume accessible to water and does not reflect the easiness with which water can enter the concrete. Thus, the sample void indexes were measured in analyses, according to NBR 9779 (2012) [47]. The mean values calculated in void index test were

performed for each mixture with three 5 cm × 10 cm cylindrical mortar specimens, according to the following equation:

$$I_{v(\%)} = \frac{M_{sat} - M_s}{M_{sat} - M_i} \times 100, \quad (10)$$

where M_i is the immersed saturated sample mass of water, M_{sat} is the saturated sample after immersion mass, and M_s is the sample dried mass.

2.4.3. Resistance to Accelerated Carbonation. The carbonation camera Caron, which refrigerated CO_2 incubator and has automatic digital control of temperature of ±1°C, relative humidity of ±2%, and controlled CO_2 content, was used, as can be seen in Figure 1(a). In this sense, the samples were placed in a dry chamber until they reached constancy of masses (Figure 1(b)) and remained in this environment for 19 days. Because the mass constancy was reached, samples were extracted from the dry chamber and placed in carbonation chamber where they remained for 30 days (Figure 1(c)).

The samples were fractured in three parts each, in which carbonation front verification process was carried out in specimen slices with about 3.3 cm. For rupture of the samples, an EMIC press with a 100 kN maximum capacity was used. The carbonation depth was then measured using a 0.01 mm precision caliper. The temperature in carbonation chamber was kept constant at temperature of 23°C, relative humidity of 65%, and CO_2 content of 5%. On a regular period, 6 readings were performed in each slice with a chemical solution of phenolphthalein used as a chemical indicator of pH. In preparation of chemical solution and in test performance, the RILEM CPC-18 standard [49], which stipulates a chemical solution of 1 g of phenolphthalein dissolved in 100 g of 70% ethyl alcohol, was considered. After its preparation, phenolphthalein solution was stored in a container for later use. The chemical solution used presented colour change in pH range between 8.3 and 10.0 presenting with a rosy/crimson red colour. The first rupture was performed immediately after 1 month, and the carbonation front advance was measured. The second rupture was performed after 2 months of samples confinement in the carbonation chamber, as shown in Figure 2.

2.4.4. Accelerated Chloride Ion Migration. The standard test method for electrical indication of the concrete's ability to resist chloride ion penetration (Cl^-) was based on ASTM C1202 standard [50]. In this sense, in the present article, the tests of accelerated chloride ion migration were performed by considering 365-day-old samples. The tests were performed with the application of a 60 V voltage over 6 hours with the passing current every 30-minute measurement. The passing current Amps readings in seconds over time generated a curve. The test result was the integral representing the area between the curve and the axis, obtained from passing the load over 6 hours in A/s or Coulombs (C). The specimens were dried in an oven at 100°C until mass constancy; then, they were packed for 24 hours in a dry chamber to cool down. At the second moment, protection systems (coating) were applied to one of the circular faces of each specimen with silicone layer on its side. Finally, a saturation method was applied by vacuum and immersion. In the cathodic chamber, an aqueous solution with 3% NaCl was placed, and in the anodic chamber, a solution of NaOH 0.3 N was placed. In addition, the samples (REF, SCBA, FA, MET, and SIL) with a diameter of 100 mm and a height 50 mm and 365 days of submerged curing were positioned between two cells (Figure 3), negative and positive, containing solutions of sodium chloride (3% by mass) and sodium hydroxide (0.3 N), respectively. They were subjected to a potential difference of 60 V for a period of 6 hours.

The applied voltage to a 0.1 Ω resistor was checked every 30 min. Therefore, the electric current (Ohm's law) and, consequently, the passing load through equation (11) according to ASTM C1202 [50] were calculated. For each mixture of the different samples, electrical loads were calculated by arithmetic mean of two determinations in different specimens:

$$Q = KC/A\left(I_0 + 2I_{30} + 2I_{60} + \cdots + 2I_{300} + 2I_{330} + 2I_{360}\right), \quad (11)$$

where Q is the electric charge; KC/A is the constant equal to 900 C/A and I_n is the electric current after applying the voltage.

3. Results and Discussion

3.1. Characterizations. The XRF experiments revealed a large predominance of the chemical compositions of CaO, SiO_2, Fe_2O_3, Al_2O_3, MgO, and K_2O for the precursor materials employed, where for Portland cement samples (REF) the XRF data for these oxide compounds were 62%, 22%, 4%, 4%, 2%, and 0.4%, respectively. In this sense, for the SCBCA-A, the corresponding values were 7%, 44%, 3%, 2%, 5%, and 7%, respectively. For the SCBA-B, these values were 3%, 71%, 2%, 5%, 2%, and 3%, respectively. For the FA samples, compositions of 2%, 70%, 5%, 17%, 0.8%, and 2% were obtained, respectively, for CaO, SiO_2, Fe_2O_3, Al_2O_3, MgO, and K_2O compounds. In addition, for the MET samples, the corresponding values were 0.1%, 64%, 3%, 28%, 1%, and 3%, respectively. For the SIL samples, the corresponding chemical compositions were 0.3%, 96%, 0.8%, 0.1%, 0.5%, and 1%, respectively.

On the other hand, the tests of particle distributions, specific masses determinations, specific materials surface areas, materials unit masses, and loss to fire are shown in Table 2.

According to particle size distribution analysis, Portland cement grains (PCV) revealed results for medium particles distribution, with diameter at 50% (D_{50}) equal to 5.90 μm, while SCBA-A, SCBA-B, FA, MET, and SIL presented the average diameters equal to 8.25 μm, 10.32 μm, 9.76 μm, 5.72 μm, and 63.67 μm, respectively. To bestow these results, electron microscopy scanning technique was used to ascertain the shape and values of particles found in

(a) (b)

Figure 1: Continued.

(c)

Figure 1: (a) Carbonation chamber; (b) measurement for mass constancy; (c) carbonation chamber with specimens.

granulometry. In this sense, Figure 4 shows microstructural differences between SCBA-A and SCBA-B systems from SEM/EDS analyses.

On the other hand, for the estimated accuracy of fire loss test, the validation was made according to NBR NM 18 [51] and results were compared with mass loss obtained by thermogravimetry. Table 2 shows the values of six fire loss determinations, 6.37%, 19.89%, 13.64%, 2.03%, 3.07, and 3.09%, for samples (CP-V, SCBA-A, SCBA-B, FA, MET, and SIL), respectively. By thermogravimetry assay, mass loss at the approximate temperature of 1000°C was 6.08%, 22.22%, 11.65%, 1.34, 2.63, and 2.98%, respectively. The difference between values achieved by the two techniques was only 0.29%, 2.33%, 1.99%, 0.69%, 0.44%, and 0.11% for each sample. It can be concluded that the fire loss test was significantly accurate and presents an excellent correlation ($R^2 = 0.9756$), as shown in Figure 5, with thermogravimetric analysis results presented in Figure 6.

On the other hand, from Figure 6, it is possible to verify the mass loss occurring in respective thermal events, particularly highlighted thermal events happening between 400°C and 450°C with portlandite decomposition. Therefore, thermogravimetry was the analytical technique used to monitor possible pozzolanic reactions of cement pastes containing 15% ash addition (SCBA-A and SCBA-B). Dweck et al. [52] employed thermogravimetric analysis in Portland cement pastes and revealed that it is possible to determine the chemically combined water content of all hydrated compounds in a thermal event ranging from 50°C to portlandite final decomposition temperature. Thus, studies were performed through reference pastes thermoanalysis (without SCBA) and in pastes containing SCBA-A or SCBA-B. The samples were analyzed by thermogravimetry after 28, 63, and 91 days of cure identifying hydrated phases formed, together with observing possible consumption of Portlandite reactions with sugarcane bagasse ash. According to Hoppe Filho et al. [53], it is possible to observe the characteristics of each phase in thermal events. In addition, Table 3 and Figure 7 show data of chemically combined water and portlandite (AQC and $Ca(OH)_2$).

Through the $\Delta H > 0$ and exothermic $\Delta H < 0$ endothermic structural transformations, it was possible to perform a quantitative analysis [54]. Thus, analyses were

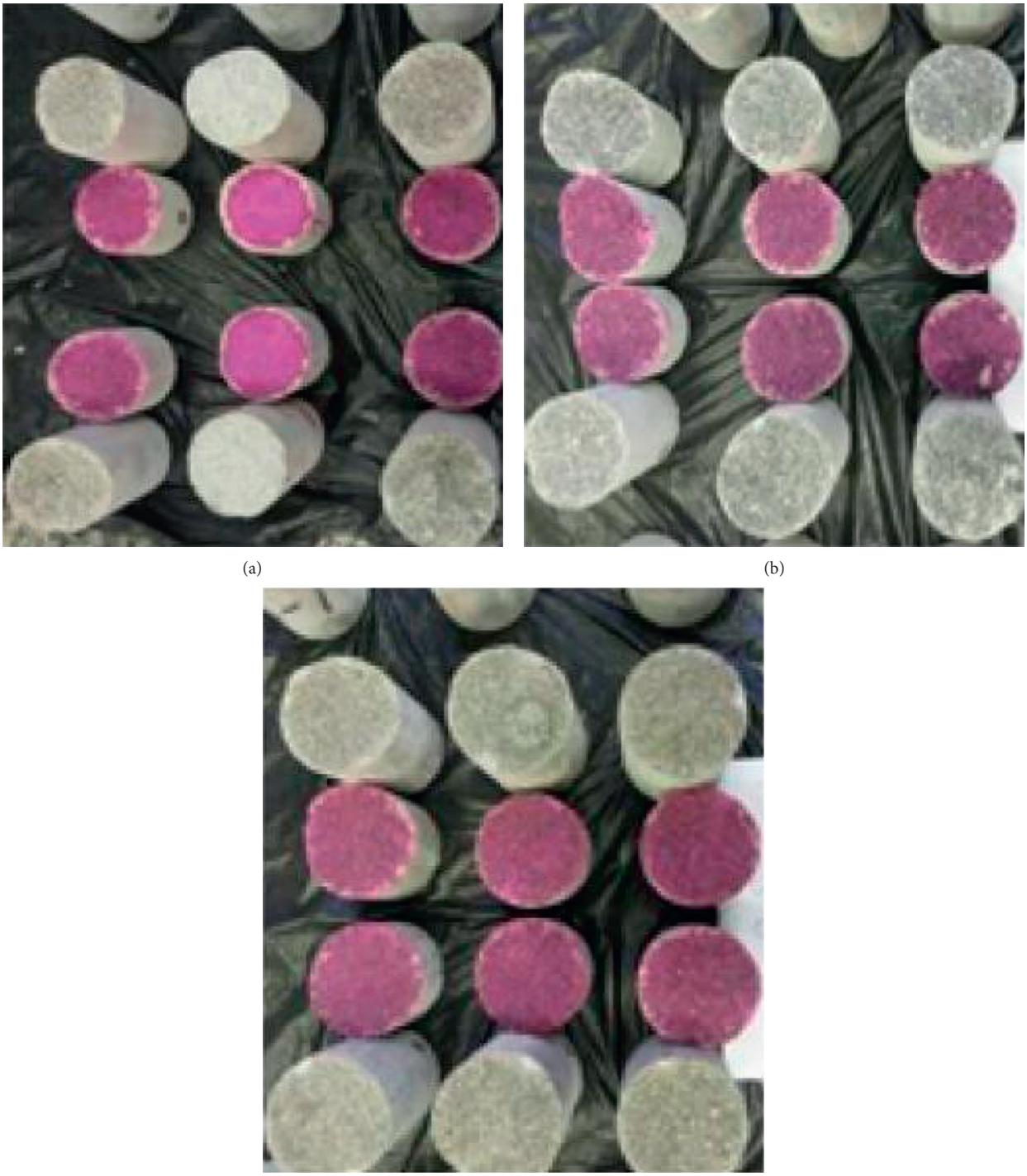

Figure 2: Samples after testing for carbonation evaluation: (a) reference; (b) fly ash; (c) active silica.

made in pastes at 28, 63, and 91 days through stochiometric calculations and quantifying contents of hydrated compounds formed, with portlandite content remaining in hydrated matrix and calcium carbonate content.

From Figure 7, the paste thermogravimetric analysis results of the chemically combined water content (AQC) can be associated with the C-S-H formation and hydrated aluminate phases, calcium hydroxide ($Ca(OH)_2$) and calcium carbonate content ($CaCO_3$), which were quantified through equations (1)–(6). Table 3 shows the results after stochiometric calculations of hydrated compounds analyzed.

According to Hoppe Filho et al. [53], the cement hydration evolution provides an increase in portlandite phase ($Ca(OH)_2$), as well as in chemically combined water content (AQC), due to hydration of anhydrous phases C_3A, C_3S, C_2S, and C_4AF, as can be seen in Table 3 and Figure 6. For

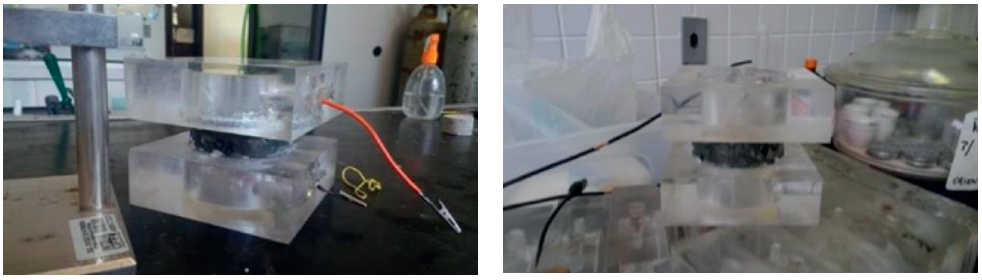

(a) (b)

Figure 3: Cells for chloride migration assay and chloride migration assay preparation.

Table 2: Summary of the materials characterization.

Properties	Cement	SCBA-A	SCBA-B	FA	MET	SIL
Unit mass (kg/dm^3)	1.00	0.075	0.089	0.693	0.703	0.550
Specific mass (kg/dm^3)	3.17	2.72	2.37	2.39	2.81	2.22
Specific surface area (m^2/g) (Blaine Electronic)	0.452	0.655	0.654	0.678	0.474	0.718
Specific surface area (m^2/g) (BET)	1.784	5.461	22.849	1.158	16.908	20.341
Particle distribution D_{10}, μm	0.94	0.21	0.94	0.18	0.34	2.99
Particle distribution D_{50}, μm	5.90	8.25	10.32	9.76	5.72	63.67
Particle distribution D_{90}, μm	29.15	43.95	43.28	92.30	34.36	372.00
Mass loss, % (TG)	6.08	22.22	11.65	1.34	2.63	2.98
Fire loss, % (FL)	6.37	19.89	13.64	2.03	3.07	3.09

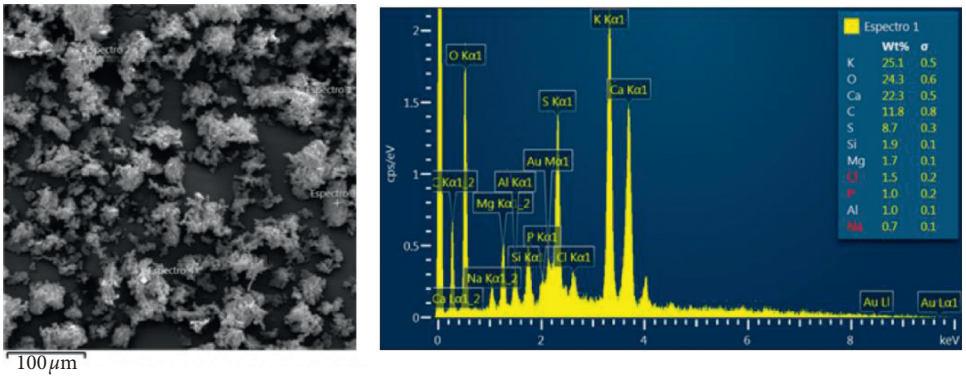

(a)

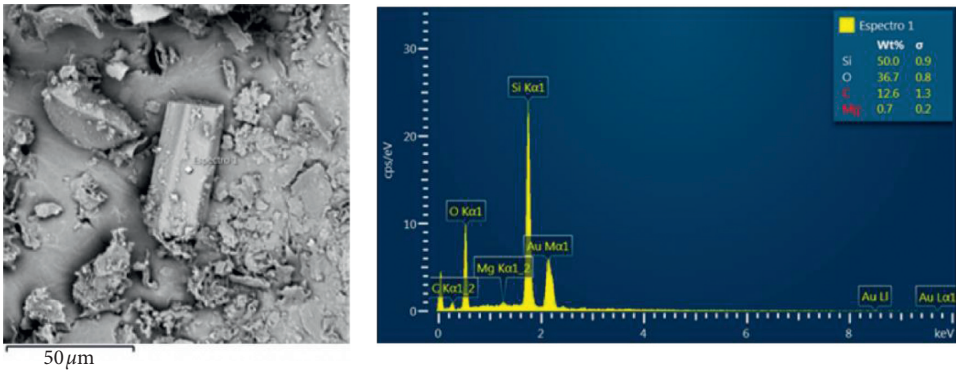

(b)

Figure 4: Scanning electron microscopy-EDS detector of (a) SCBA-A and (b) SCBA-B.

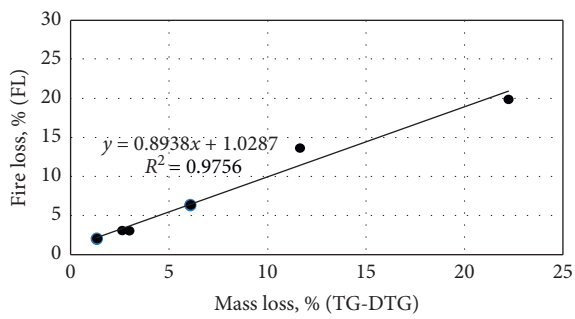

Figure 5: Fire loss (FL) versus mass loss (TG).

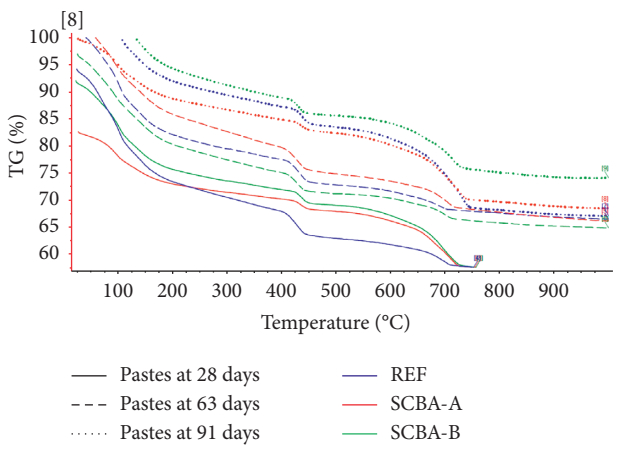

Figure 6: Thermogravimetric analysis (TG/DTG) of the pastes at 28, 63, and 91 days.

reference sample hydrated compounds (NDF) analysis contents, no significant evolution was perceived, as the results remained almost constant. When analyzing the event that occurred between 400°C and 450°C, the hypothesis of portlandite decomposition ($Ca(OH)_2$) can be attributed, since there was an evolution in portlandite increase for reference samples (CP V ARI). In calcium carbonate content analysis event, it is possible to observe at 91 days a significant increase described in Table 3, revealing that a sample carbonation may have occurred, which is suitable for other generating sources. For samples (SCBA-A and SCBA-B), the contents of hydrated compounds (AQC) analyses which increased in these compounds were observed over time in a discrete but noticeable way as shown in Figure 6. Regarding portlandite content ($Ca(OH)_2$), the samples containing 15% ash became quite expressive in quantitative terms for both samples. It can suggest that ash as the main action, the nucleation hypothesis, is a source that generates portlandite. On the other hand, if (AQC) evolution and ($Ca(OH)_2$) consumption became noticeable according to Figure 5, this trend confirmed the hypothesis of pozzolanic reactions of the samples in the paste. In this sense, ashes (SCBA-A and SCBA-B) may have acted through pozzolanic reaction in microstructure refinement, due to the fact that secondary C-S-H crystals decrease the pore diameter average of cement matrix, and are associated with filler effect.

Figure 7 also shows chemically combined water content (2C) and portlandite content in pastes studied at 91 days of hydration, obtained by thermogravimetry. Both are related to Portland cement hydration and are influenced by pozzolanic reaction occurrence in cement paste.

The increase in AQC content and the reduction of portlandite content of series with sugarcane bagasse ash related to reference series indicate that addition presented a higher amount of C-S-H. This occurred due to consumption of typical portlandite of pozzolanic reaction.

3.2. Pozzolanic Activities by the Direct Method. According to Hoppe Filhoet al. [53] and to NBR 15895 [55], the modified Chapelle's method can be employed to evaluate the kinetics of pozzolanic reaction in pozzolan/lime system. At the beginning of the essay, during the samples chemical reactions, the samples' vitreous fraction was gradually solubilized by actions of hydroxyl ions, which react with calcium ions to hydrates precipitation [56]. However, according to the results presented in Table 4, there is an indication that SCBA-A has a lower value than the minimum pozzolanic activity index suggested by Raverdy et al. [40]. In addition, SCBA-B ash presented results slightly above pozzolanic activity minimum value index. Therefore, it is possible to conclude that the increase in pozzolanic activity is associated with amorphous material amount considering other samples also with the same characteristics, specific surface area, as well as the change from quartz-α to quartz-β.

It is noteworthy that NBR 15895 [55] does not define the minimum value for $I_{Ca(OH)2}$ through Chapelle's test; however, French standard NFP 18-513 [57] brings a minimum pozzolanic activity value of 700 mg of $Ca(OH)_2$/g pozzolan, which indicates that samples SCBA-A, SCBA-B, and FA do not fit as pozzolanic material for this test. Following Raverdy et al.'s [40] suggestion, at a minimum value of 330 mg of $Ca(OH)_2$/g, the only sample that could not fit would be the SCBA-A. There is a possibility that values below the minimum established by the same authors in the SCBA-A samples may be related to their respective calcination temperatures, due to the direct influence on pozzolanic reactions when calcination temperatures are different from 600°C.

3.3. Pozzolanic Activities by the Indirect Method. The data of electrical conductivity of the sugarcane bagasse ash (SCBA-A and SCBA-B), fly ash (AF), metakaolin (MET), and active silica (SIL) are shown in Figure 8.

From Figure 8, except for the fly wheel ash exception (Figure 8(c)), there was a drop in electrical conductivity over time after insertion of these materials, indicating a pozzolanic potential for all samples. Regarding fly ash considered as exception sample, Payá et al. [58] observed the behavior for measurements up to 1000 seconds, where there was conductivity, but virtually no conductivity was observed in longer times (10000 seconds). Regarding metakaolin and active silica (Figures 8(d) and 8(e)), it was observed that conductivity is sharply reduced in the test's first 20 seconds, and after this period it continues to fall in a slower manner. On the other hand, all samples showed an initial drop in the first twenty seconds.

Table 3: Summary of chemically combined water and portlandite (AQC and $Ca(OH)_2$).

Cement paste	Cure	AQC (%)	H_2O (%) (mass loss)	$Ca(OH)_2$	CO_2 (%) (mass loss)	$CaCO_{3real}$	Residual mass
Cement CP V ARI		10.69	3.26	17.28	3.91	2.56	73.46
SCBA-A	28 days	10.28	1.89	25.00	10.69	19.30	73.12
SCBA-B		10.73	1.90	21.42	8.66	14.68	72.85
Cement CP V ARI		10.70	3.61	19.48	4.30	3.31	71.03
SCBA-A	63 days	13.11	3.59	25.29	5.26	7.23	71.84
SCBA-B		10.96	2.80	18.37	3.87	3.80	75.74
Cement CP V ARI		10.83	2.49	24.86	11.75	17.70	68.10
SCBA-A	91 days	13.11	1.69	23.54	10.62	24.14	68.59
SCBA-B		11.67	1.85	17.66	6.59	9.97	72.66

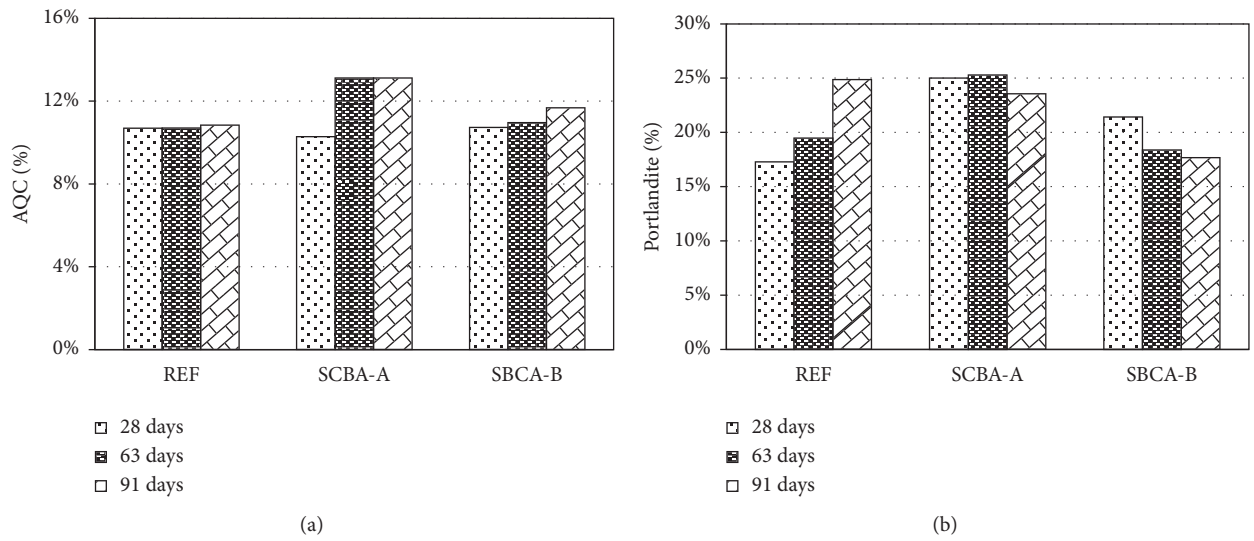

Figure 7: Chemically combined water content (AQC) and portlandite ($Ca(OH)_2$).

Table 4: Data of modified Chapelle's method for all mineral additions.

	SCBA-A	SCBA-B	FA	MET	SIL
$ICa(OH)_2$ mg CaO/g modified Chapelle's method	293	337	382	1194	1503

The electrical results showed that the essay up to 1000 s was sufficient concerning conductivity loss, attributing it to pozzolanic reactions hypothesis. In addition, Table 5 shows the variation values between initial conductivity and final conductivity for each time, 100 s and 1000 s. At the end, the conductivity loss percentage for a given time interval is determined, and this value is dependent of the reaction temperature and water, calcium hydroxide, and pozzolan ratio contained in the solution.

From Figure 8(e), the calcium hydroxide is quickly consumed, followed by direct metakaolin competitor (Figure 8(d)). In addition, the active silica and metakaolin obtained large loss of conductivities when compared with other samples in two times analyzed, 100 s and 1000 s, seemingly due to the super pozzolanic material. In addition, the results of fly ash samples (Figure 8(c)) corroborate those reported by Payá et al. [58]. It was also verified that for fly ash results up to 1000 seconds did not significantly express the entire fly ash pozzolanic potential, being necessary to extrapolate to times equal to or greater than 10000 seconds, as suggested. From Table 5, the corresponding values of %PRCond1000, for Δ1000 equal to or greater than 1.22, reveal a conductivity loss equal to 37.91% and 23.96%, respectively.

3.4. Durability Aspects. Table 6 shows the values of absorption by immersion and voids index, as well as the values of void indices, carbonation depth, passing charge, and chloride depth for all types of concrete considered in this article.

From Table 6, the reference samples exhibited larger behavior of absorption, in which the samples of silica fume obtained the lowest water absorption values. In this sense, samples with sugarcane bagasse ash have acceptable results throughout the tests. This test provided information on how much each sample absorbed water being immersed for 72 continuous hours, as well as the voids index and specific mass of each specimen. In addition, the void indices' values

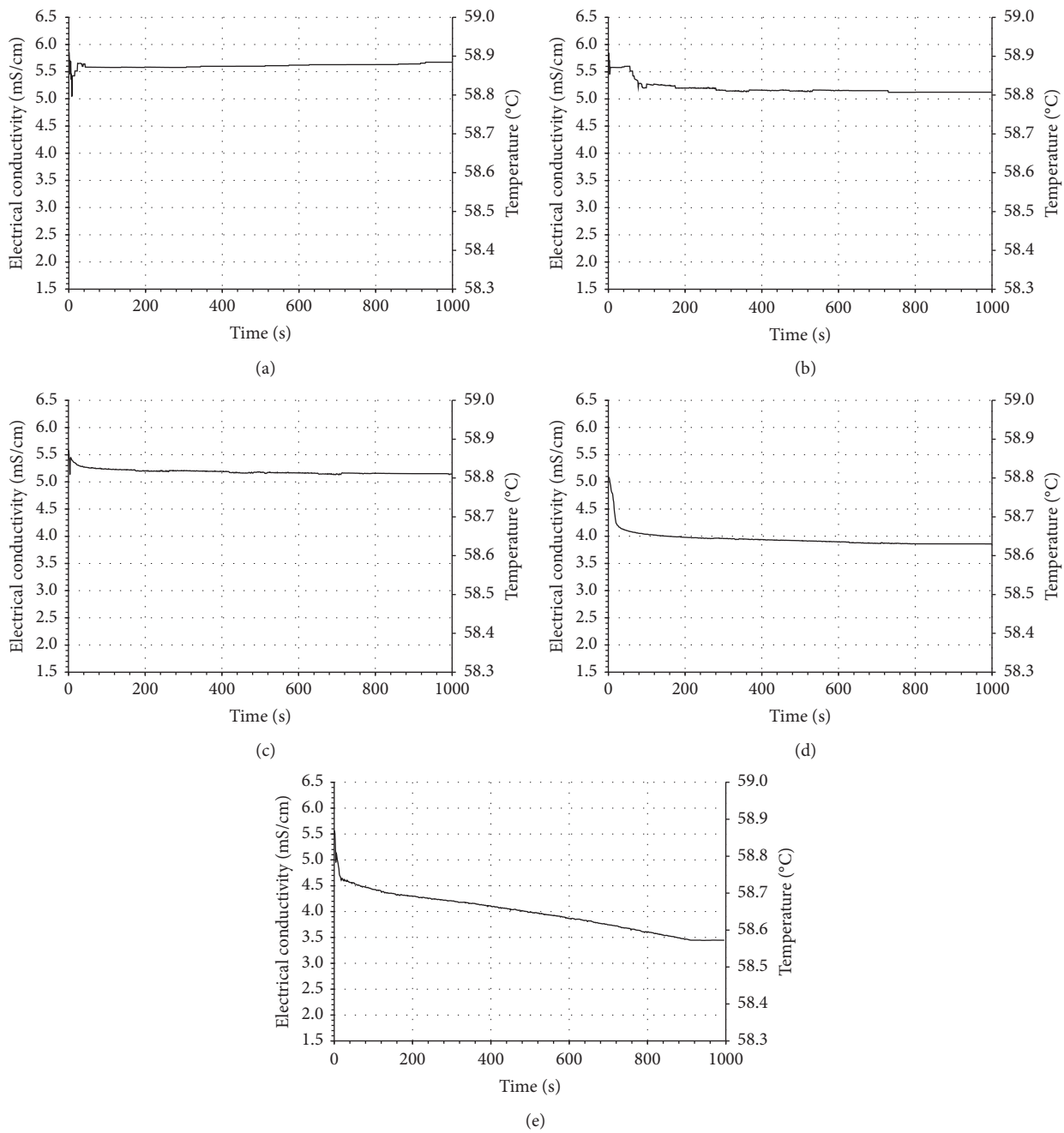

Figure 8: Electrical conductivity of (a) SCBA-A ash, (b) SCBA-B ash, (c) fly ash, (d) metakaolin, and (e) active silica.

Table 5: Summary of electrical conductivity and performance indices.

Samples	Electrical conductivity		Performance index with Portland cement (%)
	Δ_{100}	Δ_{1000}	
REF	—	—	100
SCBA-A	0.11	0.16	93
SCBA-B	0.22	0.30	98
FA	0.33	0.42	—
MET	1.04	1.22	—
SIL	1.14	2.10	—

Table 6: Data of the durability analyses.

Samples	Absorption by immersion (%)	Void indexes (%)	Carbonation depth (mm)	Passing charge (C)	Chloride depth (mm)
REF	7.39	15.58	4.7	3036	12.7
SCBA-B	7.16	15.22	6.2	1800	9.2
FA	7.34	15.67	4.9	506	5.9
MET	7.20	15.36	—	1076	3.9
SIL	6.03	12.94	2.5	86	3.3

of the reference samples were larger when compared with the other systems, especially when the silica fume is employed and when the lowest void indices were verified. In the samples of silica fume, some chemical reactions occur with the refinement of the pores, leading to a physical effect, that is, a filler effect. The samples with ash from the sugarcane bagasse CBC revealed satisfactory results, where the SCBA-B presented a lower mean void index when compared with fly ash samples.

On the other hand, for the ability of the materials to resist the carbonation processes, after the first rupture, it was possible to observe that the sugar cane bagasse ash specimens showed less depth of carbonation when compared with the active silica specimens. For specimens with fly ash addition, the carbonation progress was observed at some points that were larger than the reference samples. By considering the second rupture of the samples, the trends of the advance of the carbonation front obtained a uniform continuity, being observed that the samples with active silica obtained their values of the advance of the carbonation front at 63 days in 2.5 mm, for the samples containing fly ash obtained an advance of 4.9 mm, followed by ashes from the 6.2 mm sugarcane bagasse. The contribution of the carbonation depth values as a function of the precursor materials shown, in the thermogravimetric analyses, a significant quantity of carbonates for the SCBA-B and FA samples. Therefore, the samples containing the sugarcane bagasse ash seemingly are more suitable to react with the CO_2 molecules, allowing the advance on the carbonation front. However, regarding the results of the carbonation front, all results were promising with the depths of the carbonation front varying between 2.5 mm and 6.2 mm. Regarding the natural exposure, the mineral additions incorporated in this article were favorable to the durability of the concrete. Besides, according to ASTM C1202 [50], the reference samples (REF) obtained a moderate classification as an evaluation criterion, the SCBA-B samples obtained a low classification, and samples containing the addition of fly ash (FA) and metakaolin (MET) obtained a very low classification, in relation to the samples with the addition of active silica (SIL), which stood out with an insignificant classification and with a passing electric charge of 86 C.

From the perspective of durability associated with the resistance to chloride ions, from Table 6, a reduction in the depth of penetration with the use of mineral additions was observed; that is, all samples containing mineral additions obtained values less than 10 mm. However, the reference material presented the largest depth of penetration (12.7 mm), being the material more suitable to react with chloride ions.

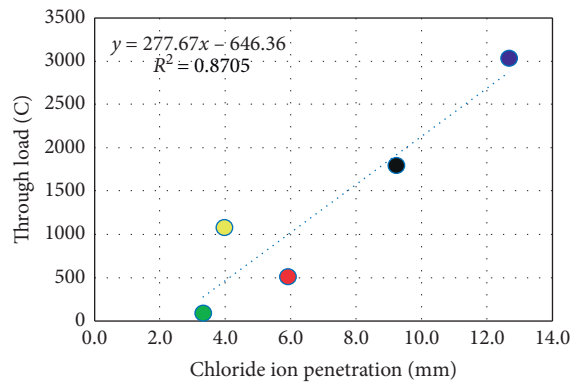

Figure 9: Linear regression analysis between the parameters of through load and depth of penetration of chloride ions.

The phenomenon of attack on reinforced concrete structures by chloride ions can be considered as a complex phenomenon due to the wide range of possible interactions between the ions and the pores of the solid; also the chloride ions also can react with hydrated phases and nanosystems present in the material [59–62]. It is also noted that the samples with mineral additions (SCBA-B) are shown as a promising material in terms of durability to resist deterioration via chloride ions. In addition, Figure 9 shows the linear regression analysis between the throughput and depth of penetration of chloride ions, where there is a considerable correlation ($R^2 = 0.8705$) between the parameters of through load and depth of penetration of chloride ions.

Finally, from the sustainability perspective, the reuse of the supplementary material SCBA-B can be useful because this material is often discarded, and significant results are obtained when compared with more popular mineral additions of samples contributing to the sustainability and preservation of natural resources.

4. Conclusions

With the analyses and results obtained, it is possible to conclude the following:

(i) Mineral addition improved concrete's properties, improving mechanical properties, refining capillary pores, and so forth. In view of pozzolanic determination analyses' results, in sugarcane bagasse samples, SCBA-A and SCBA-B, it was observed that, in some trials, SCBA-A was considered as a pozzolanic material, but in other analyses it was considered to have low reactivity, not reaching the minimum expected.

(ii) SCBA-A and SCBA-B samples did not have any type of processing (besides being dried and sifted in the 0.075 mm opening sieve), although results revealed that sugarcane bagasse ash SCBA-A can be considered as a low-pozzolanicity material. It is possible to be used as a pozzolanic material with some improvements, such as calcination and grinding, increasing its specific surface area and reactivity. Sugarcane bagasse ash SCBA-B samples were considered as medium reactivity pozzolanic material, because in analyses and assays performed the obtained results were higher than or close to the minimum of expected performance, becoming susceptible to be used as mineral addition.

(iii) Therefore, it can be concluded that there is no evident correlation between accelerated methods (modified Chapelle's and electrical conductivity) used during this research. However, in relation to nonaccelerated methods, some techniques presented a good correlation.

(iv) With SCBA-B obtaining satisfactory results, it becomes possible to use it, maintaining the same conditions of research with proportions of 15% addition.

(v) From the durability perspective, samples with 15% of sugarcane bagasse ash showed good results. Likewise, it is important to highlight that, despite some satisfactory initial results obtained, the mortar and concrete durability analyses require further research on structures' durability when sugarcane bagasse ash is added.

(vi) The phenomena that occurred during the pozzolanic reaction were complex, making it difficult to determine the reactivity of a given material, so it is only possible to identify general trends of its behavior.

Sugarcane bagasse ash has today its end in dumps; adding it to cement matrix is one more step to give concrete industry an opportunity to raise its sustainable responsibility and enhance cement performance.

Data Availability

Data are available upon request to the corresponding author.

Conflicts of Interest

The authors declare that there are no conflicts of interest regarding the publication of this paper.

Acknowledgments

This work was supported by the following: base funding, UIDB/04708/2020, and programmatic funding, UIDP/04708/2020, of the CONSTRUCT-Instituto de I&D em Estruturas e Construções. It was also funded by national funds through the FCT/MCTES (PIDDAC) and CNPq, CAPES, and FINEP (Brazilian Research Agencies). The authors also acknowledge the L'Oréal-UNESCO-ABC "For Women in Science."

References

[1] A. Saffari, M. Ataei, F. Sereshki, and M. Naderi, "Environmental impact assessment (EIA) by using the Fuzzy Delphi Folchi (FDF) method (case study: Shahrood cement plant, Iran)," *Environment, Development and Sustainability*, vol. 21, no. 2, pp. 817–860, 2019.

[2] W. Shen, Y. Liu, B. Yan et al., "Cement industry of China: driving force, environment impact and sustainable development," *Renewable and Sustainable Energy Reviews*, vol. 75, pp. 618–628, 2017.

[3] M. U. Hossain, C. S. Poon, I. M. C. Lo, and J. C. P. Cheng, "Comparative LCA on using waste materials in the cement industry: a Hong Kong case study," *Resources, Conservation and Recycling*, vol. 120, pp. 199–208, 2017.

[4] E. Wilk, M. Krówczyńska, and B. Zagajewski, "Modelling the spatial distribution of asbestos-cement products in Poland with the use of the random forest algorithm," *Sustainability*, vol. 11, no. 16, p. 4355, 2019.

[5] S. Sánchez Berriel, A. Favier, E. Rosa Domínguez et al., "Assessing the environmental and economic potential of limestone calcined clay cement in Cuba," *Journal of Cleaner Production*, vol. 124, pp. 361–369, 2016.

[6] A. Shirkhani, H. Kouchaki-Penchah, and A. Azmoodeh-Mishamandani, "Environmental and exergetic impacts of cement production: a case study," *Environmental Progress & Sustainable Energy*, vol. 37, no. 6, pp. 2042–2049, 2018.

[7] C. Chen, G. Habert, Y. Bouzidi, and A. Jullien, "Environmental impact of cement production: detail of the different processes and cement plant variability evaluation," *Journal of Cleaner Production*, vol. 18, no. 5, pp. 478–485, 2010.

[8] S. A. Miller and R. J. Myers, "Environmental impacts of alternative cement binders," *Environmental Science & Technology*, vol. 54, no. 2, pp. 677–686, 2020.

[9] M. U. Hossain, C. S. Poon, Y. H. Dong, and D. Xuan, "Evaluation of environmental impact distribution methods for supplementary cementitious materials," *Renewable and Sustainable Energy Reviews*, vol. 82, pp. 597–608, 2018.

[10] A. Sagastume Gutiérrez, J. J. Cabello Eras, C. A. Gaviria, J. Van Caneghem, and C. Vandecasteele, "Improved selection of the functional unit in environmental impact assessment of cement," *Journal of Cleaner Production*, vol. 168, pp. 463–473, 2017.

[11] D. Song, J. Yang, B. Chen, T. Hayat, and A. Alsaedi, "Life-cycle environmental impact analysis of a typical cement production chain," *Applied Energy*, vol. 164, pp. 916–923, 2016.

[12] I. Vázquez-Rowe, K. Ziegler-Rodriguez, J. Laso, I. Quispe, R. Aldaco, and R. Kahhat, "Production of cement in Peru: understanding carbon-related environmental impacts and their policy implications," *Resources, Conservation and Recycling*, vol. 142, pp. 283–292, 2019.

[13] M. Wu, Y. Zhang, Y. Ji et al., "Reducing environmental impacts and carbon emissions: study of effects of superfine cement particles on blended cement containing high volume mineral admixtures," *Journal of Cleaner Production*, vol. 196, pp. 358–369, 2018.

[14] S. Z. Carvalho, F. Vernilli, B. Almeida, M. D. Oliveira, and S. N. Silva, "Reducing environmental impacts: the use of basic oxygen furnace slag in portland cement," *Journal of Cleaner Production*, vol. 172, pp. 385–390, 2018.

[15] A. P. Gursel and C. P. Ostertag, "Impact of Singapore's importers on life-cycle assessment of concrete," *Journal of Cleaner Production*, vol. 118, pp. 140–150, 2016.

[16] P. Xu, Q. Zhao, W. Qiu, Y. Xue, and N. Li, "Microstructure and strength of alkali-activated bricks containing municipal solid waste incineration (MSWI) fly ash developed as construction materials," *Sustainability*, vol. 11, no. 5, p. 1283, 2019.

[17] J. Szulej, P. Ogrodnik, and B. Klimek, "Zeolite tuff and recycled ceramic sanitary ware aggregate in production of concrete," *Sustainability*, vol. 11, no. 6, pp. 1782–1816, 2019.

[18] M. Singh, K. Choudhary, A. Srivastava, K. Singh Sangwan, and D. Bhunia, "A study on environmental and economic impacts of using waste marble powder in concrete," *Journal of Building Engineering*, vol. 13, pp. 87–95, 2017.

[19] S. Ruan and C. Unluer, "Influence of supplementary cementitious materials on the performance and environmental impacts of reactive magnesia cement concrete," *Journal of Cleaner Production*, vol. 159, pp. 62–73, 2017.

[20] S. Sakir, S. N. Raman, M. Safiuddin, A. B. M. A. Kaish, and A. A. Mutalib, "Utilization of by-products and wastes as supplementary cementitious materials in structural mortar for sustainable construction," *Sustainability*, vol. 12, no. 9, p. 3888, 2020.

[21] T. Y. Huang, P. T. Chiueh, and S. L. Lo, "Life-cycle environmental and cost impacts of reusing fly ash," *Resources, Conservation and Recycling*, vol. 123, pp. 255–260, 2017.

[22] W.-J. Long, D. Zheng, H.-b. Duan, N. Han, and F. Xing, "Performance enhancement and environmental impact of cement composites containing graphene oxide with recycled fine aggregates," *Journal of Cleaner Production*, vol. 194, pp. 193–202, 2018.

[23] G. K. Warati, M. M. Darwish, F. F. Feyessa, and T. Ghebrab, "Suitability of scoria as fine aggregate and its effect on the properties of concrete," *Sustainability*, vol. 11, no. 17, p. 4647, 2019.

[24] Y. Kim, A. Hanif, M. Usman, M. J. Munir, S. M. S. Kazmi, and S. Kim, "Slag waste incorporation in high early strength concrete as cement replacement: environmental impact and influence on hydration & durability attributes," *Journal of Cleaner Production*, vol. 172, pp. 3056–3065, 2018.

[25] T. Nguyen, H. Mai, D. Phan, and D. Nguyen, "Responses of concrete using steel slag as coarse aggregate replacement under splitting and flexure," *Sustainability*, vol. 12, 2020.

[26] M. Sofi, Y. Sabri, Z. Zhou, and P. Mendis, "Transforming municipal solid waste into construction materials," *Sustainability*, vol. 11, no. 9, pp. 2661–2722, 2019.

[27] H.-J. Chen, N.-H. Shih, C.-H. Wu, and S.-K. Lin, "Effects of the loss on ignition of fly ash on the properties of high-volume fly ash concrete," *Sustainability*, vol. 11, no. 9, p. 2704, 2019.

[28] N. M. Azmee and N. Shafiq, "Investigating the impacts of ultra-fine calcium carbonate in high-volume fly ash concrete for structural rehabilitation for sustainable development," *Sustainability*, vol. 11, 2019.

[29] S. Pushkar, "The effect of different concrete designs on the life-cycle assessment of the environmental impacts of concretes containing furnace bottom-ash instead of sand," *Sustainability*, vol. 11, no. 15, p. 4083, 2019.

[30] E.-J. Elizondo-Martinez, P. Tataranni, J. Rodriguez-Hernandez, and D. Castro-Fresno, "Physical and mechanical characterization of sustainable and innovative porous concrete for urban pavements containing metakaolin," *Sustainability*, vol. 12, no. 10, p. 4243, 2020.

[31] G. Araya-Letelier, P. Maturana, M. Carrasco, F. C. Antico, and M. S. Gómez, "Mechanical-damage behavior of mortars reinforced with recycled polypropylene fibers," *Sustainability*, vol. 11, no. 8, p. 2200, 2019.

[32] C. Parra, E. M. Sánchez, I. Miñano, F. Benito, and P. Hidalgo, "Recycled plastic and cork waste for structural lightweight concrete production," *Sustainability*, vol. 11, no. 7, pp. 1876–1915, 2019.

[33] E. Arif, M. W. Clark, and N. Lake, "Sugar cane bagasse ash from a high-efficiency co-generation boiler as filler in concrete," *Construction and Building Materials*, vol. 151, pp. 692–703, 2017.

[34] R. G. D. Molin Filho, D. A. Longhi, R. C. T. d. Souza, R. D. Vanderlei, P. R. Paraíso, and L. M. d. M. Jorge, "Study of the compressive and tensile strenghts of self-compacting concrete with sugarcane bagasse ash," *Revista IBRACON de Estruturas e Materiais*, vol. 12, no. 4, pp. 874–883, 2019.

[35] J. P. Moretti, S. Nunes, and A. Sales, "Self-compacting concrete incorporating sugarcane bagasse ash," *Construction and Building Materials*, vol. 172, pp. 635–649, 2018.

[36] S. Singh, R.N., G. D. Ransinchung, S. Debbarma, and P. Kumar, "Utilization of reclaimed asphalt pavement aggregates containing waste from sugarcane mill for production of concrete mixes," *Journal of Cleaner Production*, vol. 174, pp. 42–52, 2018.

[37] R. A. Berenguer, A. P. B. Capraro, M. H. F. de Medeiros, A. M. P. Carneiro, and R. A. De Oliveira, "Sugar cane bagasse ash as a partial substitute of Portland cement: effect on mechanical properties and emission of carbon dioxide," *Journal of Environmental Chemical Engineering*, vol. 8, no. 2, p. 103655, 2020.

[38] ABNT NBR 16605: 2017, "Portland cement and other powdered material—determination of the specific gravity," 2020, https://www.abntcatalogo.com.br/norma.aspx?ID=372002.

[39] ABNT NBR 16372: 2015, "Portland cement and other powdered materials—determination of fineness by the air permeability method (Blaine method)," 2020, https://www.abntcatalogo.com.br/norma.aspx?ID=332676.

[40] M. Raverdy, F. Brivot, A. M. Paillere, and R. Bron, "Appréciation de l'activité pouzzolanique de constituents secondaires," in *Proceedings of the 7e Congrés International de la Chimie des Ciments*, pp. 36–41, Paris, France, 1980.

[41] M. P. Luxán, F. Madruga, and J. Saavedra, "Rapid evaluation of pozzolanic activity of natural products by conductivity measurement," *Cement and Concrete Research*, vol. 19, no. 1, pp. 63–68, 1989.

[42] ABNT NBR 12653:2014, Pozzolanic materials—requirements, 2020, http://www.consorciobradesco.com.br/.

[43] ABNT NBR 5752: 2014, "Pozzolanic materials—determination of the performance index with Portland cement at 28 days," 2020, https://www.abntcatalogo.com.br/norma.aspx?ID=315344.

[44] ABNT NBR 5739:2018, Concrete-compression test of cylindrical specimens, 2020, https://www.abntcatalogo.com.br/norma.aspx?ID=398444.

[45] ABNT NBR 7215:2019, Portland cement-determination of compressive strength of cylindrical test specimens, 2020, https://www.abntcatalogo.com.br/norma.aspx?ID=413557.

[46] ABNT NBR 7214:2015, Standard sand for cement tests-specification, 2020, https://www.abntcatalogo.com.br/norma.aspx?ID=348035.

[47] ABNT NBR 9779:2012, Mortar and hardened concrete—determination of water absorption by capillarity, 2020, https://www.abntcatalogo.com.br/norma.aspx?ID=193710.

[48] ABNT NBR 9778:2009 Hardened mortar and concrete-determination of absorption, voids and specific gravity, 2020, https://www.abntcatalogo.com.br/norma.aspx?ID=52163.

[49] R. T. 56-MHM, "CPC-18 Measurement of hardened concrete carbonation depth," *Materials and Structures*, vol. 21, pp. 453–455, 1988.

[50] ASTM C1202-19 test method for electrical indication of concretes ability to resist chloride ion penetration, 2020, http://astm.org/Standards/C1202.

[51] NBR NM 18, "Portland cement-chemical anlysis-determination of loss on ignition," 2012, https://www.abntcatalogo.com.br/norma.aspx?ID=91002.

[52] J. Dweck, A. L. Cherem da Cunha, C. A. Pinto, J. Pereira Gonçalves, and P. M. Büchler, "Thermogravimetry on calcined mass basis-hydrated cement phases and pozzolanic activity quantitative analysis," *Journal of Thermal Analysis and Calorimetry*, vol. 97, no. 1, pp. 85–89, 2009.

[53] J. Hoppe Filho, A. Gobbi, E. Pereira, V. A. Quarcioni, and M. H. F. d. Medeiros, "Atividade pozolânica de adições minerais para cimento Portland (Parte I): Índice de atividade pozolânica (IAP) com cal, difração de raios-X (DRX), termogravimetria (TG/DTG) e Chapelle modificado," *Matéria (Rio de Janeiro)*, vol. 22, no. 3, 2017.

[54] A. M. Betioli, J. Hoppe Filho, M. A. Cincotto, P. J. P. Gleize, and R. G. Pileggi, "Chemical interaction between EVA and Portland cement hydration at early-age," *Construction and Building Materials*, vol. 23, no. 11, pp. 3332–3336, 2009.

[55] ABNT NBR 15895:2010, Pozzolanic materials-determination of calcium hydroxide fi xed-modified Chapelle's method, 2020, https://www.abntcatalogo.com.br/norma.aspx?ID=80644.

[56] M. H. F. Medeiros, J. H. Filho, and P. Helene, "Influence of the slice position on chloride migration tests for concrete in marine conditions," *Marine Structures*, vol. 22, no. 2, pp. 128–141, 2009.

[57] E. Ferraz, "Pozzolanic activity of metakaolins by the French standard of the modified Chapelle test: a direct methology," *Acta Geodynamica et Geomaterialia*, vol. 12, no. 3179, pp. 289–298, 2015.

[58] J. Payá, M. V. Borrachero, J. Monzó, E. Peris-Mora, and F. Amahjour, "Enhanced conductivity measurement techniques for evaluation of fly ash pozzolanic activity," *Cement and Concrete Research*, vol. 31, no. 1, pp. 41–49, 2001.

[59] X. Liu, B. Ma, H. Tan et al., "Effect of aluminum sulfate on the hydration of Portland cement, tricalcium silicate and tricalcium aluminate," *Construction and Building Materials*, vol. 232, Article ID 117179, 2020.

[60] X. Liu, B. Ma, H. Tan et al., "Effects of colloidal nano-SiO_2 on the immobilization of chloride ions in cement-fly ash system," *Cement and Concrete Composites*, vol. 110, Article ID 103596, 2020.

[61] X. Liu, B. Ma, H. Tan et al., "Chloride immobilization of cement-based material containing nano-Al_2O_3," *Construction and Building Materials*, vol. 220, pp. 43–52, 2019.

[62] X. Liu, B. Ma, H. Tan, L. Gao, and P. Chen, "Improvement in chloride immobilization of cement-metakaolin system by triisopropanolamine," *Applied Clay Science*, vol. 193, Article ID 105656, 2020.

Hindawi
Advances in Materials Science and Engineering
Volume 2020, Article ID 5035763, 8 pages
https://doi.org/10.1155/2020/5035763

Research Article

Mechanical Performance of Concrete Made with Recycled Aggregates from Concrete Pavements

Yancong Zhang,[1,2] **Lingling Gao**,[3] **and Wei Bian**[2]

[1]*College of Highway, Chang'an University, Xi'an 710064, China*
[2]*Key Lab of Highway Construction & Maintenance Technology in Loess Region, Shanxi Provincial Transportation Technology R&D Co. Ltd., Taiyuan 030032, China*
[3]*Department of Engineering Management, Shanxi Conservancy Technical Institute, Taiyuan 030027, China*

Correspondence should be addressed to Yancong Zhang; yc_zhang@chd.edu.cn

Received 27 June 2020; Revised 28 August 2020; Accepted 29 August 2020; Published 15 September 2020

Academic Editor: Robert Černý

This research aims at analysing the mechanical performance of concrete with recycled aggregates from concrete pavements. First, the characteristics of various natural and recycled aggregates used in the concrete were thoroughly analysed. The composition of the recycled aggregates was determined and several physical and chemical tests of the aggregates were performed. In order to evaluate the mechanical performance of recycled concrete, cube compressive strength and flexural tensile strength tests were performed. The effect of recycled aggregates on the strength of recycled concrete is related to the strength of recycled aggregates, the strength of natural aggregates, and the strength of old concrete. The strength of recycled concrete decreases with increasing water-cement ratio. However, due to the water absorption of the recycled aggregate, it has a certain inhibitory effect on the strength reduction. As the replacement rate of recycled aggregates increases, the optimal sand ratio decreases. The sand ratio is controlled between 32% and 38%, which is ideal for recycled concrete. With the increase of fly ash content, the 7 d strength of recycled concrete has decreased to some extent, but the 28 d strength has been slightly improved. In addition, for compressive strength and flexural tensile strength, the optimal content of fly ash is different.

1. Introduction

In several developed countries such as Europe and the United States, the use of recycled aggregates for concrete has been for many years [1]. According to De Vries, the application of recycled aggregate in construction engineering has become a priority in many places around the world [2]. 78000 tons of recycled aggregates were used in the Netherlands in 1994. According to Collins, 10% of the total aggregates used in the United Kingdom are recycled aggregates. Meanwhile, Germany has been aiming a target of 40% recycling rate of its building and demolition waste since 1991 [3]. In the United States, nearly 100 highway paving projects by the mid-1990s had incorporated recycled aggregates in concrete for pavements.

In China, the consumption of cement is 13.71 billion tons in 2018, a year-on-year increase of 6.6%. It is estimated that approximately 246 million tons of waste concrete are currently produced annually in the mainland of China [4, 5]. The difficulties of a developing scarcity of virgin aggregate together with disposing of the concrete waste have prompted an urge to recycle waste concrete as aggregates in fresh concrete. In recent years, many Chinese investigators have engaged in the studying of recycled aggregates and nearly all aspects of mechanical property and structural performance have been covered.

Recycled aggregates from concrete pavements are concrete fragments obtained by recycled concrete pavement slabs after being crushed, washed, and classified [6–8]. Many scholars have carried out research on the mechanical

properties of concrete made with recycled aggregates from concrete pavements and have achieved many interesting results. Recycled aggregates contain certain amount of cement mortar which is characteristic of low density, big porosity, high water absorption, rough surface, and many microcracks, thus resulting in the poor property of pavement mixture containing recycled aggregates [9–12]. The majority of research conducted on recycled aggregate concrete focuses on using recycled coarse aggregates as a granular material [13–15] and as cement stabilised materials in base and subbase layers [16–18]. In contrast, there are few studies on the replacement of coarse and fine aggregate at the same time to prepare recycled concrete.

Strength is the most important mechanical indices of recycled concrete. The strength of recycled concrete is usually defined as the ability to resist external damage, sometimes the damage is equivalent to the occurrence of cracks [19]. For recycled aggregate concrete, the performance of aggregate is one of the most important factors affecting the strength of recycled aggregate concrete due to the addition of recycled aggregate [20]. Aggregate has two effects on the strength of concrete. One is the influence of the strength of the aggregate itself; the other is the influence on the interface bonding performance. In ordinary concrete, the elastic modulus of aggregate and cement mortar differ greatly. Due to cement hydration, temperature change, and load, the deformation of the two is inconsistent, resulting in interface cracks, which become the weakest link in concrete strength. In recycled concrete, the surface of recycled aggregate is covered with cement mortar. The difference between the elastic modulus of recycled aggregate and cement mortar is small, and the interface between the two is strengthened. At the same time, the recycled aggregate is highly hydrophilic and can be quickly wetted by water. Many microcracks on the surface of the recycled aggregates will suck in new cement particles, making the hydration of the contact area more complete and then forming a dense interface structure.

Based on the previous research, this study replaces coarse and fine aggregate at the same time and compares the effects of recycled aggregate replacement rate, water-cement ratio, sand ratio, and fly ash content on the mechanical properties of recycled aggregate concrete, such as cube compressive strength and flexural tensile strength.

2. Test Materials and Methods

2.1. Test Materials. Waste concrete was directly collected from concrete pavement demolishing spot, and sorting was conducted. After secondary crushing using an impact crusher or an E-crusher aggregate crushing plant, the concrete was graded into three types of fine and coarse recycled aggregates with sizes of 10–30 mm, 5–10 mm, and smaller than 5 mm. The natural aggregate used in the test was granite, including 10–30 mm, 5–10 mm, and smaller than 5 mm. The test results of physical and mechanical indices of aggregates are shown in Tables 1 and 2 according to Test methods of Aggregate for Highway Engineering (JTG E42-2005) of China.

The recycled aggregate behaved higher crushed value than the granite aggregate, but it still met the requirement of not higher than 30% in Technical Specifications for Construction of Highway Base of China. Recycled aggregate had higher needle-chip particle content than the granite aggregate. Its water absorption was far higher than that of granite aggregate.

The recycled fine aggregate showed higher sand equivalent and angularity than granite fine aggregate, but was sturdy. These indicate that recycled aggregate meets the requirements of pavement slab of highway in China.

The solid content of the water reducing agent used in the test is 23%, and the pH value is 6.8. The water reduction rate is 21%, and the chloride ion content is 0%.

2.2. Mix Proportion of Concrete. Coarse aggregate was the basis of forming the skeleton of cement concrete, while fine aggregate mainly fills in the internal void of the skeleton. The aggregate gradation had a direct impact on the performance of cement concrete [21]. The flexural strength of concrete that was made of continuous graded gravel was higher than that of discontinuous gradation.

In the test, eleven groups of continuous gradations' aggregates were prepared by replacing granite with 0%, 10%, 20%, 30%, 40%, 50%, 60%, 70%, 80%, 90%, and 100% of recycled aggregate. In each grading, fine and coarse aggregate were replaced in the same proportion. The eleven continuous gradations were shown in Figure 1. In this figure, curve "RA = 0%" is the gradation curve of natural aggregate, and curve "RA = 100%" is the gradation curve of recycled aggregate.

The mechanical properties of several kinds of recycled aggregates concrete were investigated to understand the change rule. Firstly, recycled aggregate concrete was studied with 0.10, 0.20, 0.30, 0.40, 0.50, 0.60, 0.70, 0.80, 0.90, and 1.0 aggregates replacement rate. Then, the concrete was studied with 0.29, 0.31, 0.33, 0.35, and 0.37 water-cement ratio. For sand ratio, the doping amount mainly included 0.35, 0.37, 0.39, 0.41, and 0.43. For fly ash, the doping amount mainly included 0, 0.10, 0.20, 0.30, and 0.40. The mix proportion of concrete with recycled aggregates is shown in Table 3.

It can be seen from Tables 1 and 2 that the water absorption rate of recycled aggregate is significantly higher than that of natural aggregate. To ensure that the slump of recycled concrete and natural aggregate concrete is similar, the recycled coarse and fine aggregate must be prewetted before mixing. Referring to the existing results [22], the recycled aggregates are prewetted in this test, and the water consumption is 70% of the water absorption rate of the recycled aggregates. The water consumption shown in Table 3 does not include prewetting water.

2.3. The Preparation and Test Methods of Concrete. The mixing of recycled aggregates concrete was carried out according to the test methods of cement and concrete for highway engineering (JTG E30-2005). The slump of concrete should be measured and predicted to ensure the mixing quality of recycled aggregate concrete. The vibration table

Table 1: Physical and mechanical performance of coarse aggregates.

Aggregate types	Crushed value (%)	Apparent relative density		Water absorption (%)		Needle-chip particle content (%)	
		5–10 mm	10–30 mm	5–10 mm	10–30 mm	5–10 mm	10–30 mm
Natural	18.4	2.650	2.693	1.25	1.18	2.4	3.6
Recycled	24.5	2.627	2.671	4.88	4.29	4.2	6.6

Table 2: Physical and mechanical performance of fine aggregates.

Aggregate types	Apparent relative density	Sand equivalent (%)	Water absorption rate (%)	Sturdiness (%)	Angularity (s)
Natural	2.741	60.5	1.52	7.4	46
Recycled	2.627	79.8	5.04	6.2	47

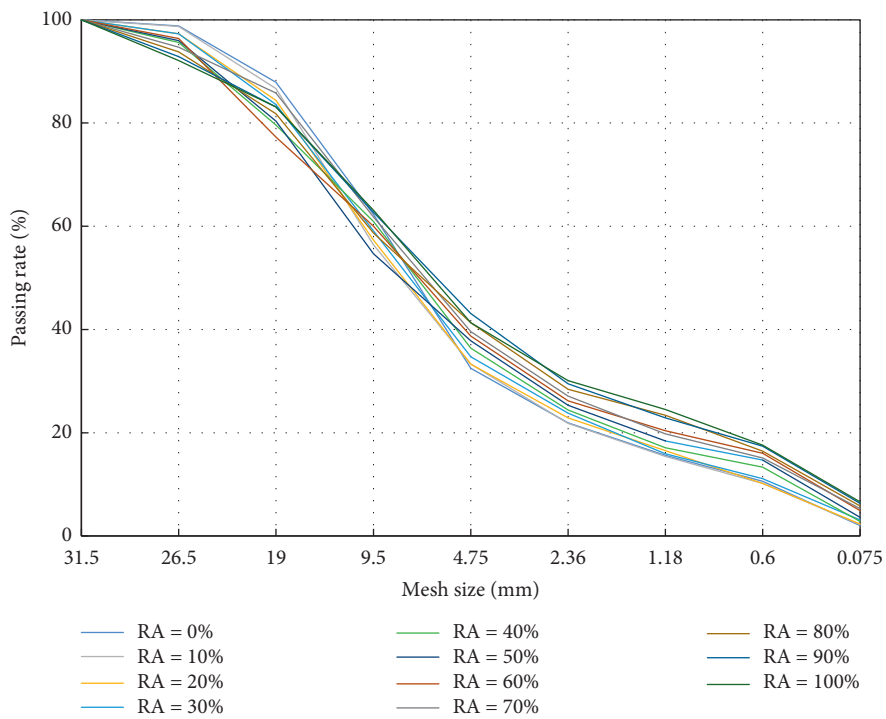

Figure 1: Grading curve.

should be used to vibrate, until the floating slurry appears on the concrete surface. Plastic film was used to seal the sample surface to reduce the moisture loss after forming. After 24 h, demould and store with a constant temperature of 20°C and humidity of 95%.

The mixing of recycled aggregate concrete was carried out according to the specification "test methods of cement and concrete for highway engineering (JTG E30-2005)".

The test methods of mechanical properties such as compressive strength and flexural tensile strength of recycled aggregate concrete were carried out according to the specification JTG E30-2005.

3. Results and Discussion

3.1. Effect of Replacement Rate of Recycled Aggregate on Strength. When the water-cement ratio is the same, the apparent density of recycled aggregate concrete decreases continuously with the increase of recycled aggregate replacement, as shown in Figure 2. As the replacement rate of recycled aggregates continues to increase, the apparent density of concrete continues to decrease. When the substitution rate is between 30% and 70%, the decrease in apparent density is larger, as shown in the curve inside the ellipse. This is due to the fact that a certain amount of mortar is attached to the surface of the recycled aggregate, resulting in a lower density of recycled aggregate than the natural aggregate. Therefore, as the replacement rate of recycled aggregate increases, the apparent density of recycled aggregate concrete decreases regularly. From another perspective, the apparent density of recycled concrete is lower than that of conventional concrete, which is beneficial to reduce the weight of concrete structure and increase the span of the structure.

Table 3: The mix proportion of concrete.

No.	Water-cement ratio (%)	Content (kg·m^3)							
		Water	Cement	Fly ash	Fine aggregates		Coarse aggregates		Water-reducing agent
					Natural	Recycled	Natural	Recycled	
RA0	0.33	122.77	370.00	0	763.00	0.00	1193.00	0.00	1.11
RA10	0.33	122.77	370.00	0	686.70	76.30	1073.70	119.30	1.11
RA20	0.33	122.77	370.00	0	610.40	152.60	954.40	238.60	1.11
RA30	**0.33**	**122.77**	**370.00**	**0**	**534.10**	**228.90**	835.10	**357.90**	**1.11**
RA40	0.33	122.77	370.00	0	457.80	305.20	715.80	477.20	1.11
RA50	0.33	122.77	370.00	0	381.50	381.50	596.50	596.50	1.11
RA60	0.33	122.77	370.00	0	305.20	457.80	477.20	715.80	1.11
RA70	0.33	122.77	370.00	0	228.90	534.10	357.90	835.10	1.11
RA80	0.33	122.77	370.00	0	152.60	610.40	238.60	954.40	1.11
RA90	0.33	122.77	370.00	0	76.30	686.70	119.30	1073.70	1.11
RA100	0.33	122.77	370.00	0	0.00	763.00	0.00	1193.00	1.11
W/C29	0.29	107.30	370.00	0	534.10	228.90	835.10	357.90	1.43
W/C31	0.31	114.70	370.00	0	534.10	228.90	835.10	357.90	1.30
W/C33	**0.35**	**129.50**	**370.00**	**0**	**534.10**	**228.90**	835.10	**357.90**	**1.09**
W/C35	0.37	136.90	370.00	0	534.10	228.90	835.10	357.90	0.98
SR29	0.35	129.50	370.00	0	479.22	205.38	889.98	381.42	1.09
SR31	0.35	129.50	370.00	0	506.60	217.12	862.60	369.68	1.09
SR35	0.35	129.50	370.00	0	561.37	240.59	807.83	346.21	1.09
SR37	0.35	129.50	370.00	0	588.76	252.32	780.44	334.48	1.09
FA10	0.35	129.50	333.00	37	534.10	228.90	835.10	357.90	1.09
FA20	**0.35**	**129.50**	**296.00**	**74**	**534.10**	**228.90**	835.10	**357.90**	**1.09**
FA30	0.35	129.50	259.00	111	534.10	228.90	835.10	357.90	1.09
FA40	0.35	129.50	222.00	148	534.10	228.90	835.10	357.90	1.09

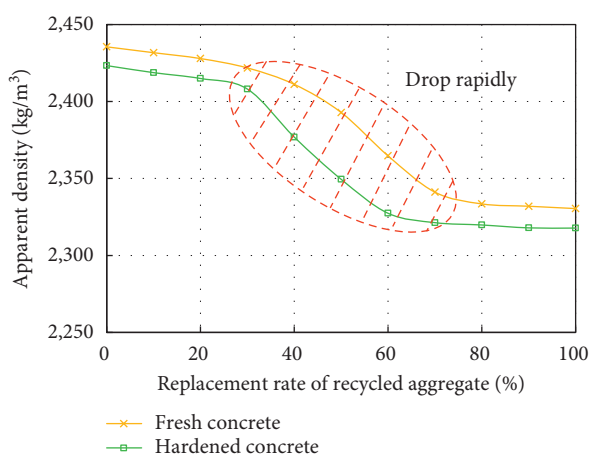

Figure 2: Apparent density of recycled aggregate concrete with different replacement rates.

The compressive strength and flexural tensile strength of recycled concrete with different recycled aggregate replacement rates are shown in Figure 3. Compared with the specimens with RA = 0, as the replacement rate of recycled aggregate continues to increase, the compressive strength and flexural tensile strength of recycled concrete decrease. Meanwhile, as the replacement rate increases, the decline is becoming more obvious. It can be seen from the two figures that even if the same mix proportion, the strength of concrete with aggregate made of recycled aggregate is still significantly lower than that of concrete with aggregate made of natural aggregate. However, due to the influence of the water absorption rate of the recycled aggregate, the true water-cement ratio of the specimens with different replacement rates is different, and the strength change is not regular.

A large number of studies have shown that [5], with the increase of recycled aggregate in recycled concrete, the strength of concrete is getting lower and lower. However, there are also data [6] shown that if the old concrete has a higher compressive strength, that is, the strength of the recycled aggregate is higher than the strength of the recycled concrete, the strength of the recycled concrete will increase as the replacement rate of the recycled aggregate increases. There are three reasons for the results of this test. First of all, the strength of recycled aggregate itself is low, resulting in a decrease in the strength of recycled concrete. It can be seen from Table 1 that the crushing value of recycled aggregate is about 32.4% lower than that of natural aggregate. Therefore, as the amount of recycled aggregate replacing natural aggregate increases, the strength of recycled concrete gradually decreased. Secondly, the water absorption rate of recycled aggregates is relatively large. After the raw material is added with water, the recycled aggregate absorbs water and causes the true water-cement ratio of the cement slurry to decrease. Therefore, as the replacement rate of recycled aggregate increases, the water-cement ratio of cement slurry continues to decrease, and the interfacial bonding between aggregates is further strengthened, resulting in an increase in the strength of recycled concrete. This is similar to the previous conclusion that replaces coarse aggregate only. Thirdly, a certain amount of cement mortar adheres to the surface of the recycled aggregate, and the surface roughness is greater

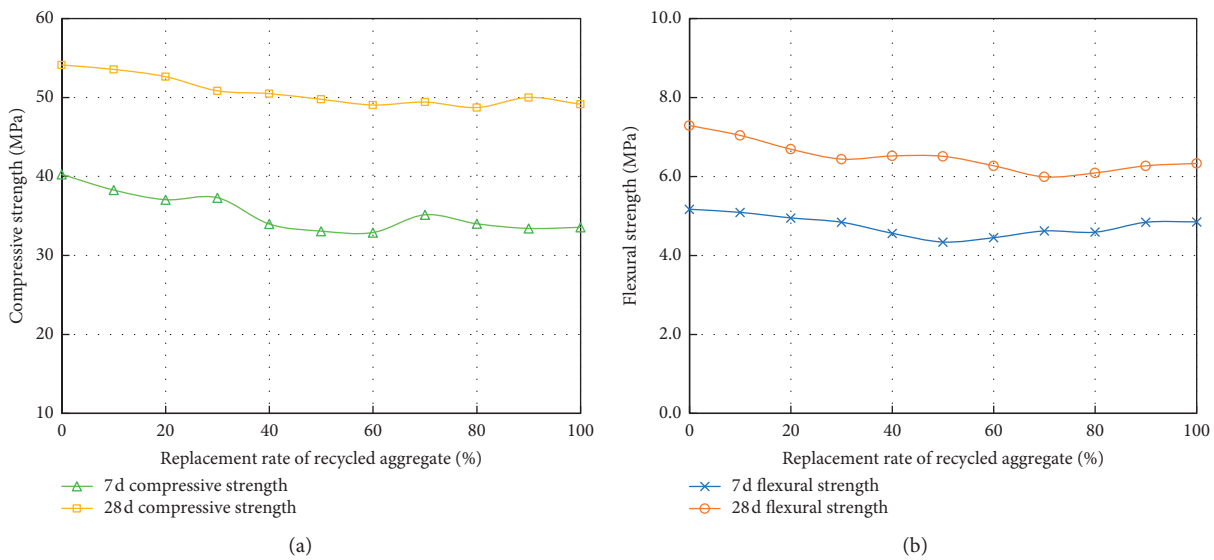

Figure 3: Strength of recycled aggregate concrete with different replacement rates. (a) The compressive strength. (b) The flexural tensile strength.

than that of natural aggregate. So, the bonding ability with the new hydration product is enhanced, and the strength of the recycled concrete is also increased.

3.2. Effect of Water-Cement Ratio on Strength of Recycled Aggregate Concrete. Water-cement ratio is one of the key factors affecting the strength of concrete. In order to study the effect of water-cement ratio on the strength of recycled concrete, five kinds of concrete with water-cement ratio were prepared in the experiment. Among them, the replacement rate of recycled aggregates is 30%. The results of strength at 7 d and 28 d tests are shown in Figure 4. It can be seen from the figures that, with the increase of water-cement ratio, the compressive strength and flexural tensile strength of recycled concrete both showed a downward trend. The water-cement ratio increased from 0.29 to 0.37, and the 28 d compressive strength and flexural tensile strength decreased by 17.9% and 14.7%, respectively. This result is consistent with the general law of the effect of water-cement ratio on concrete strength.

For the compressive strength of recycled concrete, before the water-cement ratio is less than 0.34, the decrease in compressive strength at 7 d and 28 d is greater. After the water-cement ratio is greater than 0.34, the decrease is significantly weakened. For the flexural tensile strength, there is also a turning point similar to the change law of compressive strength. After the water-cement ratio is greater than 0.32, the decrease in the flexural tensile strength at 28 d of recycled concrete is significantly weakened. The main reason for this phenomenon is that the recycled aggregate has water absorption. When the water-cement ratio is relatively small, the water is mainly absorbed by the cement and the surface of the aggregate and recycled aggregates cannot fully absorb water. As the water-cement ratio increases, a large amount of free water appears in the mixture, and this part of water is gradually absorbed by the recycled aggregate. This actually reduces the effective water-cement ratio of the recycled concrete, resulting in a decrease in the strength reduction.

3.3. Effect of Sand Ratio on Strength of Recycled Aggregate Concrete. Sand ratio has a greater impact on the workability of concrete, which in turn affects the strength of concrete. The test used a water-cement ratio of 0.35 and a recycled aggregate replacement rate of 30% to prepare recycled concrete that with 5 kinds of sand ratio. The effect of sand ratio on compressive strength and flexural tensile strength was measured. The results are shown in Figure 5. As the sand ratio increases, the strength of recycled concrete shows a trend of increasing first and then decreasing. This is true regardless of compressive strength or flexural tensile strength. This is similar to the effect of sand ratio on the strength of conventional concrete. The reason is that as the sand ratio increases, the concrete becomes denser. However, too high a sand ratio will destroy the skeleton structure of the aggregate, resulting in a drop in concrete strength.

It can be seen from the figure that the compressive strength at 28 d, the flexural tensile strength at 7 d, and the flexural tensile strength at 28 d of recycled concrete reach maximum values when the sand ratio is 39%. Therefore, recycled concrete has the same optimum sand ratio as conventional concrete. Using this sand ratio, recycled concrete can obtain maximum compressive strength and flexural tensile strength. Through a large number of experiments, when the replacement rate of recycled aggregate is 30%, the optimal sand ratio of recycled concrete is 38%–39%. As the replacement rate of recycled aggregates increases, the optimal sand ratio decreases. The sand ratio is controlled between 32% and 38%, which is ideal for recycled concrete.

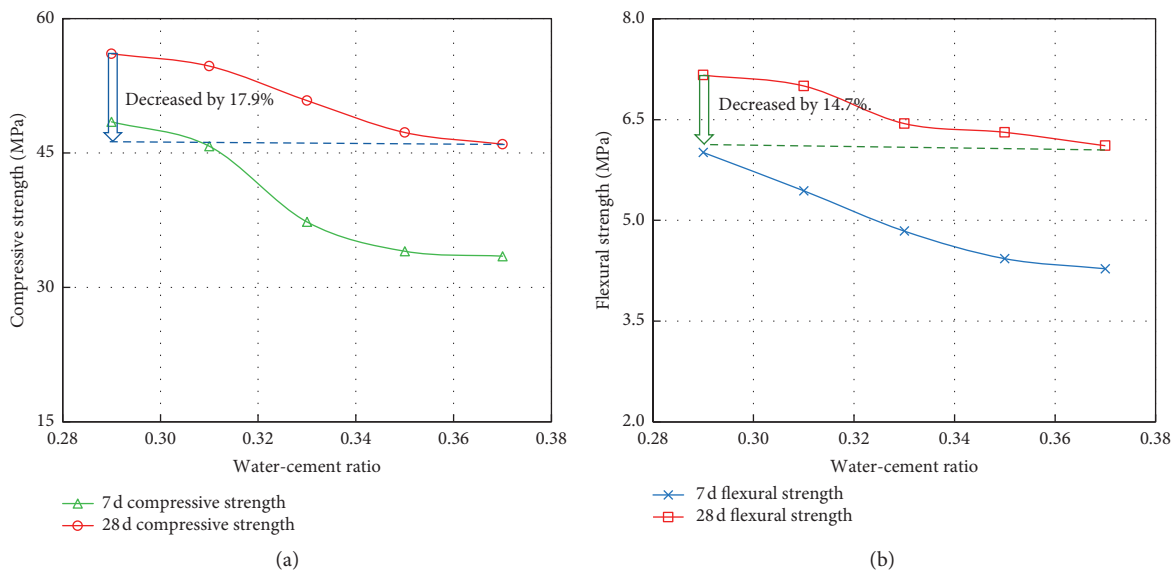

Figure 4: Strength of recycled aggregate concrete with different water-cement ratios. (a) The compressive strength. (b) The flexural tensile strength.

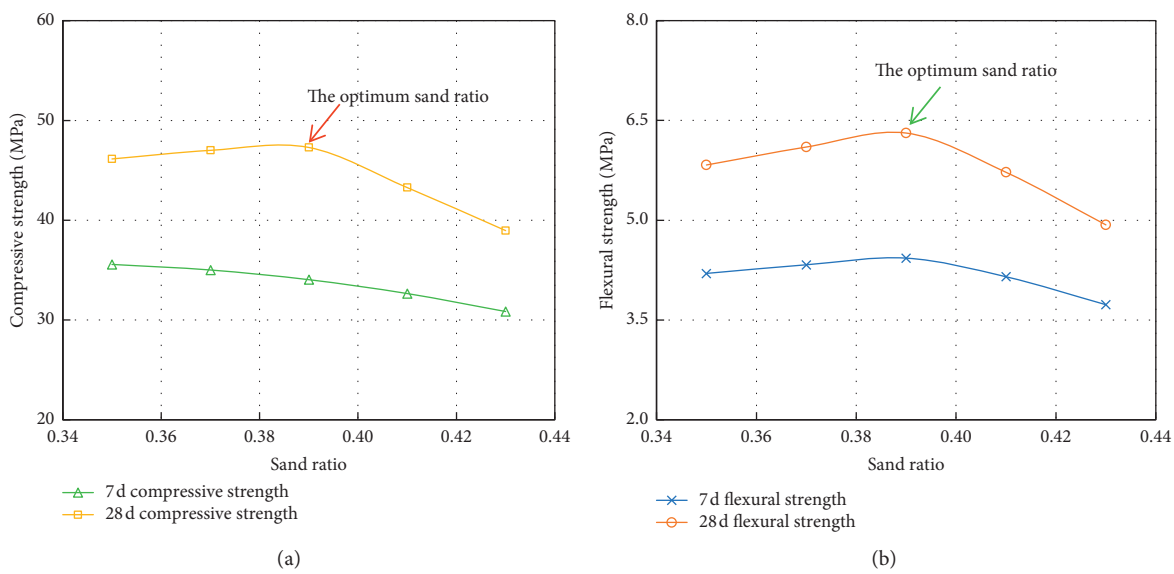

Figure 5: Strength of recycled aggregate concrete with different sand ratios. (a) The compressive strength. (b) The flexural tensile strength.

3.4. Effect of Fly Ash on Strength of Recycled Aggregate Concrete. Adding fly ash to concrete can improve the workability, compactness, and durability of concrete. Several groups of recycled concrete specimens with different contents of fly ash were prepared in the experiment. The water-cement ratio of these specimens is 0.35, and the replacement rate of recycled aggregates is 30%. Then, the effect of the fly ash content on the compressive strength and flexural tensile strength was measured. The results are shown in Figure 6. With the increase of fly ash content, the strength of recycled concrete at 7 d has decreased to some extent, but the strength at 28 d has been slightly improved. This is similar to the effect of fly ash content on the strength of conventional concrete [7]. There are two main reasons for this result: on the one hand, fly ash has a volcanic ash effect, but the effect is not obvious in the first 7 d; on the other hand, the addition of fly ash improves the density of concrete, making 28 d strength has been greatly improved.

However, for recycled concrete, the more fly ash is not the better even for 28 d strength. It can be seen from the figure that, during the increase of the fly ash content from 0 to 30%, the compressive strength and flexural tensile strength at 28 d increased by 16% and 4.9%, respectively. However, when the fly ash content increased to 40%, the 28 d compressive strength and flexural tensile strength decreased to varying degrees. For compressive strength and flexural

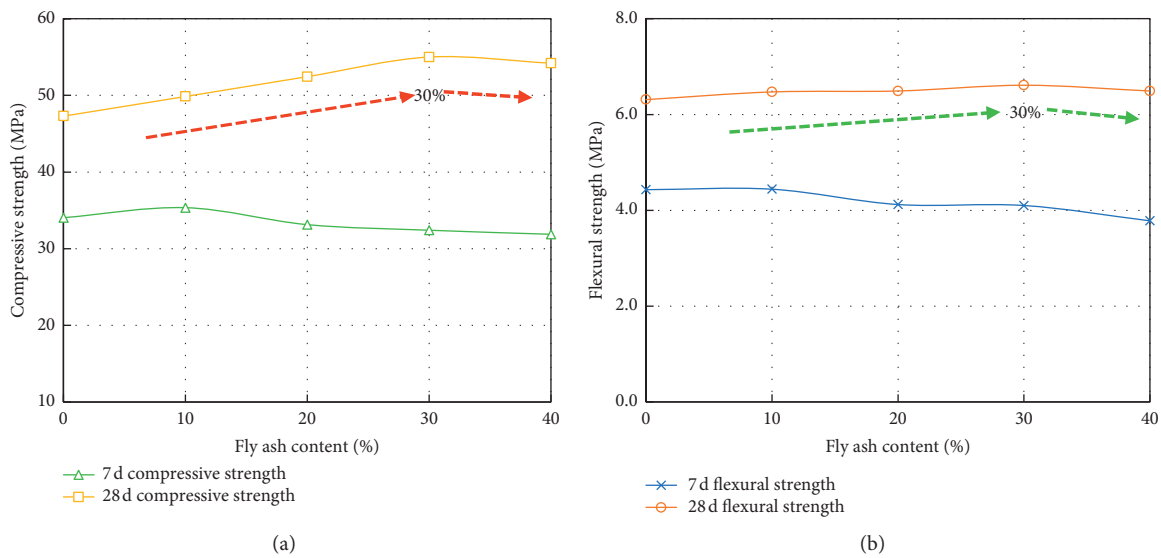

Figure 6: Strength of recycled aggregate concrete with different fly ash contents. (a) The compressive strength. (b) The flexural tensile strength.

tensile strength, the optimal content of fly ash is different. Therefore, for recycled concrete, the content of fly ash should be determined according to the compressive or flexural needs of the structure and the changes in compressive strength and flexural tensile strength.

4. Conclusion

(1) The effect of recycled aggregates on the strength of recycled concrete is related to the strength of recycled aggregates, the strength of natural aggregates, and the strength of old concrete. As the replacement rate of recycled aggregates increases, the strength of recycled concrete may increase or decrease.

(2) The strength of recycled concrete decreases with increasing water-cement ratio. However, due to the water absorption of the recycled aggregate, it has a certain inhibitory effect on the strength reduction. The greater the content of recycled aggregates, the more obvious the inhibition effect of the strength reduction of recycled concrete.

(3) Recycled concrete has the optimum sand ratio as conventional concrete. When the replacement rate of recycled aggregate is 30%, the optimal sand ratio of recycled concrete is 38%–39%. As the replacement rate of recycled aggregates increases, the optimal sand ratio decreases. The sand ratio is controlled between 32% and 38%, which is ideal for recycled concrete.

(4) With the increase of fly ash content, the strength of recycled concrete at 7 d has decreased to some extent, but the strength at 28 d has been slightly improved. In addition, for compressive strength and flexural tensile strength, the optimal content of fly ash is different.

Data Availability

The data used to support the findings of this study are available from the corresponding author upon request.

Conflicts of Interest

The authors declare that there are no conflicts of interest regarding the publication of this paper.

Acknowledgments

This work was supported by the National Natural Science Foundation of China (no. 51808329) and Science and Technology Project of Shanxi Transportation Holding Group Co., Ltd. (nos. 19-JKKJ-6 and 19-JKKJ-67).

References

[1] K. Verian, "Using recycled concrete as coarse aggregate in pavement concrete," MS Thesis, Purdue University, West Lafayette, IN ,USA, 2012.

[2] N. D. Oikonomou, "Recycled concrete aggregates," *Cement and Concrete Composites*, vol. 27, no. 2, pp. 315–318, 2005.

[3] A. V. Acker, "Recycling of concrete at a precast concrete plant," in *Proceedings of the Sustainable Construction: Use of Recycled Concrete Aggregate*, pp. 321–332, London, UK, November 1998.

[4] L. Wang and C. Li, "Research progress on the development and utilization of fly ash resources technology," *Mineral Protection and Utilization*, vol. 39, no. 4, pp. 38–45, 2019.

[5] T. Liu, Y. Zhang, M. Xu et al., "Research on the calculation of CO_2 emission of raw material carbonate decomposition in cement enterprises," *China Cement*, vol. 26, no. 2, pp. 77–80, 2019.

[6] M. S. Rahman and S. I. Ahmad, "Strength properties of concrete made from recycled brick concrete and EAF slag blended as coarse aggregate," *Materials Science Forum*, vol. 984, pp. 207–212, 2020.

[7] J. Xiao, J. Li, and Y. Lan, "The latest progress and comments on the research of recycled concrete technology," *Concrete*, vol. 10, pp. 17–20+57, 2003.

[8] D. Yang, Y. Hao, and T. Wang, "Experimental research on recycled aggregate concrete for highway pavement," in *Proceedings of the ICCTP 2010*, Beijing, China, August 2010.

[9] Y. Hou, X. Ji, X. Su, W. Zhang, and L. Liu, "Laboratory investigations of activated recycled concrete aggregate for asphalt treated base," *Construction and Building Materials*, vol. 65, pp. 535–542, 2014.

[10] J. Qiu, D. Q. S. Tng, and E.-H. Yang, "Surface treatment of recycled concrete aggregates through microbial carbonate precipitation," *Construction and Building Materials*, vol. 57, pp. 144–150, 2014.

[11] C. Shi, Y. Li, J. Zhang, W. Li, L. Chong, and Z. Xie, "Performance enhancement of recycled concrete aggregate - a review," *Journal of Cleaner Production*, vol. 112, pp. 466–472, 2016.

[12] Y. Hou, X. Ji, and X. Su, "Mechanical properties and strength criteria of cement-stabilised recycled concrete aggregate," *International Journal of Pavement Engineering*, vol. 20, no. 3, pp. 339–348, 2019.

[13] C. S. Poon and D. Chan, "Feasible use of recycled concrete aggregates and crushed clay brick as unbound road sub-base," *Construction and Building Materials*, vol. 20, no. 8, pp. 578–585, 2006.

[14] I. Vegas, J. A. Ibañez, A. Lisbona, A. Sáez de Cortazar, and M. Frías, "Pre-normative research on the use of mixed recycled aggregates in unbound road sections," *Construction and Building Materials*, vol. 25, no. 5, pp. 2674–2682, 2011.

[15] M. Diagne, J. M. Tinjum, and K. Nokkaew, "The effects of recycled clay brick content on the engineering properties, weathering durability, and resilient modulus of recycled concrete aggregate," *Transportation Geotechnics*, vol. 3, pp. 15–23, 2015.

[16] A. Arul, J. Piratheepan, Y. Ali et al., "Geotechnical properties of recycled concrete aggregate in pavement sub-base applications," *Geotechnical Testing Journal*, vol. 35, no. 5, pp. 1–9, 2012.

[17] M. M. Disfani, A. Arulrajah, H. Haghighi, A. Mohammadinia, and S. Horpibulsuk, "Flexural beam fatigue strength evaluation of crushed brick as a supplementary material in cement stabilized recycled concrete aggregates," *Construction and Building Materials*, vol. 68, pp. 667–676, 2014.

[18] M. Alireza, A. Arul, S. Jay et al., "Laboratory evaluation of the use of cement-treated construction and demolition materials in pavement base and subbase applications," *Journal of Materials in Civil Engineering*, vol. 27, no. 6, pp. 1–12, 2015.

[19] B. Huang and X. Pi, *Building Materials*, China Construction Industry Press, Beijing, China, 1995.

[20] T. C. Hansen and H. Narud, "Strength of recycled concrete made from crushed concrete coarse aggregate," *Concrete International*, vol. 5, no. 1, pp. 79–83, 1983.

[21] J. Shen and Y. Zhang, "Fiber-reinforced mechanism and mechanical performance of composite fibers reinforced concrete," *Journal of Wuhan University of Technology-Mater. Sci. Ed.*, vol. 35, no. 1, pp. 121–130, 2020.

[22] S. Zhang, "Water absorption and water return characteristics of recycled aggregate and its effect on concrete shrinkage," PhD Thesis, Beijing Architecture University, Beijing, China, 2019.

Hindawi
Advances in Materials Science and Engineering
Volume 2020, Article ID 8037131, 15 pages
https://doi.org/10.1155/2020/8037131

Research Article

Structural Behavior of Concrete Beams Containing Recycled Coarse Aggregates under Flexure

In-Hwan Yang,[1] **Jihun Park**,[1] **Kyoung-Chul Kim**,[2] **and Hyungbae Lee**[3]

[1]*Department of Civil Engineering, Kunsan National University, Kunsan, Jeonbuk 54150, Republic of Korea*
[2]*Structural Engineering & Bridges Research Division, Korea Institute of Civil Engineering and Building Technology, Goyang, Gyeonggi 10223, Republic of Korea*
[3]*Department of Environmental Management Business, EPS Engineering, Anyang, Gyeonggi 13930, Republic of Korea*

Correspondence should be addressed to In-Hwan Yang; ihyang@kunsan.ac.kr

Received 30 January 2020; Revised 30 April 2020; Accepted 15 June 2020; Published 4 July 2020

Academic Editor: Robert Černý

The structural behavior of concrete beams containing recycled coarse aggregates (RCAs) was investigated in this study using detailed experimental data. Twelve concrete beams were tested in the experimental program: nine beams with varying RCA contents and three control beams with natural coarse aggregates (NCAs). The parameters for investigating the structural behavior of the RCA concrete beams under flexure were the RCA content (30%, 50%, and 100%) and tensile rebar ratio (0.50%, 0.79%, and 1.14%). The crack pattern of the RCA beams was similar to that of the NCA beams; however, the RCA beams exhibited smaller crack spacing than the NCA beams. The flexural strength was slightly affected by the RCA content. However, the ductility of the beam was not significantly influenced by the RCA content. A comparison of the experimental results and the calculations from the ACI 318 and EC 2 provisions for the flexural strength showed that the current provisions conservatively predicted the flexural strength of the RCA concrete beams.

1. Introduction

The replacement of aging infrastructures and buildings results in large quantities of construction waste, especially concrete waste. Concrete waste generated from demolition work contains many aggregates. Because aggregates occupy the majority of the concrete volume, it is reasonable to investigate reusing the aggregates from concrete waste to create new concrete [1–3]. Recycled coarse aggregates (RCAs) have been used in many laboratory experiments [4–6].

Due to the potential economic and environmental benefits, interest in technology for processing waste concrete and the use of RCAs is rapidly increasing [7, 8]. The advantages of using RCAs include a reduction in the use of natural coarse aggregate (NCA) resources and a decrease in the amount of waste disposed in landfills, thereby diminishing environmental pollution.

Despite the high demand, RCAs are primarily used in road bases and nonstructural concrete. Only a small percentage of RCAs is used in structural concrete because the quality of RCAs is less reliable than that of NCAs. Comprehensive experimental research has been performed to assess the properties of both NCA and RCA concrete at the material level [9–14]. Several experimental studies have investigated the flexural behavior of RCA concrete beams at the structural level [15–21]; however, the results from these studies are contradictory.

Seare-Paz et al. [15] studied the structural behavior of concrete beams containing three different RCA contents: 20%, 50%, and 100%. Their results showed that the moment capacity of the RCA beams was similar to that of conventional concrete beams. They also reported that the crack pattern in the RCA beams was similar to that in conventional concrete beams.

Sunayana and Barai [16] performed an experimental study on concrete beams with 100% recycled aggregates at three different rebar ratios. Their results showed that the moment capacity of the RCA and conventional concrete

beams was similar at low rebar ratios. In addition, numerous closely spaced cracks were present in the RCA beams.

To investigate the flexural behavior of semiprecast T-beams, Fahmy and Idriss [17] performed bending tests on three beams containing a combination of recycled fine aggregates and RCAs and compared the results to those from the NCA concrete beam. Their test results showed that the load capacity of the RCA beams was greater than that of the control beam.

Kang et al. [18] tested RCA beams with $135 \times 270\,\text{mm}^2$ cross sections for both normal- and high-strength concrete. The RCA beams had RCA contents up to 30% for high-strength concrete and up to 50% for normal-strength concrete. The test results showed that the RCA beams sustained more cracks and exhibited less ductility than the conventional concrete beams.

Arezoumandi et al. [19] tested eight beams, including four RCA beams. Their test results showed that the crack spacing in the RCA beams was smaller than that in the conventional concrete beams. Moreover, the RCA beams exhibited a higher ultimate deflection than the conventional concrete beams. However, the ultimate moments of the RCA beams and the conventional concrete beams were similar.

Although several studies have investigated the flexural performance of RCA concrete beams, the results are conflicting. In addition, there are few test results of large-scale RCA beams with RCA contents up to 100%. Therefore, the purpose of this study was to explore the structural behavior of RCA concrete beams under flexure.

A total of twelve concrete beams were created and then tested under four-point bending. Nine beams were constructed with RCA concrete, and three control beams were constructed with NCA concrete. The parameters in this study were the RCA content (30%, 50%, and 100%) and tensile rebar ratio (0.50%, 0.79%, and 1.14%). The investigation of structural behavior included the cracking pattern, ductility, and ultimate flexural strength.

2. Research Significance

Extensive experimental studies of flexural characteristics are scarce for RCA beams, especially for concrete beams with RCA contents above 50%. The use of RCAs is increasing as worldwide environmental problems require more eco-friendly solutions. Therefore, in this study, the characteristics of the structural behavior, crack patterns, failure patterns, ductility, and ultimate strength of concrete beams with RCA contents ranging from 0 to 100% were investigated under flexure. The experimental data presented in this study provide valuable information for understanding the flexural strength and structural behavior of concrete beams containing RCAs.

3. Material Properties

3.1. Materials and Mixture Properties. Two types of coarse aggregates were used in this experimental setup, as shown in Figure 1. The RCAs used in this study were obtained from the demolition of concrete structures, and accordingly, they did not include ceramic. The RCAs were produced by crushing waste concrete to a maximum size of 13 mm, whereas the NCAs were produced by crushed stone to a maximum diameter of 25 mm.

NCAs with a maximum size of 25 mm are commonly used in Korea. Therefore, the 25 mm NCAs were applied in this study. The RCAs were obtained by demolishing existing aged concrete structures and crushing the concrete, which reduced the size of the RCAs. In Korea, the maximum size of RCAs is usually less than 18 mm. The effect of the coarse aggregate size on the mechanical properties of RCA concrete was investigated in the study by Meddah et al. [22]. This study showed that concrete mixtures with small RCAs (3–15 mm) had 1.8% higher compressive strength than the concrete mixtures with large RCAs (15–25 mm). Therefore, the size effect of the RCAs on the strength of the RCA concrete was not considered in this study.

Natural sand was used as the fine aggregates. The properties of the coarse aggregates, including the even-dry density (or specific gravity), absorption, and maximum diameter, are shown in Table 1. As expected, the RCAs had a lower specific gravity and higher absorption than the NCAs.

The mixture proportions for the test beams containing RCAs and NCAs are given in Table 2. The volume of NCAs in the mixtures was replaced by RCAs at three different replacement ratios: 30%, 50%, and 100%. The concrete mixtures had a target compressive strength of 35 MPa. Portland cement was used in the concrete mixture. The water-to-cement (w/c) ratio was 0.38. In addition, for this experiment, a high-range water reducer (HRWR) was used to control the workability of the concrete.

3.2. Mechanical Properties of the Materials. The compressive strength of the concrete was obtained through compressive testing of cylindrical specimens with diameters of 100 mm and heights of 200 mm. When the test beams were fabricated, cylindrical specimens were fabricated with each batch.

Two types of compression test shapes are normally used: cubes and cylinders. Cylinders are the standard specimens used in the United States [23] and Korea [24]. According to KS F 2405 [24], the standard cylindrical specimen has dimensions of $100\,\text{mm} \times 200\,\text{mm}$ or $150\,\text{mm} \times 300\,\text{mm}$, and the diameter of the cylinders must be greater than three times the maximum size of the coarse aggregates.

A cylinder with dimensions of $100\,\text{mm} \times 200\,\text{mm}$ was selected for this study because the maximum size of the coarse aggregates used in this study was 25 mm. To calculate the compressive strength of a cylinder with a diameter of 150 mm, a correction factor of 0.97 should be multiplied to the compressive strength of a cylinder with a 100 mm diameter [25].

The samples were loaded with a universal testing machine operating in displacement control mode. The axial deformations of the cylinders were measured accurately from the initiation of loading through failure. The load and the output from the three linear variable displacement transducers (LVDTs) were digitally recorded throughout the tests.

(a) (b)

Figure 1: Coarse aggregates. (a) NCAs. (b) RCAs.

Table 1: Properties of the coarse aggregates.

	Even-dry density (g/cm^3)	SD (g/cm^3)	Absorption (%)	SD (%)	Fineness modulus	Maximum diameter (mm)
Recycled coarse aggregate	2.49	0.13	2.95	0.37	6.36	13
Natural coarse aggregate	2.62	0.17	0.57	0.11	6.55	25

SD: standard deviation.

Table 2: Mix proportions for the test beams.

	RCA content by volume (%)	Unit weight (kg/m^3)					
		Water	Cement	Fine aggregate	Coarse aggregate		HRWR
					Natural	Recycled	
R000 series	0	183	482	767	888	0	3.37
R030 series	30	183	482	767	622	253	3.62
R050 series	50	183	482	767	444	422	3.86
R100 series	100	183	482	767	0	844	4.82

The stress-strain curve of each batch of concrete was obtained based on the load-displacement relationship measured during the test, which was subsequently used to compute the compressive strength and elastic modulus. The mean values of the compressive strength and the elastic modulus of each concrete beam are listed in Table 3. The test results show that the compressive strength and elastic modulus of the concrete decreased as the RCA content increased. However, the decrease in the rupture modulus of the concrete was not significant, when the RCA content increased to 50%, whereas the decrease in the rupture modulus became significant when the RCA content increased to 100%.

In addition, although HRWR was used to ensure the workability of the RCA concrete mixture, the real water-cement ratio in each mixture might not be maintained due to the high water absorption from the RCAs. Accordingly, the mechanical properties of the RCA concrete may be affected.

For each test beam, two D13 (nominal diameter = 13 mm), two D16 (nominal diameter = 16 mm), or two D19 (nominal diameter = 19 mm) reinforcing bars were used as tensile reinforcement. For each size, yield strength values of 516.3 MPa, 434.9 MPa, and 517.5 MPa were obtained from the rebar tension test. In addition, the ultimate strains at the peak stress for each rebar size were 0.0192, 0.0212, and 0.0136.

4. Test Program

4.1. Beam Specimen Design. Twelve concrete beams were tested, the experimental parameters of which are listed in Table 3. All beams had rectangular cross sections with widths of 200 mm and heights of 300 mm. The test parameters in the experiment were the RCA content and tensile rebar ratio. Three RCA contents (30%, 50%, and 100%) and three tensile reinforcement ratios (0.50%, 0.79%, and 1.14%) were adopted in this study.

Table 3: Concrete properties and experimental parameters of the test beams.

Test beam	Concrete properties						Experiment parameters		
	Compressive strength (MPa)	SD (MPa)	Elastic modulus (MPa)	SD (MPa)	Rupture modulus (MPa)	SD (MPa)	RCA content (%)	Tensile rebar size	Rebar ratio (%)
R000-S1								2 × D13	0.50
R000-S2	38.3	1.5	22,685	836	4.7	0.8	0	2 × D16	0.79
R000-S3								2 × D19	1.14
R030-S1								2 × D13	0.50
R030-S2	35.6	0.5	21,890	431	4.6	1.1	30	2 × D16	0.79
R030-S3								2 × D19	1.14
R050-S1								2 × D13	0.50
R050-S2	33.2	2.1	20,661	336	4.4	0.6	50	2 × D16	0.79
R050-S3								2 × D19	1.14
R100-S1								2 × D13	0.50
R100-S2	31.7	0.9	18,915	501	3.9	0.7	100	2 × D16	0.79
R100-S3								2 × D19	1.14

SD: standard deviation.

The test beams in Table 3 were named to indicate the RCA content and tensile rebar ratios. The three different tensile reinforcement ratios, 0.50%, 0.79%, and 1.14%, were denoted as S1, S2, and S3, respectively. For example, R050-S2 indicates that the beam has an RCA content of 50% and a tensile rebar ratio of 0.79%. R000 series beams are reference beams containing no RCAs. Four groups of test beams with different RCA contents were studied, and each group contained three beams with different rebar ratios.

For all beams, transverse reinforcements were provided to prevent shear failure. Stirrups with nominal diameters of 10 mm (D10) were used for transverse reinforcement, but no stirrups were used in the constant moment region to avoid the confinement effect on the flexural behavior. Two top rebars with a nominal diameter of 10 mm were used to hold the stirrups. The test beam dimensions are shown in Figure 2.

4.2. Fabrication of the Beam Specimens. Steel molds were used to fabricate the beam specimens. After assembling the forms, the rebar was arranged, and the rebar strain gauges were installed in the midspan to measure the strain in the tensile rebar at each loading step during the test.

After pouring, the concrete was compacted using vibration. The beam specimens were covered with both wet burlap and plastic sheets upon completion of the concrete casting. All beams and companion concrete cylinders were moist-cured for seven days. The beam specimens were then demolded and air-cured until 28 days after the concrete was poured.

4.3. Test Setup and Instrumentation. The beams were tested under simply supported four-point loading conditions, as shown in Figure 3. The total length of each test beam was 3.3 m, and the simple supports were located 150 mm from each end of the beam; that is, the clear span length was 3.0 m. A steel spreader beam was installed between the test beam specimen and the actuator to distribute the single point load into two point loads. The two loads were applied 300 mm from the midspan through the steel spreader beam. Therefore, the shear span of each beam was 1.2 m, and the constant moment region was the center 0.6 m of the beam.

The instrumentation system shown in Figure 4 consisted of LVDTs and electrical resistance strain gauges. Electrical resistance strain gauges were used to measure the strain in the concrete and the steel rebar. Five strain gauges were located on the side surface of the beam in the midspan to measure the strain at different heights. These strain gauges were mounted on the surface of the rear side of the beam specimen. The length of the strain gauges mounted on the concrete was 60 mm. Individual gauges were used until their readings became unreliable due to cracking in the underlying concrete. They were able to detect strain from small crack openings at each location. However, the concrete strain gauges became unreliable as the crack width increased. Three steel strain gauges were bonded to each tensile rebar in the beam midspan. In addition, the LVDTs were placed in the midspan and at the loading points to measure the beam deflections.

The load was applied to the beams using hydraulic jacks. Each beam test was conducted at a crosshead displacement rate of 1.5 mm/min. The test was performed until beam failure. The applied load, deflection, and strain in both the concrete and the rebar, the development and propagation of cracks, and the width of each crack were recorded until beam failure.

4.4. Calculating the Ductility and Flexural Strength of the Concrete Beams. The ductility of a concrete structure can be interpreted as a measure of the energy absorption capacity of the structural member. In general, the ductility of a concrete structure can be quantified via the ductility index, which can be expressed in terms of the deflection ductility index [26]. Midspan deflection measurements are necessary only for the deflection ductility index, and its measurement is relatively easy. The deflection ductility index, shown in (1), was used to

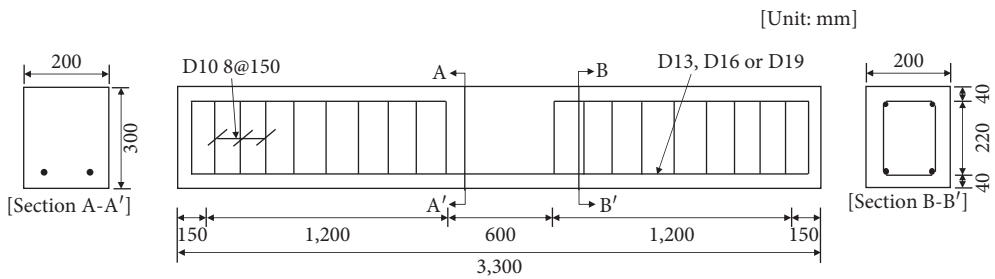

Figure 2: Test beam dimensions.

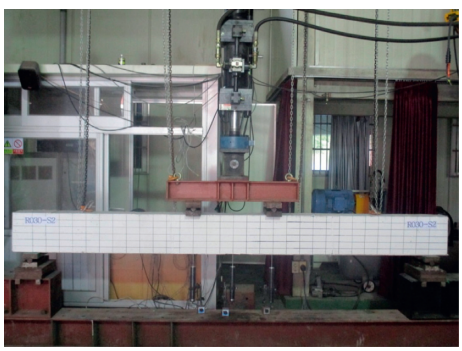

Figure 3: Test setup for the beam specimens.

examine the ductility characteristics of the members as follows:

$$\mu = \frac{\Delta_u}{\Delta_y}, \tag{1}$$

where μ is the ductility index of the member, Δ_u is the deflection of the member at the ultimate load, and Δ_y is the deflection of the member at the yielding load. The deflection at the ultimate load corresponds to the peak point in the load-deflection curve.

For the flexural strength of the concrete beams, the experimental results were compared with the calculations from the ACI 318 flexural design provision [27], EC 2 provision [28], and modified compression field theory (MCFT) using the Response 2000 program [29, 30]. The ACI 318 flexural design provision [27] is as follows:

$$M_n = A_s f_y \left(d - \frac{a}{2}\right), \quad a = \frac{A_s f_y}{0.85 f_c' b}, \tag{2}$$

where A_s is the area of the tensile rebar, f_y is the measured yield strength of the rebar, d is the effective depth, a is the depth of an equivalent rectangular compressive stress block, f_c' is the concrete measured compressive strength, and b is the width of a rectangular beam.

The EC 2 provision [28] for flexural capacity is as follows:

$$M_n = Tz = T \cdot \left(d - \frac{a}{2}\right), \quad T = A_s f_{yd}, \quad a = \frac{A_s f_{yd}}{\eta f_{cd} b}, \quad f_{cd} = \frac{\alpha_{cc} f_{ck}}{\gamma_c}, \quad f_{yd} = \frac{f_y}{\gamma_s}, \tag{3}$$

where T is the tensile force on the rebar, f_{yd} is the design yield strength of the rebar, f_y is the measured yield strength of the rebar, f_{cd} is the design value of the concrete compressive strength, f_{ck} is the measured concrete compressive strength, γ_c is the partial safety factor for the concrete, γ_s is the partial safety factor for the rebar, and α_{cc} is a coefficient (=0.85 in this study) that considers the long-term effects on the compressive strength and the unfavorable effects resulting from the way the load is applied.

To calculate the nominal flexural strength of the NCA and RCA concrete beams as accurately as possible, γ_c and γ_s are assumed to be 1.0. For the design of concrete structures, the selected values of the partial safety factors, γ_c and γ_s, are less than 1.0 to ensure the structural safety of the concrete structures. However, these values are set to 1.0 in this study to predict the actual flexural strength of the test beams.

The Response 2000 program incorporating the MCFT is a sectional analysis program that can calculate the strength of a reinforced concrete cross section subjected to shear, flexure, and axial loading [30].

5. Test Results and Discussion

5.1. Crack and Failure Patterns. Measurements of the crack and failure patterns of the beams were performed. In addition, measurements of the propagation of the cracks were performed at each loading step. At the initial cracking stage, the RCA concrete beams exhibited a higher number of cracks than the control beam, as shown in Figure 5. This phenomenon might occur because the interfacial transition

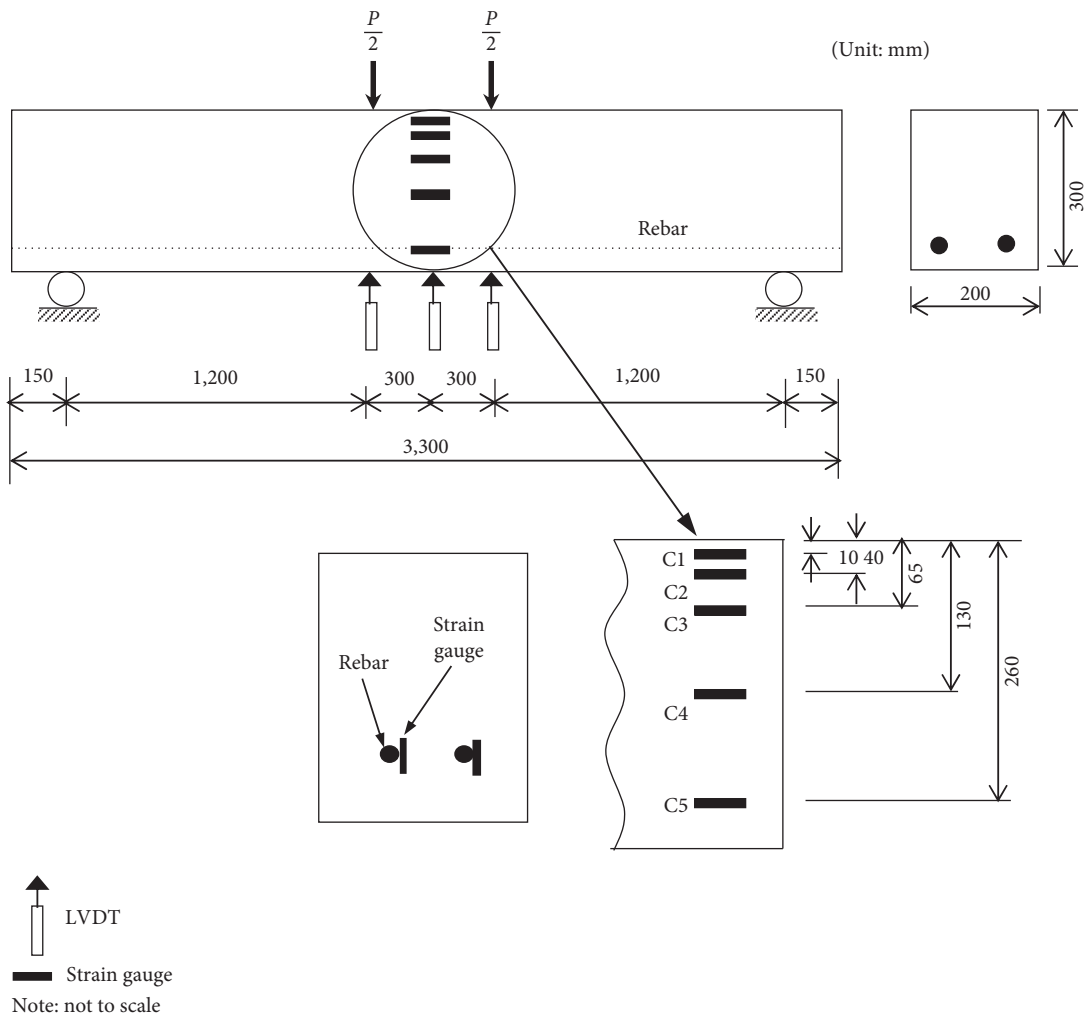

Figure 4: Instrumentation system.

zone between the RCAs and paste was weaker than that between the NCAs and paste. The weak interfacial transition zone in the RCA concrete was due to residual mortar on the surface of the RCAs.

The crack patterns of the S1 series beams in the service loading stage are shown in Figure 6. The load corresponding to 60% of the rebar yield strength was considered a typical service load. The crack propagation of the RCA beams was similar to that of the control beam. After the initial cracking stage, new cracks occurred inside and outside the constant bending zone in both NCA and RCA beams as the load increased. These new and existing cracks propagated up to the compressive zone until failure occurred in both types of beams. However, the number of cracks in the RCA beams was higher than that in the control beam.

In addition, the crack patterns at failure for the S1 series beams are shown in Figure 7. The overall crack patterns of both NCA and RCA beams were similar to experimental results reported in the study of Sera-Paz et al. [15]. The RCA beams generally sustained more cracks than the NCA beams. Hence, the crack spacing was closer in the RCA beams than in the NCA beams. According to the studies by Sunayana and Barai [16] and Sturm et al. [31], the closer cracking spacing in the RCA beams might be due to the effect of high shrinkage in the RCA beams.

All test beams failed in flexure. The test results indicate that the tensile cracks occurred first, and then the tensile rebar yielded, followed by concrete crushing, which is usually referred to as tension failure. Cracks did not appear at the beginning of the test, during which the load increased linearly. The first cracks occurred on the bottom face of the beam between the loading points, where the beam was subjected to pure bending. The cracks propagated toward the upper face. As the load increased after the initial cracking, additional flexural cracks formed between the load and supports. As the applied load was further increased, most of the flexural cracks developed vertically, and subsequently, inclined flexure-shear cracks began to appear.

The relation of the load to the crack width for each beam series is shown in Figure 8. For each beam series, the beams had the same rebar ratio but different RCA contents. For series S1, the crack widths of the RCA and NCA beams up to the rebar yield point were similar. For series S2, the crack widths of the RCA and NCA beams up to the rebar yield point were similar except for beam R050-S2. The crack width of beam R05-S2 was slightly larger than that of the other

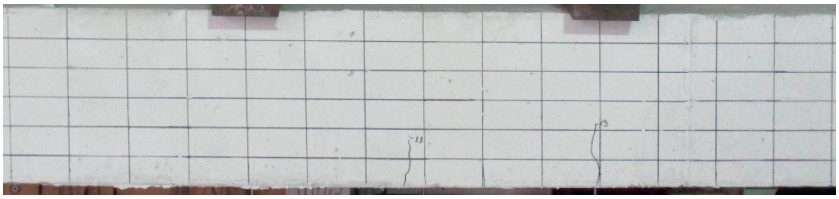

(a)

(b)

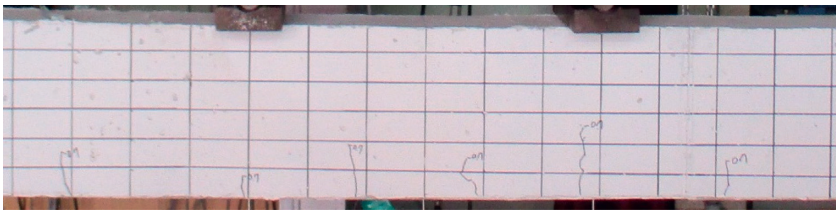

(c)

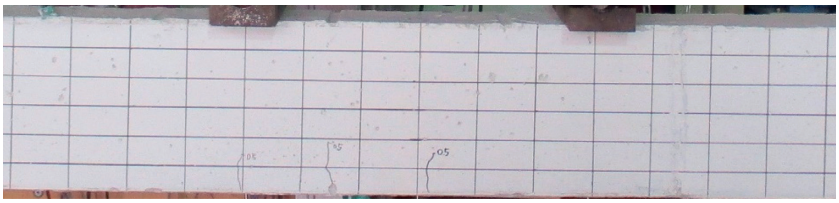

(d)

Figure 5: Typical crack patterns at the initial cracking stage ($P = P_{cr}$) (S2 series beams). (a) Beam R000-S2. (b) Beam R030-S2. (c) Beam R050-S2. (d) Beam R100-S2.

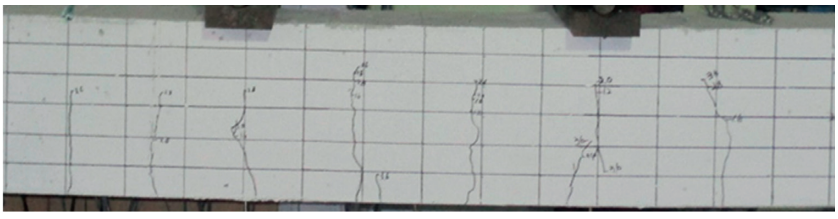

(a)

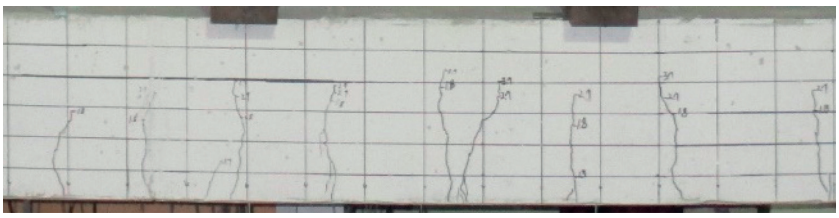

(b)

Figure 6: Continued.

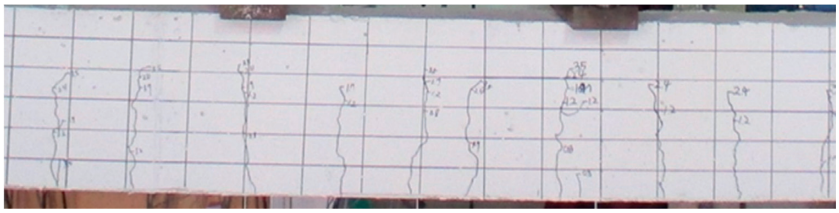

(c)

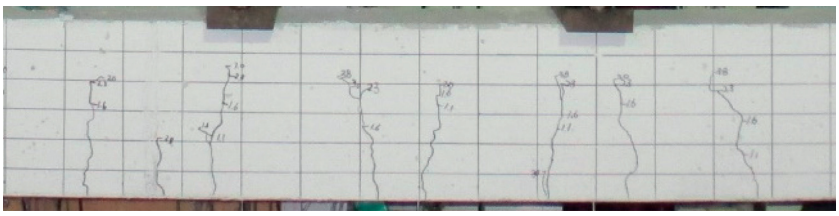

(d)

Figure 6: Typical crack patterns at the service load stage ($P = 0.6P_y$, S1 series beams). (a) Beam R000-S1. (b) Beam R030-S1. (c) Beam R050-S1. (d) Beam R100-S1.

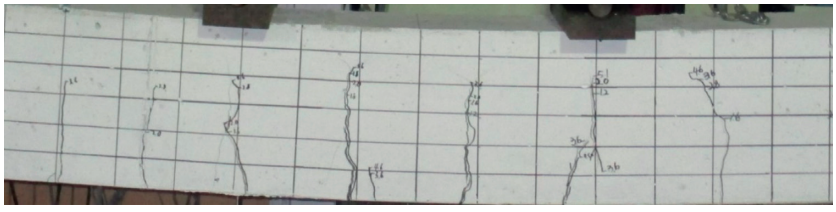

(a)

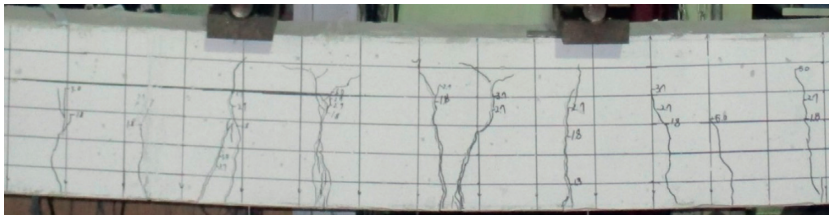

(b)

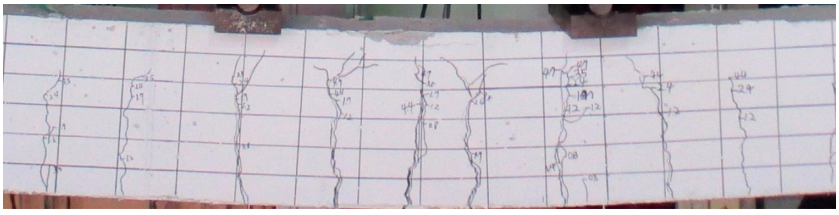

(c)

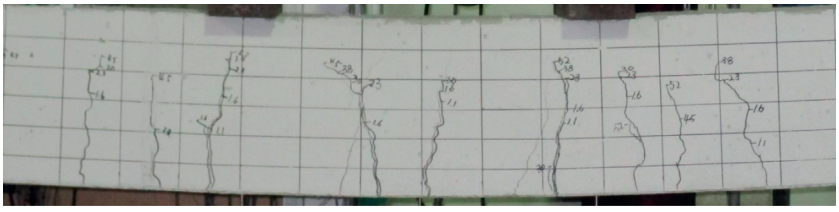

(d)

Figure 7: Typical crack failure patterns (S1 series beams). (a) Beam R030-S1. (b) Beam R030-S1. (c) Beam R050-S1. (d) Beam R100-S1.

beams. For series S3, the crack widths of the RCA and NCA beams up to the rebar yield point were similar except for beam R100-S3. The crack width of beam R100-S3 was slightly larger than that of the other beams.

Finally, the test results indicate that the number of cracks in the RCA beams was greater than that in the NCA beams and that the crack widths were similar in the RCA and NCA beams.

5.2. Load-Deflection Relationship. The load-deflection curves of the beams, measured at each loading step by the LVDTs installed in the midspan of the beams, are shown in Figures 9 and 10. Table 4 shows the first cracking load, the yield load, and the ultimate load for each specimen.

The first cracking load is the value of the load at the end of the initial linear zone in the load-deflection curve. The yield load is the load at which the rebar yielded, and the ultimate load is the maximum load of the load-deflection curve.

The deflection of the beam up to the point of crack initiation increased linearly and proportionally to the load. After the initial cracking began, each beam specimen showed nearly linear behavior until the tensile rebar yielded. From the yield point of the rebar, each beam specimen exhibited nonlinear behavior until failure.

The test results showed that the initial cracking load of the beam with 100% RCA content was lower than that of the control beam. The two lowest initial cracking loads were found in beams R100-S2 and R100-S3. This is likely because the RCA concrete has lower tensile strength than the NCA concrete. These test results are similar to those in the study by Arezoumandi et al. [19], which investigated the flexural behavior of RCA beams with an RCA content of 100%. The lower cracking load of the RCA beams was related to the interfacial transition zones between the RCAs and cement paste, which is weaker than that of the NCA beams.

The load-deflection curves for the control concrete beam and RCA concrete beams (30%, 50%, and 100%) with the same rebar ratio are shown in Figure 9. For series S1 and S2, the RCA content affected the ultimate load. As an example, the ultimate loads of beams R000-S2, R030-S2, R050-S2, and R100-S2 were 91.5, 88.3, 82.2, and 81.0 kN, respectively. This indicates that the flexural ultimate strength decreased as the RCA content increased.

However, for the S3 series, the effect of the RCA content on the ultimate load was not significant. The tensile rebar ratios in the S3 series beams were higher than those in the S1 and S2 series beams. Therefore, in terms of the flexural strength, the S3 series beams may be controlled more by the tensile rebar than by the concrete strength.

The slopes of the load-deflection curves of the RCA beams were slightly less than those of the NCA beams. This finding indicates that the RCA content affected the stiffness of the concrete beams, which could be attributed to the RCA beams having a lower elastic modulus than the NCA beams. This could result from the decrease in bonding in the RCA beams. The interfacial bonding between RCAs and mortar is known to be less substantial than that between NCAs and mortar [32].

To investigate the effects of the rebar ratio on the flexural strength, the load-deflection curves for beams with different rebar ratios are shown in Figure 10. As expected, the ultimate flexural strength increased as the rebar ratio increased. A comparison of the load-deflection curves of the beams with an RCA content of 50% is shown in Figure 10(c). The results show that the ultimate flexural strength values for beams with rebar ratios of 0.79% (R050-S2) and 1.14% (R050-S3) were 43.8% and 107.6% greater than that of a beam with a rebar ratio of 0.50% (R050-S1), respectively. In addition, the flexural stiffness of the beams after initial cracking increased as the rebar ratio increased.

5.3. Ductility. The ductility index for each beam is listed in Table 4. The ductility index ranged from 4.7 to 4.9 for beams with a rebar ratio of 0.50% (S1 series). The difference in the ductility index among the four beams in the S1 series was not remarkable. This result indicates that the ductility index was not affected significantly by the RCA content in the S1 series.

The ductility index ranged from 6.3 to 7.0 for beams with a rebar ratio of 0.79% (S2 series) and from 1.7 to 2.5 for beams with a rebar ratio of 1.14% (S3 series). This result also indicates that the ductility index was not affected significantly by the RCA content but was affected by the tensile rebar ratio for the S2 and S3 series.

5.4. Bending Moment versus Curvature. Strain gauge measurements were used to determine the curvature, and the planar sections were assumed to remain planar. The strain profile for the height of the beam could be used to compute the curvature of the cross section. Individual gauge measurements were used until their readings became unreliable due to cracking in the underlying concrete. The applied bending moment is plotted against the curvature in the midspan of the test beams in Figure 11. The curvature developed linearly up to approximately 0.17×10^{-5}/mm, which corresponds to the initial cracking load.

The slopes of the bending moment-curvature curves between the initial cracking state and the yield state are less than they are between the origin and the initial cracking state; however, the slopes remain nearly linear. The slope of the bending moment-curvature curve between the initial cracking state and the yield state is the cracked stiffness.

For the S1 series, the cracked stiffness values of beams R030-S1 and R050-S1 were lower than that of beam R000-S1. For the S2 series, the cracked stiffness values of beams R030-S2 and R050-S2 were lower than that of beam R000-S2. For the S3 series, the cracked stiffness values of beams R030-S3, R050-S3, and R100-S3 were lower than that of beam R000-S3. These results indicate that, overall, the stiffness of the RCA beams was lower than that of the NCA beams. This also corresponds to the

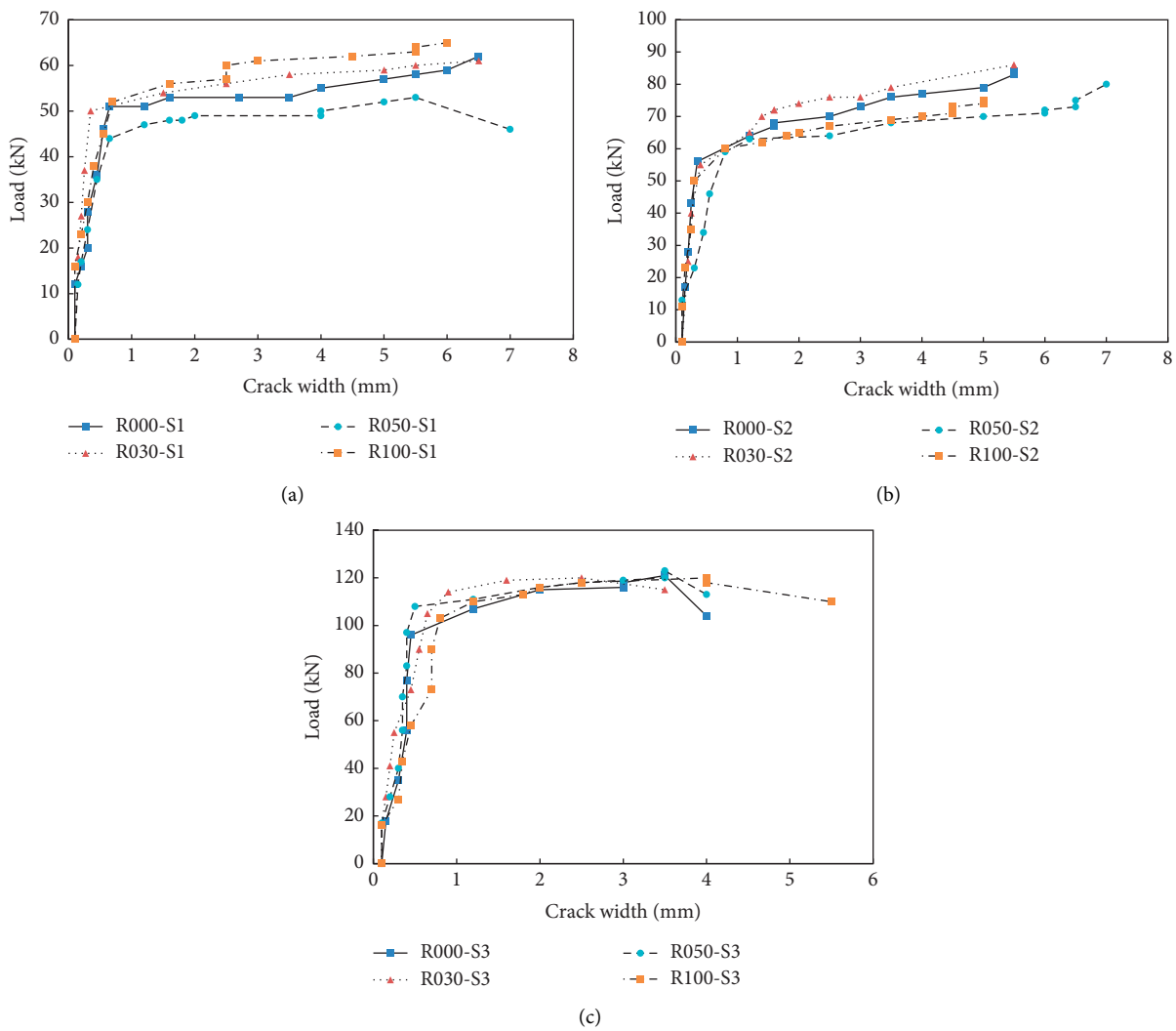

Figure 8: Load versus crack width. (a) S1 series beams (rebar ratio of 0.50%). (b) S2 series beams (rebar ratio of 0.79%). (c) S3 series beams (rebar ratio of 1.14%).

fact that the slopes of the load-deflection curves of the RCA beams were slightly lower than those of the NCA beams.

5.5. Flexural Strength of RCA Concrete Beams. The experimental results and calculations for the nominal flexural strength are plotted in Figure 12. The measured flexural strength values of both NCA and RCA beams were greater than the nominal flexural strength values calculated by the ACI 318 provision and EC 2 provision.

The ACI 318 provision underestimated the experimental flexural strength for both NCA and RCA concrete beams. The ratio of the experimental flexural strength to the calculation from the ACI 318 provision ranged from 1.08 to 1.33 for the NCA concrete beams and from 1.09 to 1.30 for the RCA concrete beams.

The EC 2 provision also underestimated the experimental flexural strength. The calculation from the EC 2 provision is similar to that from the ACI 318 provision. The study by Arezoumandi et al. [19] also revealed that the ACI 318 and EC2 provisions underestimated the flexural capacity for RCA beams by 5% to 14%. Underestimating the flexural strength of RCA beams might occur because the tension stiffening effect was not considered when predicting the flexural strength with the ACI and EC2 provisions. Therefore, the ratio of the experimental results to the calculated results indicates that the current provisions conservatively predicted the flexural strength of the RCA concrete beams.

The ratio of the experimental flexural strength to the calculation from the MCFT ranged from 0.92 to 1.05 for NCA beams and from 0.88 to 1.09 for RCA beams. Overall, the MCFT method slightly overestimated the experimental flexural strength. This might be due to the difference between the effect of tension stiffening incorporated in the program and that in the actual RCA concrete beams. The Response 2000 program considers the effect of tension stiffening based on conventional concrete.

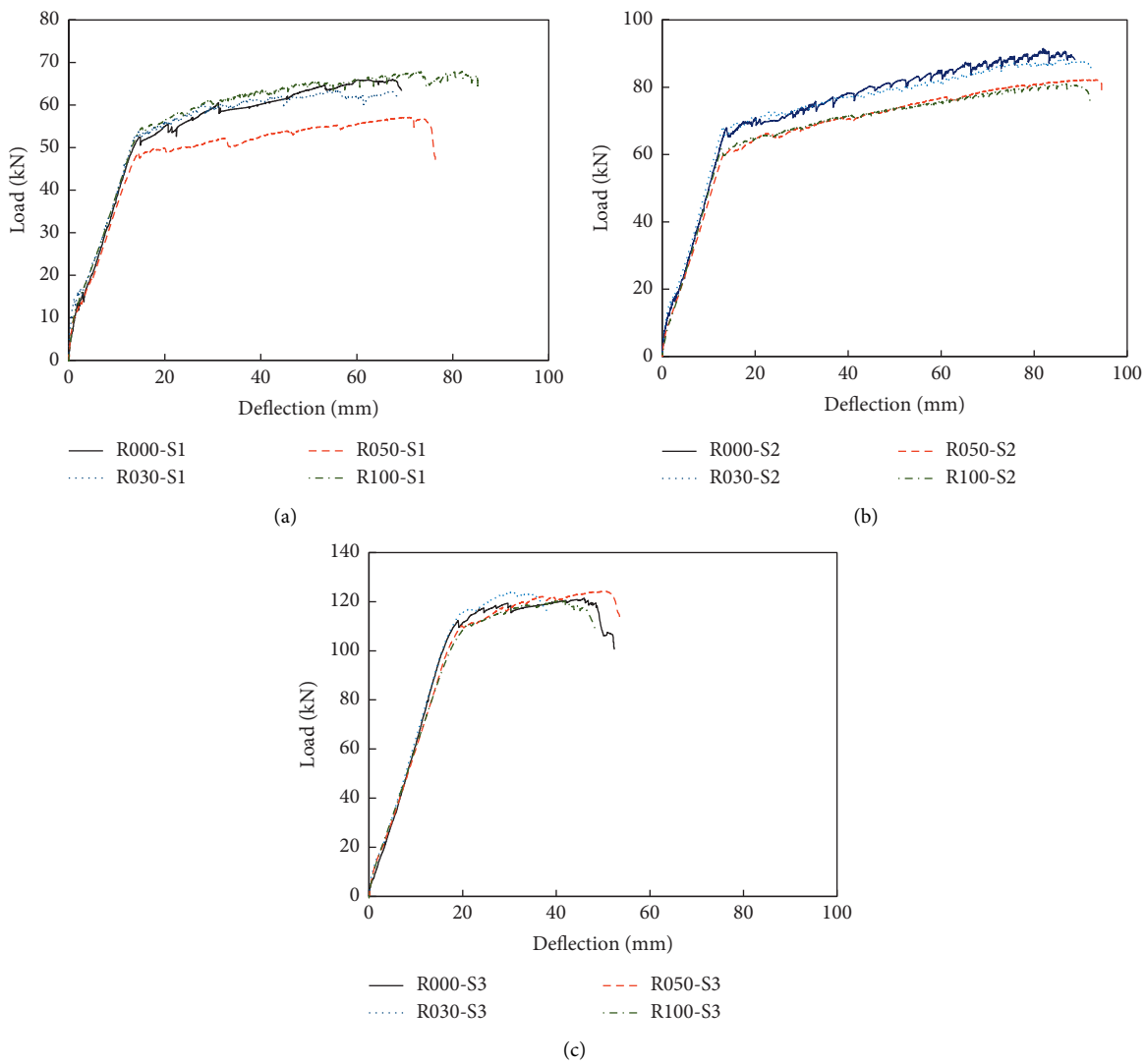

Figure 9: Effect of the RCA content on the load-deflection curves. (a) S1 series beams (rebar ratio of 0.50%). (b) S2 series beams (rebar ratio of 0.79%). (c) S3 series beams (rebar ratio of 1.14%).

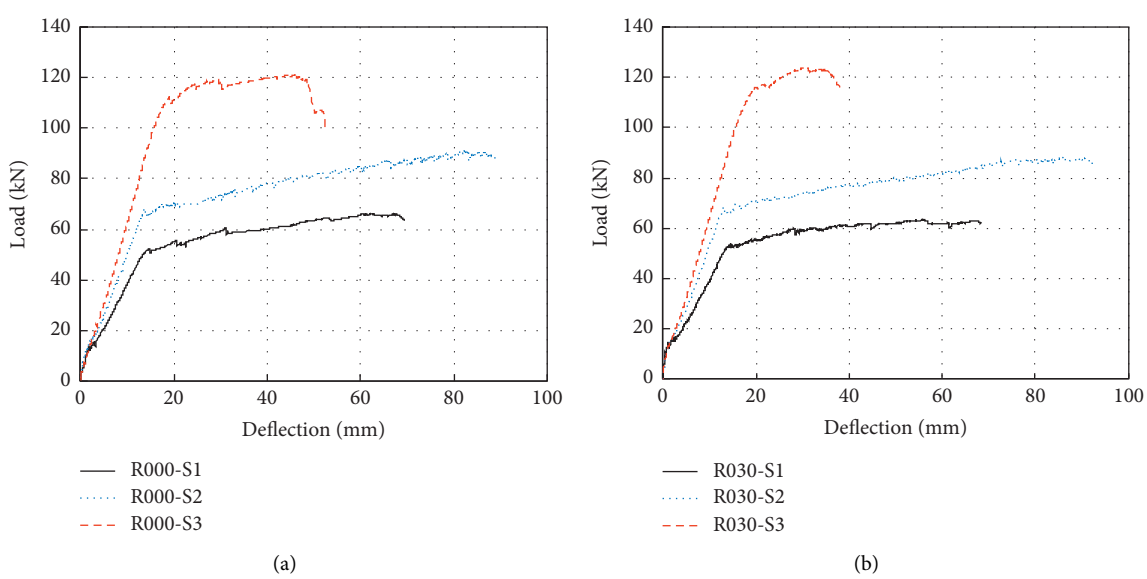

Figure 10: Continued.

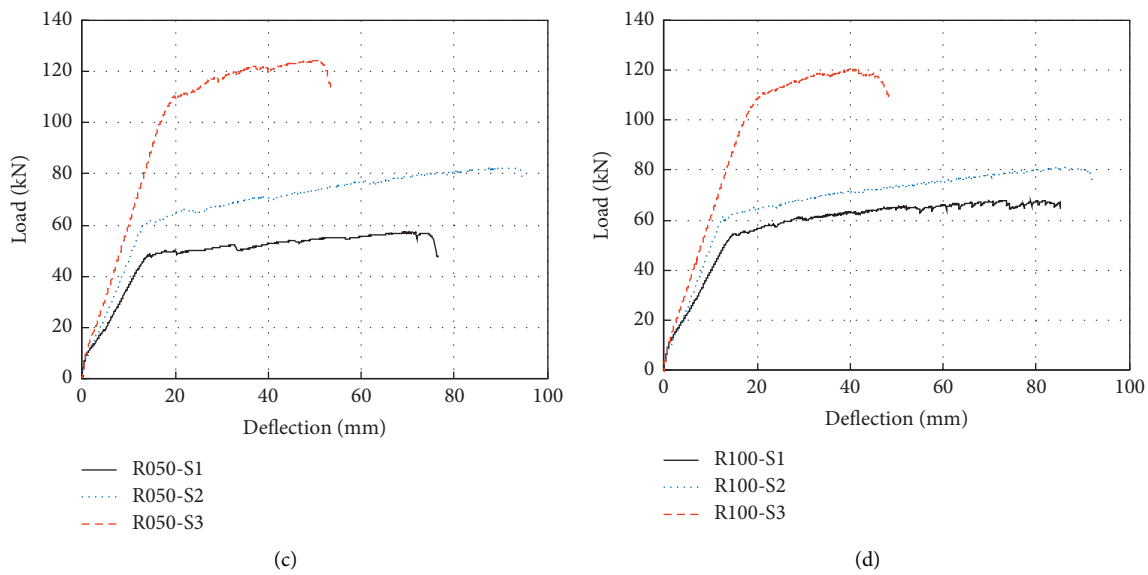

Figure 10: Effect of the rebar ratio on the load-deflection curves. (a) R000 series beams (control concrete). (b) R030 series beams (RCA content of 30%). (c) R050 series beams (RCA content of 50%). (d) R100 series beams (RCA content of 100%).

Table 4: Experimental values of the cracking, yield, and ultimate loads.

Beam specimen	Initial cracking		Yield state		Ultimate state		Ductility index
	P_{cr} (kN)	Δ_{cr} (mm)	P_y (kN)	Δ_y (mm)	P_u (kN)	Δ_u (mm)	Δ_u/Δ_y
R000-S1	13.4	1.90	52.5	14.9	66.3	90.3	4.7
R000-S2	13.0	1.50	68.0	13.8	91.5	96.8	6.4
R000-S3	7.2	0.80	112.4	19.0	121.5	46.0	2.4
R030-S1	14.7	1.10	53.9	14.5	65.2	86.3	4.7
R030-S2	16.1	1.84	68.5	13.1	88.3	92.2	7.0
R030-S3	15.3	1.63	115.9	20.0	123.7	34.9	1.7
R050-S1	10.0	1.12	48.7	14.5	57.1	70.9	4.9
R050-S2	8.9	1.13	61.6	14.7	82.2	93.5	6.3
R050-S3	11.9	1.18	110.2	19.8	124.3	50.3	2.5
R100-S1	11.9	1.39	54.7	15.2	67.9	73.3	4.8
R100-S2	5.0	0.60	61.9	12.9	81.0	84.7	6.6
R100-S3	5.9	0.50	110.9	21.5	120.4	41.2	1.9

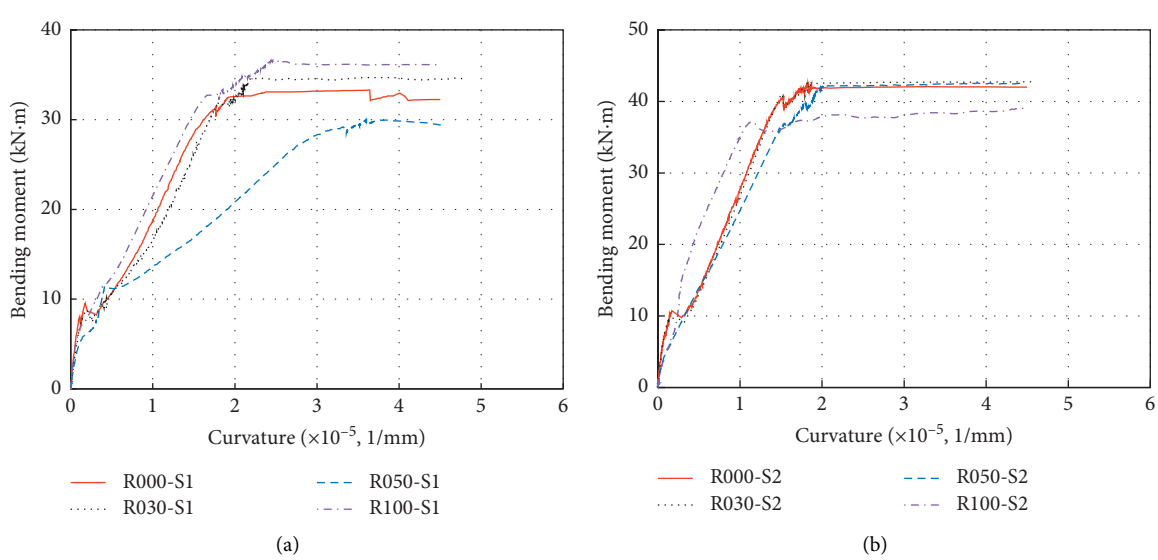

Figure 11: Continued.

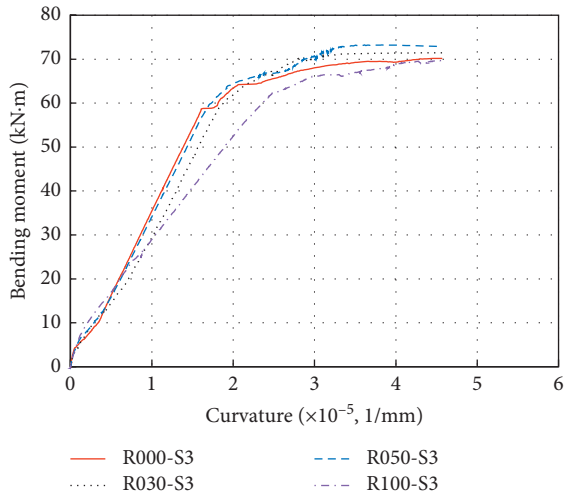

(c)

Figure 11: Bending moment versus curvature. (a) Beams with a rebar ratio of 0.50%. (b) Beams with a rebar ratio of 0.79%. (c) Beams with a rebar ratio of 1.14%.

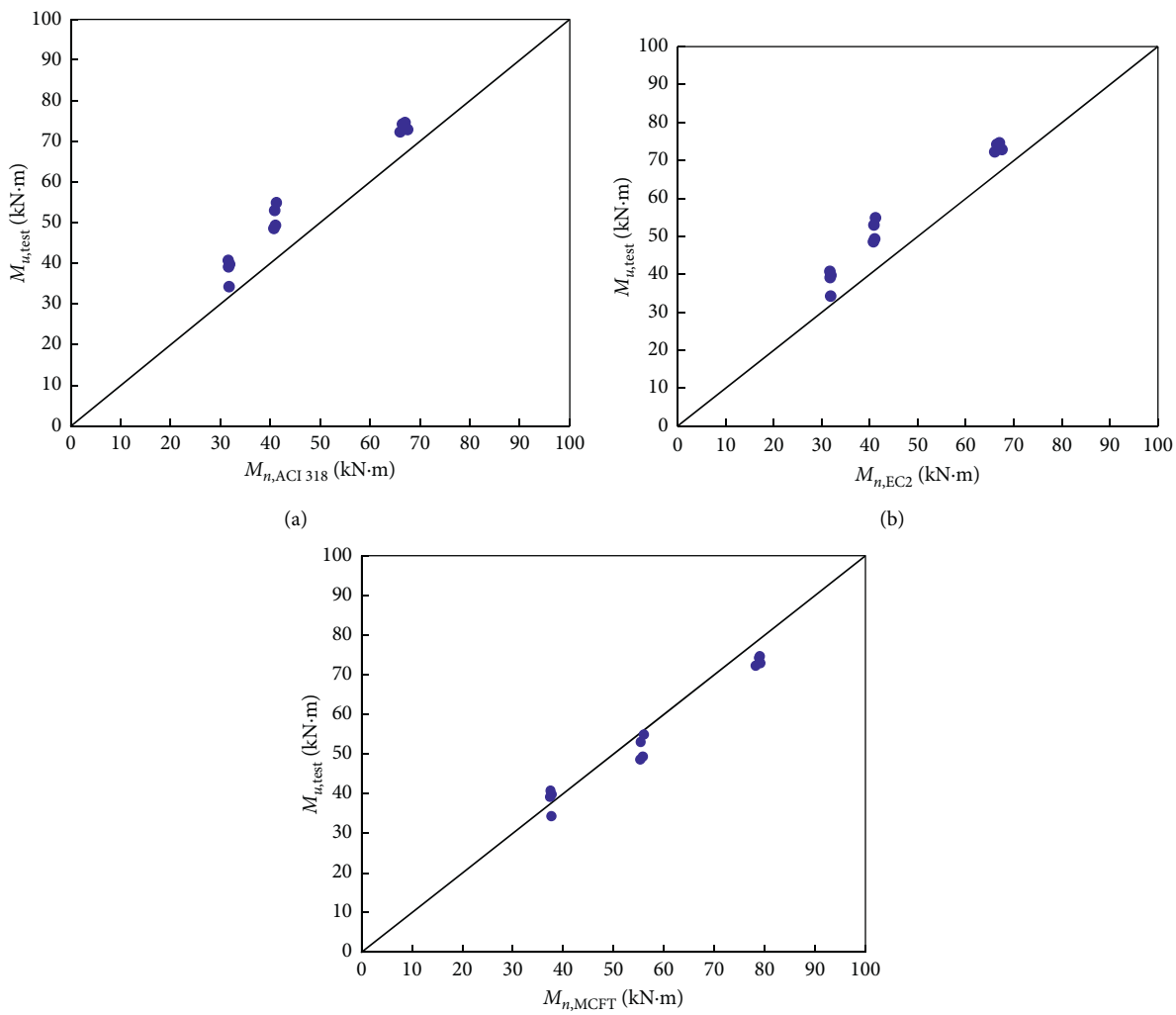

(c)

Figure 12: Comparison of flexural strength values. (a) ACI 318 provision. (b) EC 2 provision. (c) MCFT method.

6. Conclusions

This paper presents an experimental study on the flexural characteristics of concrete beams containing RCA contents up to 100%. The following conclusions are drawn from the test results:

(1) The test results showed that the number of cracks in the RCA beams was higher than that in the control beams. Therefore, the cracking pattern indicated that the RCA beams generally had closer crack spacing than the NCA beams. The closer cracking spacing in the RCA beams might be due to the effect of high shrinkage in the RCA beams.

(2) The overall flexural strength was affected by the RCA content. For beams with low rebar ratios of 0.50% and 0.79%, the flexural strength values of the RCA beams significantly decreased as the RCA content increased. In contrast, for beams with a high rebar ratio of 1.14%, the effect of the RCA contents on the flexural strength of the RCA beams was not significant.

(3) The ductility index was not significantly affected by the RCA content. The ductility of the RCA beams decreased slightly as the RCA content increased. Meanwhile, the ductility of the RCA beams decreased significantly as the rebar ratio increased.

(4) A comparison of the experimental flexural results with the calculated flexural results from the ACI 318 and EC 2 provisions indicated that the calculations underestimated the experimental results. This means that the prediction of flexural strength of the RCA members using the current provisions was conservative.

Data Availability

The data used to support the findings of this study are available from the corresponding author upon request.

Conflicts of Interest

The authors declare that they have no conflicts of interest.

Acknowledgments

This research was supported by the Korea Environment Industry and Technology Institute (KEITI) through the Public Technology Program based on the Environmental Policy Project, which was funded by the Korean Ministry of Environment (MOE) (2016000700002).

References

[1] S. Frondistou-Yannas, "Waste concrete as aggregate for new concrete," *ACI Journal Proceedings*, vol. 74, no. 8, pp. 373–376, 1977.

[2] M. Etxeberria, A. R. Marí, and E. Vázquez, "Recycled aggregate concrete as structural material," *Materials and Structures*, vol. 40, no. 5, pp. 529–541, 2007.

[3] A. D. Buck, "Recycled concrete as a source of aggregate," *ACI Journal Proceedings*, vol. 74, no. 5, pp. 212–219, 1977.

[4] V. Corinaldesi, "Mechanical and elastic behaviour of concretes made of recycled-concrete coarse aggregates," *Construction and Building Materials*, vol. 24, no. 9, pp. 1616–1620, 2010.

[5] A. Ajdukiewicz and A. Kliszczewicz, "Influence of recycled aggregates on mechanical properties of HS/HPC," *Cement and Concrete Composites*, vol. 24, no. 2, pp. 269–279, 2002.

[6] W. H. Bai and B. X. Sun, "Experimental study on flexural behavior of recycled coarse aggregate concrete beam," *Applied Mechanics and Materials*, vol. 29-32, pp. 543–548, August 2010.

[7] K. Eguchi, K. Teranishi, A. Nakagome, H. Kishimoto, K. Shinozaki, and M. Narikawa, "Application of recycled coarse aggregate by mixture to concrete construction," *Construction and Building Materials*, vol. 21, no. 7, pp. 1542–1551, 2007.

[8] S. Huda and M. S. Alam, "Mechanical behavior of three generations of 100% repeated recycled coarse aggregate concrete," *Construction and Building Materials*, vol. 65, pp. 574–582, 2014.

[9] S.-C. Kou, C.-S. Poon, and H.-W. Wan, "Properties of concrete prepared with low-grade recycled aggregates," *Construction and Building Materials*, vol. 36, pp. 881–889, 2012.

[10] S. W. Tabsh and A. S. Abdelfatah, "Influence of recycled concrete aggregates on strength properties of concrete," *Construction and Building Materials*, vol. 23, no. 2, pp. 1163–1167, 2009.

[11] N. Deshpande, S. Kulkarni, and N. Patil, "Effectiveness of using coarse recycled concrete aggregate in concrete," *International Journal of Earth Science and Engineering*, vol. 4, pp. 913–919, 2011.

[12] A. Domingo-Cabo, C. Lázaro, F. López-Gayarre, M. A. Serrano-López, P. Serna, and J. O. Castaño-Tabares, "Creep and shrinkage of recycled aggregate concrete," *Construction and Building Materials*, vol. 23, no. 7, pp. 2545–2553, 2009.

[13] L. Butler, J. S. West, and S. L. Tighe, "The effect of recycled concrete aggregate properties on the bond strength between RCA concrete and steel reinforcement," *Cement and Concrete Research*, vol. 41, no. 10, pp. 1037–1049, 2011.

[14] M. Kikuchi, T. Mukai, and H. Koizumi, "Properties of concrete products containing recycled aggregate," in *Proceedings of 2nd International Symposium on Demolition and Reuse of Concrete and Masonry*, vol. 2, pp. 595–604, Tokyo, Japan, November 1988.

[15] S. Seara-Paz, B. González-Fonteboa, F. Martínez-Abella, and J. Eiras-López, "Flexural performance of reinforced concrete beams made with recycled concrete coarse aggregate," *Engineering Structures*, vol. 156, pp. 32–45, 2018.

[16] S. Sunayana and S. V. Barai, "Flexural performance and tension-stiffening evaluation of reinforced concrete beam incorporating recycled aggregate and fly ash," *Construction and Building Materials*, vol. 174, pp. 210–223, 2018.

[17] M. F. M. Fahmy and L. K. Idriss, "Flexural behavior of large scale semi-precast reinforced concrete T-beams made of natural and recycled aggregate concrete," *Engineering Structures*, vol. 198, Article ID 109525, 2019.

[18] T. Kang, W. Kim, Y.-K. Kwak, and S.-G. Hong, "Flexural testing of reinforced concrete beams with recycled concrete aggregates," *ACI Structural Journal*, vol. 111, no. 3, 2014.

[19] M. Arezoumandi, A. Smith, J. S. Volz, and K. H. Khayat, "An experimental study on flexural strength of reinforced concrete

beams with 100% recycled concrete aggregate," *Engineering Structures*, vol. 88, pp. 154–162, 2015.

[20] H. R. Chaboki, M. Ghalehnovi, A. Karimipour, and J. de Brito, "Experimental study on the flexural behaviour and ductility ratio of steel fibres coarse recycled aggregate concrete beams," *Construction and Building Materials*, vol. 186, pp. 400–422, 2018.

[21] J. D. Brito, J. Ferreira, J. Pacheco, D. Soares, and M. Guerreiro, "Structural, material, mechanical and durability properties and behaviour of recycled aggregates concrete," *Journal of Building Engineering*, vol. 6, pp. 1–16, 2016.

[22] M. S. Meddah, S. Zitouni, and S. Belâabes, "Effect of content and particle size distribution of coarse aggregate on the compressive strength of concrete," *Construction and Building Materials*, vol. 24, no. 4, pp. 505–512, 2010.

[23] American Society for Testing and Materials (ASTM), *Standard Test Method for Compressive Strength of Cylindrical Concrete Specimens*, ASTM C39, West Conshohocken, PA, USA, 2020.

[24] Korea Industrial Standard, *Standard Test Method for Compressive Strength of Concrete; KS F 2405*, Korea Industrial Standards, Seoul, South Korea, 2010.

[25] Korea Concrete Institute, *Korea Design Code for Structural Concrete*, Korea Concrete Institute, Seoul, South Korea, 2012.

[26] S. H. Ahmad and R. Barker, "Flexural behavior of reinforced high-strength lightweight concrete beams," *ACI Structural Journal*, vol. 88, no. 1, 1991.

[27] ACI Committee 318, "Building code requirements for structural concrete (ACI 318-14) : an ACI standard : commentary on building code requirements for structural concrete (ACI 318R-14), an ACI Report," 2014.

[28] European Committee for Standardisation, *EN 1992-1-1: Eurocode 2: Design of Concrete Structures—Part 1-1: General Rules and Rules for Buildings*, European Committee for Standardisation, Brussels, Belgium, 2004.

[29] E. Bentz, *Sectional Analysis of Reinforced Concrete Members*, University of Toronto, Toronto, Canada, 2000.

[30] Response 2000 Program, http://www.ecf.utoronto.ca/~bentz/r2k.htm.

[31] A. B. Sturm, P. Visintin, and D. J. Oehlers, "Time-dependent serviceability behavior of reinforced concrete beams: partial interaction tension stiffening mechanics," *Structural Concrete*, vol. 19, no. 2, pp. 508–523, 2018.

[32] H. Dong, Y. Song, W. Cao, W. Sun, and J. Zhang, "Flexural bond behavior of reinforced recycled aggregate concrete," *Construction and Building Materials*, vol. 213, pp. 514–527, 2019.

Hindawi
Advances in Materials Science and Engineering
Volume 2020, Article ID 6326178, 11 pages
https://doi.org/10.1155/2020/6326178

Review Article

Reuse of Clay Brick Waste in Mortar and Concrete

Lihua Zhu [1,2] and Zengmei Zhu [1,2]

[1] *State Key Laboratory of Green Building in Western China, Xi'an University of Architecture & Technology, Xi'an 710055, China*
[2] *School of Civil Engineering, Xi'an University of Architecture & Technology, Xi'an 710055, China*

Correspondence should be addressed to Lihua Zhu; zhulihuaxa@163.com

Received 18 April 2020; Revised 8 June 2020; Accepted 16 June 2020; Published 3 July 2020

Academic Editor: J. M. P. Q. Delgado

The application of recycled clay brick can not only solve the disposal problem of demolished solid waste but also reduce ecological environment damage caused by the excessive development of resources. Clay brick powder (CBP) exhibits pozzolanic activity and can be used as cement replacement. Recycled clay brick aggregate (RBA) can be used to substitute natural coarse aggregate. Recycled clay brick aggregate concrete (RBAC) can attain suitable strength and be used in the production of medium- and low-strength concrete. Clay brick waste as potential partial cement and aggregate replacement material is reviewed herein. Performances in terms of mechanical and durability-related properties of mortar and concrete are discussed. Understanding the properties of clay bricks is crucial to further research and applications.

1. Introduction

Clay brick structures are widely used worldwide. In the early days of the founding of China, many clay brick structures were built. Over time, many buildings reached their design lifetime or became defective because of the use of faulty construction or inappropriate materials. Additionally, frequent earthquakes destroyed many buildings and produced a large amount of waste. Owing to the needs of urban development and reconstruction, old buildings had to be demolished, thereby resulting in the accumulation of clay brick waste [1, 2] (Figure 1). China produced approximately 15.5 million tonnes of construction waste each year, primarily concrete and brick. According to the report of the European Union in 2011, approximately 1 billion tonnes of construction and demolition waste (CDW) were produced in the European Union each year, which contained plenty of bricks [3]. Additionally, clay brick waste from demolished brick walls accounted for approximately 54% of construction and demolition waste in Spain [4]. In the capital of Valle del Cauca, Cali, an average volume of 1900 m^3 of CDW was produced by construction companies and public construction [5]. Furthermore, private constructions and renovation projects generated 580 m^3 of CDW [5].

The main method to handle CDW is through landfill or reclamation sites. The foundation of a landfill is of poor quality. Additionally, using landfill or reclamation sites is an expensive approach. It costs approximately \$21/ton to recycle one ton of concrete, brick, and masonry, while it costs approximately \$136/ton to landfill the same material [6]. In addition, the distance between demolition sites and disposal areas is becoming larger, and the transportation costs are becoming higher. As landfills and reclamation areas are limited, the landfill of waste clay bricks occupies valuable land resources and damages the soil structure, resulting in a poor grain yield. Waste storage and disposal is becoming a serious environmental problem, especially in most cities lacking disposal sites. By recycling construction waste, the amount of waste to be transferred to landfills would be significantly reduced [6].

The production of concrete and mortar has consumed a large number of nonrenewable resources and caused serious environmental pollution. Concrete is made of sand, gravel, cement, and water, which are difficult to obtain. At the world level, civil engineering and construction consumed 60% of raw materials extracted from the lithosphere [7]. Furthermore, an increase in population resulted in an increase in construction activity and the consumption of natural

(a) (b)

Figure 1: Clay bricks waste: (a) construction and demolition waste; (b) processing brick aggregate (colour figure can be viewed at http://3g.163.com/dy/article/DEDFJ5M60520EK8D.html).

resources. In areas lacking high-quality rocks or gravel, it would not be economical to import aggregates. In many urban areas, good natural aggregates are scarce, sand and stone resources have gradually exhausted, and mining has become more difficult. Meanwhile, the production of cement is not environment-friendly. As an important raw material of concrete, cement will produce plenty of dust and carbon dioxide during its production [8]. With the current technology, the production of 1 ton of cement consumes 1.7 tonnes of raw materials, approximately 7000 MJ of electricity and fuel energy [9], and 0.75 tonnes of carbon dioxide, and 12 kilograms of sulphur dioxide and dust [10]. In China, 2.5 billion tonnes of cement, accounting for approximately 60% of the world cement production, were produced in 2014 [11, 12].

Clay brick wastes have a high resource value and many countries are reusing them for many applications in construction activities. A waste framework for moving toward a European recycling society with a high level of resource efficiency was provided in the European Directive (2008/98/EC) of 19 November 2008 [13]. The European Union has set a goal of recycling 70% of its construction waste by 2020 [14]. In Germany, Denmark, and Netherlands, reuse rates are approximately 80%, compared with an average of 30% in other countries [15]. Although Germany first used crushed bricks in Portland cement to produce concrete products in 1860 [16], crushed brick as aggregate was significantly used in fresh concrete for reconstruction after the Second World War [17]. It was reported that 11.5 million m^3 of crushed brick aggregates was used to build 175,000 dwelling units [18].

The concept of sustainable development includes energy conservation, environmental protection, and protection of nonrenewable natural resources. Because of limited landfill space and costly natural aggregates, the application prospect of crushed clay bricks as a new civil engineering material must be investigated. Waste reuse and recycling is a method of energy conservation in modern society. Reuse of clay bricks as aggregates not only reduces the problem of waste storage but also helps to preserve natural aggregate resources [19]. The use of waste clay bricks not only reduces the cost of site cleaning and disposal but also yields significant social and economic benefits.

To provide a reference for further research on waste clay bricks, the reuse of waste clay bricks in concrete engineering is summarised extensively. The mechanical properties and durability of mortar using clay brick waste as cement or sand are described, and the mechanical properties and durability of concrete containing RBA are summarised. The potential application of RBAC on structural members is discussed as well.

2. Clay Brick Waste Used in Mortar

Clay brick waste can be ground into tiny particles to be used in mortar. It can exist in two forms: CBP and fine aggregates. The former exhibits pozzolanic activity to yield a denser mixture, and the latter can be used as sand replacement. The mechanical and durability properties of mortar have been studied in previous studies.

2.1. Pozzolanic Activity of CBP. Several studies [20, 21] have determined that CBP is a pozzolanic material. Its pozzolanic activity is the result of the transformation of crystalline structures of clay silicates in amorphous compounds during the manufacture of bricks, where clay is exposed to high temperatures from 600°C to 1000°C. The pozzolanic activity of CBP can be confirmed by microstructure characterisation. As shown in Figure 2, the CBP grain has a semioval shape and a semismooth surface, and it comprises morphologically irregular particles, which are mainly quartz and feldspar, the components required for the pozzolanic activity.

Generally, burned clay may not exhibit pozzolanic activity. Clay contains a high proportion of quartz and feldspar, which are crystalline minerals and do not produce active substances. Therefore, clay cannot be considered a pozzolan. However, if clay is exposed to a temperature of 600–1000°C, the crystal structure of the silicate will often change into an amorphous compound reacting with lime at room temperature [22]. The assessment of pozzolanic activity is typically based on a strength activity index specified by ASTM C618, which limits the sum of silicon, ferric, and aluminium oxides to be at least 70% for pozzolans [23]. Plenty of studies have shown that those oxides of CBP were beyond 70% and exhibit high pozzolanic activity

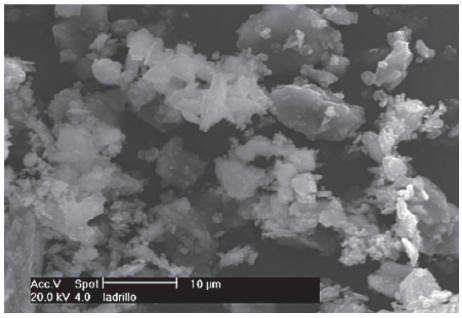

Figure 2: SEM micrograph of brick powder [21].

[20, 21, 23–40]. As shown in Table 1, the sum of silicon, ferric, and aluminium oxide of CBP exceeded 70%, which proved that CBP had high pozzolanic activity; these components will promote the formation of C-S-H (calcium silicate hydrates) or C-A-H (calcium aluminate hydrates) and thus affected the performance of mortar and concrete.

Pozzolanic activity refers to the ability of substances to react with calcium hydroxide to form hydration products at ordinary temperatures. The pH value of saturated calcium hydroxide solution is 12.45 at 25°C. High concentrations of OH^- ions can break bonds in silica, silicates, and aluminosilicates to generate simple ions [41, 42], according to the following chemical reaction:

$$\begin{aligned} &\equiv \text{Si-O-Si} \equiv + 8\text{OH}^- \longrightarrow 2\left[\text{SiO}(\text{OH})_3\right]^- + \text{H}_2\text{O} \\ &\equiv \text{Si-O-Al} \equiv + 7\text{OH}^- \longrightarrow \left[\text{SiO}(\text{OH})_3\right]^- + \left[\text{Al}(\text{OH})_4\right]^- \end{aligned} \tag{1}$$

The resulting silicate and aluminate ions accompany Ca^{2+} ions form C-S-H (calcium silicate hydrates) or C-A-H (calcium aluminate hydrates) [43, 44]. As the dissolution rate of silicate is more rapid than that of aluminate and the formation of calcium aluminate requires a higher concentration of calcium ions, first, CSH gels would appear on the particles of pozzolans, and then hexagonal sheets of calcium aluminates precipitate on the surface of the CSH gels.

Studies have shown that the pozzolanic activity of CBP increased with the content in the amorphous phase. Furthermore, the larger the specific surface area is, the smaller the particles are and the higher the pozzolanic activity is, because the powder in the pozzolanic reaction has a large reaction surface [27]. Moreover, CBP presented a higher specific surface than cement and exhibited high pozzolanic activity [20].

2.2. Mechanical Properties of Mortars with Clay Brick Waste. CBP can be considered as a promising filler that reduces the effect of the greater shrinkage phenomenon, which is likely produced by a higher pore refinement owing to the development of pozzolanic activity of CBP. Several studies [21, 27, 28, 45] have shown that the microstructure was more refined for mortars with CBP. Moreover, the microstructure became more refined and the percentage of finer pores gradually increased over time. CBP improves the structure of mortar and reduces the size and number of pores in it, resulting in a stronger and denser hardened paste. Aliabdo et al. [23] studied the pore structure of paste specimens with CBP. They discovered that the pozzolanic reactivity of CBP and possibly the rehydration of unhydrated cement particles in attached mortar improved the density of the matrix and refined the pore structure. The pore structure of the investigated paste specimens is displayed in Figure 3, and the sample containing 25% CBP has the smallest pore diameter and the best pore structure. The mortar with CBP has a higher degree of microstructure refinement, which may be related to the combined action of the additional reinforcement phase formed by the products of pozzolanic reaction of CBP and the filling effect of this additive. Furthermore, the addition of CBP affects the proportion of pores in the mortar. With the partial replacement of cement by CBP, the proportion of macropores reduced and the proportion of mesopores increased [26]. Although the study demonstrated the filling effect of CBP, Gonçalves et al. [26] reported that the packing density did not change significantly with the replacement of cement by CBP. They concluded that this might be attributed to the similarity between the particle size distributions of CBP and Portland cement, resulting in no change in the packing density. Furthermore, it is also possible that the product of pozzolanic activity of CBP makes up for the weight loss caused by CBP replacing Portland cement.

In addition, water/cement (w/c) ratio affects the density of mortar containing CBP. Under different w/c ratios, the effect of replacing cement with CBP on density is different. Toledo Filho et al. [25] discovered that the mixes of series M1 ($w/c = 0.40$) yielded porosity values that were 28% to 35% lower than those observed for mixes of series M2 ($w/c = 0.50$).

Alkaline activation can transform aluminosilicate materials into more compact binding materials. Robayo et al. [29] discovered that the addition of ordinary Portland cement and Na_2SiO_3 to the mixture promoted the dissolution of some phases in clay brick waste and increased alkali-activating processes, which improved the mechanical behaviour. Reig et al. [30] demonstrated that CBP could form alkali-activated cement pastes and mortars using NaOH and sodium silicate solution as activators. The compressive strength of the mortar was approximately 30 MPa with a w/b ratio of 0.45, which proved that it was feasible to use CBP in cement after CBP was activated by NaOH and sodium silicate solution. Additionally, Rovnaník et al. [31] studied alkali-activated CBP and discovered that the specimens exhibited a less compact structure with more pores located between sharp-edged grains, and geopolymers containing alkali-activated CBP exhibited lower flexural and compressive strengths.

Some previous studies reported that using CBP as cement addition improved the compressive strength of mortar. The pozzolanic activity of these CBP may contribute to the higher initial and final strengths of the mortars containing them. The chemical composition of CBP also explained the mechanism of this phenomenon that the presence of CBP provided to continue strength gain of mortars up to the 90th day since CBP activated hydrations of silica based

Table 1: Composition of CBP.

Chemical composition (%)											Reference
SiO_2	Al_2O_3	Fe_2O_3	CaO	SO_3	MgO	Na_2O	K_2O	TiO_2	MnO	P_2O_5	
41.47	39.05	12.73	0.63	1.59	—	—	2.81	1.03	—	—	[20]
41.47	39.05	12.73	0.63	1.59	—	—	2.81	1.03	—	—	[21]
54.2	15.4	7.6	6.8	1.1	2.5	—	—	—	—	—	[23]
39.55	15.71	14.05	12.88	0.48	3.29	—	1.98	—	—	—	[24]
63.89	25.49	7.73	0.29	—	0.04	Traces	0.95	—	—	—	[25]
63.89	25.49	7.73	0.29	—	0.04	Traces	0.95	Traces	Traces	—	[26]
58.5	15.61	3.52	13.79	2.04	2.07	0.38	2.81	0.46	0.03	0.15	[27]
58.12	15.25	3.26	15.1	2	1.87	0.38	2.84	0.41	0.03	0.18	
58.34	15.14	3.22	14.1	2.02	2.22	0.39	2.82	0.49	0.04	0.17	
59.12	15.19	4.81	10.15	1.33	4.28	1.39	3.07	0.4	0.05	0.16	
58.13	15.24	4.63	10.57	1.42	4.32	1.42	3.08	0.39	0.05	0.16	
58.87	15.1	4.61	10.24	1.23	4.28	1.44	3.06	0.4	0.05	0.16	
77.43	9.27	3.9	2.89	0.11	1.36	0.8	2.26	0.62	0.06	—	[28]
73.83	12.94	5.52	1.67	0.12	1.36	0.9	2.18	0.84	0.08	—	
77.52	9.85	4.4	2.03	0.07	1.15	0.84	2.28	0.63	0.06	—	
72.83	12.01	5.73	2.95	0.09	1.7	0.99	1.94	0.72	0.09	—	
65.92	20.08	9.1	0.73	—	0.86	0.44	0.97	1.09	—	—	[29]
49.9	16.6	6.5	9.7	3.3	5.5	0.5	4.4	0.8	0.1	0.2	[30]
57.67	14.91	5.02	9.81	1.86	3.74	1.45	3.2	—	—	—	[31]
54.83	19.05	6	9.39	2.9	1.77	0.5	3.15	0.97	—	0.2	[32]
69.99	10.62	4.02	8.86	0.038	1.39	1.02	2.61	0.55	—	0.11	
68.79	15.23	6.28	1.79	0.127	2.02	0.26	3.71	0.85	—	0.07	
72.75	15.89	4.97	0.87	0.07	1.2	0.27	2.17	0.84	—	0.1	
67.58	18.94	8.084	0.948	0.13	0.719	0.246	1.884	1.06	—	—	[33]
69.26	14.17	6.3	4.28	0.02	2.25	0.28	1.34	—	—	—	[34]
53.8	14.1	12.1	9.2	—	8.9	1.3	—	—	—	—	[35]
69.43	17.29	6.4	0.51	2.54	1.14	—	—	—	—	—	[36]
67.9	15.2	5.1	0.6	—	1.2	0.8	1.5	0.8	0.1	—	[37]
75.06	14.25	5.61	1.3	0.7	1.35	0.19	0.08	—	—	—	[38]
52	40	1.5	0.5	—	0.3	—	—	5			[39]
50.91	15.29	8.97	12.7	0.2	4.06	0.83	0.76	—	—	—	[40]

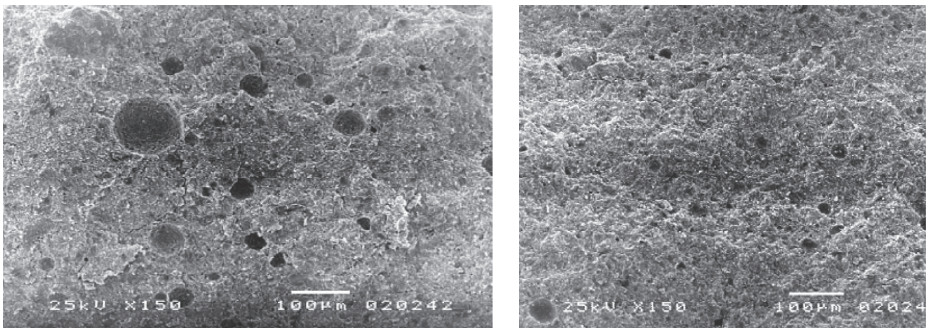

(a) (b)

Figure 3: Microstructure of paste samples. (a) Pore structure of 15% CBP paste and (b) pore structure of 25% CBP paste [23].

compounds in cement pastes. With the increase in the percentage of additions, the compressive strength increases [24]. The compressive strength of mortar also increases with the age and fineness of CBP. The finer the particle size of the CBP is, the denser the microstructure of the paste matrix is and the higher the compressive strength of the pastes is [25, 32]. Additionally, a high curing temperature can improve the hydration activity of CBP efficiently [33]. O'Farrell et al. [32] confirmed an important connection between compressive strength and threshold radius of mortar. For threshold radii down to 0.1 μm, compressive strength was not very sensitive to threshold radius, and it had only a small increase for a large decrease in threshold radius. However, when the threshold radius decreased below 0.1 μm, the strength increased significantly with a small decrease in the threshold radius. It showed that the compressive strength

increased with the increase in pore fineness and decrease in pore volume, and it also showed the effect of this additional C-S-H gel on the development of compressive strength.

Furthermore, the substitution ratio of CBP significantly affects the strength of mortar. Ortega et al. [21] revealed that the effect of pozzolanic activity was more pronounced for mortars with 10% CBP compared with those having 20% of this addition. This may be attributed to the former containing more clinker; therefore, at the same hardening ages, it was expected that a large amount of portandite had been formed for 10% CBP specimens compared to 20% specimens. Meanwhile, in the study of Liu et al. [33], the substitution ratio indicated by intensity change should not exceed 15%. Moreover, the substitution of high amounts of CBP will reduce the compressive strength of mortar significantly; when the replacement rate reaches 25%, the strength of the mortar will decrease by 25.2% [23]. This may be due to the following: pozzolanic activity produces metastable C-A-H partially; the metastable C-A-H can transform into a stable hydrogarnet with a variable composition at higher temperatures or with a longer curing time [30], and the hydrogarnet results in the reduced volume, compactness, and strength of mortars [46].

Although the replacement of CBP in mortar yielded reduced compressive strength, studies by Ortega et al. [21] confirmed that the addition of CBP did not reduce the compressive strength of the mortars, which satisfied the requirements of corresponding standards. It showed the beneficial effect of pozzolanic activity and filling effect of CBP in the performance of mortars. The compressive strength of all the studied mortars increased with hardening age, and the value for BP10 (10% brick powder) specimens was slightly higher than those noted for CEM I (a commercial ordinary Portland cement) ones at 400 days. Moreover, the flexural strength was slightly greater for mortars with CBP in comparison with CEM I ones over the 400-day period. Similarly, Boukour and Benmalek [34] discovered that CBP fillers induced only a small decrease in flexural and compressive strength with the level (2.5%, 5.0%, 7.5%, and 10%) used. The rigidity of the replaced natural sand portion might have compensated for the pozzolanic activity provided by the fine portion of the CBP filler. Moreover, Toledo Filho et al. [25] discovered that the addition of CBP had almost no effect on the compressive strength and elastic modulus until the percentage of 20% cement replacement. However, under a high w/c ratio, the strength and elastic modulus of mortar will decrease with the increase in CBP.

Studies regarding clay brick waste as fine aggregate in mortar have been reported. Bektas et al. [47] demonstrated that the high water absorption capacity of clay brick significantly affected the flow of mortar. However, even 30% of the brick mixture demonstrated sufficient workability and good consolidation with the given mixture proportions. This confirmed that brick aggregates did not reduce the strength of mortar with the levels used. Moreover, Mobili et al. [48] discovered that mortar with RBAs exhibited the highest amount of water absorbed by the capillary action.

2.3. Durability of Mortars with Clay Brick Waste. Durability is an important property of mortar. Water capillary absorption is essential for determining the durability of construction materials. Some findings on the addition of CBP revealed that CBP with low substitution rate (less than 20%) could make a higher difficulty of water ingress in the mortars containing CBP [25, 26]. This behaviour may be related to more refined porous structures, which reduced water penetration. The addition of CBP improved the sulphate resistance of cement mortar. An appropriate replacement for providing high sulphate resistance appears to be approximately 15% [35, 48, 49]. Additionally, the use of CBP significantly reduced the penetration rate of chloride ions, which is a typical cause of steel corrosion in mortars; the mechanism that can explain this phenomenon is that CBP promotes the formation of additional hydrates, which can reduce the permeability and increase the densification of the materials making the penetration of chloride ions much more difficult [21, 25, 26, 45, 50]. Additionally, Aliabdo et al. [23] found that the incorporation of CBP reduced the weight loss of mortar under high temperature. The reference specimens (without CBP) had highest weight loss attribute to the dehydration of C-S-H and ettringite contents and calcium hydroxide, while the pozzolanic reactivity of mortar with CBP consumed much more of these substances, resulting in lower weight loss; it can be concluded that the replacement of cement by CBP may result in a higher fire resistance of the mortar.

With regard to clay brick fine aggregates in mortar, Bektas et al. [47] studied the freeze-thaw process of mortar with fine brick aggregates; they concluded that the use of fine brick aggregates reduced the freeze-thaw expansion of mortar. As the aggregates contained more air bubbles preventing freeze-thaw-associated cracking, the pressure caused by ice formation and water flow was relieved, and the water flow paths were cut; in other words, tightly distributed air void structure provided space for expansive mechanisms.

In terms of drying shrinkage, Bektas et al. [47] reported a reduction in drying shrinkage after incorporating 20% recycled brick as fine aggregate. This was because additional water stored in the brick aggregate maintained plenty of moisture during hydration. Furthermore, they observed the effect of brick aggregates on the expansion of mortar immersed in NaOH solution and water. As brick aggregates are abundant in silica in nature, the possible formation of ASR can increase expansion and subsequent cracking. Similarly, Bektaş [51] investigated the ASR susceptibility of fine RBAs, and he concluded that ASR occurred in the form of reaction product of mortar bars, and the mortar expansion rate was proportional to the content of CBP.

3. Clay Brick Waste Used in Concrete

To reduce resource wastage, recycled clay brick was considered as an aggregate substitute in concrete. The physical properties of RBAs have been studied. As a mix design is key in RBAC, it was also studied. Additionally, some researchers have studied the mechanical properties and durability of RBAC.

3.1. Physical Properties of RBA. Brick aggregates exhibit a higher porosity and absorption than natural aggregates. The density of RBAC decreases with increasing brick content [52–54]. The apparent density and bulk density of recycled clay brick as aggregates are lower than those of natural aggregates, and the water absorption rate and crushing index are higher than those of natural aggregates [36, 48, 55]. As the RBA particles were angular in shape, they bonded well with cement [52]. The strength of RBA has a greater effect on the strength of concrete. The higher the strength of RBAs is, the higher the strength of RBAC is [54, 56, 57]. The microscopic images of the cut surface of concrete with natural and brick aggregates are shown in Figure 4. From the visual observation of the concrete surface, compared with natural aggregates, the brick aggregates had more pores in their structure [36].

3.2. Mix Design of RBAC. Owing to the porous nature of RBAs, the change in water demand and the adjustment of the w/c ratio should be considered in the mixing design [52, 58]. Porous RBAs may consume water for mixing concrete, which affects the workability of concrete. Hence, prewetting brick aggregates are recommended to avoid this problem [23]. Additionally, the RBAs must be in the saturated surface-dry condition before mixing, because additional water may affect the workability of RBAC [52]. Adamson et al. [36] studied the workability of concrete with RBAs; they discovered that the workability of concrete increased with the amount of coarse aggregates when the w/c ratio was constant. This may be owing to the higher porosity of the brick, which can hold more water and hence improve the workability of concrete.

The performance of RBAC is affected by the w/c ratio, sand ratio, and average particle size of brick [36, 59–62]. Moreover, the replacement level of RBAs significantly affected the properties of RBAC [59]. Coarse aggregates with flat gradation can yield more uniform aggregate particle sizes, which would be beneficial for concrete performance [36, 60]. The mechanical properties of RBAC degraded significantly with the increasing crushing index of recycled aggregates; however, the effects of increasing the crushing index on the permeability coefficient and total void ratio of RBAC can be ignored [61]. Some researchers have studied the mix design of RBAC using different methods. Ge et al. [62] adopted the orthogonal design method and obtained the optimal concrete mix in terms of compressive strength, flexural strength, and static elasticity modulus. Similar to normal concrete, the w/c ratio was the most significant factor affecting the mechanical properties of concrete containing CBP. Šipoš et al. [59] used neural network modelling to study the mix design of RBAC; they discovered that compressive strength could be affected significantly by aggregate size (fine or coarse): the compressive strength value of fine aggregates was lower than that of coarse aggregates.

RBAs from different sources exhibit different properties; therefore, the optimal replacement rate of RBAs varies with the strength of RBAs and cannot be unified. Zhang and Zong [58] suggested that 30% was an appropriate replacement level of coarse aggregates. Cachim [63] revealed that crushed bricks could be replaced by natural aggregate substitutes by up to 15% without strength reduction. When the replacement rate of RBA is 30%, the concrete properties will be reduced (up to 20%, depending on the brick type).

As the RBA exhibited lower strength, some methods were used to improve the strength of RBAC during the mix design. Adding additives can improve some properties of the specimens [64]. The use of an air-entraining admixture and superplasticiser can improve workability during mixing [52, 60]. The performance of concrete can be partially improved by the appropriate amount of CBP [45, 62]. The strength gain could be due to an increase in SiO_2, which had a favourable effect on the formation of CSH gels as a result of pozzolanic reactions [23, 32, 34, 65]. Additionally, the mixed use of CBP and RBA could yield better RBAC performances [48, 59], likely because the fine RBA particles formed a compact and dense ITZ of mortar and filled the pores of RBAC. Manzur et al. [66] found that the corrosion susceptibility of concrete increased with the increase of water-cement ratio; moreover, a concrete mix with higher compressive strength was beneficial to concrete corrosion resistance, because it meant that the concrete will have a greater density and a lower permeability, resulting in less chloride ions entering. In addition, fibre can effectively inhibit the development of cracks and improve the toughness and deformation capacity of concrete [64].

3.3. Mechanical Properties of RBAC. The porosity of RBA increases the porosity of concrete, and it may increase the water absorption and reduce the strength properties of concrete [35]. The increase in water absorption of brick aggregates results in an increase in concrete water permeability. Moreover, the water permeability coefficient of RBAC and the compressive strength of RBA exhibit a linear relationship. The water permeability of RBAC decreased as the compressive strength of RBA increased [54, 67]. Aliabdo et al. [23] studied the relationship between compressive strength and porosity, and they discovered that increased porosity was crucial in reducing the strength of concrete.

Additionally, the mechanical properties of RBAC and the maximum aggregate size (MAS) were correlated. Uddin et al. [68] reported the effects of MAS on RBAC. They revealed that the effect of cement content on compressive strength was more significant when the coarse aggregate MAS was smaller. Mohammed and Mahmood [69] reported that ultrasonic pulse velocity (UPV) increased with the maximum aggregate size. As the compressive strength and Young's modulus of the RBAC changed with the UPV, the maximum aggregate size, compressive strength, and Young's modulus may be correlated.

In addition, RBAC exhibits some properties similar to normal concrete. Martínez-Lage et al. [70] reported that Poisson's ratio of concrete was not significantly affected by the coarse aggregate replacement level, and the experimental group values were 0.14–0.20. Additionally, studies have

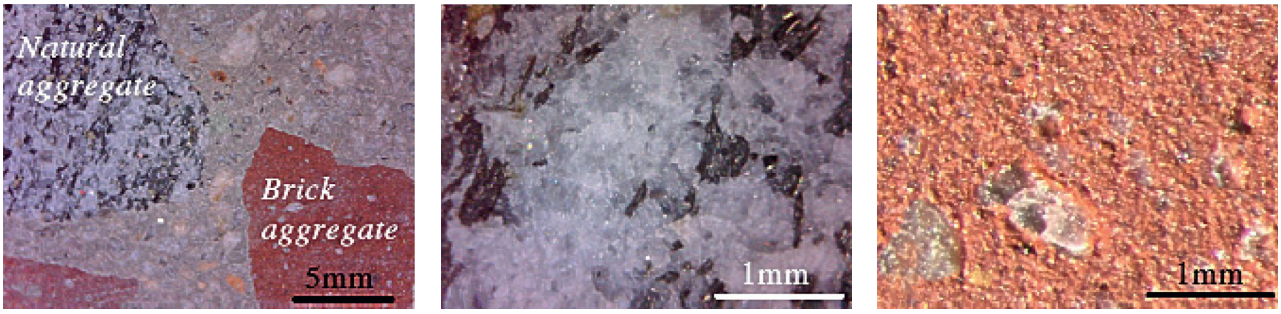

(a) (b) (c)

Figure 4: Images of the surface of concrete: (a) both natural and brick aggregates, (b) natural aggregate,and (c) brick aggregate [36].

shown that the higher the density of the RBAs is, the higher the strength of RBAC is [37, 45, 71].

Because strength is fundamental in design, some researchers have studied the mechanical properties of RBAC. Khalaf [52] and Zong et al. [53] discovered that the compressive and flexural strengths of RBAC reduced when RBAs were used. The higher the replacement rates of RBAs are, the greater the strength loss was. The reduction in compressive strength was 44% in RBAC prepared with 50% RBAs after 28 days. This conclusion was supported by the observations of Nepomuceno et al. [72] and Heikal et al. [38]. They revealed that the flexural and compressive strengths of concrete reduced as the brick replacement level increased. The interface between the mortar and aggregates is shown in Figure 5. As shown, RBAC contained microcracks in the ITZs, and a few internal voids appeared in the RBAs. This may have contributed to the compressive strength of RBAC being lower than that of normal concrete [60].

Although some studies have shown decreased compressive strength of RBAC, Adamson et al. [36] reported that the average strength of cylinders containing RBAs was slightly higher than that of the control mixture, and the strength increased with the brick content. They speculated that it may be due to the relatively low strength of natural aggregates compared to that of RBAs used in the experiment. In addition, the surface roughness and angular shape of RBAs contributed to the formation of a good bond between the aggregates, thereby increasing the splitting tensile strength of the geopolymer [37]. Uddin et al. [68] revealed that the splitting tensile strength of concrete decreased with an increase in the maximum aggregate size, regardless of the variation of sand to total aggregate volume (s/a) ratio and cement content. However, the results showed that the compressive strength of concrete increased with the increase in maximum aggregate size only under certain conditions. On the contrary, some studies showed that the particle size of CBP had no significant effect on the flexural strength of RBAC [39, 45, 58, 62].

Owing to the high porosity of RBAs, the elastic modulus of RBAC is lower than that of normal concrete [45, 48, 58, 70]. Debieb and Kenai [19] discovered that the modulus of elasticity reduced by of 30%, 40%, and 50% for coarse, fine, and both coarse and fine crushed brick concrete, respectively. Furthermore, Zhang and Zong [58] and

Figure 5: SEM image of specimen: RBA1-100 (w/c = 0.55) [60]. RBA-recycled clay brick aggregate, 1 − w/c = 0.55, 100-replacement level = 100%.

Aliabdo et al. [23] concluded that the presence of RBAs reduced the modulus of elasticity and splitting tensile strength of concrete. However, Disfani et al. [73] showed that the modulus of rupture and flexural modulus for all cement-stabilised blends were satisfactory, complying with the road authority requirements for pavement base applications.

Additionally, the alkali reactivity of RBA has been studied. Bektaş [51] confirmed that RBAs exhibited alkali reactivity, and the formation of ASR gel was confirmed by visual observations and microscope studies. An ettringite band formed around limestone particles was observed under a microscope. Rovnaník et al. [31] revealed that high-alkali concrete mixes with brick aggregates demonstrated higher expansions compared with the control mix.

With regard to the drying shrinkage, a few researchers revealed higher shrinkage strains in concrete containing recycled clay brick with fine and coarse aggregates [19, 74]. This may have been due to the lower restraining effect of brick aggregates compared with that of natural aggregates. Debieb and Kenai [19] observed that the early shrinkage rate of recycled brick fine aggregate concrete was six times that of normal concrete. Furthermore, some findings on the factors affecting drying shrinkage have been reported. Khatib [74] reported that a recycled fine brick aggregate replacement level of up to 100% exhibited only a 10% shrinkage, that is,

even a high replacement level did not result in strength reduction. Because of the internal curing effect and the dilution of CBP, replacing cement with CBP can significantly reduce the autogenous shrinkage of concrete [45].

3.4. Durability of RBAC. The durability of concrete must be considered when designing structures. It is affected by the permeability of the material used. In fact, the water permeability could be almost doubled when incorporating RBAC [19]. Apart from increased water permeability, an increase in the air permeability of concrete by using RBAs has been discovered by Zong et al. [53]. This was attributed to the more porous characteristics of RBAs.

Although water permeability has negative effects on the freezing and thawing resistances of concrete [40], Adamson et al. [36] discovered that no samples failed within 300 cycles of the freeze-thaw tests. With the increase in the replacement rate of the RBAs, the frost-thaw resistance of concrete improved [45, 75]. Additionally, RBAC produced with RBAs exhibited a lower carbonation resistance and higher water permeability [53, 58, 76]. On the contrary, Gu [77] discovered that brick aggregate replacement had no significant negative effect on carbonation depth. In addition, according to Adamson et al. [36], by increasing the content of brick, the resistance to chloride penetration decreased. This could be attributed to higher porosity and absorption in brick aggregates compared with those in natural aggregates. Nevertheless, Ge et al. [45] revealed that concrete's resistance to chloride ion penetration improved. Furthermore, corrosion of steel in samples containing RBA initiated earlier than that in samples with natural aggregates; the existence of RBAs accelerated the corrosion of steel reinforcement [36, 53, 66].

In addition, as the porosity of RBA itself is reflected directly on the global porosity of concrete, the RBAC demonstrated lower thermal conductivity and better fire performance. Wongsa et al. [37] revealed that the thermal conductivity and UPV of RBAC increased as the concrete density increased and that the thermal conductivity of RBAC was approximately three times lower than that of normal concrete. Furthermore, the concrete with RBAs showed slightly higher fire resistance than normal concrete [23, 57, 78]. Moreover, the presence of RBAs to produce lightweight high-calcium flies ash geopolymer concrete yielded excellent thermal insulation and good density [37, 79].

4. Structural Performance of RBAC

The RBA products used in the structure are our primary concern. Therefore, studies regarding the structural performance of RBAC are necessary. Owing to the low density of brick aggregates, the block with RBAs was much lighter and can reduce the weight of the structure. The mechanical properties of RBAC beams and columns are studied.

4.1. RBAC Masonry Units. Studies regarding concrete masonry units have been performed. The use of RBAs as an alternative to aggregates can reduce the weight of the units. The test results of Aliabdo et al. [23] showed that the complete replacement of fine and coarse aggregates with RBAs reduced the compressive strength of the units. The dry unit weight of concrete masonry units decreased by approximately 25%. The water absorption of concrete masonry units increased with the increase in the content of RBAs. With the increase in RBAs, the thermal resistance of masonry concrete units improved significantly. Therefore, compared with natural aggregates, modified concrete masonry blocks demonstrate better thermal properties. They suggested that the replacement level of coarse aggregates should not exceed 50%; otherwise it would lead to a significant decline in compressive strength. As 20% fly ash was used to replace cement and 3% bubble was added in renewable brick aggregate concrete, the compressive strength of the specimens reached 19.4 MPa, thereby satisfying the requirements of load-bearing blocks; furthermore, the thermal conductivity was lower than that of normal concrete [80]. MU5 RBA block was studied; the size of the specimen was 390 mm × 190 mm × 190 mm, with a 57% pore rate. The results showed that the average compressive strength of the MU5 RBA block was 6%~12% lower than the calculated value of China standard formula. Additionally, the average flexural strength of the MU5 RBA block was 1.15 MPa, which satisfied the requirements of the test material. This block can be used in practice [81]. Zhan [82] reported that a block containing RBAs had higher water, carbonisation, and frost resistances.

Furthermore, waste clay bricks were used directly as half scale or full scale to build walls. The effects of scale on the masonry compressive strength, Young's modulus, shear modulus, and diagonal tensile strength based on component and material testing at two scales were studied. The results showed that the shear failure of the walls was affected by the diagonal tensile strength, axial load, and material properties (coefficient of friction and cohesion), and the flexural failure of the specimens was controlled by the aspect and axial load ratios [71].

4.2. RBAC Column and Beam. The performances of columns and beams containing RBAs were studied. Wang et al. [83] studied the seismic performance of columns with RBAs. Four columns were used; they exhibited natural aggregates, recycled concrete, RBAs, and fibre and silicon powder added in RBAs, respectively. They discovered that the seismic resistance of the three recycled concrete columns decreased compared with the normal concrete column. However, the addition of silica powder and fibre improved the elastic modulus and ductility. Liu et al. [84] revealed that the use of steel tubes improved the bearing capacity of columns. Ji et al. [85] and Wang et al. [86] observed the bending and shear properties of RBA beams; they reported that the specimens exhibited the similar damage form compared with normal concrete and that the reinforcing steel bar and concrete were bonded well. In addition, FRP-confined square plain concrete columns with RBAs were studied, and RBAC exhibited a lower stiffness than normal concrete; furthermore, confined RBAC columns showed higher ultimate loads and axial strains, indicating their stronger ductility [87–89].

5. Conclusions

The potential use of waste clay brick as a binder and aggregate substitute in mortar and concrete was summarised in this article. The pozzolanic activity of CBP allowed CBP to partially replace cement for the production of mortar. RBAs could be used to produce RBAC, even though the mechanical properties of RBAC were worse than those of normal concrete. The addition of RBAs improved the durability of RBAC in some cases. Furthermore, RBAC could reduce transportation costs and dead loads, and it could be used for the production of units, beams, and columns.

Completely replacing natural aggregates with RBAs has been shown to be feasible; it could reduce the consumption of natural resources and encourage the reuse of construction waste. As the structural performance of RBAC is important for constructional engineering, the application of RBAC in structures can be strengthened.

Conflicts of Interest

The authors declare that they have no conflicts of interest.

Acknowledgments

This work was funded by the Project of the Shaanxi Province Key Research and Development Program on Industry Innovation Chain (2018ZDCXL-SF-03-03-01) and the National Natural Science Foundation of China (51878552).

References

[1] A. Rao, K. N. Jha, and S. Misra, "Use of aggregates from recycled construction and demolition waste in concrete," *Resources, Conservation and Recycling*, vol. 50, no. 1, pp. 71–81, 2007.

[2] Z. Xiao, T.-C. Ling, S.-C. Kou, Q. Wang, and C.-S. Poon, "Use of wastes derived from earthquakes for the production of concrete masonry partition wall blocks," *Waste Management*, vol. 31, no. 8, pp. 1859–1866, 2011.

[3] S. Manfredi, R. Pant, D. W. Pennington, and A. Versmann, "Supporting environmentally sound decisions for waste management with LCT and LCA," *The International Journal of Life Cycle Assessment*, vol. 16, no. 9, pp. 937–939, 2011.

[4] M. F. España, *Actualización del Catálogo de Residuos Utilizables en Construcción*, 2010.

[5] R. A. Robayo Salazar, P. E. Mattey Centeno, Y. F. Silva Urrego, D. M. Burgos Galindo, and S. Delvasto Arjona, "Construction and demolition wastes: analysis of its management and reuse in Cali," *Revista Tecnura*, vol. 19, no. 44, pp. 157–170, 2015.

[6] M. Lennon, *Recycling Construction and Demolition Wastes: A Guide for Architects and Contractors*, Commonwealth of Massachusetts, Department of Environmental Protection, Boston, MA, USA, 2005.

[7] I. Zabalza Bribián, A. Valero Capilla, and A. Aranda Usón, "Life cycle assessment of building materials: comparative analysis of energy and environmental impacts and evaluation of the eco-efficiency improvement potential," *Building and Environment*, vol. 46, no. 5, pp. 1133–1140, 2011.

[8] A. A. Shakir, S. Naganathan, and K. N. B. Mustapha, "Effect of quarry dust and billet scale additions on the properties of fly ash bricks," *Iranian Journal of Science and Technology-Transactions of Civil Engineering*, vol. 38, no. C1, pp. 51–60, 2014.

[9] S. Mindess, J. F. Young, and D. Darwin, *Concrete*, Prentice Hall, Upper Saddle River, NJ, USA, 2nd edition, 2003.

[10] C. Chao, "Resource depletion and environmental discharge of cement production in China," *Journal of Anhui Agricultural Sciences*, vol. 35, no. 28, p. 8986, 2008.

[11] General Administration of Customs of the People's Republic of China, 2015.

[12] S. Jewell and S. M. Kimball, "Mineral commodity summaries 2015," *U.S. Geological Survey 2015*, vol. 9, p. 196, 2015.

[13] E. C. Directive, "Directive 2008/98/EC of the European parliament and of the council of 19 November 2008 on waste and repealing certain directives," *Official Journal of the European Union*, vol. 312, no. 3, pp. 3–30, 2008.

[14] EU Commission, *Roadmap to a Resource Efficient Europe*, European Commission, Brussels, Belgium, 2011.

[15] M. Bravo, J. de Brito, J. Pontes, and L. Evangelista, "Mechanical performance of concrete made with aggregates from construction and demolition waste recycling plants," *Journal of Cleaner Production*, vol. 99, pp. 59–74, 2015.

[16] A. Devenny and F. M. Khalaf, "Use of crushed brick as coarse aggregate in concrete," *Masonry International*, vol. 12, no. 3, pp. 81–84, 1999.

[17] T. C. Hansen, *Recycling of Demolished Concrete and Masonry*, E And FN Spon, New York, NY, USA, 1992.

[18] F. M. Khalaf and A. S. DeVenny, "Recycling of demolished masonry rubble as coarse aggregate in concrete: review," *Journal of Materials in Civil Engineering*, vol. 16, no. 4, pp. 331–340, 2004.

[19] F. Debieb and S. Kenai, "The use of coarse and fine crushed bricks as aggregate in concrete," *Construction and Building Materials*, vol. 22, no. 5, pp. 886–893, 2008.

[20] V. Letelier, J. Ortega, P. Muñoz, E. Tarela, and G. Moriconi, "Influence of waste brick powder in the mechanical properties of recycled aggregate concrete," *Sustainability*, vol. 10, no. 4, p. 1037, 2018.

[21] J. M. Ortega, V. Letelier, C. Solas, G. Moriconi, M. Á. Climent, and I. Sánchez, "Long-term effects of waste brick powder addition in the microstructure and service properties of mortars," *Construction and Building Materials*, vol. 182, pp. 691–702, 2018.

[22] P. K. Mehta and P. J. M. Monteiro, *Concrete: Microstructure, Properties, and Materials*, McGraw-Hill Education, New York, Ny, USA, 2017.

[23] A. A. Aliabdo, A.-E. M. Abd-Elmoaty, and H. H. Hassan, "Utilization of crushed clay brick in concrete industry," *Alexandria Engineering Journal*, vol. 53, no. 1, pp. 151–168, 2014.

[24] M. S. Kirgiz, "Strength gain mechanisms of blended-cements containing marble powder and brick powder," *KSCE Journal of Civil Engineering*, vol. 19, no. 1, pp. 165–172, 2015.

[25] R. D. Toledo Filho, J. P. Gonçalves, B. B. Americano, and E. M. R. Fairbairn, "Potential for use of crushed waste calcined-clay brick as a supplementary cementitious material in Brazil," *Cement and Concrete Research*, vol. 37, no. 9, pp. 1357–1365, 2007.

[26] J. P. Gonçalves, L. M. Tavares, R. D. Toledo Filho, and E. M. R. Fairbairn, "Performance evaluation of cement mortars modified with metakaolin or ground brick," *Construction and Building Materials*, vol. 23, no. 5, pp. 1971–1979, 2009.

[27] E. Navrátilová and P. Rovnaníková, "Pozzolanic properties of brick powders and their effect on the properties of modified

lime mortars," *Construction and Building Materials*, vol. 120, pp. 530–539, 2016.

[28] N. R. Rakhimova and R. Z. Rakhimov, "Alkali-activated cements and mortars based on blast furnace slag and red clay brick waste," *Materials & Design*, vol. 85, no. 11, pp. 324–331, 2015.

[29] R. A. Robayo, A. Mulford, J. Munera, and R. Mejía de Gutiérrez, "Alternative cements based on alkali-activated red clay brick waste," *Construction and Building Materials*, vol. 128, pp. 163–169, 2016.

[30] L. Reig, M. M. Tashima, M. V. Borrachero, J. Monzó, C. R. Cheeseman, and J. Payá, "Properties and microstructure of alkali-activated red clay brick waste," *Construction and Building Materials*, vol. 43, pp. 98–106, 2013.

[31] P. Rovnaník, B. Řezník, and P. Rovnaníková, "Blended alkali-activated fly ash/brick powder materials," *Procedia Engineering*, vol. 151, pp. 108–113, 2016.

[32] M. O'Farrell, S. Wild, and B. B. Sabir, "Pore size distribution and compressive strength of waste clay brick mortar," *Cement and Concrete Composites*, vol. 23, no. 1, pp. 81–91, 2001.

[33] S. Liu, R. Dai, K. Cao, and Z. Gao, "The role of sintered clay brick powder during the hydration process of cement pastes," *Iranian Journal of Science and Technology, Transactions of Civil Engineering*, vol. 41, no. 2, pp. 159–165, 2017.

[34] S. Boukour and M. L. Benmalek, "Performance evaluation of a resinous cement mortar modified with crushed clay brick and tire rubber aggregate," *Construction and Building Materials*, vol. 120, pp. 473–481, 2016.

[35] H. Binici, S. Kapur, J. Arocena, H. Kaplan, and H. Kaplan, "The sulphate resistance of cements containing red brick dust and ground basaltic pumice with sub-microscopic evidence of intra-pore gypsum and ettringite as strengtheners," *Cement and Concrete Composites*, vol. 34, no. 2, pp. 279–287, 2012.

[36] M. Adamson, A. Razmjoo, and A. Poursaee, "Durability of concrete incorporating crushed brick as coarse aggregate," *Construction and Building Materials*, vol. 94, pp. 426–432, 2015.

[37] A. Wongsa, V. Sata, P. Nuaklong, and P. Chindaprasirt, "Use of crushed clay brick and pumice aggregates in lightweight geopolymer concrete," *Construction and Building Materials*, vol. 188, pp. 1025–1034, 2018.

[38] M. Heikal, K. M. Zohdy, and M. Abdelkreem, "Mechanical, microstructure and rheological characteristics of high performance self-compacting cement pastes and concrete containing ground clay bricks," *Construction and Building Materials*, vol. 38, pp. 101–109, 2013.

[39] M. Nematzadeh, J. Dashti, and B. Ganjavi, "Optimizing compressive behavior of concrete containing fine recycled refractory brick aggregate together with calcium aluminate cement and polyvinyl alcohol fibers exposed to acidic environment," *Construction and Building Materials*, vol. 164, pp. 837–849, 2018.

[40] K. Jankovic, D. Bojovic, D. Nikolic, L. Loncar, and Z. Romakov, "Frost resistance of concrete with crushed brick as aggregate," *Facta Universitatis—Series: Architecture and Civil Engineering*, vol. 8, no. 2, pp. 155–162, 2010.

[41] P. Rovnaníková, *Plasters*, Society for Monument Protection Techniques, Prague, Czech Republic, 2002.

[42] C. Shi and R. L. Day, "Pozzolanic reaction in the presence of chemical activators: part II—reaction products and mechanism," *Cement and Concrete Research*, vol. 30, no. 4, pp. 607–613, 2000.

[43] J. Cabrera and M. F. Rojas, "Mechanism of hydration of the metakaolin-lime-water system," *Cement and Concrete Research*, vol. 31, no. 2, pp. 177–182, 2001.

[44] A. Gameiro, A. Santos Silva, R. Veiga, and A. Velosa, "Hydration products of lime-metakaolin pastes at ambient temperature with ageing," *Thermochimica Acta*, vol. 535, pp. 36–41, 2012.

[45] Z. Ge, Y. Wang, R. Sun, X. Wu, and Y. Guan, "Influence of ground waste clay brick on properties of fresh and hardened concrete," *Construction and Building Materials*, vol. 98, pp. 128–136, 2015.

[46] M. F. Rojas, "Study of hydrated phases present in a MK–lime system cured at 60°C and 60 months of reaction," *Cement and Concrete Research*, vol. 36, no. 5, pp. 827–831, 2006.

[47] F. Bektas, K. Wang, and H. Ceylan, "Effects of crushed clay brick aggregate on mortar durability," *Construction and Building Materials*, vol. 23, no. 5, pp. 1909–1914, 2009.

[48] A. Mobili, C. Giosuè, V. Corinaldesi, and F. Tittarelli, "Bricks and concrete wastes as coarse and fine aggregates in sustainable mortars," *Advances in Materials Science and Engineering*, vol. 2018, Article ID 8676708, 11 pages, 2018.

[49] L. G. Li, Z. Y. Zhuo, J. Zhu, and A. K. H. Kwan, "Adding ceramic polishing waste as paste substitute to improve sulphate and shrinkage resistances of mortar," *Powder Technology*, vol. 362, pp. 149–156, 2020.

[50] L. G. Li, Z. Y. Zhuo, A. K. H. Kwan, T. S. Zhang, and D. G. Lu, "Cementing efficiency factors of ceramic polishing residue in compressive strength and chloride resistance of mortar," *Powder Technology*, vol. 367, pp. 163–171, 2020.

[51] F. Bektaş, "Alkali reactivity of crushed clay brick aggregate," *Construction and Building Materials*, vol. 52, pp. 79–85, 2014.

[52] F. M. Khalaf, "Using crushed clay brick as coarse aggregate in concrete," *Journal of Materials in Civil Engineering*, vol. 18, no. 4, pp. 518–526, 2006.

[53] L. Zong, Z. Fei, and S. Zhang, "Permeability of recycled aggregate concrete containing fly ash and clay brick waste," *Journal of Cleaner Production*, vol. 70, pp. 175–182, 2014.

[54] S. I. Ahmad and M. A. Hossain, "Water permeability characteristics of normal strength concrete made from crushed clay bricks as coarse aggregate," *Advances in Materials Science and Engineering*, vol. 2017, Article ID 7279138, 9 pages, 2017.

[55] J. S. González, F. L. Gayarre, C. L.-C. Pérez, P. S. Ros, and M. A. S. López, "Influence of recycled brick aggregates on properties of structural concrete for manufacturing precast prestressed beams," *Construction and Building Materials*, vol. 149, pp. 507–514, 2017.

[56] F. M. Khalaf and A. S. DeVenny, "Properties of new and recycled clay brick aggregates for use in concrete," *Journal of Materials in Civil Engineering*, vol. 17, no. 4, pp. 456–464, 2005.

[57] F. M. Khalaf and A. S. Devenny, "Performance of brick aggregate concrete at high temperatures," *Journal of Materials in Civil Engineering*, vol. 16, no. 6, pp. 556–565, 2004.

[58] S. Zhang and L. Zong, "Properties of concrete made with recycled coarse aggregate from waste brick," *Environmental Progress & Sustainable Energy*, vol. 33, no. 4, pp. 1283–1289, 2013.

[59] T. K. Šipoš, I. Miličević, and R. Siddique, "Model for mix design of brick aggregate concrete based on neural network modelling," *Construction and Building Materials*, vol. 148, pp. 757–769, 2017.

[60] C. Zheng, C. Lou, G. Du, X. Li, Z. Liu, and L. Li, "Mechanical properties of recycled concrete with demolished waste

concrete aggregate and clay brick aggregate," *Results in Physics*, vol. 9, pp. 1317–1322, 2018.

[61] Z. Zhang, Y. Zhang, C. Yan, and Y. Liu, "Influence of crushing index on properties of recycled aggregates pervious concrete," *Construction and Building Materials*, vol. 135, pp. 112–118, 2017.

[62] Z. Ge, Z. Gao, R. Sun, and L. Zheng, "Mix design of concrete with recycled clay-brick-powder using the orthogonal design method," *Construction and Building Materials*, vol. 31, pp. 289–293, 2012.

[63] P. B. Cachim, "Mechanical properties of brick aggregate concrete," *Construction and Building Materials*, vol. 23, no. 3, pp. 1292–1297, 2009.

[64] M. S. Islam and M. A. A. Siddique, "Behavior of low grade steel fiber reinforced concrete made with fresh and recycled brick aggregates," *Advances in Civil Engineering*, vol. 2017, Article ID 1812363, 14 pages, 2017.

[65] A. Naceri and M. C. Hamina, "Use of waste brick as a partial replacement of cement in mortar," *Waste Management*, vol. 29, no. 8, pp. 2378–2384, 2009.

[66] T. Manzur, B. Baten, M. J. Hasan, H. Akter, A. Tahsin, and K. M. A. Hossain, "Corrosion behavior of concrete mixes with masonry chips as coarse aggregate," *Construction and Building Materials*, vol. 185, pp. 20–29, 2018.

[67] L. G. Li, J. J. Feng, J. Zhu, S. H. Chu, and A. K. H. Kwan, "Pervious concrete: effects of porosity on permeability and strength," *Magazine of Concrete Research*, pp. 1–35, 2019.

[68] M. T. Uddin, A. H. Mahmood, M. R. I. Kamal, S. M. Yashin, and Z. U. A. Zihan, "Effects of maximum size of brick aggregate on properties of concrete," *Construction and Building Materials*, vol. 134, pp. 713–726, 2017.

[69] T. U. Mohammed and A. H. Mahmood, "Effects of maximum aggregate size on UPV of brick aggregate concrete," *Ultrasonics*, vol. 69, pp. 129–136, 2016.

[70] I. Martínez-Lage, F. Martínez-Abella, C. Vázquez-Herrero, and J. L. Pérez-Ordóñez, "Properties of plain concrete made with mixed recycled coarse aggregate," *Construction and Building Materials*, vol. 37, no. 3, pp. 171–176, 2012.

[71] C. L. Knox, D. Dizhur, and J. M. Ingham, "Experimental study on scale effects in clay brick masonry prisms and wall panels investigating compression and shear related properties," *Construction and Building Materials*, vol. 163, pp. 706–713, 2018.

[72] M. C. S. Nepomuceno, R. A. S. Isidoro, and J. P. G. Catarino, "Mechanical performance evaluation of concrete made with recycled ceramic coarse aggregates from industrial brick waste," *Construction and Building Materials*, vol. 165, pp. 284–294, 2018.

[73] M. M. Disfani, A. Arulrajah, H. Haghighi, A. Mohammadinia, and S. Horpibulsuk, "Flexural beam fatigue strength evaluation of crushed brick as a supplementary material in cement stabilized recycled concrete aggregates," *Construction and Building Materials*, vol. 68, no. 5, pp. 667–676, 2014.

[74] J. M. Khatib, "Properties of concrete incorporating fine recycled aggregate," *Cement and Concrete Research*, vol. 35, no. 4, pp. 763–769, 2005.

[75] K. Jankovic, D. Nikolic, and D. Bojovic, "Concrete paving blocks and flags made with crushed brick as aggregate," *Construction and Building Materials*, vol. 28, no. 1, pp. 659–663, 2012.

[76] K. S. Baek and Y. S. Kim, "A study on the carbonation resistance of concrete using crushed clay bricks as coarse aggregate," *Journal of the Regional Association of Architectural Institute of Korea*, vol. 10, no. 4, pp. 233–240, 2008.

[77] Y. Gu, "Research on the application of recycled aggregates from waste brick in concrete," Master's thesis, Anhui Jianzhu University, Hefei, China, 2015.

[78] A. Baradaran-Nasiri and M. Nematzadeh, "The effect of elevated temperatures on the mechanical properties of concrete with fine recycled refractory brick aggregate and aluminate cement," *Construction and Building Materials*, vol. 147, pp. 865–875, 2017.

[79] L. Zhu, J. Dai, G. Bai, and F. Zhang, "Study on thermal properties of recycled aggregate concrete and recycled concrete blocks," *Construction and Building Materials*, vol. 94, pp. 620–628, 2015.

[80] L. Wu, J. Yao, S. Gao, X. Zhu, B. Zhou, and X. Xu, "Research on factors affecting physical and mechanical properties of pre-placed concrete slabs with recycled brick aggregate manufactured by grouting," *Journal of Water Resources and Architectural Engineering*, vol. 13, no. 6, pp. 214–220, 2015, in Chinese.

[81] W. Cao, L. Huang, Q. T. Gao, T. Bao, F. Li, and Y. Li, "Experimental study on the basic mechanical properties of recycled brick aggregate masonry," *Journal of Railway Science and Engineering*, vol. 16, no. 2, pp. 114–120, 2019, in Chinese.

[82] N. Zhan, "Experimental research on durability of crushed bricks as aggregate in recycled concrete wall bricks," Master's thesis, Anhui Jianzhu University, Hefei, China, 2016.

[83] S. Wang, T. Yang, and T. Li, "An experimental research on regenerated brick granules effect on seismic behavior of recycled concrete columns," *Industrial Construction*, vol. 43, no. 11, pp. 26–29, 2013.

[84] P. Liu, X. Du, J. Liang, Z. Niu, and J. Shi, "Exerimental study on short column axial compression performance of recycled aggregate concrete filled square steel tube," *Journal of Agricultural University of Hebei*, vol. 5, pp. 112–118, 2017, in Chinese.

[85] C. Ji, A. Zhai, W. Zhai, S. Chen, and C. Wang, "Experimental study on flexural performance of recycled brick coarse aggregate concrete beam," *Hydro-science and Engineering*, vol. 6, pp. 59–64, 2012, in Chinese.

[86] C. Wang, A. Zhai, S. Chen, C. Ji, and A. Zhao, "Analysis of anti-shear capacity of slope section for recycled brick aggregate concrete beam," *Journal of Water Resources and Water Engineering*, vol. 24, no. 2, pp. 151–154, 2013, in Chinese.

[87] B. Yan, L. Huang, L. Yan, C. Gao, and B. Kasal, "Behavior of flax FRP tube encased recycled aggregate concrete with clay brick aggregate," *Construction and Building Materials*, vol. 136, no. 2, pp. 265–276, 2017.

[88] L. Huang, L. Chen, L. Yan et al., "Behavior of polyester FRP tube encased recycled aggregate concrete with recycled clay brick aggregate: size and slenderness ratio effects," *Construction and Building Materials*, vol. 154, pp. 123–136, 2017.

[89] M. M. Islam, M. S. I. Choudhury, and A. F. M. S. Amin, "Dilation effects in FRP-confined square concrete columns using stone, brick, and recycled coarse aggregates," *Journal of Composites for Construction*, vol. 20, no. 1, Article ID 04015017, 2015.

Hindawi
Advances in Materials Science and Engineering
Volume 2020, Article ID 3575709, 10 pages
https://doi.org/10.1155/2020/3575709

Research Article

Shrinkage and Strength Properties of Coal Gangue Ceramsite Lightweight Aggregate Concrete

Yunsen Wang,[1] **Jingping Qiu**,[1] **and Chao Zeng**[2]

[1]*Key Laboratory of Ministry of Education on Safe Mining of Deep Metal Mines, Northeastern University, Shenyang, China*
[2]*Department of Civil, Architectural and Environmental Engineering, Missouri University of Science and Technology, Rolla, MO, USA*

Correspondence should be addressed to Yunsen Wang; wangyunsen@mail.neu.edu.cn

Received 16 February 2020; Revised 17 April 2020; Accepted 30 April 2020; Published 15 May 2020

Guest Editor: Ana S. Guimarães

It is a promising and effective method for waste treatment by using coal gangue to make lightweight aggregate concrete. However, lightweight aggregate concrete with low-density coal gangue ceramsite is prone to cracking during volume shrinkage, which limits its application in the construction industry. In an attempt to resolve the problem of cracking in shrinkage, this study investigated the effect of prewetting time and shrinkage reducing agents on shrinkage volume and concrete strength through a series of concrete shrinkage and strength tests. The experimental results show that shrinkage volume reduced at a prewetting time of 12 hrs or with a 2% addition of D-230 polyether amine reductant. With the optimal conditions of 12 hrs prewetting time and 2% addition of the reductant, the concrete shrinkage volume significantly decreased with a negligible impact on its strength. Appropriate amount of shrinkage reducing agent and adjustment of prewetting time of coal gangue ceramsite are necessary to reduce the shrinkage rate and improve the stability of the specimen. This is of great significance to wide application of lightweight aggregate concrete with coal gangue ceramsite.

1. Introduction

Coal gangue is a kind of solid waste generated by the coal mining and washing. Long-term storage not only takes up space but also causes serious pollution and destruction of the surrounding environment [1–3]. The treatment and utilization of coal gangue has attracted the interest of many researchers [4] since the 1970s. Coal gangue has been widely used for power generation, the extraction of chemical products, and the creation of chemical fertilizers and ceramsite [5–9].

Coal gangue can be converted into low-density ceramsite aggregates, which can be used to make low-density coal lightweight aggregate concrete, usually with an apparent density <1950 kg/m^3 [10].There are three types of coal gangue ceramsites (CGC): self-igniting coal gangue, burning coal gangue, and coal gangue mixed with binder [11]. Utilizing coal gangue to make CGC instead of natural, ordinary aggregate can reduce coal gangue disposal and lead to a significant reduction in the consumption of natural aggregates in the construction industry.

Compared with ordinary concrete, lightweight aggregate concrete has many attractive characteristics, such as lower density, higher strength, better antiseismic performance, and so on [12]. Many studies have been conducted on the preparation and expansion behavior of this concrete (the densities not exceeding 1950 kg/m^3) in the presence of additives including carbon fiber, waste materials [13, 14], and reductants [15–21]. However, owing to the high water absorption and porosity, large volume shrinkage of lightweight aggregate concrete causes the formation of cracks. These cracks connect to flow paths for gases, water, and aggressive substances. It is harmful for the durability and compromise of the performance of concrete structures [13]. This limits its application in the construction industry to a large extent. Many attempts to tackle this problem have been made in LWAC. For reefs aggregate, Cheng et al. [22] studied the drying shrinkage behavior of the concrete with

different moisture contents. It is found that increasing the moisture content significantly reduced its shrinkage rate and the concrete made of saturated reef aggregates showed good performance in reducing autogenous shrinkage. For saturated lightweight aggregate, Henkensiefken et al. [23] studied the effect of the amount of cementitious material on LWAC shrinkage and found that specimens with larger volume fractions of SLWA reduced its shrinkage rate. For fly ash-clay ceramsite, Wang et al. [24] studied the effect of ceramsite prewetting on LWAC autogenous shrinkage by using microstructural analysis of the concrete and found that moisture content had influence on the shrinkage but was not dominant. For the shale ceramsite, Gong et al. [25] verified that the presence of a reductant can reduce the drying shrinkage and autogenous shrinkage of the concrete, thus mitigating the cracking issue. These studies have shown that adjusting the prewetting time or addition of a certain amount of reductant can effectively suppress shrinkage of the concrete. However, for coal gangue ceramsite, systematic tests on wetting time and shrinkage reducing agents have not been reported in any prior study. Three problems remain: (1) the lack of a quantitative relationship between CGC prewetting time and concrete shrinkage, (2) the lack of a quantitative relationship between the amount of SRA used and concrete shrinkage, and (3) the lack of a quantitative understanding of the combined effect of lightweight aggregate prewetting time and SRA amount on volume shrinkage and concrete strength.

The present study is conducted to fill these research gaps by investigating shrinkage and strength properties of coal gangue ceramsite lightweight aggregate concrete. A series of concrete shrinkage and strength tests were undertaken for different CGC prewetting times and SRA doses, separately. Through these experiments, the effects of CGC prewetting time and SRA on concrete shrinkage and strength will be analyzed, and the results will provide effective guidance for solving the concrete shrinkage problem.

2. Experimental Investigation

2.1. Materials Preparation. Ceramsite is a main component of coal gangue ceramsite lightweight aggregate concrete and accounts for approximately 50% of its total volume. Its properties have significant influence on the performance of the concrete. The coal gangue ceramsite used in this study was produced by Chaoyang Hualong Kejian Co., Ltd, and its morphology is shown in Figure 1. This product has similar physical characteristics and particle size distribution to ordinary concrete, as seen in Tables 1 and 2, respectively. It is widely used for concrete testing experiments.

JEEFMINE® D-230 polyether amine, with an average molecular weight of approximately 230, was used as a reductant. Limestone sand with a particle size ranging from 0.15 mm to 2.34 mm was used as a fine aggregate. Tap water was used in all experiments. In this study, the dose of the added reductant ranged from 0.5% to 1.0% while the water-cement ratio ranged from 15% to 20%.

The fraction of the coal gangue ceramsite with a particle size ranging within 9.5~16 mm was 87.8% (see Table 2), which meets the standard requirements for concrete materials (ASTM C330/C330M).

Figure 1: Morphology of the coal gangue ceramsite used in this study.

The cement used was P • O • A32.5 grade slag Portland cement. Its physical properties and chemical composition are shown in Tables 3 and 4, respectively.

The compressive strength at 28 d was 40.1 MPa, as shown in Table 3, and the loss on ignition was 1.06%, as shown in Table 4. The physical properties of the cement in terms of strength, chemical composition, and loss on ignition meet the quality requirements laid out in GB175-2007 entitled "General Portland Cement" and also meet the test requirements.

2.2. Design of Mixing Proportions for LWAC and CGC. In JGJ12-2006, which is entitled "Technical Regulations for Lightweight Aggregate Concrete Structure," the strength grade for structural LWAC is specified. In this test, LWAC was designed with compressive strength grade LC30. The initial mixing proportions are in Table 5. The following experiments are adjusted on the basis of the proportions.

2.3. Preparation and Experimental Procedure

2.3.1. LWAC Mixing and Curing. In the LWAC mixing process, the following stirring procedures were applied: first stir the cement, ceramic, and fine aggregate evenly, and then add the appropriate amount of water and superplasticizer (Figure 2). The mold size was 100 mm × 100 mm × 515 mm, and the mixture well mixed by hand was placed in the mold to vibrate for 120 s; after 24 h, it was stripped for standard curing, and finally, the test was performed. Similarly, the following CGC prewetting procedure was followed: weigh the CGC; immerse the CGC in water for a certain period of time; drain the water to keep the saturated surface dry; and vibrate the mixture for 60 s.

The specimens were cured at a temperature of $20 \pm 2^{\circ}$C and immersed in a saturated solution of $Ca(OH)_2$. Then, concrete performance tests were carried out according to the GBT50081-2002 standard.

Table 1: Physical characteristics of coal gangue ceramsite (based on GB/T 17431-2010).

Type of aggregate	Packing density (kg/m3)	Apparent density (kg/m3)	Compressive strength (MPa)	Water absorption rate(%)			
CGC	975	1730	35	5.07	6.50	7.02	7.43

Table 2: Particle size distribution for coal gangue ceramsite.

Sieve size (mm)	19.0	16.0	9.50	4.75
Cumulative screen residue (%)	0	12	99.8	99.8

Table 3: Physical properties of the cement.

Setting time (min)		Stability	Flexural strength (MPa)		Compressive strength (MPa)		Fineness 80 μm sieve residue (%)	Density (g/m^3)
Initial setting	Final setting		3 d	28 d	3 d	28 d		
204	312	Qualified	3.8	6.5	18.3	40.1	5.6	3.03

Table 4: Chemical composition of the cement.

CaO (%)	SiO_2 (%)	Al_2O_3 (%)	Fe_2O_3 (%)	MgO (%)	SO_3 (%)	Loss on ignition (%)
63.48	21.30	5.55	3.46	2.54	2.67	1.06

Table 5: Mixing proportions for LWAC with CGC.

Mix proportions (kg/m^3)					28 d compressive strength (MPa)
Cement	Water	Sand	CGC	Apparent density (kg/m3)	
420	155	564	702	1749	38.4

Figure 2: Forming a concrete specimen.

2.3.2. Compressive Strength Test for LWAC. The test machine was an NYL-200D. The instructions were as follows: place the specimen in the center of the lower press plate, keeping the center of the specimen in line with the center of the press plate (Figure 3). Start the press with the lower surface of the press plate facing upward. When the specimen is close to the upper plate and the upper pressure surface is in contact with the balanced test body, apply a uniform continuous load at a loading rate of 0.6 ± 0.1 MPa. When the deformed specimen is close to destruction, stop adjusting the throttle of the press, and continue to load until destruction. Then, record the failure load. The compressive strength of LWAC was calculated as follows:

$$f_{cu} = \frac{F}{A}, \tag{1}$$

Figure 3: A picture after the specimen is damaged.

where f_{cu} denotes the compressive strength of LWAC, MPa; F represents the specimen failure load, N; and A is the specimen bearing area, mm^2.

F and A are readily measured experimentally. From equation (1), the compressive strength for the test specimen size can be calculated. However, it must be noted that the product of this value and the size conversion factor (set to 0.95 in this study based on the standard set in GBT 50082-2009) is the final compressive strength for the standard size concrete.

2.3.3. Shrinkage Experiment for LWAC. The LWAC shrinkage test comes from GBT 50082-2009 entitled "ordinary concrete long-term performance and durability test method standards." After the specimen is modeled, it should be cured for 24 ± 2 h with a membrane (Figure 4). The specimen's initial length (L_0) is measured by an HSP-540 contraction expansion instrument, and then the specimen is placed in an environment in which the temperature is 20 ± 3°C and the humidity is 60 ± 5% at the proper time point to measure the specimen's length (L_t). The resolution for the length measurement is 0.01 mm.

The shrinkage rate for the specimen is calculated by using the following formula:

$$\varepsilon_{st} = \frac{L_0 - L_t}{L_b} \tag{2}$$

where ε_{st} is the shrinkage rate of the concrete at time t, t is the time elapsed after the initial length is measured, days; L_b is the measured gauge of the specimen, that is, the distance between the inner sides of the concrete specimen, mm; L_0 is the initial length of the specimen, mm; and L_t is the length of the specimen measured at t, mm.

The shrinkage rates for the three specimens are averaged to calculate the shrinkage rate for the group, and the resolution of the final shrinkage rate is approximately 1.0×10^{-6}.

3. Results and Discussion

3.1. Effect of CGC Prewetting Time on Volume Shrinkage of LWAC. Five sets of LWAC were prepared according to the reference mixture proportions (see Table 5 for the mixture proportions). The selected prewetting times for the ceramsite are 0 h, 1 h, 6 h, 12 h, and 24 h. Three specimens were formed for each concrete test set. After the specimens were molded for 1 d, they were demolded, and their initial length was determined according to the GBT 50082-2009 method. Thereafter, the shrinkage and strength of the specimens were measured at 1 d, 3 d, 7 d, 14 d, 28 d, and 56 d.

As seen from Figure 5, the shrinkage of LWAC develops gradually. LWAC shrinkage increases with time. Early on, the slope of the curve is large, indicating that the LWAC shrinkage rate is maximal. In the later stage, the LWAC shrinkage tends to level off. For example, the shrinkage rate for concrete at 3 d is more than 70% of the shrinkage rate at 28 d.

It can be seen from Figure 6 that the shrinkage rate for LWAC decreases as the CGC prewetting time increases, but this decrease is not constant. When the prewetting time goes from 0 h to 1 h, the shrinkage rate at 56 d (in Figure 6(b)) decreases by approximately 25×10^{-6} mm/mm, while when the prewetting time goes from 12 h to 24 h, the shrinkage rate at 56 d (in Figure 6(b)) decreases by only approximately 9×10^{-6} mm/mm. This is because CGC water absorption increases rapidly in the early flooding stage, and the absorption rate reaches 5.07% at 1 h. However, when the ceramsite is almost fully saturated after 12 h, the water absorption rate for the ceramsite is only 0.38%.

Therefore, the described approach is an effective way to reduce the drying shrinkage of LWAC for longer prewetting times because the prewet ceramsite contains a certain amount of water, and some of the water is gradually released in the late hydration process; thus, the relative humidity decreases slowly to compensate for the shrinkage. However, when the prewetting time exceeds 24 h, the moisture content of the CGC has negligible variation, and the effect of the prewetting time on the shrinkage reduction rate is insignificant.

3.2. Effect of CGC Prewetting Time on the Strength of LWAC. Figure 7 shows that the prewetting time improves the mechanical resistance at 14 and 28 d, and the only decrease is observed when the test is performed early (at 7 d). This improvement is probably because the strength of the concrete and the cement stone depends on the interfacial adhesion of the aggregate and the cement stone. The denser the interface area of the structure, the greater the cohesive force and, hence, the higher the strength of the concrete. This trend probably also originates from a deficiency in the LWAC preparation due to a minor operation error. At 7 d, as the moisture content of the CGC increases from 0 to 7.43% (from C0 to C4), its ability to absorb moisture from the cement slurry decreases, resulting in a decrease in the water-cement ratio at the interface. The larger the water-cement ratio at the interface is, the greater the porosity is, so the early strength decreases. At 28 d, with the further progression of the hydration reaction, the internal humidity of the cement slurry gradually decreases. The water return capacity increases with an increase in the prewetting time, so the cement in the interface area can be fully hydrated. This causes an increase in the density of the interface structure, so the compressive strength at 28 d increases. As seen in Figure 8, with an increase in the degree of ceramsite prewetting, the strength growth rate for LWAC also increases. The growth rate for LWAC (C0) prepared with dry ceramic is 17.5%, while the growth rate for LWAC (C4) is 35.9%.

In the results of the preceding analysis, it can be seen that the strength of the LWAC decreases at a certain rate in the early stage after CGC prewetting, and the internal curing effect on the prewet ceramsite enhances its strength. This enhancement will increase with the degree of prewetting.

3.3. Effect of SRA on the Volume Shrinkage of LWAC. In the experiment, five groups of LWAC were prepared by

Figure 4: Shrinkage test device and concrete specimen.

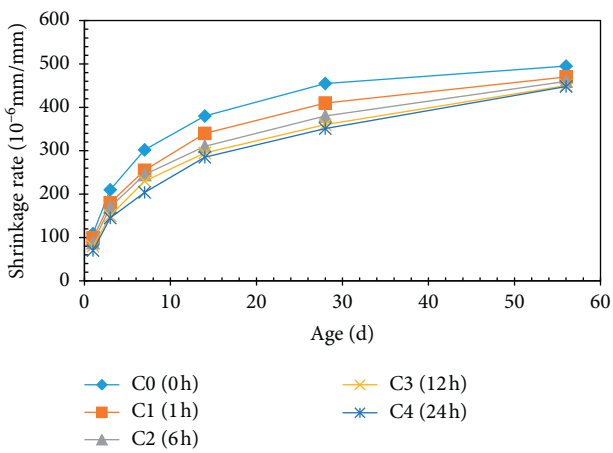

Figure 5: Effect of prewetting time on shrinkage rate for different CGC prewetting times.

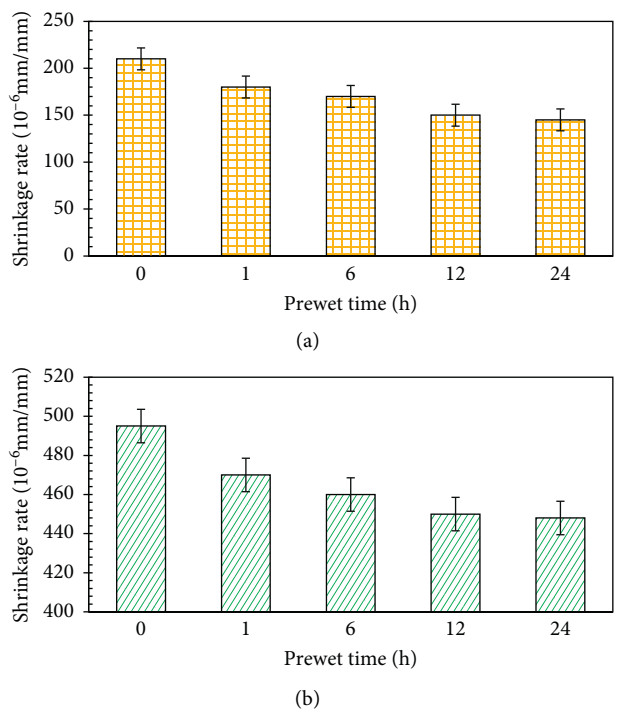

Figure 6: Shrinkage rate for different prewetting times (a) at 3 d and (b) 56 d.

adjusting the dose of SRA (0%, 0.5%, 1.0%, 2.0%, and 4.0% of the cement mass, respectively): the groups are denoted as C0, D1, D2, D3, and D4, respectively. The initial length of the specimens was determined by the GBT 50082-2009 method, and then the shrinkage was calculated at the following time points: 1 d, 3 d, 7 d, 14 d, 28 d, and 56 d.

It can be seen in Figure 9 that the addition of SRA considerably reduces the shrinkage of LWAC. With an increase in SRA, the LWAC shrinkage decreases gradually for each sample time point. For example, the shrinkage rates at 14 d, 28 d, and 56 d for C1 are approximately 79%, 82%, and 79% of those for C0. In the case of C1, when the concentration of water is approximately 1.3%, the cement paste internal capillary solution for the surface tension drops significantly, thereby reducing the negative pressure inside the gap and reducing the shrinkage of the specimen.

However, the shrinkage rate for LWAC instead decreases with an increase in SRA content. As shown in Figures 10(a) and 10(b), the shrinkage rate for LWAC is influenced by the amount of SRA, which decreases monotonically with decreasing slope. A slower shrinkage reduction rate beyond 2% can be seen in both graphs. When SRA content increases from 2.0% to 4.0%, the shrinkage at 3 d decreases by approximately 6%, and the shrinkage at 56 d decreases by 3%. This slower reduction after the 2% dose can be explained by the reduction of the solution surface tension. When SRA makes up over 2.0% of the cement, its concentration in the water is more than

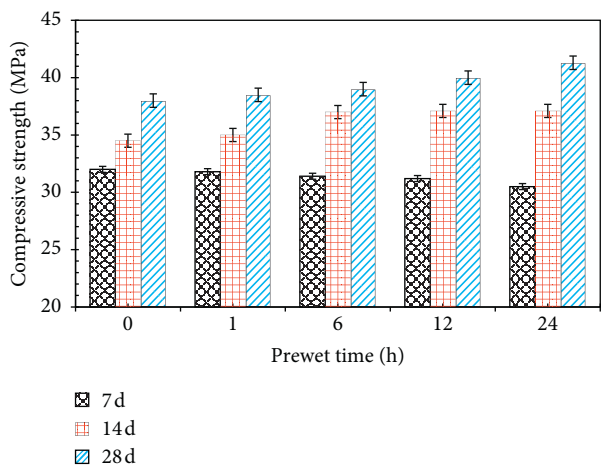

Figure 7: Effect of prewetting time of CGC on the compressive strength of the concrete.

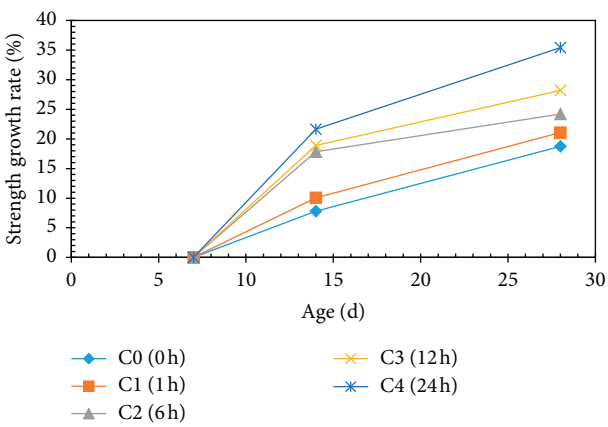

Figure 8: Strength growth rate for the concrete at different ages.

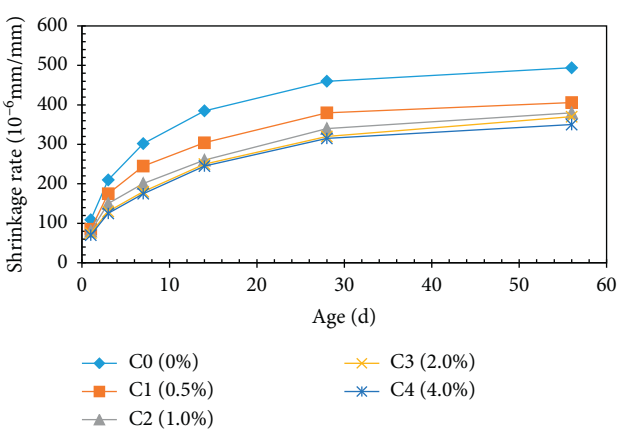

Figure 9: Effect of SRA dose on concrete shrinkage.

5.0%. Considering the dependence of the solution surface tension on the SRA, the reduction in surface tension slows after a certain dose, leading to a smaller effect of SRA on LWAC shrinkage. This finding is also consistent with the dose recommended in the product specification (1.0–3.0% of the mass of the cement).

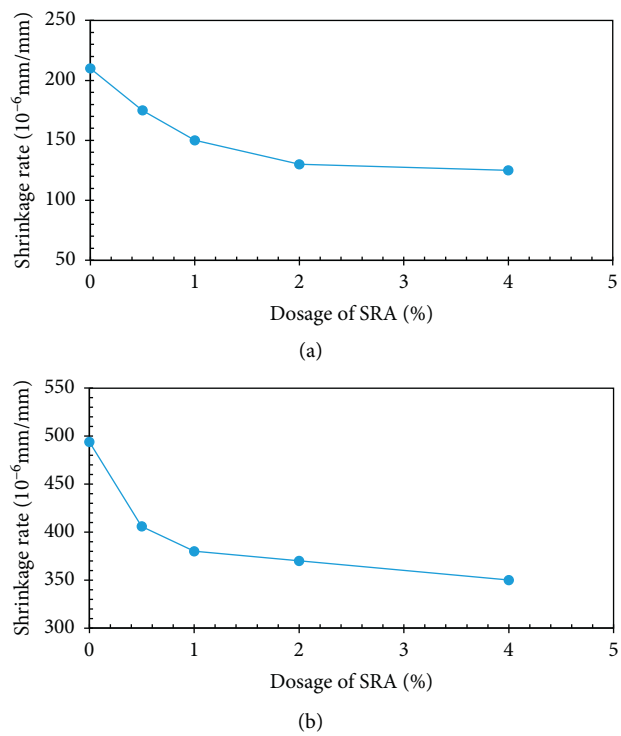

Figure 10: Concrete shrinkage with different doses of SRA (a) at 3 d and (b) 56 d.

3.4. Effect of SRA on LWAC Strength. As described above, five different percentages of SRA (0%, 0.5%, 1%, 2%, and 4%) were used in the construction of the cement test groups. Three sets of samples were prepared in each test group. After 1 d of stripping, they were placed in saturated $Ca(OH)_2$ solution. According to the methods of GB/T 50081-2002 "Test method of mechanical properties of ordinary concrete," the compressive strength was measured at 7 d, 14 d, and 28 d. Then, the compressive strength of the concrete was measured.

Figure 11 illustrates that the SRA mixture has an adverse effect on the compressive strength of LWAC. With an increase in SRA, the compressive strength of LWAC gradually decreases. Compared to the reference group (0% SRA), the compressive strength for LWAC with 2% SRA decreases by 6% and 3% at 7 d and 28 d, respectively. When the SRA dose increases to 4%, the compressive strength of the concrete decreases significantly, by 10% and 5% at 7 d and 28 d, respectively. This is consistent with Rajabipour's study [26], which suggested that when the SRA dose is less than 2%, there is no adverse effect on strength, whereas the strength of the concrete is reduced when SRA is increased to 5% of the cement content.

3.5. Combined Effect of SRA and Prewetting Time on LWAC Shrinkage. Figure 12 presents the conditions in which a combination of 2.0% SRA and different prewetting times (0 h, 1 h, 6 h, and 24 h) are used. Based on the similar curve trends with and without SRA, shrinkage suppression can mainly be attributed to prewetting. It should be noted that,

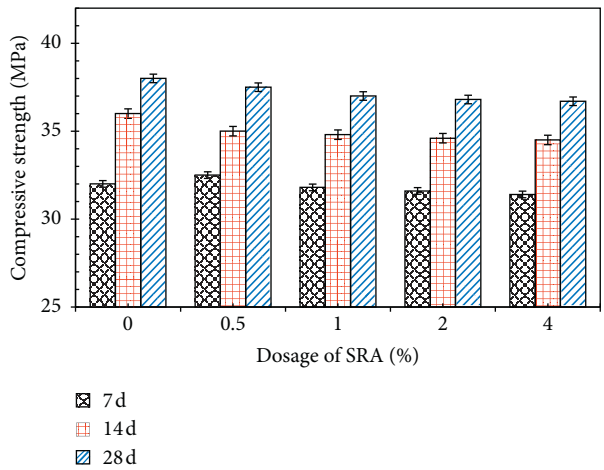

Figure 11: Effect of SRA dose on the compressive strength of concrete.

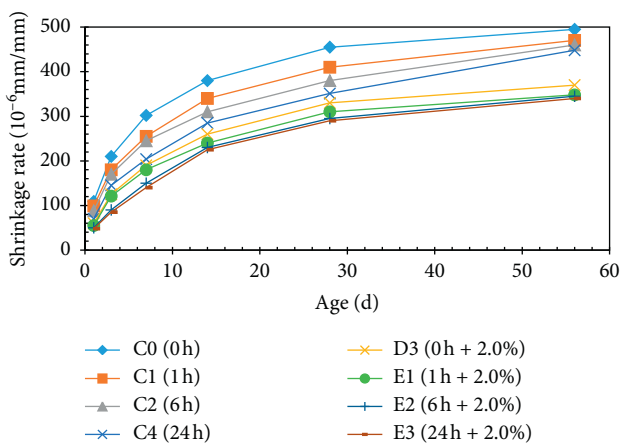

Figure 12: Effect of the prewetting time on concrete shrinkage with SRA incorporation.

since the relative ratio of water to cement in the experiment is 0.4%, the concentration in the water is approximately 5.0% with 2% SRA, indicating an increasing concentration of SRA. Therefore, tension is reduced a small amount, which is able to prevent significant shrinkage.

Figure 13 displays a similar decreasing trend with respect to the prewetting time for the shrinkage rate in both scenarios. When the prewetting time extends from 0 to 1 h, the shrinkage rate decreases markedly. However, when the prewetting time extends from 1 h to 12 h, the variation in the shrinkage rate is subtle. The difference in shrinkage variation after 1 h can be clearly seen in the two graphs. The case without SRA has a relatively larger reduction compared to the other case.

More quantitatively, the shrinkage (mm/mm) for C0, C1, C2, and C4 (in Figure 13(a)) at 56 d was 497×10^{-6}, 473×10^{-6}, 463×10^{-6}, and 449×10^{-6}. Compared with the lightweight aggregate C0 reference, the shrinkage (mm/mm) of C1, C2, and C4 decreased by 24×10^{-6}, 34×10^{-6}, and

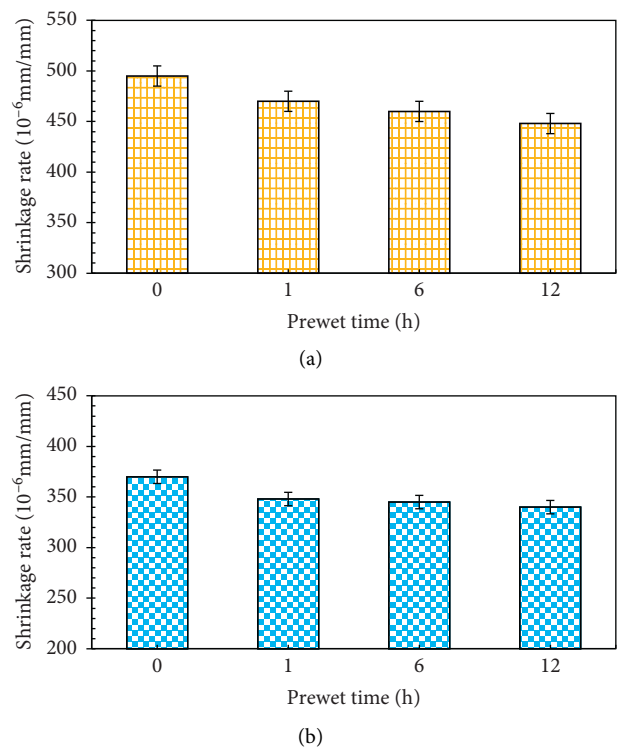

Figure 13: Shrinkage rate for concrete at 56 d (a) without SRA and (b) with SRA (2.0%).

48×10^{-6}, respectively. However, after the addition of SRA (in Figure 13(b)), the shrinkage (mm/mm) for D3, E1, E2, and E3 at 56 d was 368×10^{-6}, 348×10^{-6}, 343×10^{-6}, and 338×10^{-6}, respectively. Compared with the initial state of D3, the shrinkage (mm/mm) for E1, E2, and E3 produced a reduction of 20×10^{-6}, 25×10^{-6}, and 30×10^{-6}, respectively. It can be seen that, after the induction of shrinkage and with the incremental change in prewetting, the result is not as pronounced as when internal curing alone is applied. This difference is probably due to the inclusion of SRA in the LWAC, which reduces the capillary solution surface tension. In the case where ceramsite water absorption is constant and the capillary diameter in the semisaturated state remains constant, the smaller the surface tension of the pore solution, the smaller the corresponding capillary tension drop. Thus, lower surface tension weakens the effects of shrinkage inhibition. This speculation remains to be confirmed in later research.

In this experiment, the effect of SRA on the shrinkage of LWAC under different dose conditions is also studied by using water-treated coal gangue ceramic. The water saturation time was 24 h, and SRA concentrations of 0%, 0.5%, 1.0%, and 2.0% were selected for evaluation.

From Figures 14 and 15, it can be seen that the shrinkages (mm/mm) of D1, D2, and D3 at 56 d were 409×10^{-6}, 381×10^{-6}, and 369×10^{-6}, respectively, when dry ceramic was used. These values are approximately 82%, 77%, and 74% of that seen in the reference group C0. When saturated ceramsite was used, the shrinkages (mm/

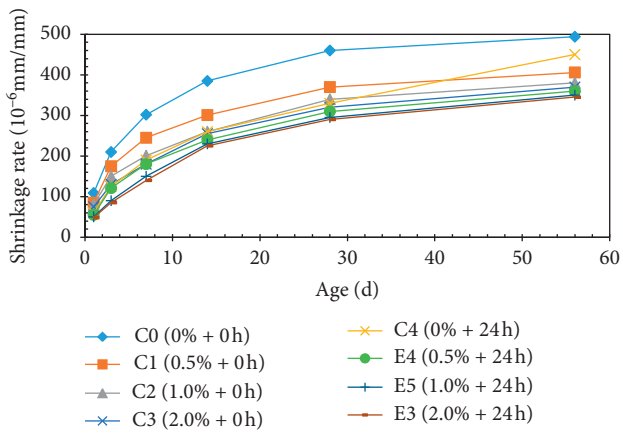

Figure 14: Effect of SRA dose on the shrinkage of the concrete for different prewetting times.

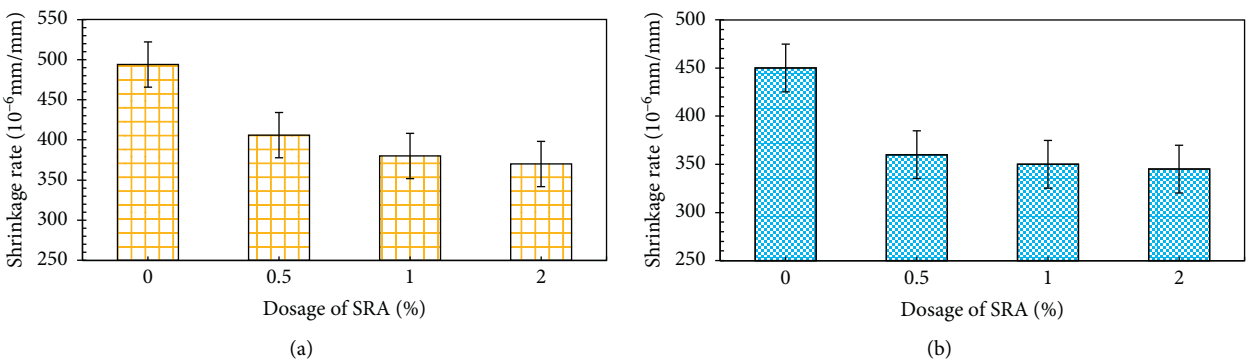

Figure 15: Shrinkage of the concrete with (a) drying and (b) CGC prewetting (24 h) at 56 d.

mm) of E4, E5, and E3 were 382×10^{-6}, 351×10^{-6}, and 338×10^{-6}, respectively. These shrinkages are 85%, 78%, and 75% of those in reference group C4. Compared with the addition of SRA alone, as shown in Figure 15(a), the combined incorporation of SRA and prewetting of the ceramic, as shown in Figure 15(b), significantly reduces LWAC shrinkage. However, the effect of SRA increase on the drying shrinkage is not obvious, and the shrinkage rate in Figure 15(b) is lower than its counterpart in Figure 15(a).

In summary, compared with the prewetting of the ceramic or SRA alone, the use of both SRA and prewet ceramic composite together can significantly inhibit LWAC shrinkage, resulting in a significant "superposition" effect.

3.6. Combined Effect of SRA and Prewet Ceramic on LWAC Strength. Figure 16 displays the effect of SRA, prewetting time, and the combination of the two on the compressive strength of LWAC under dry curing conditions. In the early hydration stages, SRA and the internal curing compound have an unfavorable effect on LWAC strength, but it is smaller at the later stage and is slightly higher than that of the reference group C0. At the same SRA dose, compared with SRA alone, the use of prewet ceramsite results in higher LWAC strength. This increased strength is mainly due to the internal curing of ceramsite. The dense structure of the cement slurry interface area increases the concrete strength and ultimately compensates for the loss of strength caused by SRA-induced delay of cement hydration. In the combined case, with elapsed prewetting time, the late strength is enhanced to a certain extent.

In addition, at 7 d, the LWAC strength in the combined case is lower than that in the reference group. However, the degree of reduction is much smaller than the sum of the drops observed when using SRA and internal curing individually. This result may be due to the addition of SRA. Under this condition, the shrinkage stress of the cement slurry decreases, and this decreased stress reduces the formation of microcracks and other defects, finally reducing the adverse effect on the strength. However, with an increase in SRA content, LWAC strength decreases, which indicates that the internal curing effect from prewetting the ceramic cannot completely eliminate the negative effect of SRA on strength when the SRA content is too large.

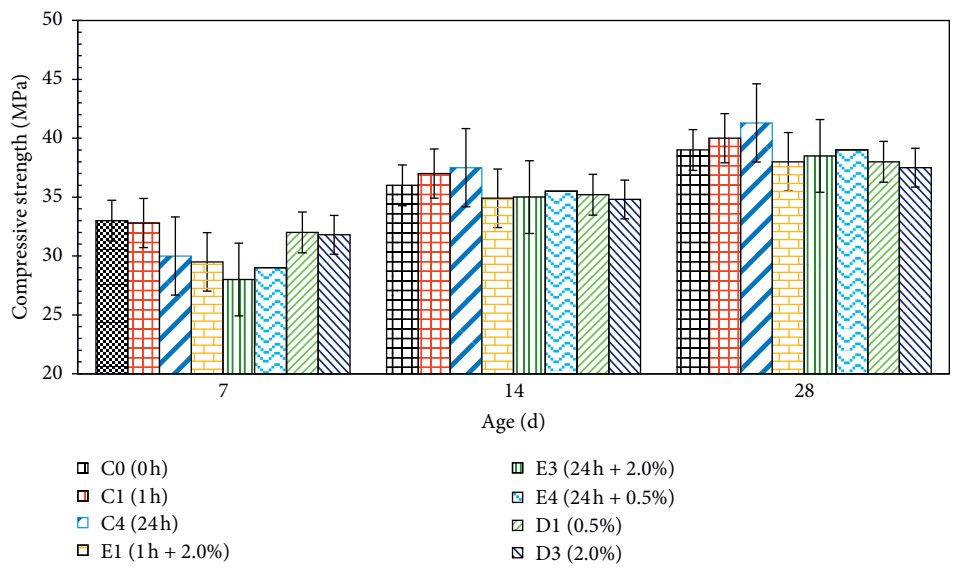

Figure 16: Influence of SRA, prewetting time, and a combination of SRA and prewetting time on the compressive strength of concrete.

4. Conclusions

In this study, the prewetting time of coal gangue ceramsite and shrinkage reducing agent were taken into account by laboratory experiments. The effects of the prewetting time and shrinkage reducing agent on the shrinkage volume and mechanical properties of LWAC are discussed. The results showed that prewetting time and shrinkage reducing agent have great influence on the shrinkage of lightweight aggregate concrete with coal gangue ceramsite. Appropriate control of prewetting time and shrinkage reducing agent in the sample preparation can increase strength of LWAC to meet the concrete strength standard and considerably reduce the shrinkage of concrete.

As prewetting time of CGC is prolonged, shrinkage volume of LWAC gradually decreases. For example, when ceramsite is initially prewetted, the shrinkage volume reduction is most notable. When CGC is prewetted for more than 12 h, the effect of prewetting time on shrinkage volume reduction becomes insignificant. In addition, prewetting time also shows influence on strength. For example, after CGC prewetting treatment, the early strength (at 7 d) of LWAC decreases. The late strength of LWAC increases and becomes higher than that without prewetting treatment.

The incorporation of SRA has a significant effect on shrinkage volume reduction of LWAC. For example, when SRA is 2% of the cement, shrinkage volume of LWAC at 56 d is reduced by approximately 26%. When the SRA dose is large, an increase in the dose has less effect on shrinkage volume reduction. In addition, addition of SRA has an adverse effect on the compressive strength of LWAC. For example, when SRA makes up 2% or less of the cement, the effect of SRA on the compressive strength of the LWAC is small. When the dose increases to 4% of the cement, LWAC strength decreases significantly. The compressive strength decreases by 10% and 5% at 7 d and 28 d, respectively.

The combined application of SRA and prewetting shows good and pronounced suppression of LWAC shrinkage. Specifically, the combined application has a certain influence on the early strength of LWAC. The late strength of the concrete enhances and effectively compensates for the adverse effect of SRA on strength.

Operation error in the preparation of LWAC, i.e., not mixing sufficiently, probably contributed to shrinkage and strength changes. The adverse effect of this operation error remains to be assessed and improved. It is suggested that the effect of different methods on the lightweight aggregate concrete with coal gangue ceramsite be presented by microstructure analysis. It can reveal the microscale mechanism of the dependence of concrete strength on prewetting time and shrinkage reducing agent.

Data Availability

The data used to support the findings of this study are available from the corresponding author upon request.

Conflicts of Interest

The authors declare that the research was conducted in the absence of any commercial or financial relationships that could be construed as a potential conflict of interest.

Acknowledgments

The authors gratefully acknowledge the financial support from National Science Foundation (51774066), the National Science and Technology Support Plan (2017YFC1503105, 2018YFC0604604, and 2019YFC1907201), Research and Development Project (Liaoning, 2019JH2/10300051) and Innovation Program for College Students Northeastern University, (201116 and 200060).

References

[1] F. Salguero, J. A. Grande, T. Valente et al., "Recycling of manganese gangue materials from waste-dumps in the Iberian Pyrite Belt - application as filler for concrete production," *Construction and Building Materials*, vol. 54, pp. 363–368, 2014.

[2] C.-L. Wang, W. Ni, S.-Q. Zhang, S. Wang, G.-S. Gai, and W.-K. Wang, "Preparation and properties of autoclaved aerated concrete using coal gangue and iron ore tailings," *Construction and Building Materials*, vol. 104, pp. 109–115, 2016.

[3] D. Wu, Y. Hou, T. Deng, Y. Chen, and X. Zhao, "Thermal, hydraulic and mechanical performances of cemented coal gangue-fly ash backfill," *International Journal of Mineral Processing*, vol. 162, pp. 12–18, 2017.

[4] Y. Yao, Y. Li, X. Liu, H. Sun, S. Jiang, and C. Feng, "Performance and energy calculation on a green cementitious material composed of coal refuse," *Clean Technologies and Environmental Policy*, vol. 16, no. 2, pp. 281–290, 2014.

[5] J. Szczypa, J. Neczaj-Hruzewicz, and J. Sablik, "Some of properties of slime coatings in coal-gangue systems," *Transactions of the Institution of Mining and Metallurgy*, vol. 82, no. 802, pp. c167–c169, 1973.

[6] X. Querol, M. Izquierdo, E. Monfort et al., "Environmental characterization of burnt coal gangue banks at Yangquan, Shanxi province, China," *International Journal of Coal Geology*, vol. 75, no. 2, pp. 93–104, 2008.

[7] L. Haibin and L. Zhenling, "Recycling utilization patterns of coal mining waste in China," *Resources, Conservation and Recycling*, vol. 54, no. 12, pp. 1331–1340, 2010.

[8] H. Xiao, X. Ma, and K. Liu, "Co-combustion kinetics of sewage sludge with coal and coal gangue under different atmospheres," *Energy Conversion and Management*, vol. 51, no. 10, pp. 1976–1980, 2010.

[9] X. Liu, X. Zhuang, O. Font et al., "Influence of soil cover on reducing the environmental impact of spontaneous coal combustion in coal waste gobs: a review and new experimental data," *International Journal of Coal Geology*, vol. 85, no. 1, pp. 2–22, 2011.

[10] R. Demirboga, I. Orung, and R. Gul, "Effects of expanded perlite aggregate and mineral admixtures on the compressive strength of low-density concretes," *Cement and Concrete Research*, vol. 31, no. 11, pp. 1627–1632, 2001.

[11] J. Wang, Q. Qin, S. Hu, and K. Wu, "A concrete material with waste coal gangue and fly ash used for farmland drainage in high groundwater level areas," *Journal of Cleaner Production*, vol. 112, pp. 631–638, 2016.

[12] M. Aslam, P. Shafigh, M. Z. Jumaat, and M. Lachemi, "Benefits of using blended waste coarse lightweight aggregates in structural lightweight aggregate concrete," *Journal of Cleaner Production*, vol. 119, pp. 108–117, 2016.

[13] A. Hanif, Z. Lu, and Z. Li, "Utilization of fly ash cenosphere as lightweight filler in cement-based composites-a review," *Construction and Building Materials*, vol. 144, pp. 373–384, 2017.

[14] B. González-Corrochano, J. Alonso-Azcárate, and M. Rodas, "Production of lightweight aggregates from mining and industrial wastes," *Journal of Environmental Management*, vol. 90, no. 8, pp. 2801–2812, 2009.

[15] A. Ben Fraj, M. Kismi, and P. Mounanga, "Valorization of coarse rigid polyurethane foam waste in lightweight aggregate concrete," *Construction and Building Materials*, vol. 24, no. 6, pp. 1069–1077, 2010.

[16] P. Shafigh, H. B. Mahmud, M. Z. B. Jumaat, R. Ahmmad, and S. Bahri, "Structural lightweight aggregate concrete using two types of waste from the palm oil industry as aggregate," *Journal of Cleaner Production*, vol. 80, pp. 187–196, 2014.

[17] F. Colangelo, F. Messina, and R. Cioffi, "Recycling of MSWI fly ash by means of cementitious double step cold bonding pelletization: technological assessment for the production of lightweight artificial aggregates," *Journal of Hazardous Materials*, vol. 299, pp. 181–191, 2015.

[18] F. Colangelo, R. Cioffi, B. Liguori, and F. Iucolano, "Recycled polyolefins waste as aggregates for lightweight concrete," *Composites Part B: Engineering*, vol. 106, pp. 234–241, 2016.

[19] F. Colangelo, F. Messina, L. Di Palma, and R. Cioffi, "Recycling of non-metallic automotive shredder residues and coal fly-ash in cold-bonded aggregates for sustainable concrete," *Composites Part B: Engineering*, vol. 116, pp. 46–52, 2017.

[20] A. Hanif, Z. Lu, Y. Cheng, S. Diao, and Z. Li, "Effects of different lightweight functional fillers for use in cementitious composites," *International Journal of Concrete Structures and Materials*, vol. 11, no. 1, pp. 99–113, 2017.

[21] M. I. Khan, M. Usman, S. A. Rizwan, and A. Hanif, "Self-consolidating lightweight concrete incorporating limestone powder and fly ash as supplementary cementing material," *Materials*, vol. 12, no. 18, 2019.

[22] S. Cheng, Z. Shui, R. Yu, T. Sun, and X. Zhang, "Multiple influences of internal curing and supplementary cementitious materials on the shrinkage and microstructure development of reefs aggregate concrete," *Construction and Building Materials*, vol. 155, pp. 522–530, 2017.

[23] R. Henkensiefken, D. Bentz, T. Nantung, and J. Weiss, "Volume change and cracking in internally cured mixtures made with saturated lightweight aggregate under sealed and unsealed conditions," *Cement and Concrete Composites*, vol. 31, no. 7, pp. 427–437, 2009.

[24] X. F. Wang, C. Fang, W. Q. Kuang, D. W. Li, N. X. Han, and F. Xing, "Experimental investigation on the compressive strength and shrinkage of concrete with pre-wetted lightweight aggregates," *Construction and Building Materials*, vol. 155, pp. 867–879, 2017.

[25] J. Gong, W. Zeng, and W. Zhang, "Influence of shrinkage-reducing agent and polypropylene fiber on shrinkage of ceramsite concrete," *Construction and Building Materials*, vol. 159, pp. 155–163, 2018.

[26] F. Rajabipour, G. Sant, and J. Weiss, "Interactions between shrinkage reducing admixtures (SRA) and cement paste's pore solution," *Cement and Concrete Research*, vol. 38, no. 5, pp. 606–615, 2008.